The effect of in-process ethylene incorporation on the evolution of particle morphology and molecular characteristics of commercial Heterophasic Ethylene Propylene Copolymers (HEPCs)

By

Linda Botha

Dissertation presented for the degree of Doctor of Philosophy (Polymer Science)

At

Stellenbosch University

Promoter: Prof. A.J. van Reenen

April 2014

Declaration

By submitting this dissertation, I declare that the entirety of the work contained herein is my own, original work, that I am the owner of the copyright thereof (unless to the extent explicitly otherwise stated) and that I have not previously in its entirety or in part submitted it for obtaining any qualification.

Signature: ..... Date: 2014/02/24

Abstract

Impact copolymers or heterophasic polypropylene-ethylene-co-propylene copolymers (HEPCs) commonly produced in industry are valued for their good mechanical properties, combining the rigidity of the polypropylene matrix with the toughness of the dispersed ethylene-propylene copolymer. The potential for further optimisation and tailoring of product properties can be realised through an improved understanding of how the copolymer phase produced in the second reactor develops with increasing ethylene incorporation, providing an intermediate link between predicted physical behaviour and the process parameters required to achieve this. To this end, the morphological development of heterophasic or impact copolymers, has been a topic of interest of many studies to date, yet due to the complexity of these polymers, there is still some uncertainty with regards to the mechanism of copolymer growth as well as the structure-function relationships that exist. These studies were limited either due to the use of autoclave products or final impact copolymer products obtained from industry.

The work presented in this study was aimed at understanding how the nascent copolymer phase develops during a transition from homopolymer to the final copolymer. This was done by selecting samples at certain intervals from two different commercial gas-phase processes, yielding two sets of four samples, each with a range of increasing ethylene contents. These samples provided the unique opportunity to study the early development of copolymer in a sequential manner (as each sample builds on the morphology of the previous one). The morphological development of copolymer in these samples was investigated by high resolution FE-SEM and it was observed that the copolymers showed different degrees of internal and external distribution as well as porosity for the different sets, determined by the initial porosity of the homopolymer. It was also found that the copolymer was radially distributed throughout the particle in all instances, suggesting that ethylene monomer diffusion limitations did not play a significant role in the copolymerization process.

A further aim of the study was to determine the effect of ethylene incorporation on bulk sample crystallinity, microstructure and chemical composition. It was observed by SCALLS and TREF that increasing ethylene incorporation attenuated the crystallinity of the homopolymer, resulting in a distribution of components with different crystallinities within the samples, suggesting some interaction between the developing copolymer and existing homopolymer. During the microstructural development of these samples, longer or more blocky ethylene sequences seemed to be favoured above isolated ethylene sequences with increasing ethylene incorporation and it was shown by solid-state NMR that ethylene partitioning between both

amorphous and rigid environments occurred. Detailed characterization (solution and solid-state ^{13}C NMR, HT-SEC and HT-HPLC) of the semi-crystalline copolymer fractions provided some information on the development of microstructure and chemical composition in these fractions that are responsible for compatibilization between the homopolymer matrix and dispersed rubber phase. Based on the different observations from the investigations outlined above, a model for copolymer development in each set was proposed and related to the physical property development observed for these samples.

Opsomming

Die impak-kopolimere – ook bekend as heterofase polipropileen-etileen-kopropileen kopolimere (HEPC's) – wat tans in die bedryf vervaardig word, is bekend vir hul goeie meganiese eienskappe, naamlik om die styfheid van 'n polipropileenmatriks met die sterkte van 'n etileen-propileen kopolimeer, wat in die matriks versprei is, te kombineer. Die potensiaal vir die optimisering en pasmaak van produkeienskappe kan bewerkstellig word deur beter begrip ten opsigte van hoe die kopolimeerfase wat in die tweede reaktor vervaardig word, ontwikkel as gevolg van toenemende inkorporasie van etileen, en hoe dit 'n skakel skep tussen voorspelbare fisiese gedrag en die prosesparameters wat nodig is hiervoor. Tot datum het heelparty studies gefokus op die morfologiese ontwikkeling van heterofase of impak-kopolimere, maar as gevolg van die komplekse aard van hierdie polimere is daar nog steeds onsekerheid oor die meganisme van kopolimeerontwikkeling, asook die verwantskappe tussen die polimeerstruktuur en -funksie. Sodanige studies was beperk omdat óf outoklaafprodukte óf finale produkte van industriële prosesse gebruik is.

Die doel van hierdie studie was om begrip te kry vir hoe die kopolimeerfase ontwikkel tydens 'n oorgang van homopolimeer tot die finale produk. Hiervoor is twee stelle van vier monsters met toenemende etileeninhoude tydens die oorgang in twee verskillende gasfaseprosesse verkry. Hierdie monsters het die unieke geleentheid gebied vir die opvolgende bestudering van die vroeë ontwikkeling van die kopolimeer, deurdat elke monster voortgebou het op die morfologie van die vorige monster. Die morfologiese ontwikkeling van die kopolimeer is ondersoek deur van hoëresolusie FE-SEM gebruik te maak. Verskillende wyses van interne en eksterne verspreiding, sowel as porositeit van die onderskeie stelle (soos bepaal deur die aanvanklike porositeit van die homopolimeer), is vir die verskillende prosesse waargeneem. Daar is ook waargeneem dat die kopolimeer in alle gevalle op verskeie straalposisies binne die partikel versprei is, waarvan afgelei kan word dat monomeerdiffusiebeperking nie 'n beduidende rol in die kopolimerisasieproses speel nie.

'n Verdere doel van hierdie studie was om die uitwerking van etileen-inkorporasie op die kristalliniteit, mikrostruktuur en chemiese samestelling van die polimeer te bepaal. Deur middel van SCALLS en TREF is bevind dat toenemende etileen-inkorporasie die kristalliniteit van die homopolimeer verswak het. Die gevolg was die vorming van 'n verskeidenheid komponente met verskillende kristalliniteite, wat dui op 'n interaksie tussen die groeiende kopolimeer en die bestaande homopolimeer. Tydens die ontwikkeling van die mikrostruktuur van die monsters

het dit geblyk dat lang, opeenvolgende etileeneenhede tydens toenemende etileen-inkorporasie vinniger ontwikkel as afgesonderde etileen- en propileeneenhede. Deur middel van soliedefase-KMR is daar bewys dat die etileen in beide amorfe en kristalagtige areas versprei is. Die semi-kristallyne kopolimere wat deur TREF verkry is, is verder gekarakteriseer met behulp van KMR in oplossing sowel as die soliede fase, HT-SEC en HT-HPLC, wat meer inligting verskaf oor die ontwikkeling van die mikrostruktuur en chemiese samestelling van hierdie fraksies wat normaalweg verantwoordelik is vir die interaksies tussen die homopolimeermatriks en die verspreide rubberfase. Op grond van die waarnemings soos hierbo vermeld, word ’n model vir die kopolimeerfase-ontwikkeling van elke stel monsters in hierdie studie voorgestel en verbind met die ontwikkeling van die waargenome fisiese eienskappe.

This thesis is dedicated to my own little family at home –
Thanks for providing the nudge when I needed it,
the comfort when I needed it
and your love regardless.

Acknowledgements

This study would not have been possible if it weren't for the following people, whom the author would like to thank below:

A huge thanks to my promoter, Prof Albert van Reenen for his guidance, helping me navigate the extensive field of Polymer Science, especially that of HEPCs and in his wisdom providing me with the exact amount of inspiration and advice exactly when I needed it!

To my business managers Dr. Francois du Toit, Monja Smith (for the initial project concept), Dr. Brian Sole and Jenny Green for your valuable feedback, IP checks, encouragement and good discussions. To Dr. John Mellor for providing the financial support for my studies while I continued to work at Sasol Polymers.

To my mentor, Ludwig van Niekerk, from whom I have learnt all about the business of making polypropylene, engineering balances and operations. You have always given me solid guidance and our discussions means a lot to me!

To the one person who probably understands the work-life-study balance best, Morne Swart, thanks for showing me that it can be done and helping out with your experience and advice whenever and however I needed it!

Thanks to Miranda Waldron at UCT for the microscopy images – only you can make it look easy. To Dr. Jaco Brand and Elsa Malherbe at CAF, thanks for running a seemingly endless number of solution NMR samples and doing magic with your shimming. Thanks to Dr. Pritish Sinha for the solid-state NMR runs and sharing your solid-state as well as polymer experience to help me make the most from this method.

A word of thanks to my Sastech colleagues, Dr. Dawie Joubert, for your valuable insights and discussions, Dr. Sandra Joubert, for your pioneering work on developing a macro for our impact copolymers, which has significantly contributed to this study and also to Heidi Duveskog for introducing me to the exciting and daunting world of NMR analysis of polymers. I am convinced that without your guidance and feedback I would never have begun to tap the potential that NMR analysis can provide.

Thanks to Dr. Gareth Harding for the HT-SEC and SEC-FTIR runs as well as your good advice and feedback. To Dr. Sadiqali Cheruthazhekatt and Phiri Mohau for the HT-HPLC runs and stimulating discussions.

To Maggie (Dr. M Brand) and Divann for the SCALLS runs and your very patient help with regards to the Origin software, as well as Madeleine and Marehette for welcoming and accommodating me in the lab. I am happy to say that I have through my studies gained a few friends. To Marie for the completion of some of the TREF experiments – I am eternally grateful for this.

Thanks to my colleagues at the Sasol Polymers' Polymer Technology Services Centre, especially Robert Kwinda, for alleviating the work pressure at the plant and to Ayanda Mfusi for your help

with the compounding of samples, Jacques Rossouw for the physical testing, the production shifts and the process laboratory personnel for their kind assistance.

A special thanks to my PP friends: Charl, Hans, Christelle, Almari, Nelius and Pierre for your support and for accommodating the crazy scientist in your midst.

I would also like to thank my moms and grandparents for their unconditional love and support.

To my husband Heinrich, without your support this would never have happened. Thanks for your help in so many different aspects, your love, understanding and encouragement.

Table of Contents

List of Figures

List of Tables

List of Abbreviations

3D	3-Dimensional
^{13}C	Carbon thirteen, a natural isotope of carbon with an isotope mass of 13
AFM	Atomic force microscopy
A-TREF	Analytical temperature rising elution fractionation
CAGR	Compounded annual growth rate
CPMAS	Cross polarization and magic angle spinning
CRYSTAF	Crystallisation analysis fractionation
DMA	Dynamic mechanical analysis
d-TCE	Deuterated tetrachloroethane
DSC	Differential scanning calorimetry
ELSD	Evaporative light scattering detector
EPC	Ethylene-propylene copolymers
EPR	Ethylene-propylene rubber
FE-SEM	Field emission scanning electron microscopy
FTIR	Fourier transform infrared spectroscopy
GC	Gas chromatography
SEC	Size exclusion chromatography
HDPE	High density polyethylene
HEPC	Heterophasic ethylene-propylene copolymers
HP	Homopolymer
HPLC	High performance liquid chromatography
HT-HPLC	High temperature high performance liquid chromatography
HT-SEC	High temperature size exclusion liquid chromatography
ICP	Impact copolymer
iPP	Isotactic polypropylene
IDREF	Dipolar dephasing or interrupted decoupling experiments
IR	Infra-red
LDPE	Low density polyethylene
LLDPE	Linear low density polyethylene
MFR	Melt flow rate
M_n	Number average molecular weight
MTA	Mega tons per annum
M_w	Weight average molecular weight

MWD	Molecular weight distribution
NMR	Nuclear magnetic resonance
PD	Polydispersity
PE	Polyethylene
PET	Polyethylene terephthalate
PP	Polypropylene
PS	Polystyrene
P-TREF	Preparative temperature rising elution fractionation
PVC	Polyvinyl chloride
RI	Refractive index
SCALLS	Solution crystallisation analysis by laser light scattering
SEC	Size exclusion chromatography
SEC-FTIR	Size exclusion chromatography Fourier transform infrared spectroscopy
SEM	Scanning electron microscopy
Tan	Tangent
TCB	Trichlorobenzene
TCE	Tetrachloroethylene
TEM	Transmission electron microscopy
TFA	Turbidity fractionation analysis
T_g	Glass transition temperature
T_m	Melting temperature
TREF	Temperature rising elution fractionation
XRD	X-ray diffraction
ZN	Ziegler-Natta

Chapter 1

Introduction and Objectives

In this chapter a brief background of the manufacture, end-uses and current challenges for heterophasic ethylene propylene copolymers (HEPCs) will be given. The problem statement and specific objectives of this study are identified and the dissertation layout provided.

1.1 Introduction

The global polypropylene (PP) demand in 2012 was estimated at 52 million metric tons comprising 26% of the global commodity thermoplastics demand and being the largest of the different plastics markets, followed by PVC (18%) and HDPE (17%) [1]. The largest portion of PP is used in injection moulding (33%), followed by film and sheet (24%) and raffia applications (18%) [1]. Homopolymers (HP) and impact copolymers (ICPs) combined comprises over 90% of the global PP production grade split and these grades also have the highest growth potential [2]. PP production volumes are forecast to grow to approximately 80 million tons by 2016, with the fastest Compounded Annual Growth Rate (CAGR) expected for the Asia-Pacific region at 8% [3]. Closer to home, factors affecting the PP markets in South Africa such as the relative high prices of feedstock (compared to those of competitor companies in the Middle-East), have placed local resin producers under increased pressure to improve the value-add of their product and service offering in order to stay competitive. The polypropylene markets have also seen increasing encroachment by other cost-effective polymers such as high-density polyethylene (HDPE) and polyethylene terephthalate (PET) [2]. Currently global PP markets are still dominated by homopolymer, as it can be produced at high instantaneous throughputs (relative to impact copolymers) and doesn't require a second in-series reactor. However these polymers are mostly used for raffia and film applications. For thin walled injection moulding (which holds a significant market share as shown above), there is a growing need for ICPs with advanced impact-stiffness properties, as well as improved melt flow rates to enable faster cycle times and the filling of highly intricate moulds.

One way of improving product competiveness is through the optimization of product properties, capitalizing on the intrinsic differences between PP and other polymers, e.g. good stiffness and heat distortion properties [2]. In fact heterophasic ethylene-propylene copolymers or impact copolymers (HEPCs or ICPs) initially came into existence by combining the excellent rigidity of propylene homopolymer and the impact resistance of an ethylene-propylene copolymer to improve the stiffness-impact balance of the polymer. The first patent specifically mentioning significant improvement in impact strength by in-series copolymerization and production of so-called in-reactor alloys was granted to the Shell Oil Company in 1965 [4]. Since then, many academic studies have been initiated to obtain a clearer understanding of the link between polymer structure and end-properties [5-10]. These polymers are however extremely complex and the underlying mechanisms between structure and function are not yet fully understood.

The complexity of commercial HEPCs is therefore the main obstacle to overcome when attempting to understand structure-function relationships. This complexity originates from the multi-site nature of the heterogeneous Ziegler-Natta (ZN) catalysts, which are typically used in current gas-phase and slurry technologies. Each different active site has its own tacticity- and kinetic profiles and resultantly different products are obtained from different active sites. The specific in-series reactor configuration, used for producing the HEPCs also results in products where the homopolymer from the first reactor is covalently bonded to the copolymer produced in the second reactor. These physical bonds between reactor products are mostly responsible for the superior physical properties observed in these polymers [4], however it makes these polymers more difficult to study in the bulk as the effect of the copolymer phase (which can comprise around 20% of the final polymer) is overshadowed by the main component which is the homopolymer. The copolymer phase itself is also very complex, ranging from highly amorphous ethylene-propylene rubber to semi-crystalline copolymer and even some crystalline polyethylene. All of these components in turn consist of chains spanning a wide range of molecular weights and chemical compositions. For this reason there are studies that have only focused on the ethylene-propylene copolymer portion, which can either be synthesised according to specification [5,7] or isolated via extraction [8]. Some work on isotactic PP/EPR blends, have also been done [6,10]. The limitation of such studies is that it negates the matrix-copolymer phase interaction and in the case of rubber extraction, the effect of semi-crystalline ethylene-propylene copolymers, which may crystallize with the matrix.

It is commonly known that the dispersion of the ethylene-propylene rubber (reflected by rubber particle sizes and inter-particle distances) can be translated into the physical performance, specifically the impact toughness of the polymer [11]. Vital to being able to control rubber particle size and distribution, is an understanding of how the rubber phase develops relative to the existing homopolymer matrix and how the semi-crystalline copolymers facilitate compatibility between the clearly incompatible homopolymer and rubber. From this point of view, a few studies focused on an improved understanding of the morphology development of these different phases have previously been conducted [5-8,12]. Some studies have tried to replicate the development of the copolymer phase as well as to focus on phase interactions, however these studies were done in laboratory scale autoclave reactors, that do not fully represent the conditions prevailing in continuous processes industrially [5,7,12].

Despite the challenges outlined above, a few theories on the evolution of the copolymer phase in relation to the existing homopolymer matrix have been put forward. These include the “solid

core" model, "polymer flow" model, "multi grain" model and "pore filling" model. These models will be described in more detail in Chapter 2. Comparing these models and the studies that led to development of them, it is clear that each model is limited to the scope of the study and the assumptions made. For example McKenna *et al.* found that the pore-filling model was highly dependent on the assumed size of the pores, which could differ as much as an order of magnitude between the micro-and macro-pores. Hence significantly different results could be obtained depending on the definition of average pore size. This remark just served as an example, but it is clear that the diversity of methods used and assumptions made for the development of these models provided different windows of understanding on the subject of developing morphology. However the sum of these different approaches doesn't necessarily constitute a full understanding and some gaps still exist.

1.2 Objectives

It is evident that within the complexity of HEPCs and the limitations of each study mentioned above, a broad scope exists for further work aimed at understanding the development of the copolymer phase and control of the rubber particle size and distribution.

The work presented in this study was unique in the sense that samples representative of an "evolving polymer" were obtained in a time-dependent manner directly from industrial processes, providing a real-time view of how the copolymer phase develops in the second reactor as ethylene incorporation increases over time. These samples have an advantage above using copolymer-matrix blends due to the fact that the two reactor products are covalently linked and thus matrix and different copolymer phase interactions are taken into account, representative of the whole polymer and its physical behaviour in end-use applications. Furthermore, since the samples were obtained from industrial gas-phase processes, large-scale effects such as particle mixing, monomer diffusion limitations, cooling effects and continuous production were reflected in the analytical results and the learning obtained from this study should be applicable to these processes in industry.

The objectives of this study were:

- To determine the effect of increasing ethylene incorporation on the development of polymer morphology and physical properties in the bulk.
- To determine the attenuation of bulk sample crystallizability by increasing ethylene incorporation.

- Relation of the underlying bulk and fractionated polymer microstructure, chemical composition and crystal packing to the observed differences in sample crystallinity, morphology and physical properties.
- To develop a model for improved understanding of how the copolymer phase evolves from low to high ethylene contents.

In this study, eight HEPCs in total were selected from two different gas-phase production facilities, employing different technologies. The samples were obtained at specific times after initial ethylene introduction (T0), yielding samples with increasing total ethylene contents. These samples were organised into two sets, one for each technology and due to significant differences in reactor configuration, catalyst system and operating parameters, the development of the copolymer phase and its effects were investigated separately for each set.

Particle phase morphology of external and internal surfaces of bulk samples as well as fracture surfaces of moulded test pieces were visualised using field emission scanning electron microscopy (FE-SEM). These images were selected in a specific manner in a radial distribution to determine how increasing amounts of incorporated ethylene affect the copolymer phase development and distribution with respect to the existing homopolymer matrix. Physical testing was done on test bars moulded from bulk samples to determine the effect of ethylene incorporation on stiffness and impact strength (which are the two most important physical properties in end-use). The physical property results were also compared to DMA trends, which provided information on polymer behaviour, phase transitions and interactions at different temperatures.

From the bulk analyses clear ethylene dependent growth trends were observed for the morphology and physical properties and these trends were also different for the two sets. This warranted further investigation of the influence on sample crystallinity and microstructure. Crystallizability of the bulk samples were analysed by solution crystallization analysis by laser light scatter (SCALLS) that indicated clear ethylene dependent differences in sample crystallinity. Preparative temperature rising elution fractionation (p-TREF) confirmed the trend of decreasing crystallizability with increasing ethylene incorporation (although with lower resolution than SCALLS) and provided fractions for further microstructural and chemical composition analysis.

Ethylene distribution within the polymer chains and in relation to crystalline structures was investigated by solution and solid-state nuclear magnetic resonance (NMR) respectively. Effects

on molecular weight and ethylene distribution were determined by high temperature size exclusion chromatography (HT-SEC) coupled to Fourier transform infrared spectroscopy (FTIR) via an LC transform interface. High temperature high performance liquid chromatography (HT-HPLC) was used to obtain ethylene content-dependent trends for the polymers according to molecular weight and chemical composition. Observations from the microstructural development and partitioning of ethylene in crystalline and amorphous phases were related back to the crystallinity, microscopic features and physical property behaviour. This was done on bulk samples and TREF fractions.

1.3 Dissertation layout

The dissertation is divided into the following six chapters:

Chapter 1

A brief introduction and background concerning heterophasic ethylene-propylene copolymers is provided and the specific objectives of this study outlined. This chapter also contains the general layout of the dissertation.

Chapter 2

In this chapter, the unique properties of HEPCs as well as the different gas-phase technologies used for their manufacture are described in more detail. A detailed background is given on previous studies aimed at elucidating HEPC structural interactions and morphological development as well as detail on existing models for this, which will highlight the main findings and limitations as well as provide the context for this particular scope of work.

Chapter 3

In this chapter the experimental detail is given for sample selection. Sample preparation and the various analytical methods used in this study are discussed. The analytical techniques and equipment used are also discussed in detail.

Chapter 4

The development of bulk polymer morphology in the nascent (growing) chains with increasing ethylene incorporation is discussed at the hand of FE-SEM images obtained from various sections of the polymer particles. The development of physical properties with increasing ethylene incorporation as obtained from DMA and physical testing is outlined. The observed growth in rubber particle size and rubber inter particle distance is related to the development of physical properties. Preliminary observations for both sets in the bulk are highlighted.

Chapter 5

The effect of ethylene incorporation on sample crystallinity is investigated. The development of polymer microstructure with increasing ethylene content (as determined by solution NMR in bulk samples and fractions) is discussed and is related to the observed differences in morphology and physical properties. Changes in ethylene partitioning between amorphous and crystalline phases and its effect on crystal packing (as determined by solid-state NMR) and chemical composition distribution (as determined by HT-HPLC) is discussed and related to the morphological and physical changes in Chapter 4.

Chapter 6

The observations from Chapter 4 and 5 are consolidated in this chapter. The effect of increasing ethylene incorporation on the morphology and physical properties of the HEPCs are summarised. The microstructural changes responsible for the observed changes in crystal packing, overall crystallinity and ultimately polymer physical properties are discussed. A model is presented for the development of the copolymer phase in each sample set and the scope for future work is outlined.

1.4 References

1. Koster, R. *Polypropylene - the success story continues?* August 2012., IHS Marketing report.
2. Schoene, W. *Polypropylene - Global Markets, Challenges & Opportunities,* 7th Novolen Technology Conference, December 2011
3. Axis Research Mind., *Polypropylene (PP) - A Global Market Watch (2011-2016)*. 2012.

4. Short, G.A., Shell Oil Company, *Production of a modified polyolefin*. US Patent: 3318976, 3 Dec 1965.

5. McKenna, T.F., Bouzid, D., Matsunami, S. and Sugano, T. *Evolution of Particle Morphology during Polymerisation of High Impact Polypropylene.* Polymer Reaction Engineering, 2003. **11**(2): p. 177-197

6. Li, Y., Xu, J., Dong, Q., Wang, X., Fu, Z. and Fan, Z., *Effect of Microstructure of EPR on Crystallization and Morphology of PP/EPR Blends.* Polymer-Plastics Technology and Engineering, 2008. **47**: p. 1242-1249

7. Debling, J.A. and Ray, W.H. *Morphological Development of Impact Polypropylene Produced in Gas-phase with a $TiCl_4/MgCl_2$ Catalyst.* Journal of Applied Polymer Science., 2001. **81:** p. 3085-3106

8. Urdampilleta, I., Gonzalez, A., Iruin, J.J., de la Cal J.C. and Asua, J.M *Morphology of High Impact Polypropylene Particles.* Macromolecules., 2005. **38**: p. 2795-2801

9. Suarez, I., Caballero, J. and Coto, B. *Characterization of ethylene/propylene copolymers by means of a SEC-4D technique.* European Polymer Journal., 2011. **47**:(2) p.171-178

10. D'Orazio, L. and Cecchin, G. *Isotactic polypropylene/ethylene-co-propylene blends: effects of composition on rheology, morphology and properties of injection moulded samples*. Polymer., 2001. **42**: p.2675-2684

11. Liang, J.Z. and Li, R.K.Y. *Rubber toughening in polypropylene: a review.* Journal of Applied Polymer Science., 2000. **77:** p. 409-417

12. Li, Y., Xu, J., Dong, Q., Fu, Z. and Fan, Z.Q. *Morphology of polypropylene/poly(ethylene-co-propylene) in-reactor alloys prepared by multi-stage sequential polymerization and two-stage polymerization.* Polymer., 2009. **50**: p.5134-5141

Chapter 2

Literature Review

In this chapter, commercial drivers for HEPCs, their unique properties and different gas-phase technologies used for their manufacture are described in more detail. A detailed background is given on previous studies aimed at elucidating HEPC morphology development as well as their derived models, which will highlight the progress and limitations of such studies and also provide the context for the particular scope of work in this thesis.

2.1 Driving forces for further development of HEPCs

2.1.1 Market outlook for polypropylene

The year 2013 marks two very important anniversaries in the polyolefin industry: the 50th anniversary of the Ziegler-Natta Nobel Prize as well as the 60th anniversary of the very first patent on polyethylene [1]. In 1957, more than half a century ago, the first commercial polypropylene resin was produced by Montecatini with a Ziegler-Natta catalyst [2]. Polypropylene soon grew into a widely used resin due to the relatively low cost of propylene feedstock as a by-product from the oil and gas industry, as well as its advanced mechanical properties, especially in the case of the impact copolymers, earning the reputation of the "poor man's engineering polymer". Its cost-effectiveness and versatility also resulted in polypropylene replacing high-density polyethylene (HDPE) and polystyrene (PS) in some of their applications.

This situation has however changed in the past few years where global polypropylene markets are placed under pressure due to rising feedstock costs. Feedstock availability can also be a limiting factor. The result of this is that polypropylene has become more expensive. There is also a situation of global oversupply of polypropylene. In this economic environment, China is considered to be the growth leader, especially driving the growth of plastics used in automotive applications. However in 2012, there was already 14.4 MTA (mega tons per annum) installed polypropylene capacity in China and this is expected to grow further up to 25.9 MTA in 2017. Hence China is expected to start importing less in the next few years. Other expected trade flow changes predicted up to 2017 include an increase in exports by the Middle East and an increase in imports by Europe and Africa [3, 4]. Facing these challenges polypropylene producers both globally and locally need to differentiate their current product portfolios and service offering to ensure a sustainable demand and sufficient product margins.

Within these challenges described above, there however exist some opportunities and potential that can be utilized: Polypropylene still holds the largest global market amongst the thermoplastics at 26% (Figure 2.1A). Furthermore when considering global demand trends over the past 22 years polypropylene is also the fastest growing polymer (up to 52 million metric tons in this time frame), compared to other commodity polymers such as high density polyethylene (HDPE), linear low density polyethylene (LLDPE), low density polyethylene (LDPE), polyvinylchloride (PVC), polystyrene (PS) and polyethylene terephthalate (PET).

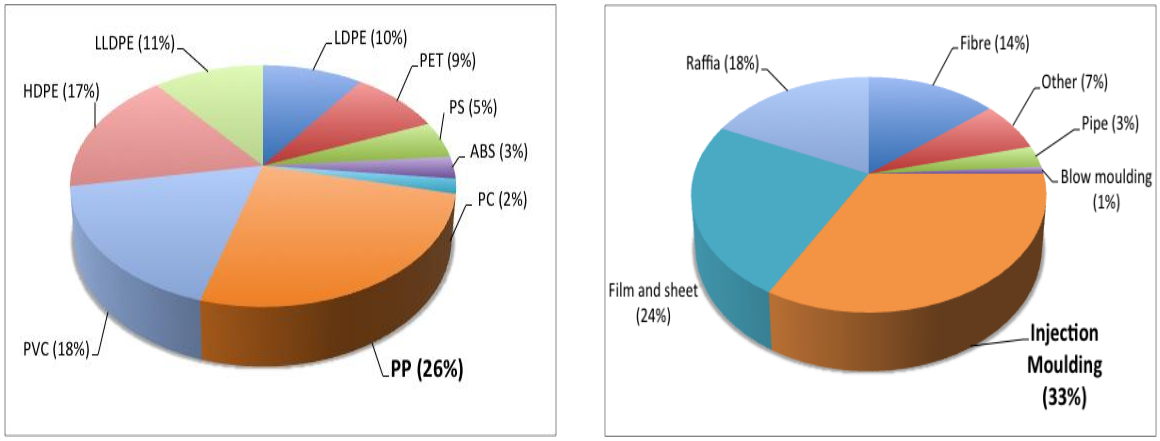

Figure 2.1 *Polypropylene marketing position: (A) Global thermoplastics demand in 2012 (B) Polypropylene demand breakdown by end-application (adapted from [4]).*

A breakdown of the different end-applications for polypropylene globally is shown in Figure 2.1B. From this data it is clear that injection moulding is the largest single application for polypropylene. HEPCs or impact copolymers are predominantly used in injection moulding to obtain the high stiffness and impact strength requirements of this type of application. Therefore, with polypropylene still being the largest thermoplastics market, injection moulding the largest application for polypropylene and impact copolymers being the predominant grade used in these applications, it is clear that there exist a large scope for further development of this specific type of polypropylene, which could potentially be used in product differentiation.

2.1.2 Present and future potential of HEPCs

Injection moulded articles or parts are typically used in food and transport packaging, domesticware, electrical appliances, building materials and automotive applications. The specific mechanical properties required of the resin can vary depending on the article produced and the end-use, however the trend in industry is to require increasing stiffness and impact strength properties, coupled with reduced weight per article (which is beneficial for downguaging and sustainability), while having improved melt flowability for faster cycle times and filling of more intricate moulds. In mentioning these different drivers influencing the design and production of HEPCs, it is clear that in order to fulfil market demand, a few conflicting requirements have to be met. For example, it is well known in industry that polymer stiffness and impact strength are driven by opposite forces, hence increase of the one property might lead to a decrease in the other. Furthermore, since there may be operational limitations (driven by condensing capacity and instantaneous volume targets) to obtain a certain maximum melt flow rate in the reactors, organic peroxides may have to be added during extrusion to obtain the

required final melt flow, which negatively impacts polymer properties. It is therefore clear that in order to obtain these required properties an advanced understanding of the HEPC structure-function relationship is of importance.

Automotive applications has been identified as the market with the best potential growth, as mentioned in the previous section. When considering that in Europe only 35% of plastics used in automotive applications are polypropylene [3] and locally this figure is even less, hence it is clear that some untapped potential for HEPCs exist in this field. The main drivers for increasing the polypropylene contribution to this market is weight reduction of the moulded articles (to curb carbon emmissions by producing lighter vehicles), recyclability and cost efficiency [3]. HEPCs have already proven that these have good mechanical properties and are lightweight compared to metals. The question is whether HEPCs would be able to significantly replace engineering resins and metals in future to provide cost-effective, lightweight (i.e. "green") solutions and grow its market share in the automotive industry. This can only be answered through a proper understanding of the complex relationship between HEPC phase morphology and mechanical properties and how these properties can be tailor-made to the application in mind.

2.2 What are heterophasic copolymers (HEPCs)?

2.2.1 Introduction

In 1965 the first patent for the production of HEPCs was granted to Shell Oil Company (US-Patent 3,318,976). This specifically addressed the problem that polypropylene in itself has high stiffness but low impact resistance. The novelty of the patent was that superior impact, stiffness and tensile strength properties could be obtained by producing in-reactor alloys of polypropylene with ethylene-propylene copolymers, compared to physical blends of polypropylene with polyethylene or elastomers. This invention paved the way for a whole new type of polymer with advanced properties and since then, much progress in this field has been made, in industry to optimize HEPC properties and in academia to improve the understanding of the mechanism behind these mechanical properties.

Currently commercial high impact polypropylene (ICP/hiPP) or heterophasic polypropylene (ethylene-co-propylene) polymers (HEPCs) are produced sequentially in a two-reactor configuration. Typically an isotactic PP matrix is produced in the first reactor and transferred to the second reactor where ethylene is introduced together with propylene to produce ethylene-

propylene copolymers, which are very diverse, ranging from atactic and rubbery to semi-crystalline.

In Fig. 2.2 two SEM micrographs are shown of the fracture surfaces of two different HEPC pellet samples [5]. This serves as an example for the typical arrangement of the different phases present in HEPCs. The ethylene-propylene rubber phase was extracted by xylene and is observed in these images as holes. It can be seen that the homopolymer forms a continuous phase or matrix in which the rubber particles are distributed. The function of the rubber particles is to dissipate forces applied to the polymer. The size and distribution can be related to physical properties, for example the polymer on the left has shown improved impact strength properties compared to the one on the right, due to a finer and more even distribution of rubber particles [5]. In these images, the position of semi-crystalline ethylene-propylene copolymers can't be observed (as some of it may crystallize with the matrix and the rest may have been removed with the rubber), however it is known that these copolymers act as a third phase with a compatibilizing function between the matrix and rubber and are therefore important for the proper distribution of rubber throughout the sample.

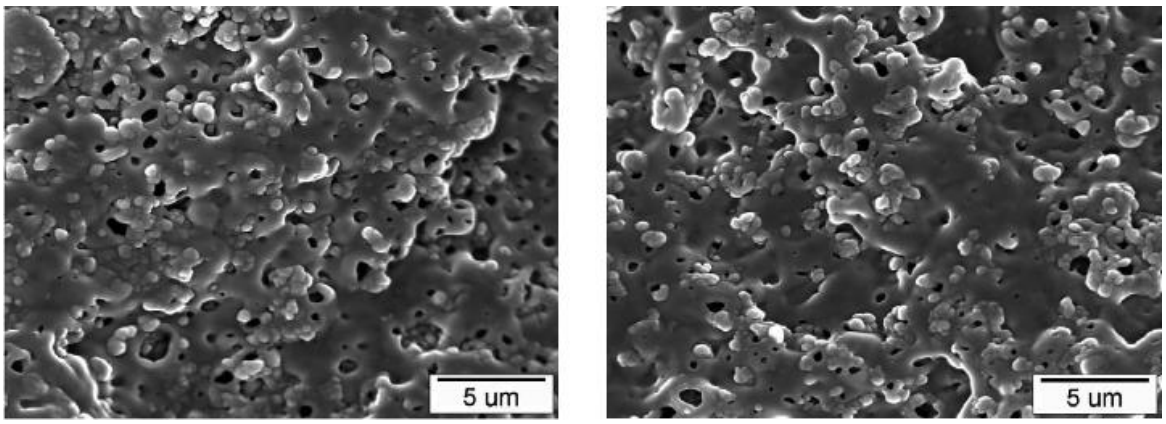

Figure 2.2 *SEM micrographs of fracture surfaces of two HEPC pellet samples with different cold impacts properties: Left – 10.5 kJ/m² and Right – 6.6 kJ/m² [5].*

2.2.2 Manufacture of heterophasic copolymers – Industrial processes

A schematic representation of current propylene polymerization technologies is shown in Fig. 2.3 below. Some of these are gas-phase only processes such as the Spherizone®-(LyondellBasell), Unipol- (Dow Plastics), Innovene®- (Ineos) and Novolen® processes. Other technologies such as the Spheripol technology from LyondellBasell and Borstar technology from Borealis use a combination of a bulk (liquid propylene) loop reactor in the first stage linked to a gas-phase copolymerization reactor in the second stage. In some instances pre-polymerization

of propylene is done at a lower activity in a smaller reactor upstream of the loop reactors to improve powder particle morphology.

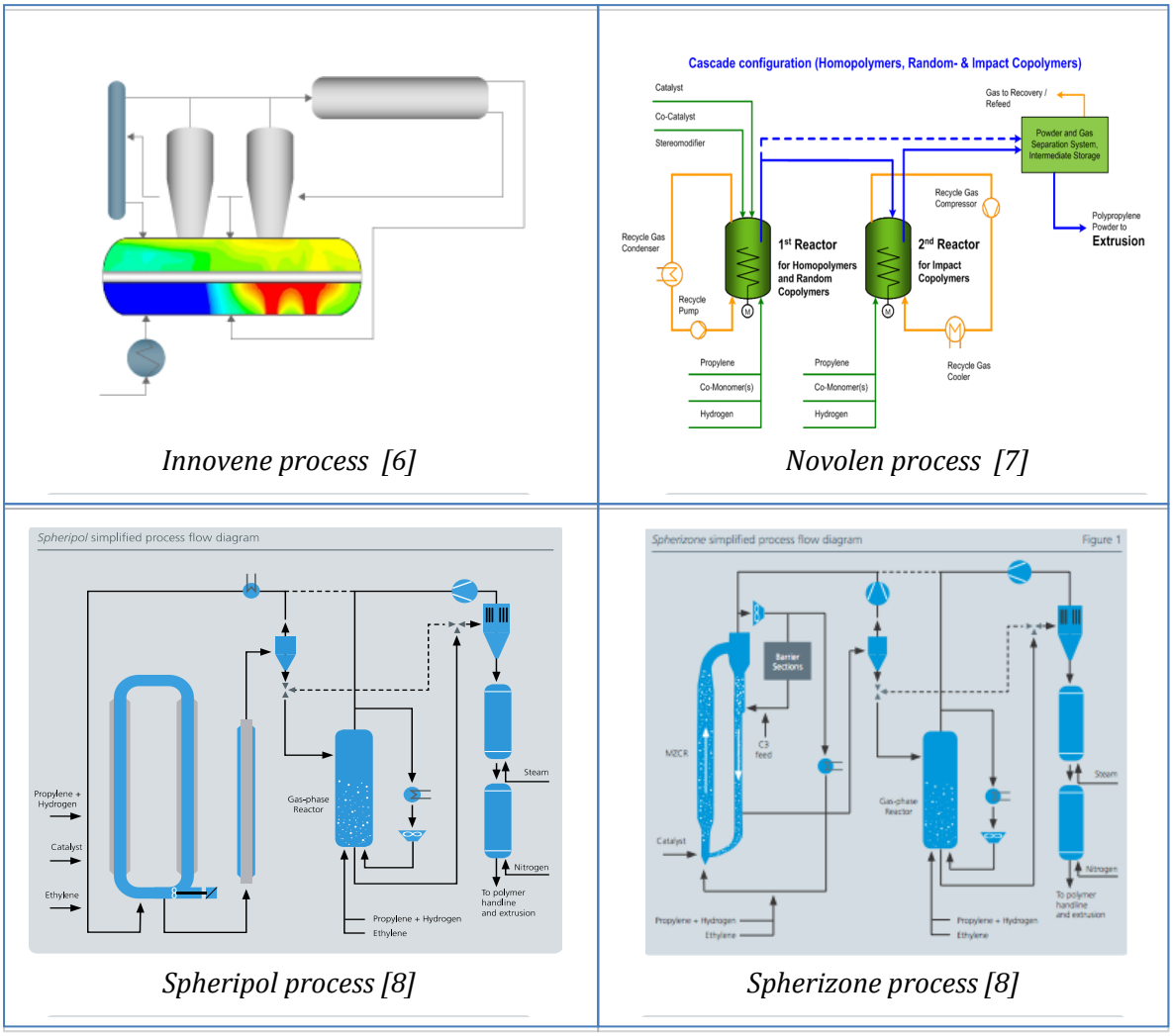

Innovene process [6]

Novolen process [7]

Spheripol process [8]

Spherizone process [8]

Figure 2.3 *Different commercial propylene polymerization processes [6-8].*

Regardless of the technology used, a single reactor is the minimum requirement for homopolymer- and random copolymer production, with the addition of a second reactor only serving to increase polymerization residence time and therefore yield. However, for the production of heterophasic ethylene–propylene copolymers a minimum of two reactors are required. This also has to be in a specific in-series configuration as the homopolymer produced in the first reactor is transferred to the second reactor where copolymerization on the existing polymer and therefore a covalent linkage between homopolymer and copolymer occurs, which is the core principle behind the advanced properties of these in-reactor alloys.

Hydrogen is introduced as a chain termination agent, thereby controlling the average polymer molecular weight, which affects the melt flow rate typically measured and controlled in

industry. In gas-phase technologies propylene monomer is added in both gas and liquid form and the evaporation of liquid propylene is used to control the exothermic polymerization reaction. This cooling mechanism is intimately dependant on the condensing capacity and the reactor gas composition. Therefore at higher ethylene and hydrogen reactor compositions, cooling capacity is limited as both ethylene and hydrogen are incondensable at operational polymerization temperatures and pressures.

For heterophasic copolymer production, the percentage copolymer in the end product is reflected by the production rate in the second reactor relative to the combined production rates of both reactors. In order to achieve a certain copolymer composition, an activity control agent is used in the second reactor to reduce the catalyst activity towards ethylene. The ethylene content of the copolymer is controlled by the relative ratio of ethylene to propylene in the second reactor.

2.2.3 Ziegler-Natta catalysis

Today, almost 97% of all polypropylene produced in industry, is made with Ziegler-Natta catalysts [1]. Ziegler-Natta catalysts are supported heterogeneous transition metal catalysts. The support material can be silica or magnesium chloride and has an important function as it is responsible for the distribution and accessibility of the active sites. The support also determines the morphology of the catalyst and eventually that of the polymer through the morphology replication effect [9]. The active sites are Ti^{2+} and Ti^{3+} cations and these are created by interaction of $TiCl_3$ or $TiCl_4$ through the cocoatalyst with the $MgCl_2$ support. The catalyst also contains an internal donor or stereomodifier which coordinates to the active site by donation of a lone pair of electrons. This creates a specific three dimensional site which enables only one mode of monomer incorporation, resulting in isotactic polypropylene (where all methyl pendant groups are oriented in the same direction). Another crucial element of the catalyst system is the use of an aluminium alkyl co-catalyst which activates the pre-catalyst and can also scavenge catalyst poisons to maintain high activity. With fourth generation ZN catalysts the internal donor may be extracted by the aluminium alkyl during polymerization and for this reason an external donor is added to maintain stereoregularity.

A schematic representation of a typical polymerization process for propylene is shown in Fig. 2.4. Here the aluminium alkyl molecule (encircled in red) is bound to the Ti centre of the active site, creating a metal-carbon bond where the polymerization takes place. In this species the Ti centre has an empty orbital that can overlap with the frontier orbital of the double bond of the

propylene monomer. After coordination of a propylene, a chain migration step occurs where the monomer is inserted in the titanium-carbon bond of the existing alkyl chain. Consecutive repetition of this process results in the growth of the polymer chain.

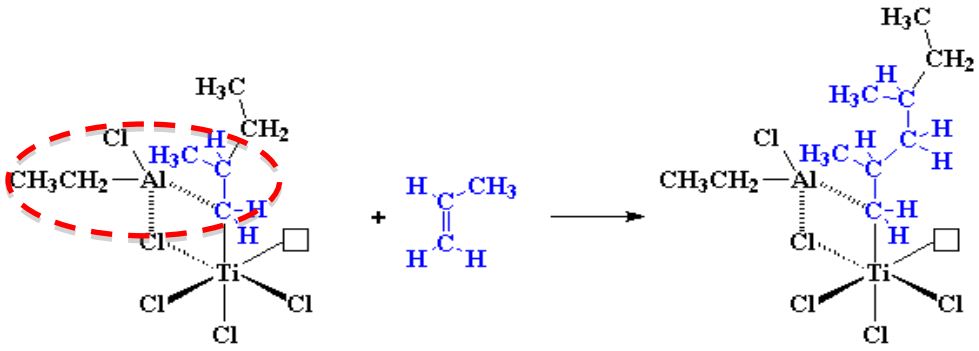

Figure 2.4 *A proposed reaction for propylene polymerization using a Ziegler-Natta catalyst [10].*

For ethylene and propylene copolymerization as it occurs in the second in-series reactor, the existing homopolymer chains produced in the first reactor may be very long and one can imagine some diffusion limitations for the ethylene and propylene monomers to reach the active sites at this stage. In this case, the original catalyst support morphology may have an influence on polymerization kinetics as it will be ultimately responsible for a network of pores leading to the active sites. It should also be noted that the proposed mechanism contains a very simplified version of the active site and in fact a feature of Ziegler-Natta catalysts is that many different types of active sites exist with different modes of stereoregulation and different relative activities towards propylene and ethylene [11]. The result of this is that a complex mixture of polymer chains with wide molecular weight- and chemical composition distributions are obtained during polymerization.

2.3 Morphological development of heterophasic copolymers

2.3.1 Introduction

Despite the many studies that have been conducted on various aspects of HEPC morphology, microstructure, chemical composition etc., [12-25] it is still unclear how the EPR phase evolves in the second reactor and how it interacts with the existing isotactic PP matrix produced in the first reactor to influence the overall particle morphology and product properties. Many of these studies have focused on characterization of the final polymer after melting and crystallization [12-19], which provides different information to what is obtained when considering the

morphology of the nascent polymer obtained directly from the reactors. While the morphological comparison of final moulded products relates more directly to physical properties, the morphological development of nascent polymer properties is a direct consequence of the polymerization conditions and provides information on what can be controlled during the process of polymerization to ultimately obtain the required polymer properties. A few studies aimed at understanding the development of nascent polymer morphology have been documented [20-25]. From these, various models (some contradicting) for the evolution of the copolymer phase have been proposed. The models with the most relevance to this particular study are described in the sections to follow:

2.3.2 The double grain model

The work of Kakugo *et al*. in 1989 is one of the first studies of this type focused on the development of nascent polypropylene morphology [9]. Using two-step staining techniques for TEM, which was novel at the time, they found that the globules (approximately 1 μm in diameter) observed previously by SEM were in fact secondary particles and that these consisted of even smaller primary particles (0.2-0.35 μm in diameter) each containing only one or a few catalyst crystallites, depending on the catalyst activity [9].

They went on further to examine the morphology development of nascent PP and HEPC particles produced with Ziegler-Natta catalysts through SEM and TEM and proposed a model (Fig. 2.5) [23]. This is commonly referred to as the double grain model and is widely accepted by later studies as the first model of its type [20-22]. In this model at the end of the propylene polymerization, each polymer particle consists of a few globules (secondary particles), which in turn consists of a few primary polymer particles, each containing a single catalyst crystallite. It was also proposed (based on TEM observations) that highly active catalyst crystallites are responsible for the growth of polypropylene chains and those crystallites with lower activity are excluded into the boundaries between primary particles. The ethylene-propylene copolymer was not found within the primary particles, but rather at the boundaries between particles; firstly migrating between secondary particles and secondly along the boundary of primary particles, forming a continuous phase (Fig. 2.5).

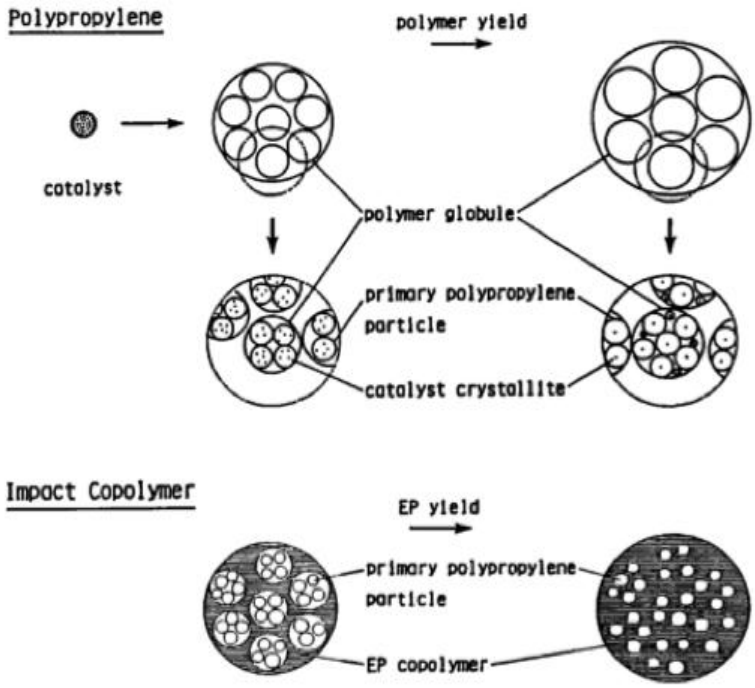

Figure 2.5 *A model for nascent polypropylene and HEPC growth by Kakugo et al. [23].*

Fibrils were also observed possibly due to the cold drawing of the crust of primary PP particles as a large amount of copolymer effused to the boundary. The assumption made by this study, as well as further work done by Debling and Ray (described in Section 2.3.3) was that the EPR is formed on active sites located on catalyst fragments underneath the PP homopolymer. As the EPR grows, the PP layer starts to experience stresses and eventually cracks, thereby releasing the EPR into the cracks, flowing from there into pores and eventually onto the particle surface. It should also be noted that the studies of Kakugo *et al.*, was conducted on lower activity Mg-Ti and δ-$TiCl_3$ catalyst systems, which have evolved greatly in industry since 1989 in terms of support technology, activity and internal- and external donor technology affecting stereoregularity.

2.3.3 The multi-grain model

Debling and Ray investigated HEPC morphology development along with reaction kinetics and selected polymer properties (molecular weight distribution and crystallinity by DSC) [21]. The presence of submicron-sized pores (micropores) and larger macropores as well as the clustering of submicron-sized particles as observed by Kakugo *et al.* was also supported by this study (Fig. 2.6). A new observation from this study was that the micropores seemed to disappear first at low copolymer contents and that at higher copolymer contents, pooling

occurred as the copolymer segregated in certain areas on the surface (Fig. 2.6). They observed that some level of porosity is maintained, regardless of total ethylene content (contents as high as 70% ethylene were evaluated). This maintenance of porosity suggested that monomer diffusion would not be limited even at very high ethylene contents.

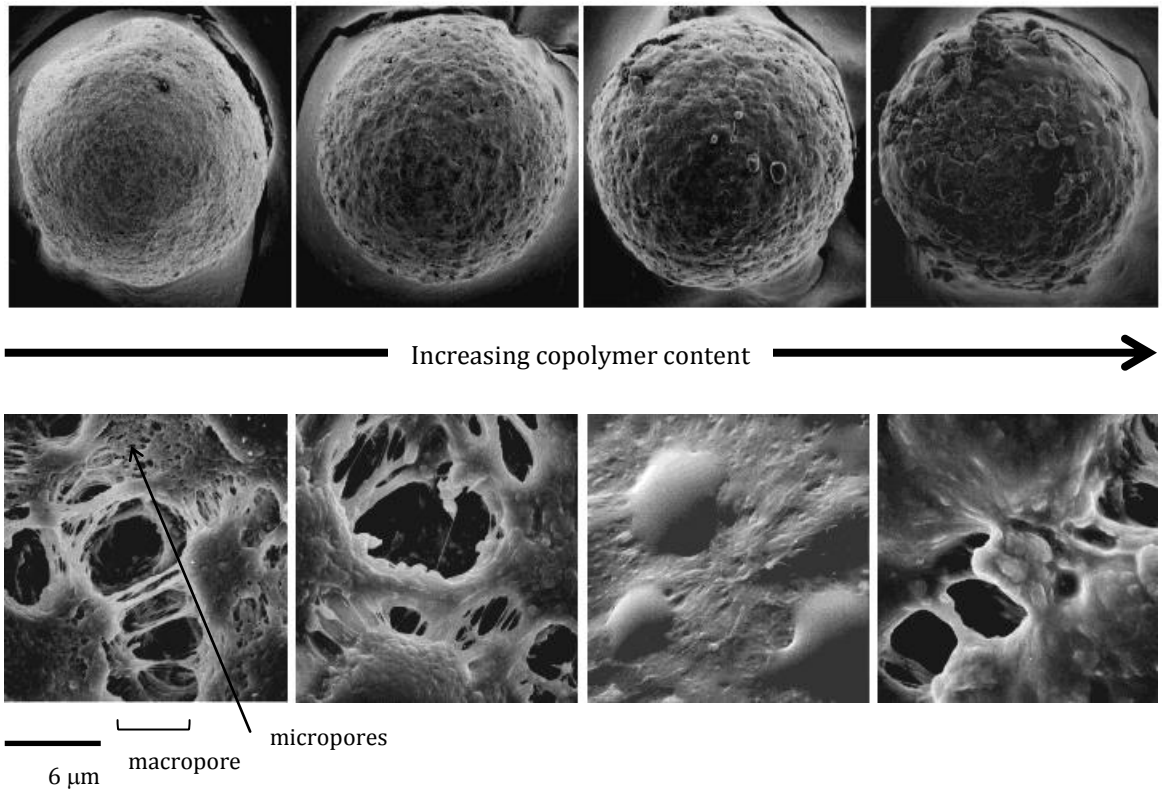

Figure 2.6 *SEM images by Debling and Ray [21] for HEPC whole particles (top row) and magnified surface area (bottom row) for samples with increasing copolymer contents (from left to right: 0%, 15%, 40% and 70% copolymer).*

From the above observations, they proposed a somewhat different order of copolymer development to that described by Kakugo *et al.*, in that the copolymer phase first expands into micropores between microparticles (primary particles containing a catalyst crystallite each) and then into the macropores between agglomerates of the micro particles (Fig. 2.7).

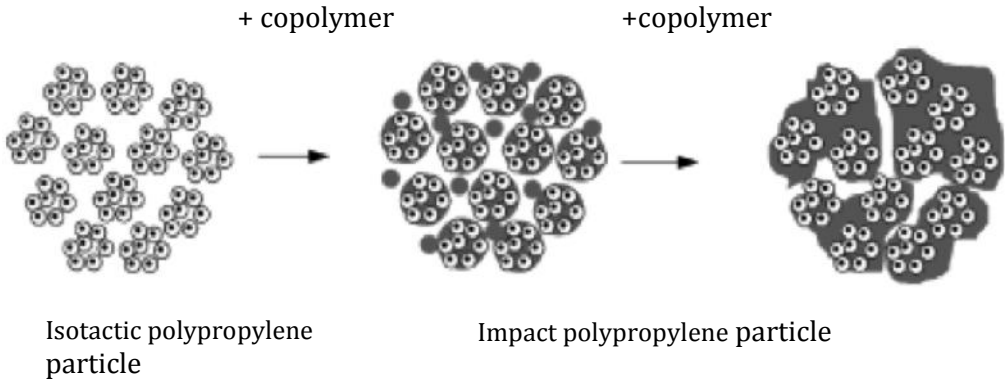

Figure 2.7 *Debling and Ray's proposed model for impact polypropylene growth [21].*

It was also noted that the resultant morphology was highly dependent on the ethylene content in the copolymer phase, where amorphous copolymers tended to form segregated phases and pooled in certain areas and crystalline copolymers tended to behave more like the homopolymer phase. The segregated phase could also become more of a continuous phase, by altering process conditions that promote low copolymer viscosity and high mobility, such as high reaction temperature, low crystallinity and low molecular weight of this phase. Of course these reaction conditions, as well as the extremely high copolymer contents (70%) could be easily obtained with the autoclave system used, but it's uncertain how this could be manipulated in industrial plants without generating an excess of "sticky" material and severe reactor fouling.

2.3.4 The combined dual grain and polymeric flow model

In contrast to the models described above, Cecchin *et al*. 2001 [24] proposed that the EPR does not form below the PP surface, but challenged the multigrain model by combining the features of a dual grain- (similar to that described above) and a polymeric flow system. In this study, autoclave products containing multiphase polypropylene, ethylene-propylene copolymer and polyethylene (PP/EPR/PE) were investigated. The reasoning behind this approach was that since polyethylene is crystalline (with assumed low mobility) and should be formed where it is observed, the position of polyethylene should indicate the polymerization front. Supported by the observation of polyethylene lamellae on the surface of the globules (secondary particles), it was proposed that catalyst fragments are moved to the surface of the subglobules where copolymerization can occur. The resultant model was described as a double-grain model with expanding microcore (Fig. 2.8).

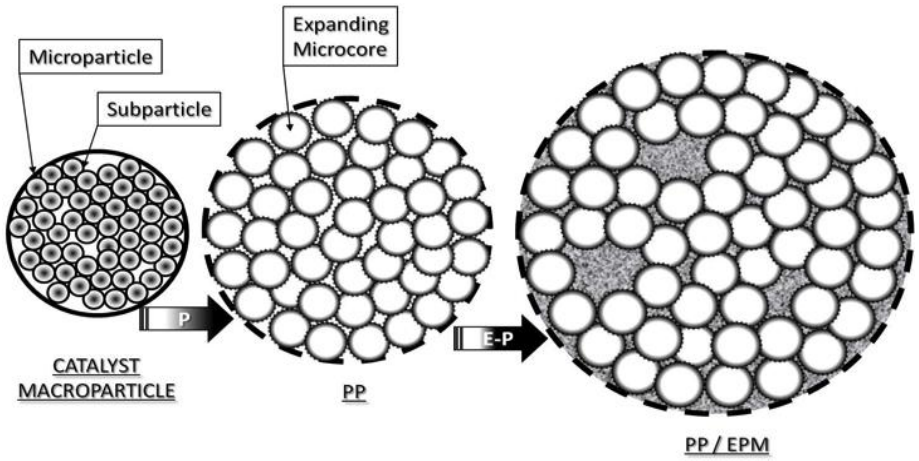

Figure 2.8 *The double grain model with expanding microcore [24].*

The theory of Kakugo *et al.*, concerning the expulsion of catalyst active sites with lower propylene activity but higher ethylene activity to the boundaries of globules where copolymerization takes place, was also challenged in this study. It was shown by copolymerization with 1-butene that polybutene lamellae were found in the same position as the polyethylene and hence the increased activity of certain sites towards certain monomers was questioned. In contrast to this, Cecchin *et al*. however did support the mechanism of migration of catalyst particles to the surface of subglobules as first identified by Kakugo *et al*. [23].

It should also be noted that in order to support their theories, Cecchin *et al*. used polymers consisting of 60 wt% PP,10 wt% EPR and 30 wt% PE or 60 wt% PP, 40 wt% PB. These polymers are significantly different compared to those represented in the current thesis and also those most commonly used in industry (80 wt% PP, 20 wt% EPR). Hence it is uncertain whether the observations in this study that forms the basis for the model development would still be valid for polymers with different compositions.

2.3.5 Mechanism of rubber distribution and the effect of porosity

McKenna *et al*. [20] identified that even though most of the available morphology models seemed to agree on some assembly of primary crystallites from which the polymer grows it was still unclear how the ethylene-propylene rubber leaves the crystallite structures. They investigated this further and found that the distribution of the ethylene-propylene copolymer seemed to depend on overall copolymer content and did not exactly match the pore distribution. Non-uniform pooling of rubber on the surface of particles was also observed.

Furthermore, removal of the rubber by solvent extraction did not significantly change the PP morphology. They concluded that the EPR was mostly found on the surface of subglobules and pre-existing cracks formed after homopolymerization and therefore not inside the particles.

Similar to the results from Debling and Ray it was observed that larger pores remained after polymerization. This observation seems to contradict the notion that the rubber is the only continuous phase as suggested in the previous section. They also proposed a model for different mechanisms of copolymer growth depending on pore size, which accounted for the preferential filling of small pores above larger ones as well as why some level of porosity is maintained, regardless of the amount of rubber in the polymer. The most significant contribution from this paper was the extensive work on porosity measurement using different techniques (mercury intrusion porosimetry and nitrogen adsorption and desorption). The authors concluded that the observed porosity can differ significantly based on the limiting pore size assumed. Therefore the scale of the observed changes limited the study: it focused mainly on macrostructure and assumed certain defined pore sizes.

2.3.6 "Before-after" comparative studies

Building on the information presented in the preceding sections, Urdampiletta *et al*. [22] set out to investigate morphology development of the ethylene-propylene rubber (EPR) phase by comparing particle morphologies before and after copolymerization. They compared the morphology of a PP homopolymer with an HEPC containing 24% EPR and specifically focused on porosity and its effect on monomer diffusion limitations, EPR distribution within the isotactic PP matrix and a more detailed characterization of the type of copolymer produced and its relation to catalyst active centre distribution.

From atomic force microscopy (AFM) scans of the HEPC particle at various radial positions it was concluded that the copolymer was not only present on the surface of subglobules but also finely distributed in the PP matrix as well as in pores between the mesoparticles (agglomerates of globules), resulting in an almost complete pore filling (Fig. 2.9). This was supported by mercury intrusion porosimetry which indicated an almost 50% loss in porosity between the homopolymer and HEPC; however as discussed in Section 2.3.4 certain assumptions with respect to pore size definition could give different observed porosities.

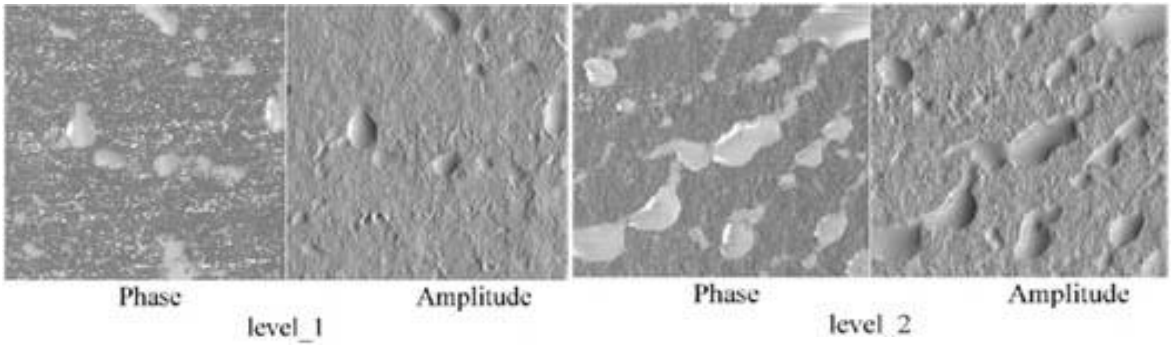

Figure 2.9 *Phase and amplitude images from atomic force microscopy (AFM) of the microtomed HEPC particles at different radial positions [22].*

Based on the above observations, Urdampilleta *et al*. [22] proposed yet another model, with some deviation from those proposed by Debling and Ray (Section 2.3.3), Cecchin (Section 2.3.4) and McKenna (Section 2.3.5). In this model, most of the EPR is finely dispersed in the mesoparticles and only some of it breaks the polypropylene matrix, flowing into pores, thereby reducing the porosity of the whole particle (Fig. 2.10). It was not clear whether the copolymer is produced on the pore surface of particles or in the PP matrix and then flowing out into the pores.

Although commercial samples with copolymer contents representative of products used in industry was used in this study, it was limited by the fact that all information was extrapolated from a "before vs. after" comparison. Hence certain questions around the development and growth of the copolymer phase and its mobility could not be answered in this study.

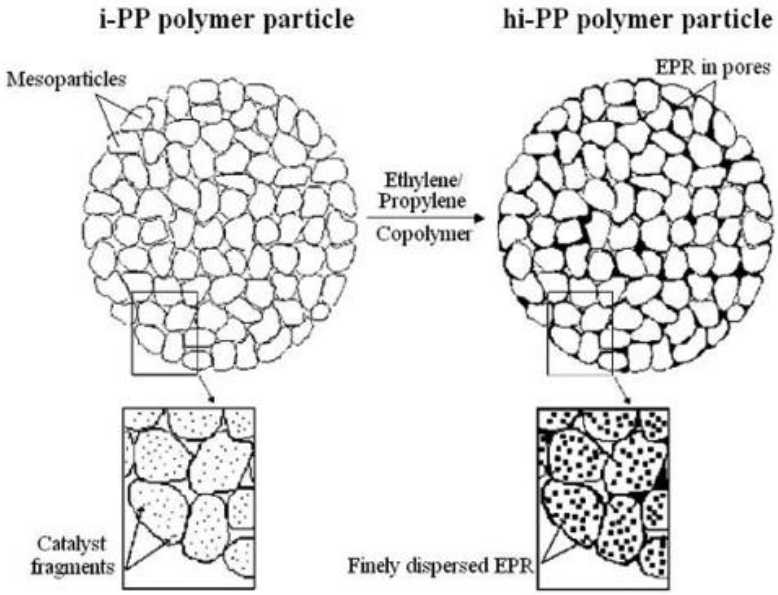

Figure 2.10 *The model proposed by Urdampilleta et al. for HEPC development [22].*

Chen *et al*. [25] used a similar model, with some elaboration on an interfacial layer of polyethylene crystallites or polyethylene-polypropylene (PE-PP) block copolymers between the copolymer rubber and the homopolymer, but further investigated differences in morphology after melt compounding of particles with 14wt% ethylene. They observed that the melt-compounding led to a multiple layer core-shell structure consisting of a rigid polyethylene core, surrounded by an ethylene-propylene rubber (EPR) intermediate layer, followed by an interfacial ethylene-propylene block-copolymer linking the EPR to the isotactic PP matrix.

2.4 Context for this thesis

Apart from the models presented above, which spans a timeframe from 1989 to 2007 and are considered the most relevant to the scope of this thesis, many other morphology studies during and after this period exist, which use similar models as those described above with some minor modifications. Smolná *et al*. reported the most recent development in this area of research in August 2013 [19]. This group published the application of combined AFM and micro-computed tomography (micro-CT) to obtain 3D visualisation of pore distribution (for isotactic PP) and EPR distribution within an HEPC particle (Fig. 2.11). They concluded that ethylene-propylene rubber exists both as a continuous network and as discrete domains in the particle.

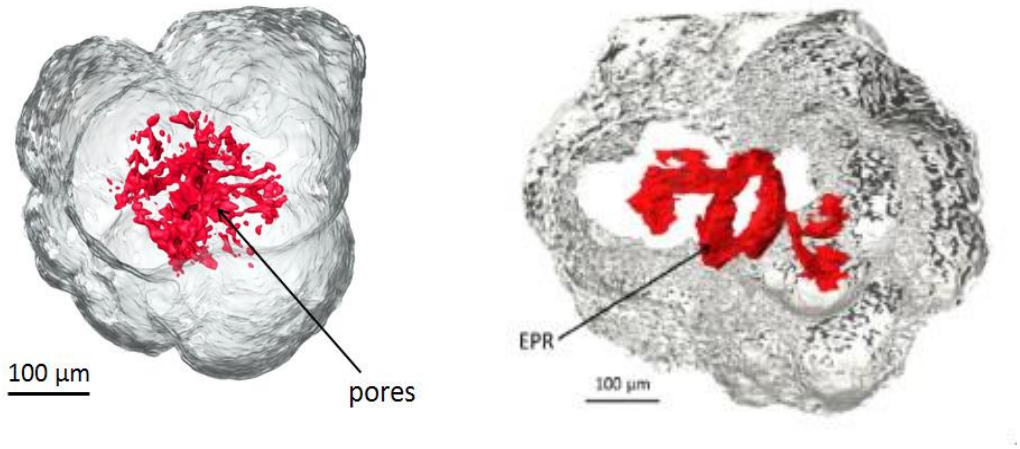

Figure 2.11 *Three-dimensional visualization of the pore distribution and EPR distribution in a homopolymer particle (left) and an impact copolymer (right) as determined by Smolná et al. [19].*

It is clear that each of the above studies provide very useful information on this highly complex system. Considering the different defined scopes and techniques used in these studies, it is not surprising that these studies have arrived at different theories for morphology development, some with areas of overlap and others completely divergent. Like the proverbial blind men describing an elephant the subject of heterophasic copolymers is too complex to be resolved in one unifying theory.

Almost all of the studies described above used polymers obtained by laboratory autoclave polymerizations [20-21, 23-24] using polymerization conditions and copolymer contents quite different from what is found in commercial products. A small number of studies used commercial products [22, 25], but these focused mainly on differences between the homopolymer and the end-product HEPC, leading to a before-after comparison, but no information on the development that occurs inbetween these processes.

This study is therefore unique in the sense that samples were obtained from typical industrial gas-phase processes and not by means of laboratory scale polymerization, thus presenting an opportunity to evaluate the morphology development for commercial polymers with specific applications in industry and relation of these morphological changes to physical performance can be made.

Furthermore this study aims to elucidate the mechanism of ethylene copolymer growth and -development by evaluating samples obtained at various times after initial ethylene introduction in industrial processes, thereby filling in the gaps between the “before” and “after” snapshots. In this way samples ranging from homopolymer to copolymers with low- and intermediate ethylene contents as typically found in commercial processes were obtained in sequence, allowing an almost “real-time” look into the growth of the copolymer phase as it occurs in industry.

Furthermore, in order to provide a clear line of sight from nascent product morphology to final product properties, the observed morphological developments in this study are also placed within the context of changes in crystallinity, development of microstructure and -chemical composition as well as phase interactions and molecular dynamics for the different samples evaluated. The observations from all the different studies mentioned above are also related to the mechanical behaviour of the polymers. This study therefore represents the first of its type due to nature of the samples used in this study, as well as the extension of the morphological study to other polymer properties.

2.5 References

1. http://www.incorep.org
2. http://www.bpf.co.uk/Plastipedia/Plastics_History/Default.aspx
3. Schoene, W. *Polypropylene - Global Markets, Challenges & Opportunities,* 7th Novolen Technology Conference, December 2011
4. Koster, R. *Polypropylene - the success story continues?* August 2012., IHS Marketing report.
5. Tan, H., Li, L., Chen, Z., Song, Y. and Zheng, Q. *Phase morphology and impact toughness of impact polypropylene copolymer.* Polymer. 2005., **46:** p. 3522-3527
6. http://www.ineos.com/en/businesses/INEOS-Technologies/Technologies/
7. http://www.cbi.com/technologies/polypropylene
8. http://www.lyondellbasell.com/technology
9. Kakugo, M., Sadatoshi, H., Sakai, J. and Yokoyama, M. *Growth of polypropylene particles in heterogeneous Ziegler-Natta polymerization.* Macromolecules., 1989. **22:** p.3172-3177
10. http://www.pslc.ws/macrog/ziegler.htm
11. Kissin, Y.V. *Isospecific polymerization of olefins.* Springer-Verlag, New York. 1985
12. Song, S., Feng, J., Wu, P. and Yang Y. *Shear-enhanced crystallization in impact-resistant polypropylene copolymer: Influence of compositional heterogeneity and phase structure*. Macromolecules., 2009. **42:** p.7067-7078
13. Li, R., Zhang, X., Zhao, Y., Hu, X., Zhao, X. and Wang, D. *New polypropylene blends toughened by polypropylene/poly(ethylene-co-propylene) in reactor alloy: Compositional and morphological influence on mechanical properties.* Polymer., 2009. **50:** p.5124-5133
14. Shangguan, Y., Zhang, C., Xie, Y., Chen, R., Jin, L. and Zheng, Q. *Study on degradation and crosslinking of impact polypropylene copolymer by dynamic rheological measurement*. Polymer., 2010. **51:** p. 500-506
15. Chen, R., Shangguan, Y., Zhang, C., Chen, F., Harkin-Jones, E. and Zheng, Q. *Influence of molten-state annealing on the phase structure and crystallization behaviour of high impact polypropylene copolymer.* Polymer., 2011. **52:** p.2956-2963
16. Tochácek, J., Jancár, J., Kalfus, J. and Hermanová, S. *processing stability of polypropylene impact-copolymer during multiple extrusion – Effect of polymerization technology*. Polymer Degradation and Stability., 2011. **96(4):** p.491-498
17. Tian, Y., Song, S., Feng, J. and Yi, J. *Phase morphology evolution upon melt annealing treatment and corresponding mechanical performance of impact resistant polypropylene copolymer*. Materials Chemistry and Physics., 2012. **133:** p.893-900
18. Zhou, X., Feng, J., Yi, Y. and Wang L. *Synergistic improvement of toughness of isotactic polypropylene: The introduction of high density polyethylene and annealing treatment.* Materials and design., 2013. **49:** p.502-510
19. Smolná, K., Gregor, T. and Kosek, J. *Morphological analysis of high-impact polypropylene using X-ray microCT and AFM*. European Polymer Journal., 2013. In press – corrected proof

20. McKenna, T.F., Bouzid, D., Matsunami, S. and Sugano, T. *Evolution of particle morphology during polymerisation of high impact polypropylene.* Polymer Reaction Engineering., 2003. **11**(2): p. 177-197

21. Debling, J.A. and Ray, W.H. *Morphological Development of Impact Polypropylene Produced in Gas-phase with a $TiCl_4/MgCl_2$ Catalyst.* Journal of Applied Polymer Science., 2001. **81:** p. 3085-3106

22. Urdampilleta, I., Gonzalez, A., Iruin, J.J., de la Cal J.C. and Asua, J.M *Morphology of high impact polypropylene particles.* Macromolecules., 2005. **38**: p. 2795-2801

23. Kakugo, M., Sadatoshi, H., Sakai, J. Chapter 27. *Morphology of nascent polypropylene produced by $MgCl_2$ supported Ti catalyst*. Catalytic Olefin Polymerization. Editors: Keii, T., Soga, K. Elsevier. 1990., p.345-354

24. Cecchin, G., Marchetti, E. and Baruzzi, G. *On the Mechanism of Polypropene growth over $MgCl_2/TiCl_4$ Catalyst Systems*. Macromolecular Chemistry and Physics., 2001. **202:** p.1987-1994

25. Chen, Y., Chen, Y., Chen, W. and Yang, D. *Evolution of phase morphology of high impact polypropylene particles upon thermal treatment.* European Polymer Journal., 2007. **43:** p.2999-3008

Chapter 3

Experimental

In this chapter the origin of the samples, method of sampling and sample selection, is provided. Methods for sample preparation as well as analytical methods are described in detail and information on the selected equipment and processing of data is given.

3.1 Production of the samples

The heterophasic copolymer (HEPC) samples used in this study were obtained from different gas-phase processes used for the commercial production of polypropylene. To provide an understanding of the effects of using commercial products as opposed to autocalve polymerization products, an example of a typical gas phase process is given in Fig. 3.1. Most polypropylene gas phase processes consists of two reactors connected in series. In the first reactor, a Ziegler-Natta catalyst is added together with a silane compound for stereocontrol, as well as an aluminium alkyl for catalyst activation and scavenging of poisons.

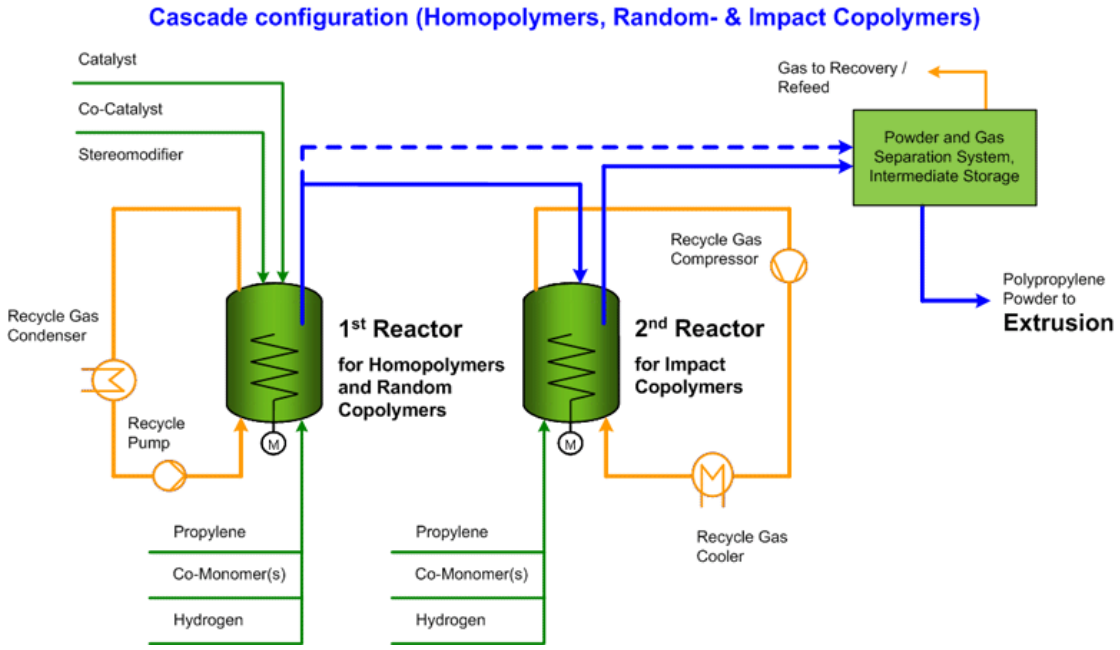

Figure 3.1 *Reactor configuration for the production of heterophasic or impact copolymers with the Novolen® gas-phase process [1].*

During HEPC production, a propylene homopolymer is produced in the first reactor, which is then transferred to the second reactor where ethylene is introduced along with propylene for copolymerization. The ratio between these two monomers in the second reactors will determine the copolymer ethylene distribution and since the samples used in this study were obtained at different points in the transition to copolymer, they will represent different copolymer compositions.

Raw materials used in the process, such as the propylene and ethylene monomers were supplied as polymerization grade material and may be purified further to reduce the composition of poisons down to ppm level.

3.2 Determination of sample composition by Fourier transform infrared spectroscopy (FTIR)

Samples for FTIR spectroscopy were prepared on a *Specac* manual hydraulic press to obtain films of approximately 190 µm thickness. approximately 0.8 g of powder was used per film. FTIR spectra were acquired on a *PerkinElmer Spectrum One* instrument using *Spectrum* software (Copyright 2007 PerkinElmer Inc.). Transmittance scans in were performed in the wavenumber range of 4400-400 cm^{-1}. The scans were then converted into absorbance mode for determination of peak heights. The determination of total ethylene content and ethylene composition of the copolymer phase was done using an in-house method.

3.3 Sample selection

Heterophasic copolymers were selected from two different commercial gas-phase processes during grade transition from propylene homopolymer to impact copolymer. Samples representing homopolymer prior to the transition were taken upon ethylene introduction into the second reactor (denoted T0) followed by sampling at 30 minute intervals thereafter, following the series T30, T60, T90, etc. These samples were analysed by FTIR to obtain an indication of the relative ethylene contents of the range (note that each transition can occur at a different rate depending on the particular plant conditions and therefore the range of samples obtained during each transition may differ in terms of the rate of ethylene introduction and development of ethylene content). From these broad ranges, a few particular samples were selected with distinctly different ethylene contents to best represent the range. In Chapter 4 (Tables 4.1 and 4.2) a summary of the different sample compositions is given. The prefixes “1” and “2” are used to distinguish sample sets for the different plants (technologies). Therefore samples denoted as 1_T0 and 2_T0 will be used to indicate samples selected from the different plants upon ethylene introduction into the second reactor.

3.4 Microscopy analysis of phase morphology development

Whole powder particles from each sample were mounted directly on stubs for microscopic evaluation (SEM and FE-SEM), providing information on the external surfaces. Particles were also imbedded in resin and microtomed to obtain 10 µm sections for the visualization of the development of internal surfaces. For comparative purposes and to ensure that a section near

the centre of a particle was used, particles of similar sizes (approximately 600 µm diameter) were selected. For the preparation of these samples an Agar 100 Resin kit (Agar Scientific, Elektron Technology UK Ltd, UK) was used and the embedding of particles in resin done according to the manual provided with the kit.

FE-SEM was also done on the fracture surfaces of moulded samples. The moulded samples were prepared as described in Section 3.6.1. These samples were prepared by placing moulded test bars in liquid nitrogen for 5 min, whereafter it was clamped and broken, yielding two fracture surfaces per sample. The fracture surfaces were extracted by complete immersion in xylene for 16 h at room temperature to remove the rubbery phase. This was done to evaluate the effect of progressive ethylene incorporation on the size and distribution of the rubber particles, as it would occur in the end application.

For the acquisition of field-emission scanning electron microscopy (FE-SEM) images a Nova NanoSEM 230 instrument (FEI, Oregon, USA) at the University of Cape Town (UCT) was used. For the purposes of this study, two detectors were used: a TLD (through the lens detector) for high resolution images and an ETD (Everhart-Thornley detector), which is a secondary electron detector. Images were captured at 5keV at magnifications of 10 000 x, 20 000 x and 50 000 x in EDX mode. The surfaces of each particle were scanned at various locations and images taken that were considered to be representative for the sample.

3.5 Determination of powder bulk density and particle size distribution

To compare the differences in porosity observed by FE-SEM, the bulk densities of the T0 samples were determined using an aluminium funnel and - measuring cup (Ray-Ran, Warwickshire, UK) and using the standard ASTM D1895-96(2010)e1 method for powder. Determination of the powder particle size distribution for the T0 samples was done with a Mastersizer 2000 instrument (Malvern, Worcestershire, UK) using an existing general-purpose analysis model on the Mastersizer 2000 software routinely used for propylene powder. The following settings were used for determination of particle size distribution: particle refractive index (1.490), dispersant refractive index (1.000), absorption (0.1) and range (0.02 to 2000 µm).

3.6 Mechanical properties

3.6.1 Dynamic mechanical analysis (DMA)

Due to a limited amount of sample, flexural test bars (83 mm in length) were prepared for each of the bulk samples in the series. The bulk powder samples were first stabilized with a general additive package consisting of Irgafos 168® , Irganox 1010® and calcium stearate (BASF, Ludwigshafen, Germany). This was done by dissolving the additives in acetone to a final concentration of 5 $mg.ml^{-1}$ and then by adding 40 ml of this solution to 20 g of each bulk powder sample to ensure a final additive concentration of 1%(w/w) in the polypropylene. The powder/additive solution mixture was left in a fume hood until all the acetone had evaporated, resulting in stabilized powder.

The test bars were produced by injection moulding on a HAAKE™ MiniJet II piston injection moulding system (Thermo Scientific, Thermo Fisher Scientific, USA). The following injection moulding parameters were used: cylinder temperature for melting of the samples (230 °C), mould temperature (70 °C), pressure: (250 bar), hold pressure time (3 s) and total cycle time (30 s). A type 5B flexural test bar mould with dimensions of (90 mm x 10 mm x 2 mm) was used. The type rating is based on the ISO527-1 and ISO527-2 test standards. The first test bar of each new sample was discarded to ensure that no carry-over from the previous sample was present in the test bar.

A Q800 Dynamic Mechanical Analysis (DMA) Instrument (TA Instruments Ltd., Herts, UK) was used to determine changes in the mechanical properties of the injection moulded samples. DMA is used to measure the deformation of a sample as a sinusoidal force is applied over a range of temperatures, yielding data on the storage modulus, which can be related to stiffness properties and damping properties which can be correlated to impact properties [2]. Test bars were clamped horizontally between the centre- and back clamps and a single cantilever clamp setting was selected on the instrument. The storage modulus and tan delta values were obtained from the custom Thermal Advantage™ for Q series™ software for this instrument.

The following temperature profile was used:

- Cooling step from 25 °C to -100 °C at a rate of -10 °C/min.
- Isothermal step at -100 °C for 10 min.
- Heating step from -100 °C to 80 °C at a rate of 3 °C/min.

3.6.2 Measurement of tensile modulus

The tensile modulus is indicative of the stiffness of an elastic material and is expressed in MPa units. In this study the tensile properties were determined on an Instron 3365 (Instron, High Wycombe, UK) instrument on moulded test bars as described in the previous section.

The samples were all processed in the same manner and were conditioned for 48 h before measurement at 23 °C.

Tensile testing was done according to the ISO527-1 and ISO527-2 test standard, where an elongation force is applied to the test specimen of known dimensions and load carried by the specimen measured [3]. The load and deflection data is then translated into a stress-strain curve.

The tensile modulus or Young's modulus is determined by the slope of a secant line between 0.05% and 0.25% strain on the stress-strain plot (Fig. 3.2). The tensile modulus is then calculated according to the formula:

$$E_1 = (\sigma_2 - \sigma_1)/(\varepsilon_2 - \varepsilon_1) \quad (3.1)$$

where: ε_1 is a strain of 0.0005 and σ_1 is the stress at ε_1

ε_2 is a strain of 0.0025 and σ_2 is the stress at ε_2

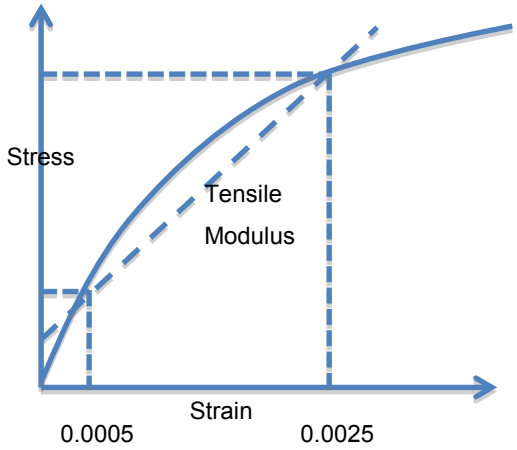

Figure 3.2 *A typical stress-strain plot with an indication on the measurement of the tensile modulus, adapted from [4].*

3.6.3 Measurement of impact strength

Impact strength measurements were obtained using a CEAST® Resil Impactor (Instron, High Wycombe, UK) according to the standard Charpy impact testing procedure outlined in the ISO179-1 standard [4]. During this testing the test specimen is placed in the instrument so that

it is supported near its ends as a horizontal beam. An impact force is applied in a single blow by means of a striker, with the line of impact in the middle of the end supports. The resultant force that is registered upon fracturing of the sample is indicative of the energy absorbed by the material and can be related to the impact resistance. This is normalised for the fracture area and the impact measurement is therefore expressed as a force per a specific surface area (kJ/m^2). Charpy impact testing was done at 23 °C, 0 °C and -20 °C for comparison of the room temperature impacts influenced by the ductile behaviour of the matrix to cold impacts influenced by the rubbery copolymer as impact modifier [5].

3.7 Crystallizability and fractionation of the samples

3.7.1 Solution crystallization analysis by laser light scattering (SCALLS)

The effect of progressively increasing ethylene content on crystallizability for the bulk samples of both sets was firstly evaluated with solution crystallization analysis by laser light scattering (SCALLS). It has been previously shown that good correlations exist between the resulting profiles from the heating step of SCALLS and temperature rising elution fractionation (TREF) [6,7]. For the SCALLS method, 40 mg of powder sample was dissolved in 20 ml of 1,2,4-trichlorobezene (TCB) at 130 °C to achieve a final concentration of 2 $mg.ml^{-1}$. The dissolved polymer was kept in a custom made quartz sample holder of the following dimensions: length = 100 mm, internal diameter 21 mm. This quartz sample holder was then placed in the aluminium heating/cooling block as seen in a schematic representation of the turbidity fractionation equipment (Fig. 3.3). The same experimental equipment was used as described by van Reenen *et al.* [7]. SCALLS runs were done by Dr. M. Brand at the Institute for Polymer Science, University of Stellenbosch.

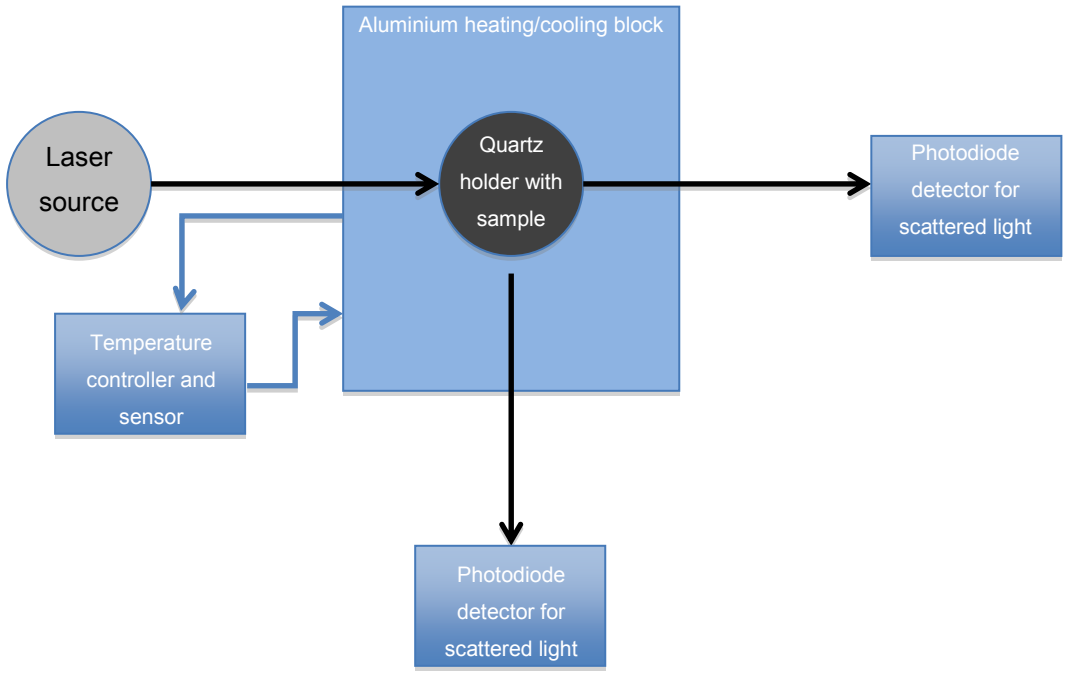

Figure 3.3 *A simplified diagram of the turbidity fractionation equipment adapted from [7].*

The aluminium heating/cooling block has its own temperature control unit for the controlled variation of the sample temperature during the experiment. The following temperature profile was used:

- Isothermal step at 130 °C for 1 h
- Controlled cooling step from 130 °C to 100 °C in 30 min
- Isothermal step at 100 °C for 15 min
- Crystallization step from 100 °C to 30 °C at a cooling rate of 1 °C/min
- Isothermal step at 30 °C for 5 min
- Heating step from 30 °C to 130 °C at a rate of 1.5 °C/min

The above steps were repeated and data generated from the repeat (second run) was used for the trends presented in this study. Even though nascent polymer particles were used, the thermal histories of these particles may still have been different due to a temperature gradient present in the reactors as would be expected for these large vessels – hence the second run was used to remove thermal history, analogous to what is normally done with differential scanning calorimetry (DSC).

3.7.2 Preparative temperature rising elution fractionation (Prep-TREF)

Preparative TREF was subsequently done on all bulk powder samples with specific elution steps at 30 °C, 60 °C, 80 °C, 90 °C, 100 °C, 110 °C, 120 °C, 130 °C and 140 °C to determine differences in crystallizability between samples of a specific technology set. The existing prep-TREF equipment of the Polymer Science department at the University of Stellenbosch was used for fractionation. Each powder sample (approximately 3 g) was completely dissolved in 300 ml of xylene at 130 °C in a glass reactor. The powder samples were stabilized by the addition of 0.02 g of a antioxidant to the xylene used for dissolution.

Crystallization step: Pre-heated sea sand or white quartz (Aldrich, South Africa) was added to the glass reactor after dissolution to completely cover the liquid level. The sand was used as a crystallization support. The glass reactor was then placed in an oil bath that was pre-heated to 130 °C and the crystallization step was initiated whereby the reactor contents were cooled to 24 °C at a rate of -0.1 °C/hr. This method of slow cooling ensured that sufficient time was given for complete crystallization to occur.

Elution step: The crystallized reactor contents were then packed into a stainless steel column (dimensions: length= 1500 mm, internal diameter= 750 mm) containing a layer of glass wool at the bottom to prevent the solvent inlet from plugging with sample and also to distribute the flow of solvent. The sample layer was compressed as evenly as possible to prevent solvent channelling and another layer of glass wool was placed on top of the sample. The packed column was connected to the inlet- and outlet ports in a modified gas chromatography column and fresh xylene feed was pumped into the column for the elution steps. The xylene was then heated in increasing steps to obtain the different fractions at the pre-determined temperatures. Elution steps were typically started 3 °C lower than the target elution temperature to ensure that the sample volume was sufficient within the temperature ramping time. The column contained a temperature probe for accurate determination of the sample temperature upon elution. Approximately 300 ml of each dissolved fraction was obtained from the column. Each of these fractions was transferred to a round-bottom flask and the xylene evaporated in a rotary evaporator. Thereafter, acetone was added to the evaporated sample to precipitate the specific fraction and these samples transferred to pre-weighed containers. The acetone was removed by drying in a vacuum oven. The sample weight was monitored throughout the drying process and the final weights of the samples recorded after no further loss in weight was observed.

3.8 Characterization techniques

3.8.1 Carbon-13 solution nuclear magnetic resonance spectroscopy (^{13}C NMR)

Samples (60 mg when available, slightly lower amounts were used for the TREF fractions) were dissolved in 0.6 ml deuterated tetrachloroethane (d-TCE, Aldrich, South Africa) to a final concentration of 100 mg.ml^{-1}. The samples were prepared by first adding 0.3 ml of solvent, then the powder sample, heating the mixture with a heat gun to melt the polymer and concentrate it in active window of the NMR tube. Thereafter, another 0.3 ml of solvent was added to the tube. The tube was then sealed with teflon tape and placed in an oven at 130 °C for at least an hour to homogenise. The 600 MHz Varian^{Unity} INOVA NMR Spectrometer at the Central Analytical Facility (CAF) in Stellenbosch was used for high resolution solution ^{13}C NMR. Spectra were acquired by Dr. J. Brand and E. Malherbe at the CAF. Solution NMR spectra were acquired using the following settings: a 90 ° flip angle of ≈7.4 μs with inverse gated proton decoupling as well as an acquisition time of 1.8 s and a pulse delay of 15 s. The spectra are considered to be 99% quantitative since only carbon atoms with T_1 relaxation delays of <3 s were taken into account. All spectra used had a signal-to-noise ratio of at least 15 for the Sδδ peak at 30 ppm. Integrals from the spectra were obtained using spectral assignments from literature [8-12]. ^{13}C NMR calculations are given below in Equations 3.1 – 3.9. Monomer contents and dyads shown below were determined according to Ray *et al.* [10] and number average sequence lengths according to Zhang *et al.* [12].

- %P = Sαα + 0.5(Sαγ + Sαδ) (3.1)
- %E = 0.5[Sββ + Sβδ + Sγγ + Sγδ + Sδδ + 0.5(Sαγ + Sαδ)] (3.2)
- mol%P = Eq.3.3/(Eq.3.3 + Eq.3.4) (3.3)
- mol%E = Eq.3.4/(Eq.3.3 + Eq.3.4) (3.4)
- PP dyad = Sαα (3.5)
- EP dyad = Sαγ + Sαδ (3.6)
- EE dyad = 0.5(Sβδ + Sδδ) +0.25(Sγδ) (3.7)
- N_e = [EE + (PE/2)]/(PE/2) (3.8)
- N_p = [PP + (PE/2)]/(PE/2) (3.9)

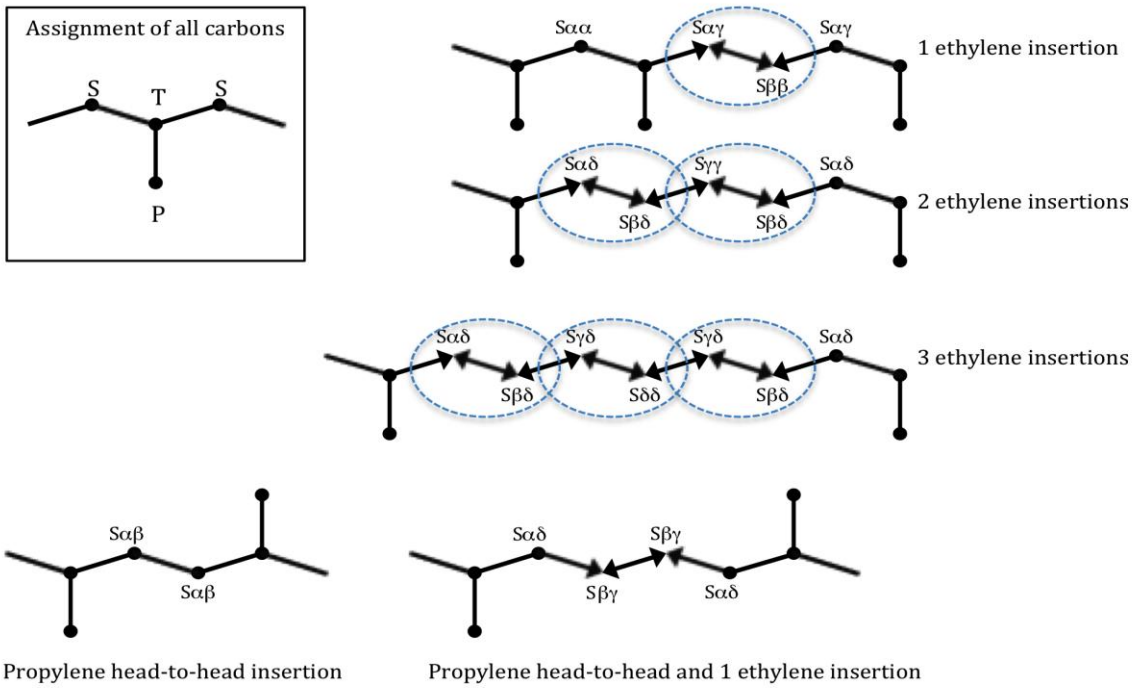

Figure 3.4 *Carbon assignment used for ^{13}C solution NMR adapted from Carman and Wilkes [10] and Ray et al. [11].*

PEP, PEE and EEE triads were determined using calculations obtained from Ray *et al*. [10] and PPP, PPE and EPE triads were determined using calculations from Kakugo *et al*. [11]. Tetrads (PPPP, PPPE, EPPE, PEEP and PEEE) were calculated by integration of the secondary carbon peaks assigned to specific tetrad sequences, normalised for total propylene and ethylene content. The chemical shifts for these assignments were obtained from Ray *et al*. [10]. The EEEE tetrad was calculated using a formula published by Zhang *et al*. [12].

3.8.2 Solid-state NMR

The solid-state NMR spectra were acquired in a Varian VNMRS 500 MHz two-channel spectrometer using 4 mm zirconia rotors and a 4 mm Chemagnetics™ T3 HX MAS probe. The ^{13}C cross-polarization (CP) spectra were recorded at ambient temperature with proton decoupling, a 3 μs 90 ° pulse and a recycle delay of 5 s. Magic-angle-spinning (MAS) was performed at 5 kHz and adamantane was used as an external chemical shift standard where the downfield peak was referenced to 38.3 ppm. The power parameters were optimised for the Hartmann-Hahn match; the radio frequency fields were $\gamma_C B_{1C} = \gamma_H B_{1H} \approx 57$ kHz. The contact time

for cross-polarization was 1 ms. The free induction decay had 442 complex points, Fourier transformed with 20 Hz line broadening.

For the dipolar dephasing or interrupted decoupling experiments (referred to as IDREF in the rest of the paper), the cross polarization conditions were used, with a 7 μs 180 ° pulse and the interrupted decoupling time constant set at 40 μs.

3.8.3 X-Ray diffraction

Room temperature (23 °C) X-ray diffractions patterns were acquired by Dr. V. Smith (Chemistry Department, University of Stellenbosch) using an X'Pert PRO MRD (XL) diffractometer (PANalytical B.V., Almelo, The Netherlands) equipped with a copper anode. A reflection-transmission spinner (PW3064/60) configuration was used and the following settings were applied: A $K\alpha_1$ wavelength of 1.540598 and a $K\alpha_2$ wavelength of 1.544426 ($K\alpha_2$:$K\alpha_1$ ratio of 0.5). A continuous scan was done between the following angles: $5° < 2\theta < 40°$.

3.8.4 High temperature size exclusion chromatography (HT-SEC)

The molecular weights of the polymer samples were determined using a High Temperature Polymer Laboratories PL220 Chromatograph (Polymer Laboratories, Varian Inc., Church Stretton, Shropshire, England) by Dr. G. Harding and P. Mohau (Institute for Polymer Science, University of Stellenbosch). The instrument was used with three PL Gel Olexis and one PL Gel Guard column with a total column set length of 950 mm. A refractive index detector was used and the expected eluent refractive index was set at 1.571. The equipment was calibrated with narrowly distributed polystyrene standards obtained from Polymer Laboratories, Church Stretton, England. The HT-SEC elutions were performed at 150 °C and TCB stabilized with 0.0125% 2,6-ditert-butyl-4-methylphenol (BHT) was used both as eluent and solvent. The eluent flow rate was 1 $ml.min^{-1}$. Samples were prepared for HT-SEC in stabilized TCB to a final concentration of 1 $mg.ml^{-1}$ and allowed to dissolve for 2 h at 160 °C. The sample injection volume was 200 μl.

3.8.5 Size exclusion chromatography coupled to Fourier transform infrared spectroscopy (SEC-FTIR)

This hyphenated technique was used to determine the chemical composition distribution over the range of molecular weights found in a sample. The HT-SEC portion of the analysis was done first (according to the procedure outlined in the preceding section), with the only difference being that different fractions eluting from the column were transferred onto a slow rotating, heated germanium disc using the Series 300 LC transform interface (Lab Connections, Carrboro, USA) which was attached directly to the column outlet. The same temperature setting (150 °C) was used for the chromatograph and LC transform, however the nozzle temperature was slightly higher at 165 °C. Solvent was evaporated by heating the disc, resulting in the deposition of samples on the disc.

FTIR spectra were subsequently obtained directly from different degree points on the germanium disc and were recorded on a Nicolet iS10 Spectrometer (Thermo Electron, Waltham, USA) using a resolution of 4 cm^{-1}. For each degree on the perimeter of the rotating disc, an FTIR spectrum was obtained, thus a large amount of data was generated. For the purpose of simplification, a few FTIR bands of interest were identified and the intensities of these were determined for each sample. The Omnic software package from Thermo Electron was used to process the data, yielding the following point values per degree analysed: Gram Schmidt values (which represent the total concentration over the elution volume), as well as the areas for the peaks at different wavenumbers, using the method previously established by de Goede *et al.* [14]. For determination of propylene content, the area ratio of the band at 1376 cm^{-1} (CH_3 bending band representing propylene) to the band at 1462 cm^{-1} (CH_2 bending band representative of total polymer content). Propylene crystallinity was calculated by the area ratio of the 998 cm^{-1} to 973 cm^{-1} band representative of long and short polypropylene 3_1 helices respectively. The ethylene content was calculated by the area ratio of the 720 cm^{-1} to 1150 cm^{-1} bands previously used to calculate comonomer composition of ethylene-propylene block copolymers. Ethylene crystallinity was determined by the 720 cm^{-1} to 730 cm^{-1} area ratio where these two bands represent long continuous methylene sequences. In polyethylene with high crystallinity, the 730 cm^{-1} band starts to appear, hence it is considered to be a good indicator of polyethylene crystallinity. SEC-FTIR data was acquired by Dr. G. Harding (Institute for Polymer Science, University of Stellenbosch).

3.8.6 Separation by chemical composition using high temperature high performance liquid chromatography (HT-HPLC)

High temperature high performance liquid chromatography (HT-HPLC) was carried out on the TREF fractions, using an HPLC instrument supplied by Polymer Char (Valencia, Spain) using similar settings as described by Cheruthazekatt *et al*. [15]. Samples were dissolved in 1-decanol to a final concentration of 1 $mg.ml^{-1}$. The chromatograph was equipped with an autosampler (injection volume of 20 μl), two separate ovens housing the columns (at 160 °C) and two pumps with vacuum degassers. The specific column used for HPLC mode was a Hypercarb column (Hypercarb, Thermo Scientific, Germany) with dimensions of 100 mm x 4.6 mm (internal diameter). The column packing consisted of porous graphite particles, 5 μm in diameter with pore size of 250 Å and a surface area of 120 m^2/g. The mobile phase first introduced into the column was 1-decanol and thereafter a linear gradient from 0 to 100% TCB in 1-decanol was established in 10 min. The flow rate was constant at 0.5 $ml.min^{-1}$. 100% TCB flow was subsequently maintained for 20 min, whereafter 100% 1-decanol was introduced into the column to restore the initial column conditions. A PL-ELS 1000 evaporative light scattering detector (ELSD) was used (Polymer Laboratories, Church Stretton, England) for monitoring of the sample eluting from the system. HT-HPLC runs were done by P. Mohau and Dr. S. Cheruthazekatt (Institute for Polymer Science, University of Stellenbosch).

3.9 References

1. http://www.cbi.com/technologies/polypropylene
2. *Thermal Analysis Application Brief (TA-130): Polypropylene impact resistance by dynamic mechanical analysis.* TA Instruments (Thermal Analysis & Rheology), http://www.tainst.com
3. http://www.ides.com/property_descriptions/ISO527-1-2.asp
4. *Plastics – Determination of Charpy impact properties. Part 1:Non-instrumented impact test.* International Standard ISO 179:1:2000(E), ISO copyright office, Geneva, Switzerland.
5. van der Wal, A., Mulder, J.J., Odekerk, J. and Gaymans, R.J. *Polypropylene-rubber blends: 1. The effect of the matrix properties on the impact behaviour.* Polymer.,1998. 39(26): p.6781-6787.
6. Shan, C.L.P., deGroot, W.A., Hazlitt, L.G. and Gillespie, D. *A new turbidimetric approach to measuring polyethylene short chain branching distributions.* Polymer., 2005. 46: p.11755-11767
7. van Reenen, A.J., Rohwer, E.G., Walters, P., Lutz, M. and Brand, M. *Development and use of a turbidity analyser for studying the solution crystallization of polyolefins.* Journal of Applied Polymer Science., 2008. 109: p.3238-3243

8. Randall, J.C. *Methylene sequence distributions and number average sequence lengths in ethylene-propylene copolymers.* Macromolecules., 1978. 11: p.33-36

9. Carman, C.J. and Wikes, C.E. *Monomer sequence distribution in ethylene propylene elastomers. I. Measurement by carbon-13 nuclear magnetic resonance spectroscopy.* Rubber Chemistry and Technology., 1971. 44(3): p.781-804

10. Ray, G.J., Johnson., P.E. and Knox, J.R. *Carbon-13 nuclear magnetic resonance determination of monomer composition and sequence distribution in ethylene-propylene copolymers prepared with a stereoregular catalyst system.* Macromolecules., 1977. 10(4): p.773-778

11. Kakugo, M., Naito Y., Mizunuma, K. and Miyatake, T. *^{13}C NMR determination of monomer sequence distribution in ethylene-propylene copolymers prepared with δ-$TiCl_3$-$Al(C_2H_5)_2Cl$.* Macromolecules., 1982. 15: p.1150-1152

12. Zhang, X., Chen, H., Zhou, Z., Huang, B., Wang, Z., Jiang, M. and Huang, B. *DSC and ^{13}C NMR studies of ethylene-propene copolymers prepared by a highly active and stereospecific catalyst.* Macromolecular Chemistry and Physics. 1994. 195: p.1063-1073

13. De Goede, E., Mallon, P. and Pasch, H. Fractionation and analysis of an impact poly(propylene) copolymer by TREF and SEC-FTIR. Macromolecular Materials and Engineering., 2010. 295(4): p. 366-373

14. Cheruthazekatt, S., Pijpers, T.J.F.,Harding, G.W., Mathot, V.B.F. and Pasch, H. *Multidimensional analysis of the complex composition of impact polypropylene copolymers: Combination of TREF, SEC-FTIR-HPer DSC, and High Temperature 2D-LC.* Macromolecules., 2012. 45: p.2025-2034

Chapter 4

Results and Discussion: Bulk morphology and physical property development

The development of bulk particle morphology, physical properties, molecular weight distribution and chemical composition distribution with progressively increasing ethylene contents is investigated for heterophasic copolymer samples from different gas-phase technologies. Based on these observations, mechanisms for the development of the copolymer phase in each set is proposed and placed within the context of previous morphology development studies found in literature.

4.1 Introduction

In Chapter 2 the commercial importance of heterophasic polypropylene–(ethylene-co-propylene) polymers (HEPCs) and the potential for further development and optimization of HEPC product characteristics were discussed. These reactor alloys are commercially valuable due to their high stiffness and impact strength properties obtained by combining the rigidity of highly crystalline isotactic polypropylene (PP) with the toughness of ethylene–propylene rubber (EPR). HEPCs, produced with Ziegler–Natta catalysts are extremely complex due to the heterogeneity of available active sites [1].

A number of studies focussing on various aspects of HEPC morphology, microstructure, chemical composition, etc., have been published and various models for the development of the copolymer phase have been proposed. These models were described in detail in Chapter 2, but the following main findings with relevance to the current chapter will be highlighted:

Kakugo *et al*. (2) published the first report of primary particles containing catalyst crystallites, which were observed by means of TEM. Previously the smallest structures observed were the globules (agglomerates of the primary particles) by SEM. This led to the development of a dual-grain model, distinguishing between primary and secondary particles. The significance of this work is that the position of catalyst crystallites in HEPC production could be monitored for the first time and it was found that during homopolymerization, lower activity crystallites were moved to the globule surfaces or edges where subsequent copolymerization took place (3). Debling and Ray (4) developed Kakugo's dual-grain model further to reflect the growing polymer as a multi-grain structure, proposing the growth of the copolymer on the active sites underneath a homopolymer layer and that the growth of copolymer resulted in rupturing of the homopolymer layer, causing copolymer to flow out into the cracks and pool on some of the surfaces. It is noteworthy that the authors could still observe some porosity in the particles even at significantly higher ethylene contents typically used in industry.

In contrast to the models above, Cecchin *et al*. 2001 [5] proposed that the EPR does not form below the PP surface, but used a model combining features of a dual grain - and a polymeric flow system. Supported by the observation of polyethylene lamellae on the surface of the globules (secondary particles), they proposed that copolymerization occurs on catalyst fragments, which are transported to the surface of the subglobules during polymerization. In contrast to what was proposed by Kakugo et *al*. [2] they didn't find any active centres with

specific activity towards ethylene monomer. McKenna *et al*. (6) also observed this growth of copolymer on the globule surface, but with some further focus on the presence of micro- and macropores and proposed different mechanisms of pore filling depending on pore size.

Urdampiletta *et al*. [7] proposed a pore-filling type of model based on the comparison of the morphology of a homopolymer and an HEPC containing 24% EPR. In this study AFM was used and a fine distribution of copolymer was observed in the matrix, but since only the samples with and without copolymer was compared it wasn't clear where the copolymer originated and whether some migration of this phase took place. Chen *et al*. [8] proposed a similar model, but also focussed on the interfacial layer of polyethylene crystallites or polyethylene–polypropylene (PE–PP) block copolymers between the copolymer rubber and the homopolymer and investigated differences in morphology after melt compounding of particles with 14% ethylene. After melt-compounding they observed a multiple layer core–shell structure with the core consisting of polyethylene, surrounded by an ethylene–propylene rubber (EPR) intermediate layer, followed by an interfacial ethylene–propylene block-copolymer layer and the isotactic PP matrix.

Each of the studies mentioned above provided useful information in the quest to unravel the morphology of these highly complex polymers. However, when considering all the information obtained from these studies, the question of where the copolymer phase starts to develop and how it is distributed relative to the existing homopolymer phase in the nascent polymer particle remains unanswered. The approach of the first four studies was to generate autoclave products with different ethylene and copolymer contents and ranges, which included much higher ethylene contents than those used in industry, but did not focus on the early development of the copolymer phase at lower ethylene contents. Furthermore autoclave polymerization is a batch process and does not account for the large-scale effects (such as monomer diffusion limitations, particle mixing and cooling effects) typically found in the continuous industry processes. The last two studies mentioned above used commercial products but these compared differences between the homopolymer and the final HEPC, hence a before–after comparison, without any information on the development of the copolymer phase.

The work presented in this thesis is therefore the first report that sheds some light on the early development of the ethylene copolymer phase. Samples were obtained from industrial processes and therefore large-scale effects are taken into account in the development of suitable

models for copolymer growth. Furthermore, the selection of samples from a homopolymer to copolymer grade transition allows for the evaluation of samples obtained after various times after initial ethylene introduction in industrial processes. Each consecutive sample therefore builds on the morphology of the previous one and in doing this an almost ''real-time'' look into the growth of the copolymer phase as it occurs in industry is provided.

In this chapter the effect of increasing ethylene incorporation on the morphology development of the copolymer phase relative to the existing homopolymer was evaluated by means of FE-SEM. The development of physical properties and rubber particle size and distribution along with increasing ethylene incorporation will also be discussed and related to the morphological changes. The effects of ethylene incorporation on molecular weight- and chemical composition distribution in the bulk will also be determined.

The characterization mentioned above will be done for two sets of polymers, each obtained from a different gas-phase propylene polymerization technology. These two sets are therefore fundamentally different due to inherent differences in reactor configuration, catalyst- and donor system and polymerization conditions (temperatures, pressures and reactor feeds). The main purpose of the study is not to compare technology differences but rather to develop a model for the morphology and physical property development within a set (technology) and also to identify common behaviours that are driven by ethylene incorporation.

The learning obtained from the ethylene-dependent morphology development and physical property development in the bulk samples will also serve as the background and point of departure for the more detailed work in Chapter 5 focused at understanding crystallinity, microstructural and chemical composition changes in the bulk and fractions due to increasing ethylene incorporation.

4.2 Experimental

The experimental methods used for the analyses in this chapter are described in detail in Chapter 3 and briefly outlined in the section below: Four HEPC samples from each technology set obtained during transition from homopolymer (denoted T0) to final impact copolymer were selected for further characterization. These samples and their specific compositions are

outlined in Table 4.1 (set 1) and Table 4.2 (set 2). For the scope of the thesis, the following prefixes "1" and "2" will be used to denote samples from set 1 and set 2 respectively. Other sample nomenclature such as T60, T90, T120, etc. will indicate the timestamp of the sample as obtained during transition, therefore within a set e.g. 2_T60, 2_T90 and 2_T120, will indicate samples with progressively increasing ethylene contents. A more detailed description of the sample selection is given in Section 3.1 (Chapter 3).

Microscopy and powder particle analysis techniques used for the morphological evaluation are described in Section 3.4. Techniques used for determination of mechanical (DMA) and physical properties are described in Section 3.6. The analytical methods used for molecular weight determination (SEC) and chemical composition distribution over molecular weight distribution (SEC-FTIR) are described in Section 3.8.

4.3 Results and Discussion

4.3.1 Sample composition

To enable the selection of samples with distinctly different ethylene contents and thus representing different stages of ethylene incorporation and copolymer phase development, an initial FTIR analysis of reactor powders was done. In Fig. 4.1 and Fig. 4.2 the FTIR spectra of the 800 to 680 cm^{-1} region is shown for samples from set 1 and set 2 respectively. In both these figures a pronounced increase in the height of the 720cm^{-1} band with increasing ethylene content is observed, relative to the 735 cm^{-1} band which is present at low ethylene contents. The copolymer ethylene composition was determined by the ratio of the absorbances at 735 cm^{-1} and 720 cm^{-1} respectively. It is known that FTIR bands observed at 720 and 730 cm^{-1} are representative of ethylene crystallinity and thus long ethylene sequences. The band at 735 cm^{-1} represents isolated ethylene groups between two propylene groups. Therefore the ratio between the 735 cm^{-1} and 720 cm^{-1} absorbances would indicate a relative random to blocky distribution of ethylene. This value expressed as a percentage is indicative of the ethylene content of the copolymer [9]. The calculated compositions of the selected samples, based on FTIR and later confirmed by ^{13}C NMR are given in Table 4.1 for set 1 and Table 4.2 for set 2. This analysis confirmed that a step-wise increase in the ethylene content of the samples occurred at different intervals during the transition and it was possible from this information to select four samples from each set with significantly different ethylene contents to provide a

representative range for the rest of the study. From Table 4.1 and Table 4.2 it is clear that similar copolymer contents are obtained for the last sample at the end of the transition. There is however technology specific differences, such as the duration of the transition, as well as the total ethylene content and copolymer ethylene content at the end of the transition. This emphasises the importance of focusing on ethylene-dependent differences and phase development within a set but not between different sets to ensure that only the effects of copolymer development are reflected in the observed changes and that the same governing principles will be valid for the results interpretation of a specific set.

Table 4.1 Composition of the set 1 samples obtained during a homopolymer to HEPC transition

Sample	Time (min)[a]	Ethylene content (mol%)[b]	Ethylene content (mol%)[c]	Copolymer ethylene composition (mol%)[c]	Copolymer content (mol%)[c]
1_T0	0	0	0	0	0
1_T150	150	2.2	1.3	23.8	5.4
1_T180	180	5.2	2.8	28.2	10.1
1_T240	240	6.4	4.0	31.3	12.9
1_T300[d]	300	10.8[d]	6.5	36.8	17.6
1_T360	360	11.7	7.1	37.8	19.6

[a] Time of sampling in minutes after introduction of ethylene to the second reactor
[b] Determined by ^{13}C NMR
[c] Determined by FTIR
[d] Sample included in DMA results set, but not used for other analyses. The NMR value for this sample was extrapolated from the NMR/FTIR correlation curve.

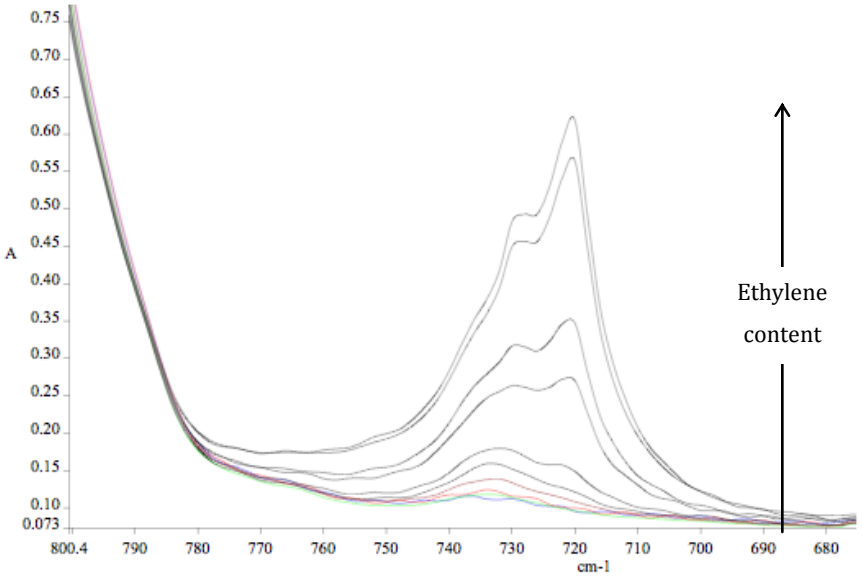

Figure 4.1 *FTIR spectra in the 800 to 680 cm^{-1} region for samples from set 1.*

Table 4.2 Composition of the set 2 samples obtained during a homopolymer to HEPC transition

Sample	Time (min)[a]	Ethylene content (mol%)[b]	Ethylene content (mol%)[c]	Copolymer ethylene composition (mol%)[c]	Copolymer content (mol%)[c]
2_T0	0	0	0	0	0
2_T60	60	5.8	3.6	39.2	9.2
2_T90	90	10.6	6.8	43.1	15.9
2_T120	120	12.6	7.8	44.7	17.5
2_T150	150	13.2	9.3	46.9	19.8

[a] Time of sampling in minutes after introduction of ethylene to the second reactor
[b] Determined by ^{13}C NMR
[c] Determined by FTIR

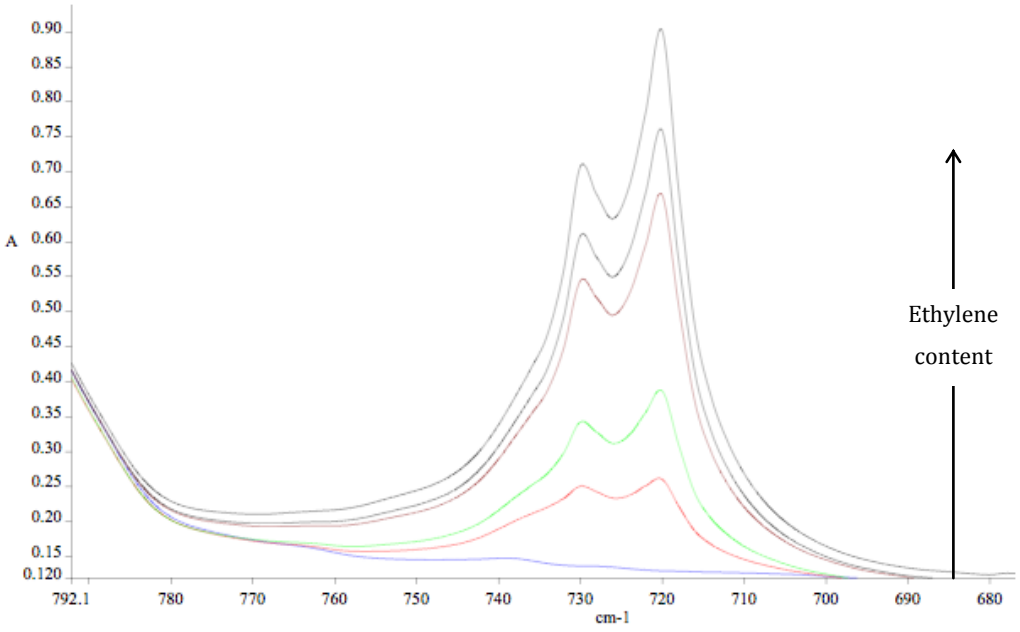

Figure 4.2 *FTIR spectra in the 800 to 680 cm^{-1} region for samples from set 2.*

4.3.2 Development of the copolymer phase by microscopy analysis of reactor powder samples

4.3.2.1 Homopolymer porosity and development of external morphology

It follows a logical order to start the discussion of morphological development with the base polymer or homopolymer prior to copolymerization. As expected, due to set specific differences, the morphology of the homopolymer samples at the start of each set transition was quite different. Scanning electron microscopy (SEM) analysis of these particles from the different sets indicated different porosities for the homopolymer matrix as observed in the T0 samples with

no ethylene present (Fig. 4.3). This was investigated further by bulk density analysis of the T0 powders and it was found that the bulk density was lower for the 2_T0 sample at 463 kg/m^3 compared to the 1_T0 sample with a bulk density of 1_T0 at 482 kg/m^3, supporting the observation of higher porosity for the 2_T0 sample. However, upon further determination of the powder particle size distribution, it was observed that on average the 2_T0 particles were larger, which may also account for the lower bulk density due to particle packing and larger inter-particle spaces (Fig. 4.4).

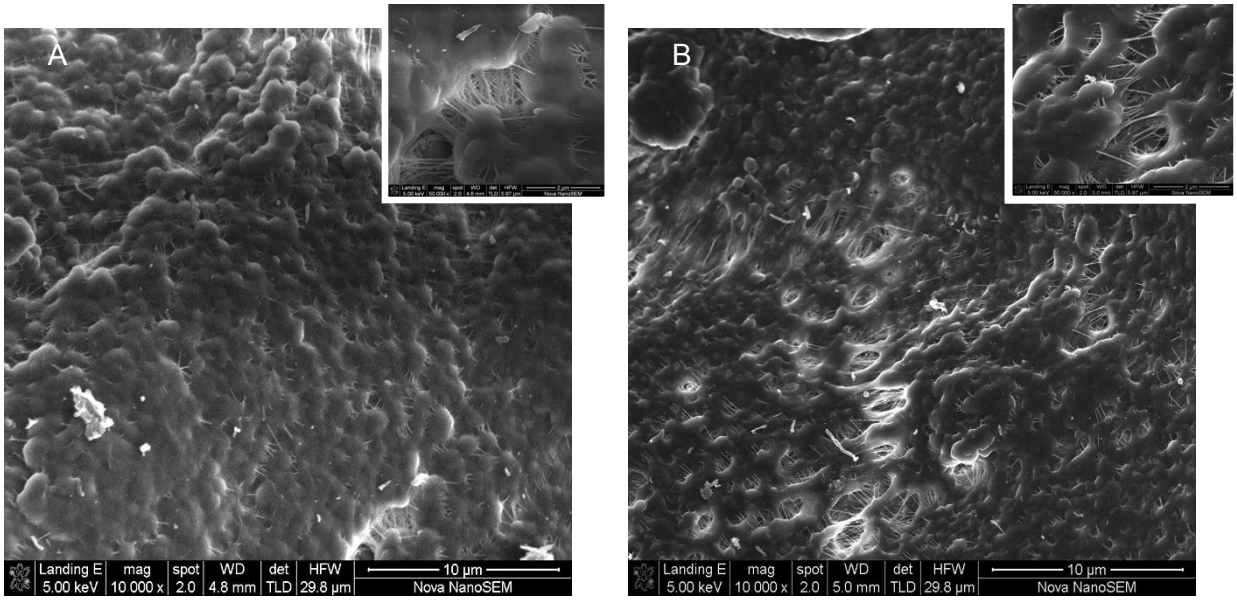

Figure 4.3 *SEM of external surfaces of whole particles from samples (A) 1_T0 and (B) 2_T0 (inlay pictures in top right corner at a greater magnification).*

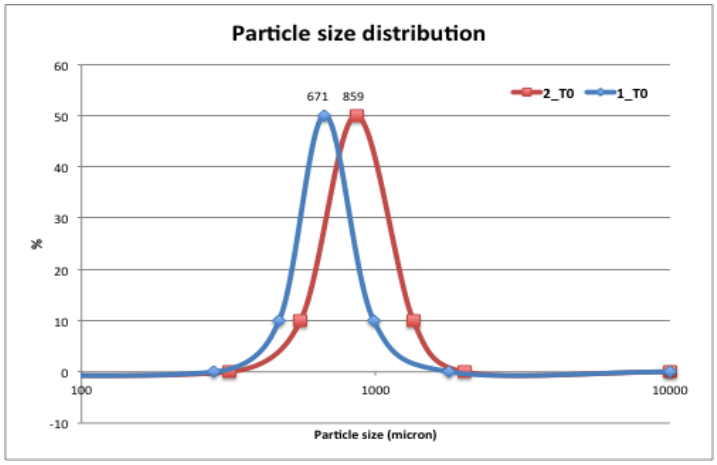

Figure 4.4 *Comparison of particle size distribution of T0 samples from different technologies.*

A preliminary investigation was done using scanning electron microscopy (SEM) to obtain images of whole powder particles (Fig. 4.5) to determine whether any obvious differences due to copolymerization could be observed. SEM as a surface technique can be used to distinguish between crystalline homopolymer, which is organized in globular structures, creating a rough surface and amorphous rubber, that doesn't crystallize, but has some mobility and results in the smoothening of surfaces. From these images it can be seen that for set 1 (Fig. 4.5A to C) there is very little porosity on the external surfaces of the particles, even in the sample with the lower ethylene content (1_T150). A gradual smoothing of the external surface can be seen as the ethylene content increases with the 1_T360 sample completely coated with a copolymer layer.

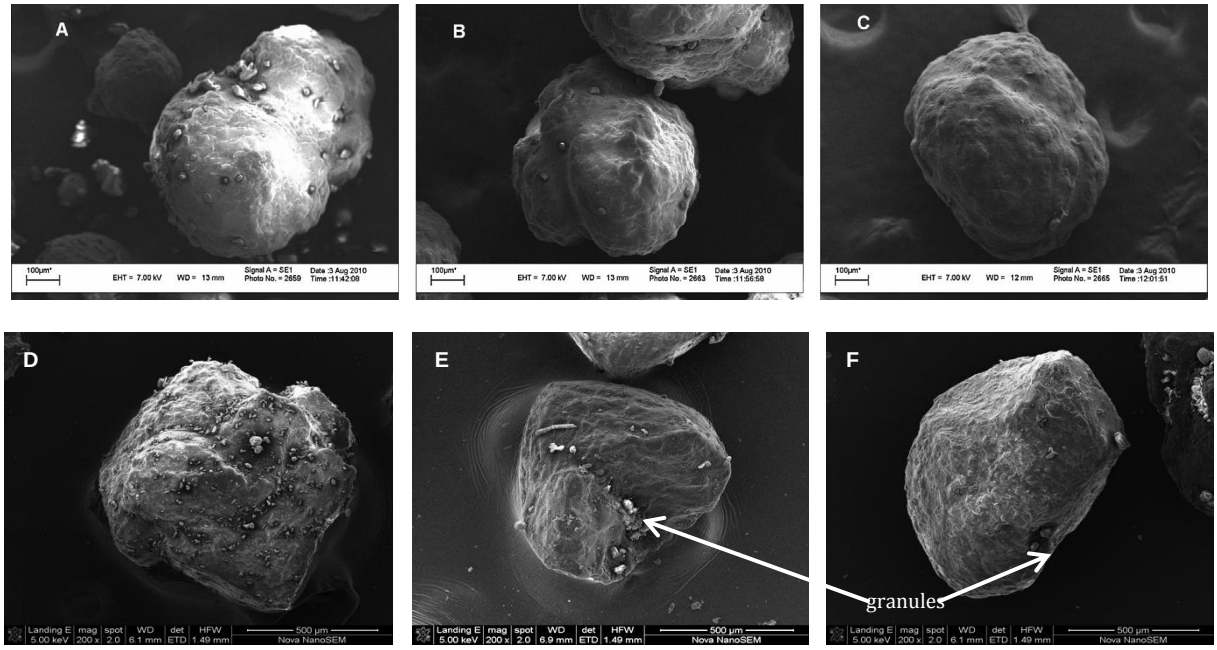

Figure 4.5 *SEM images of whole powder particles with increasing ethylene contents. Top row: (A) 1_T150, (B) 1_T240 and (C) 1_T360 from set 1 and bottom row: (D) 2_T60, (E) 2_T120 and (F) 2_T150 from set 2.*

Similar to the set 1 particles, whole particles of set 2 (Fig. 4.5D to E) have granular external surfaces, possibly due to copolymers present in pores penetrating to the surface. This granular appearance decreases with increasing ethylene content as the pores are increasingly filled and copolymer is deposited on the surface. For this set however, the granular appearance is still present at higher ethylene contents. Note that a few granules can still be seen in the sample with the highest ethylene content (2_T150), indicating that the rubbery copolymer has not completely coated the surface.

Upon more detailed investigation, higher resolution FE-SEM images of the external surface of the same samples were obtained (Fig. 4.6). In these images a typical globular surface consisting of polypropylene is observed, similar to what has been reported in other morphology studies [2-4]. Additionally, thin threads are observed in the lower ethylene content sample (Fig. 4.6A), which seems to be distributed in the spaces between the homopolymer globules as well as stretching over cracks in the surface. These thin fibrils could be due to cold-drawing of homopolymer as observed by Kakugo *et al*. [2]. This finer level of detail is lost in the higher ethylene content sample (Fig. 4.6B), where there is enough copolymer to pool in certain areas on the surface so that the structure of the underlying globules is not visible. Interestingly, there are also some cracks visible that have not been coated with copolymer.

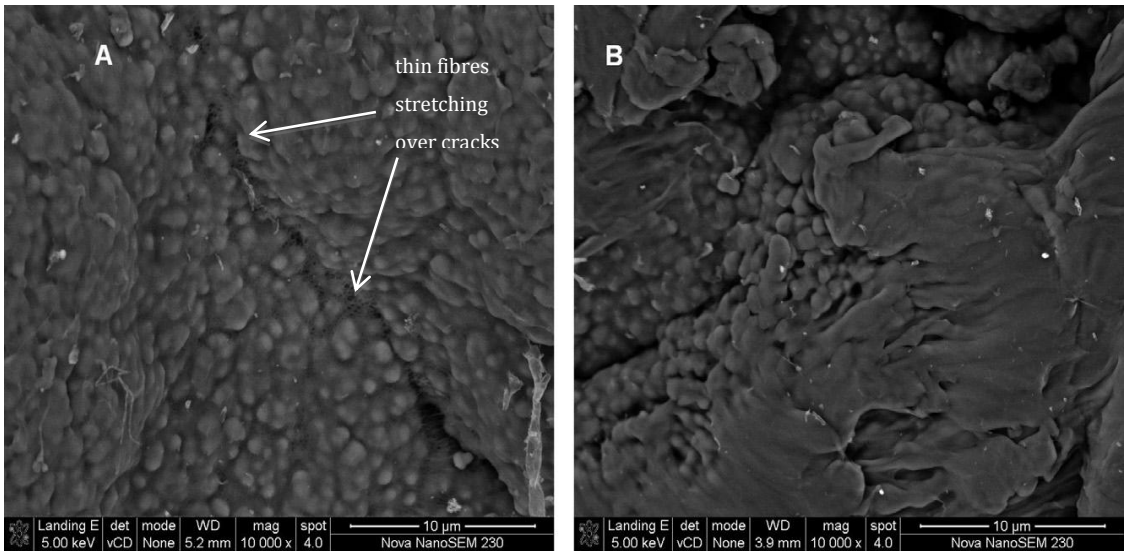

Figure 4.6 *FE-SEM of the external surfaces of sample 1_T150 with 2 mol% ethylene (A) and 1_T240 with 6 mol% ethylene (B).*

The pooling effect and incomplete filling of pores and cracks of the higher ethylene content sample, correspond to similar observations by Debling and Ray [4]; however it must be noted that the polymer surfaces in this study have considerably lower porosity than those studied by Debling and Ray even at lower copolymer content. This may be due to process differences as this study uses industrial samples compared to autoclave powders used by Debling and Ray, or due to catalyst differences. Whatever the case may be, it is clear at least for the system investigated here, that at ethylene contents as low as 6 mol% there is already a significant amount of copolymer on the external powder particle surface, which could possibly grow from thin copolymer threads present in the small gaps between polypropylene globules and stretching over larger cracks.

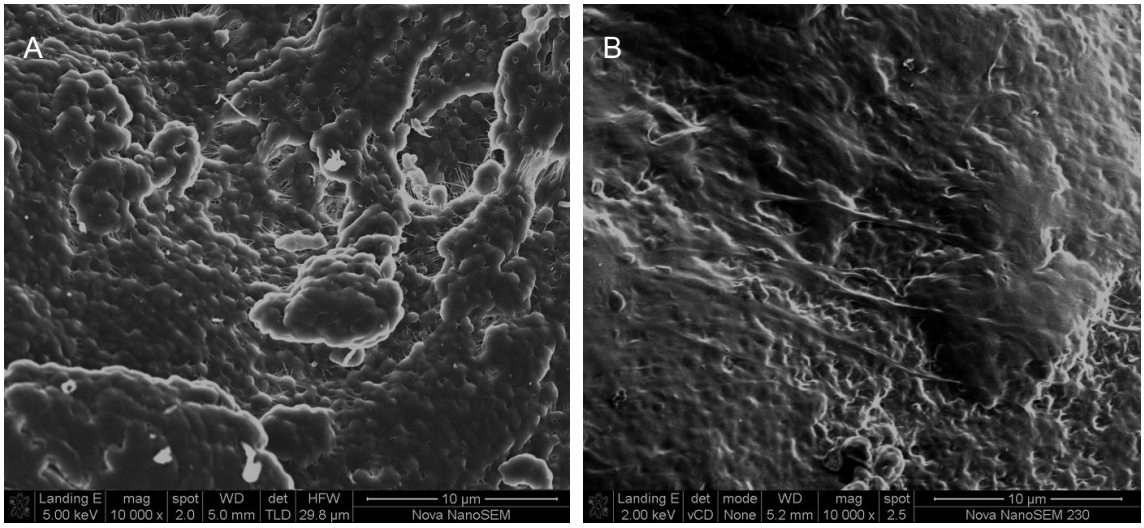

Figure 4.7 *FE-SEM of the external surfaces of (A) 2_T60 with 6 mol% ethylene and (B) 2_T150 with 13 mol% ethylene.*

For the set 2 images in Fig. 4.7, finer globular and rubbery structures are present. The same governing principle of rubber pooling in certain areas applies to samples from this set, however this only occurs at much higher ethylene and rubber contents (refer to Fig. 4.6B with 6 mol% ethylene and Fig. 4.7B with 13 mol% ethylene). Overall, there appears to be a more even copolymer distribution for the set 2 samples as the underlying globular structures are less well defined. Relating these observations to the copolymer compositions, it is also interesting that the 2_T60 sample has slightly lower total copolymer content than the set 1 equivalent (refer to Tables 4.1 and 4.2: 9 mol% compared to the 13 mol% of 1_T240), and also higher ethylene content in the copolymer phase (refer to Tables 4.1 and 4.2: 39 mol% compared to 31 mol% for 1_T240). These preliminary results indicate differences in the way ethylene is distributed for the two different sample sets, highlighting the inherent dependence of morphology on catalyst system. This observation presents an opportunity to study these differences more closely, as will be done by determination of chemical composition development for both sets in the next chapter.

The main objective of this study is however to observe how the copolymer phase develops during grade transitioning as increasing amounts of ethylene are incorporated. Since this development is clearly dependent on the morphology dictated by the catalyst system as well as that of the initial homopolymer before copolymerization occurs, it makes sense that a separate mode of copolymer phase development will be valid for each set. Therefore the development of internal phase morphology will be discussed for each set separately in the following sections. These observations will be compared and contrasted to existing models from previous studies,

where general principles that seem to govern the copolymer phase development will be highlighted.

4.3.2.2 Detailed morphology development of set 1

During an initial scanning process, a few field emission scanning electron microscopy (FE-SEM) images of some of the internal particle surfaces were obtained to determine whether the same progression observed for the external surfaces also occurred internally (Fig. 4.8). These images indicate larger cracks on the internal particle surfaces than those observed externally. A progression in the crack coverage was also observed which correlated with increasing ethylene content. Again, even with the highest ethylene content sample (corresponding to approximately 20 mol% copolymer content), some pores between globules as well as larger cracks were observed, so it is clear that internal porosity is maintained. This corresponds to what has been shown previously by Debling and Ray, i.e. that even with copolymer contents as high as 70 mol% the polymer particles can remain porous internally, leading to a lower bulk density than would be expected if a simple pore filling model were applied [4].

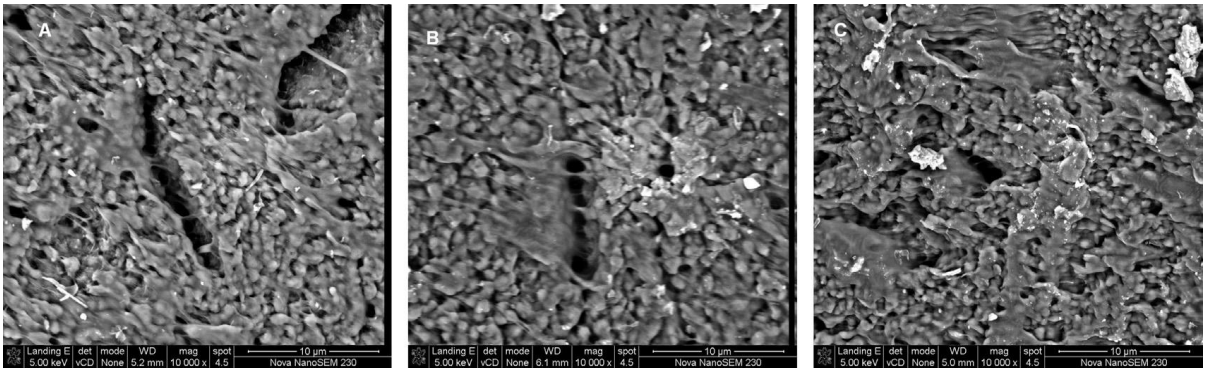

Figure 4.8 *FE-SEM images of the internal surfaces of samples from set 1 with increasing ethylene contents. (A) 1_T150 (2 mol%), (B) 1_T240 (6 mol%) and (C) 1_T360 (12 mol%).*

Following this initial survey, a more detailed FE-SEM study was conducted to determine the internal ethylene distribution along the diameter of microtomed particles. Similar to Fig. 4.8, sections of whole microtomed particles (Fig. 4.9) indicate a non-homogeneous internal surface with some cracks present. Whole particles of similar sizes (approximately 600 μm in diameter) were selected for comparison, as these are the average particle sizes found for these industrial samples (refer to Fig. 4.4). Sections from the outer- and inner surfaces (highlighted by the white squares in Fig. 4.9) were compared to determine whether there were any significant differences in rubber content and radial distribution throughout the particles.

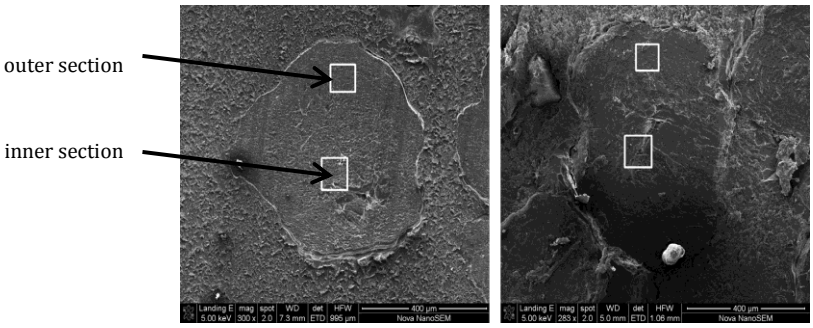

Figure 4.9 *Examples of FE-SEM images from microtomed sections of whole particles, indicating the areas selected for comparison of inner and outer regions. (A) 1_T180, (B) 1_T360.*

When comparing the development of overall morphology in Fig. 4.10 to Fig. 4.12 for set 1, a general progression in surface smoothening can be seen as the total ethylene content increases from 2 mol% to 12 mol% – to such an extent that the globular structures which are still observed in the 6 mol% ethylene samples are completely covered in the 12 mol% ethylene samples, resulting in a smoother surface area. This has resulted in a significantly reduced resolution obtained with SEM (since with SEM only the surface topography is determined). Furthermore, the changes in surface appearance are more drastic, progressing from 6 mol% to 12 mol% sample, than from 2 mol% to 6 mol%.

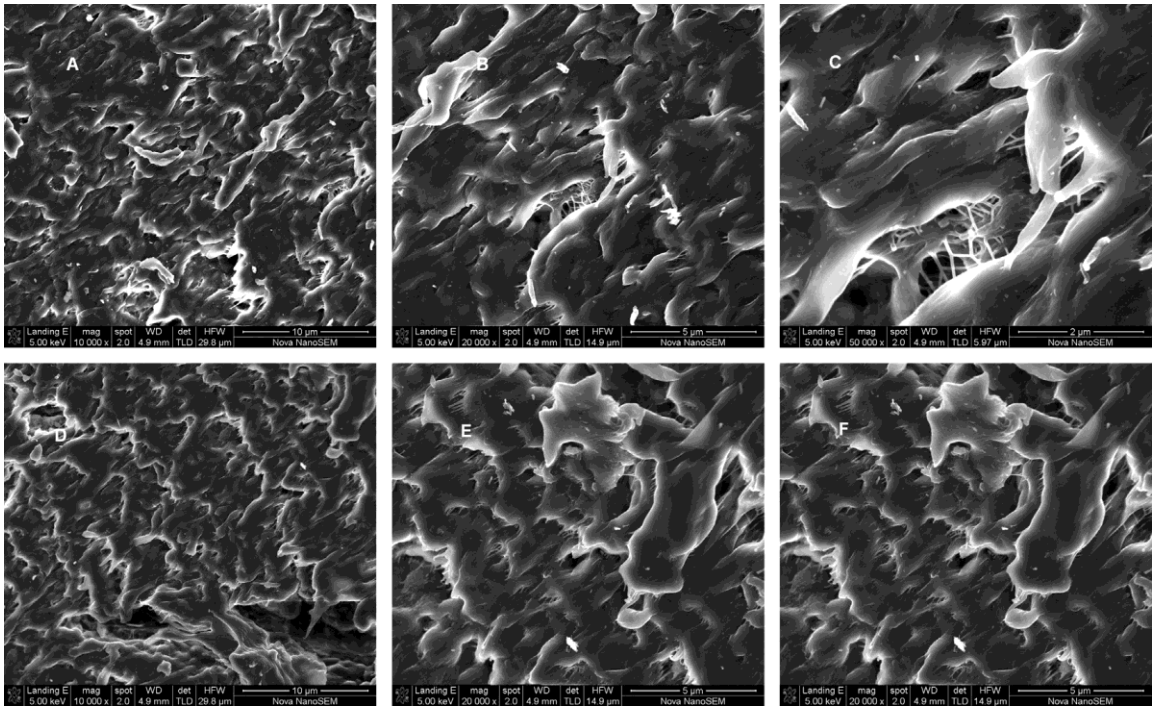

Figure 4.10 *FE-SEM images of microtomed sections of sample 1_T150 (2 mol% ethylene). Images from the inner region are shown in the top row (A-C) and from the outer region in the bottom row (D-F).*

Comparing Fig. 4.10 and Fig. 4.11, the surface areas in these images appear fairly similar, except at the highest magnification (50 000x) where a loss in the resolution of the globular structures for the higher ethylene content sample (Fig. 4.11C and Fig. 4.11F) is seen. Regardless of this detail, it appears that the ethylene copolymer is already present as a thin, uneven layer, covering the globules at low ethylene content and that this layer becomes thicker until it reaches a critical mass at high enough ethylene contents to almost completely coat the underlying globular structure. This growth however also occurs at different rates for different parts of the copolymer phase, thus resulting in the pooling effects observed in these samples in Fig. 4.6 and Fig. 4.8.

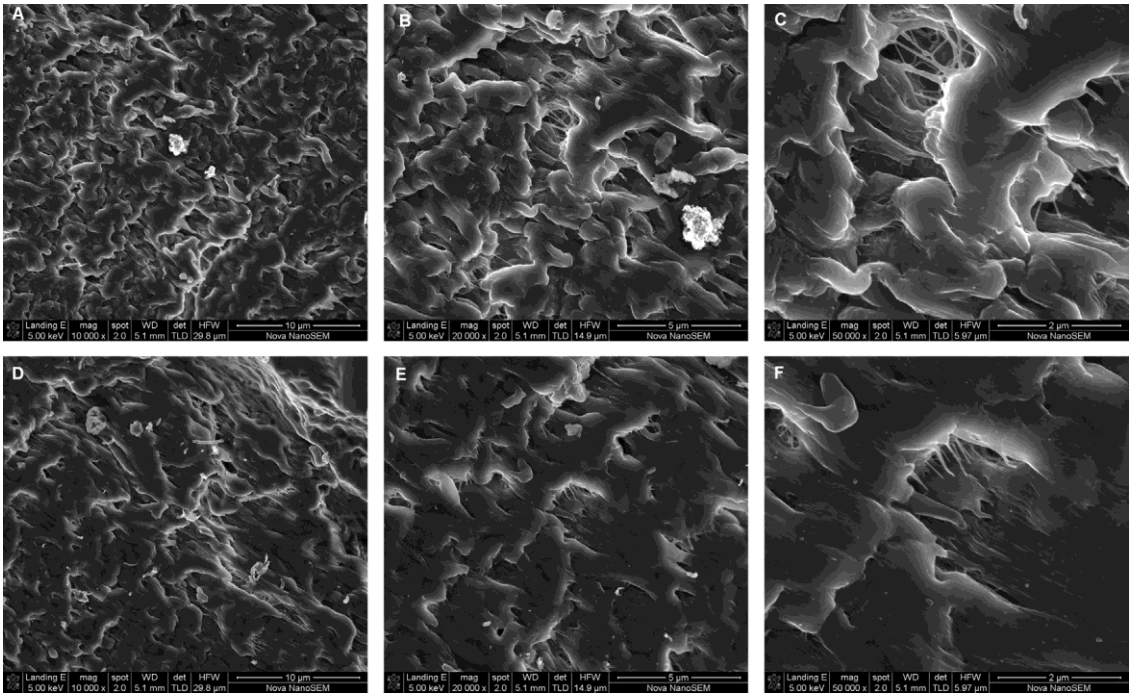

Figure 4.11 *FE-SEM images of microtomed sections of sample 1_T240 (6 mol% ethylene).*

Thin fibrils can be distinguished in all the set 1 samples, which could either be due to rubber or cold-drawn polypropylene fibrils. In the highest ethylene content sample (Fig. 4.12), these structures are however much thicker and seems to contain droplets, possibly due to rubber or copolymer with high mobility, flowing over and coating the existing fibrils.

Comparing the images of the inner surfaces (top rows) and outer surfaces (bottom rows) in Fig. 4.10 to Fig. 4.12 it is also clear that even for the lowest ethylene content sample, the copolymers are radially distributed throughout the whole particle and doesn't seem to be limited to the inner or outer areas. If significant monomer diffusion limitations existed in the particle, one

would expect at least a concentration gradient of copolymer distribution throughout the particle, which is clearly not the case here. This supports the theories of Debling and Ray [4] as well as McKenna *et al.* [6].

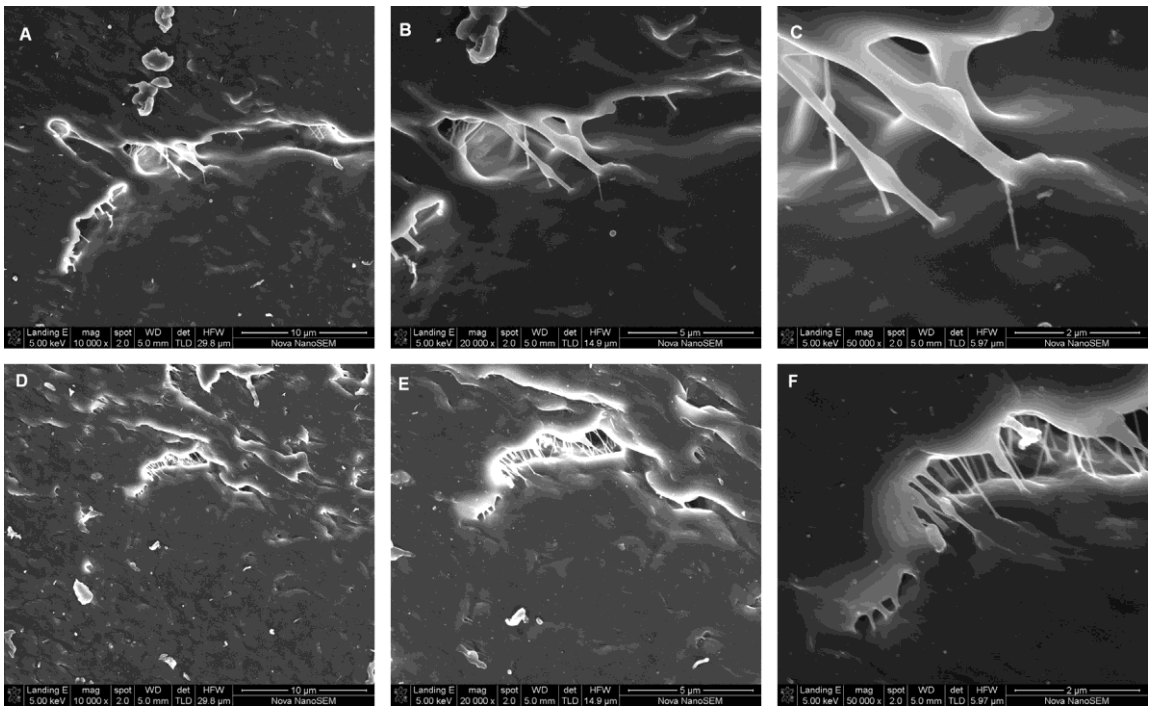

Figure 4.12 *FE-SEM images of microtomed sections of sample 1_T360 (11.7 mol% ethylene).*

Based on the observations from the FE-SEM images for set 1, the theory posed by Kakugo *et al.* [3], that ethylene specific active centres with lower activity than those responsible for polymerization of the original homopolymer are ejected to the surface of the secondary particles can be partially supported as it does appear that the copolymer phase forms and continues to grow on the surface of the globules (noting the progression in the loss of globular features between samples with increasing ethylene contents). The precise role of active centres with different ethylene preferences is however not clear from these observations and could be investigated further by comparing the microstructural development in these samples by means of solution NMR.

4.3.2.3 Detailed morphology development of set 2

For the investigation of the detailed morphology development in set 2, the same methodology was used as for set 1. In Figure 4.13 images of microtomed particles, indicating the areas selected for the outer and inner regions are shown.

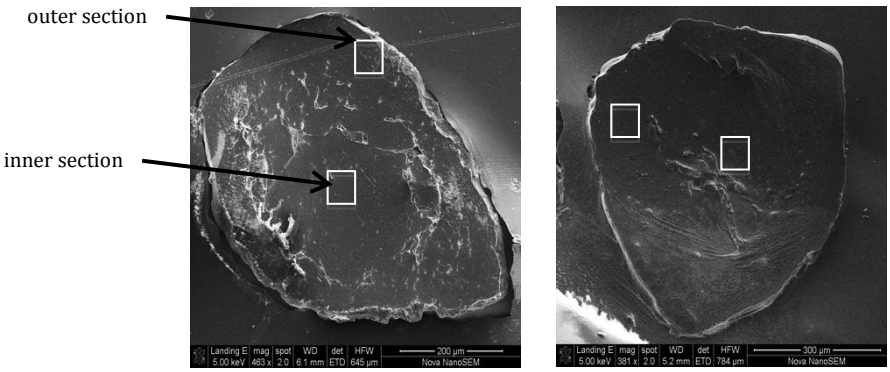

Figure 4.13 *FE-SEM images from microtomed sections of whole particles, indicating the areas selected for comparison of inner and outer regions. (A) 2_T60 and (B) 2_T120.*

Compared to the extensive network of pores observed in the homopolymer sample of this set (as shown in Fig. 4.3B), it is an interesting observation in Figure 4.14 that even for the sample with the lowest ethylene content in the set (6 mol%) a significant reduction in internal porosity has taken place.

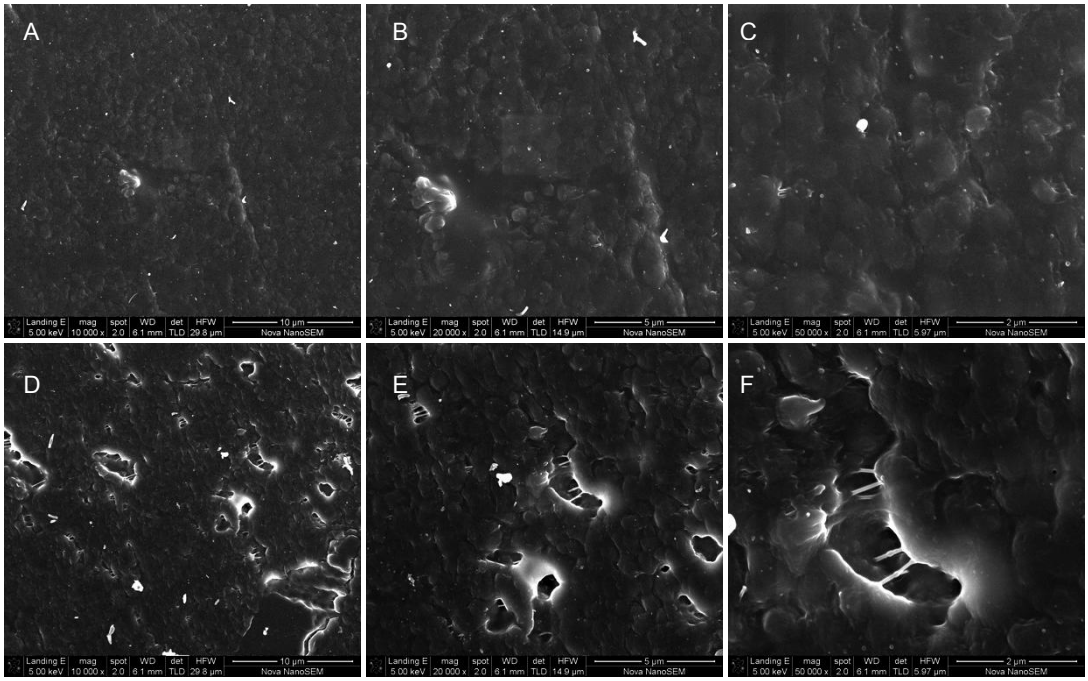

Figure 4.14 *FE-SEM images of microtomed sections of sample 2_T60 (6 mol% ethylene). Inner region: top row (A-C) and outer region: bottom row (D-F).*

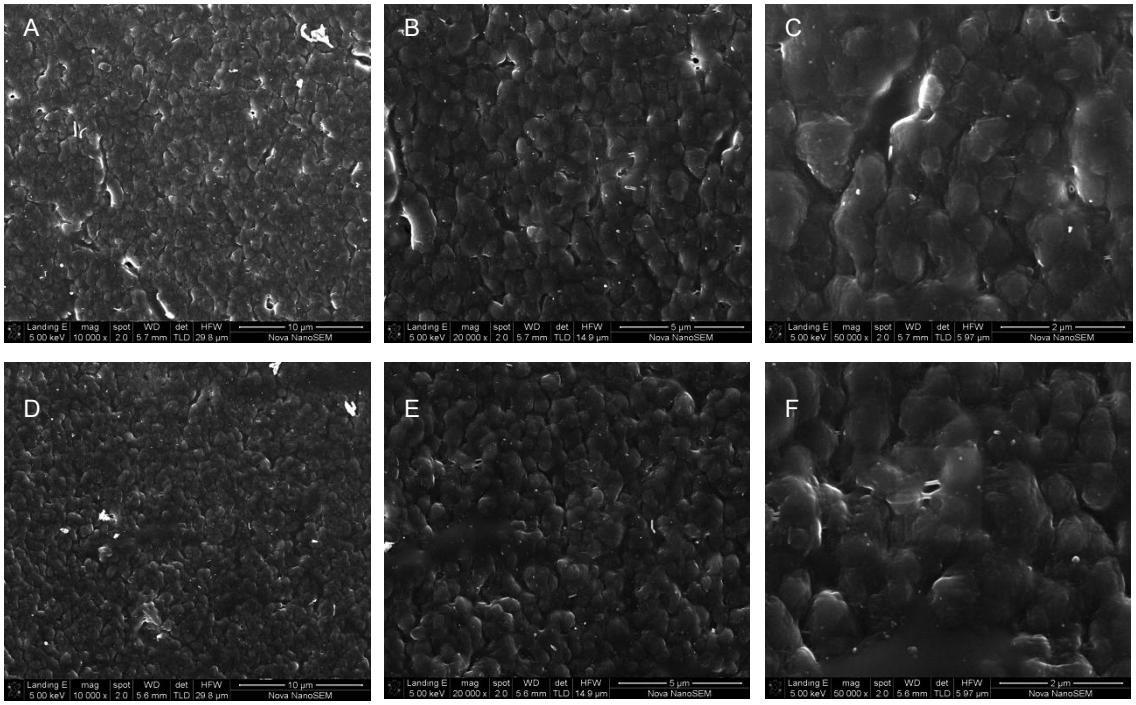

Figure 4.15 *FE-SEM images of microtomed sections of sample 2_T90 (11 mol% ethylene). Inner region: top row (A-C) and outer region: bottom row (D-F).*

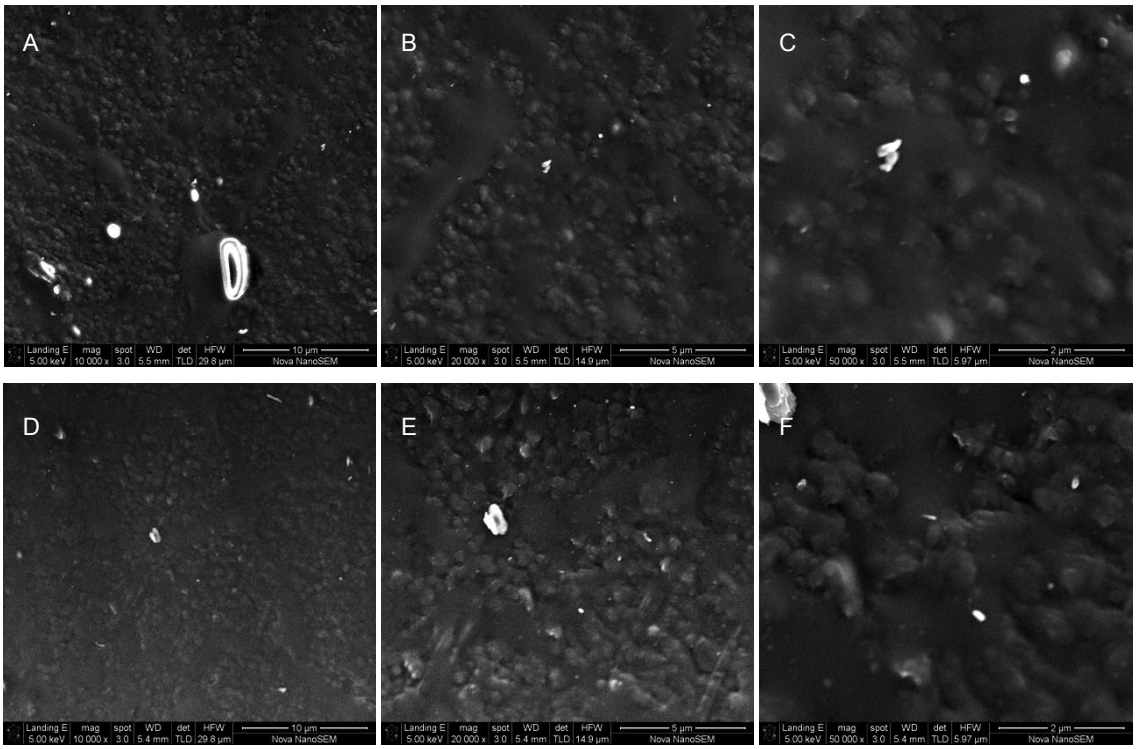

Figure 4.16 *FE-SEM images of microtomed sections of sample 2_T120 (13 mol% ethylene). Inner region: top row (A-C) and outer region: bottom row (D-F).*

The progression of ethylene incorporation for set 2 is shown in the images in Fig. 4.14 to Fig. 4.16. For this set it is also observed that the rubber phase is present throughout the whole diameter of the particle, irrespective of ethylene content. For the lowest ethylene content in this set (Fig. 4.14), the overall porosity seems greater for the outer area (bottom row) compared to the inner area (top row), suggesting that for this set the rubbery copolymer phase appears to be formed more rapidly on the inside of the particle than on the surface. For the rest of the samples in this set, the observed porosity rapidly disappears with increasing ethylene incorporation, to such an extent that there doesn't appear to be significant differences between rubber distribution for the inner and outer regions of the particle. Fibrils are also only observed in the 2_T60 sample (Fig 4.14) with the lowest ethylene content and seem to disappear along with the complete filling of available pores.

The mechanism of copolymer phase growth for set 2 appears to be different from what was discussed previously for set 1. Porosity is significantly reduced on the internal surfaces, even at relatively low ethylene contents and complete pore filling is observed at higher ethylene contents. With increasing ethylene content, some pooling of the copolymer occurs. The copolymer phase however doesn't appear to completely cover the homopolymer globules. Instead a grainy structure, possibly remnants of the homopolymer globules, persist at the highest ethylene contents with smoother "streams" of copolymer which seems to flow between the grains. This distribution of the copolymer indicates that it exists as a separate, discontinuous phase relative to the existing homopolymer structures. Based on the initial significant amount of pores present in the homopolymer of this set, one might also argue that this observation could be a function of the particle surface area, where the copolymer could be preferentially filling macropores between globules, with less pronounced globule surface coating.

4.3.2.4 Summary of morphological developments

Since the samples used in this study was distinctly different from previous morphological investigations, this allowed for the visualization of the early development of copolymer phase as it occurs in industry and also indicated how the growing copolymer is distributed relative to the homopolymer phase by comparing sequential samples. Clear ethylene dependent trends have been identified such as the pooling of copolymer in certain areas if the total ethylene content is high enough. It was concluded that the copolymer phase is indeed distributed radially throughout the polymer without being limited to any specific location or being distributed via a concentration gradient.

The development of the copolymer phase can occur in different ways, either by a gradual covering of the surface of homopolymer globules, resulting in a smooth surface, as observed for set 1, or by forming structures extending between particles, retaining a grainy surface area due to the presence of globules that have not been covered, as observed for set 2. Considering the development of the copolymer phase in each of these sets, it seems that the size the of existing pores in the homopolymer phase either drives the inclusion of the copolymer phase within the pores if they are large enough (as observed for set 2) or excludes the copolymer, causing it to preferentially coat the surface of the globules (as observed for set 1).

There are however still some limitations in that SEM and FE-SEM, being surface techniques, cannot provide any information on macro- and micropores that have been coated by a copolymer layer. For the purpose of this study it has been assumed that the microtomed sections observed should contain a representative image of the porosity distribution throughout the particle. However, future work focussing specifically in porosity changes such as mercury porosimetry or the more recent combination of AFM and X-Ray microCT techniques as described by Smolná *et al*. [10] will shed some light on macro-and microporosity changes with copolymer phase development.

4.3.3 Effect of ethylene incorporation on bulk polymer physical properties

4.3.3.1 Physical properties determined for set 1 samples

Dynamic mechanical analysis (DMA) was used to determine the effect of increasing ethylene incorporation on the mechanical properties of the different polymer samples. In this experimental technique a sinusoidal deformation force is applied to a moulded sample of known dimensions. The amount of deformation is related to the sample stiffness or elastic behaviour and is expressed as the storage modulus, which is an in-phase component (refer to the displacement in Fig 4.17). Another sample response to the applied force is a phase shift and this out-of-phase component is termed the loss modulus. The ratio of the loss modulus to the storage modulus is calculated as the tan delta (tan δ) value and this often referred to as damping, which is a measure of the energy dissipation of a material. The tan δ value can be related to the impact resistance behaviour of a material [11].

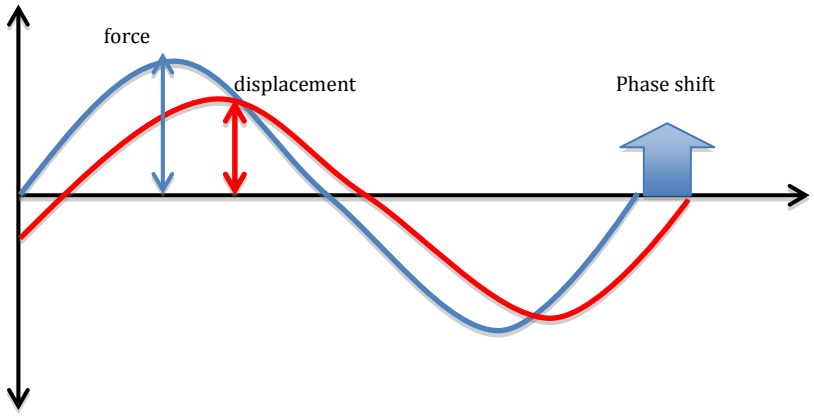

Figure 4.17 *The relationship between the applied DMA force in blue and the measured deformation in red [11].*

By varying the temperature during the measurement, the sample's mechanical properties and phase transitions over a range of different temperatures can be determined. Changes or inflection points in the storage modulus and tan δ curves plotted against temperature indicate phase transitions.

When considering the storage modulus values obtained for set 1 samples (Fig. 4.18), a steady decrease in the storage modulus with increasing ethylene incorporation can be observed, as expected. For this sample range a fifth sample in the same set obtained at 300 minutes after

ethylene introduction (1_T300) was included (Table 4.1). This sample contained approximately 6.5 mol% ethylene based on FTIR measurement. The drop in stiffness from -25 °C to 25 °C (delta storage modulus), displayed as the red trendline in Fig. 4.18, increases with increasing ethylene incorporation and reaches a plateau at sample 1_T300. Sample stiffness is therefore affected to a greater extent with increasing ethylene content, but this is only up to a certain level of ethylene incorporation (approximately 10.8 mol%), whereafter no further decrease in stiffness is observed.

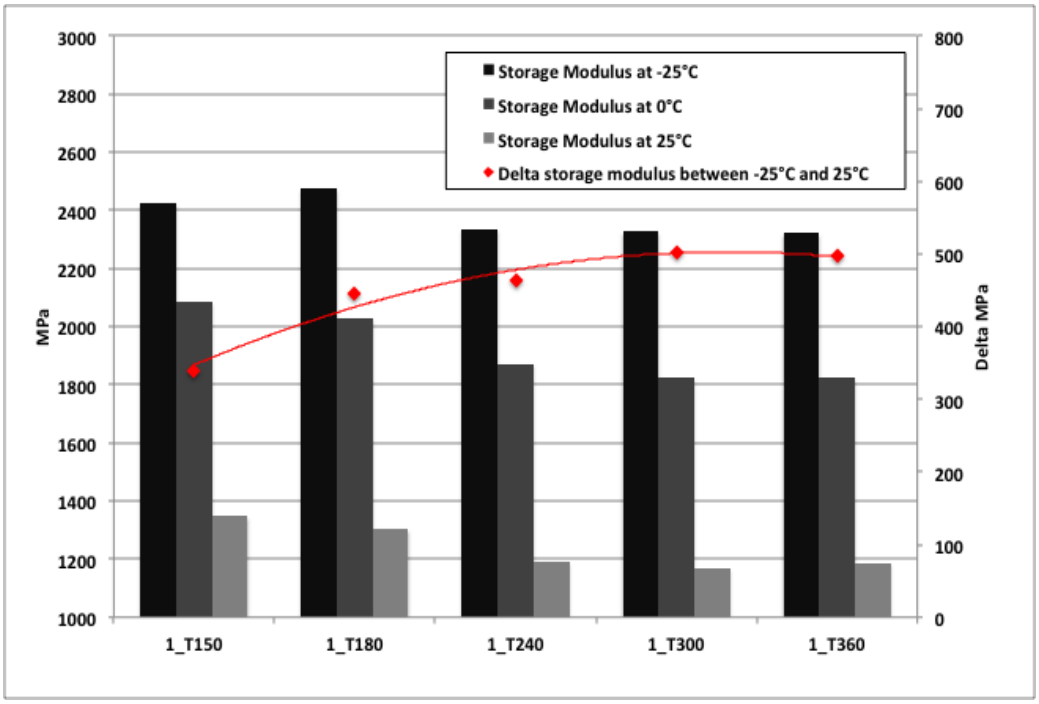

Figure 4.18 *Storage modulus as measured by DMA for moulded samples from set 1 (1_T150 to 1_T360) at different temperatures.*

The tan δ trends also display as expected an increase in damping (as indicated by the development of a second peak around -20 °C) with increasing ethylene contents (Fig. 4.19). From this data it is quite difficult to determine the glass transition temperature (T_g) from the cold temperature peak height for samples 1_T150 to 1_T240 as no real peak exists for these samples at low temperatures. In relating the observed damping behaviour from the DMA results to expected physical properties, it is clear that at these relatively low ethylene contents the effect of ethylene incorporation would have no significant impact resistance benefit, even though the stiffness is already being affected as observed in the storage modulus curves in Fig. 4.18. Towards the other end of the range, at higher ethylene contents (1_T300 and 1_T360) it does seem that the damping (and therefore the expected impact resistance) increases slightly

with increasing ethylene incorporation, without the stiffness being further affected. This measure of increase is also smaller from 1_T240 to 1_T300 and therefore it is expected that beyond the highest ethylene content a plateau in the impact strength measurement should be reached.

The horizontal distance between the two peaks is also observed to decrease with decreasing ethylene content. Doshev *et al.* [12] reported a similar observation previously where at low ethylene contents in the copolymer, the glass transition temperature (T_g) of the copolymer and propylene homopolymer phases move closer to each other. For heterophasic ethylene-propylene copolymers (HEPCs), some of the major transition regions were previously identified as (1) the α_{am} or amorphous copolymer phase relaxation occurring just above -50 °C and (2) the β_{PP} or relaxation of the polypropylene homopolymer phase between 15-20 °C [12]. In Fig. 4.19, the α_{am} relaxation is observed to occur between -40 °C and -20 °C, which is slightly higher than reported by Doshev *et al.*, however it should be noted that this value was indicated for copolymer samples containing 70 mol% and 82 mol% ethylene in the copolymer phase, which are not typically found in industrial samples, specifically not those used in this study. The β_{PP} relaxation is observed around 20 °C as expected. The movement of these relaxation peaks towards each other as observed with decreasing ethylene content could possibly indicate greater interaction between the two phases, but where a single peak is observed, it could also be that the actual rubber content in these samples are just too low to register a separate T_g value. For the 1_T150 to 1_T240 samples, only one peak is observed, representative of a glass transition at 20 °C. The presence of a single peak should however not be accepted as indicative of a miscible system, as phase separation may still exist with small dispersed domains higher than a minimum value, which was postulated as 0.18 μm [13]. This aspect was therefore investigated further by microscopy analysis of injection moulded test bars (refer to Table 4.5 and Section 4.3.4).

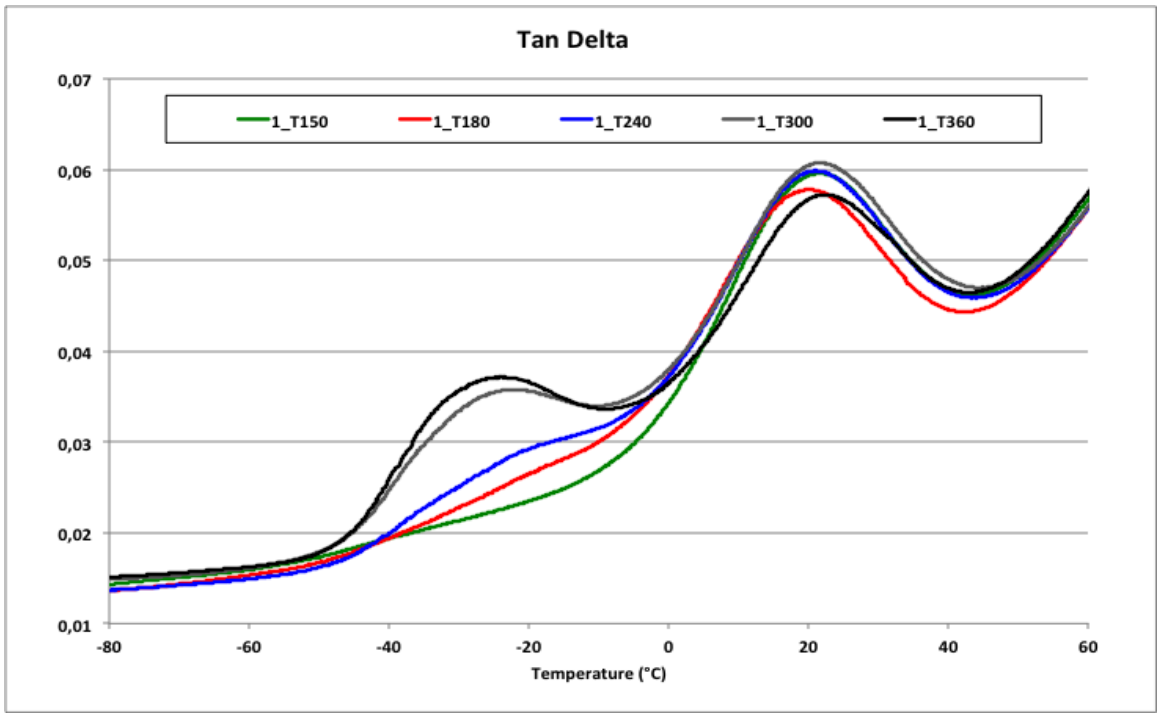

Figure 4.19 *Tan delta curves as measured by DMA for moulded samples from set 1.*

To relate the DMA observations to physical properties, larger samples (>5 kg) were obtained during a similar homopolymer to copolymer transition. Similar and overlapping ethylene contents compared to the set 1 values were obtained during this sampling and the composition and physical property results are indicated in Table 4.3 below. These samples are denoted with a "B" to indicate that these were obtained during a second sampling, e.g. 1B_T0 represents the time zero sample obtained on the same plant/technology as set 1, but during a second transition at a later date.

Table 4.3 Composition of the large samples obtained to represent set 1.

Sample	Time (min)[a]	Ethylene content (mol%)[b]	Ethylene content (mol%)[c]	Tensile Modulus (MPa)	Charpy Notched Impact (kJ/m²) 23 °C	0 °C	-20 °C
1B_T0	0	0	0	1641	3.3	1.7	1.2
1B_T90	90	2.5	4.2	1402	7.3	3.2	2.2
1B_T150	150	4.7	7.8	1340	9.9	4.8	3.7
1B_T360	360	6.9	11.4	1250	14.5	7.9	4.9
1B_T240	240	7.4	12.3	1288	14.6	7.8	4.8

[a] Time of sampling in minutes after introduction of ethylene to the second reactor
[b] Determined by FTIR
[c] Extrapolated NMR value

The values shown in Table 4.3 were used to determine trends for tensile modulus (Fig. 4.20) and impact strength (Fig. 4.21) and from these trends extrapolated values were determined for the original samples (Table 4.4). This was done by fitting the ethylene contents of the original samples to the physical property curves obtained for the samples as described in Table 4.3. In Fig. 4.20 and Fig. 4.21 it can be seen that the extrapolated physical property values for the original samples provide clear ethylene-dependent trends, which could be used to predict physical property behaviour over the range of ethylene contents investigated in this study (and also typically encountered in industry). It was observed with DMA that there is a marked decrease in stiffness with increasing ethylene content up to the higher ethylene contents (approximately 11%), whereafter the decrease in stiffness is less pronounced. The physical test results also indicate a similar decrease in tensile properties. Similarly, there is an increase in the impact strength with increasing ethylene content also reflecting the increase observed in the cold temperature damping trends by DMA. These observations are consistent with what is well known in industry and since samples with significantly different ethylene contents were used, a clear trend was easily established. It is also noteworthy that different points (as indicated by ethylene content) exist for optimal stiffness and impact strength, where the stiffness properties seem to plateau at lower ethylene contents than the corresponding impact strength plateau for this set. Depending on the physical property balance required, optimal ethylene contents could be selected from these trends to obtain a specific impact-stiffness balance.

Table 4.4 Extrapolated physical properties for set 1 original samples.

Sample	Time (min)[a]	Ethylene content (%)[b]	Tensile Modulus (MPa)	Charpy Notched Impact (kJ/m²)		
				23 °C	0 °C	-20 °C
1_T150	150	1.3	1532	4.8	2.4	1.6
1_T180	180	2.8	1412	7.7	3.9	2.6
1_T240	240	4.0	1356	9.7	4.9	3.3
1_T300	300	6.5	1280	13.1	6.8	4.5
1_T360	360	7.4	1260	14.1	7.4	4.8

[a] Time of sampling in minutes after introduction of ethylene to the second reactor
[b] Determined by FTIR

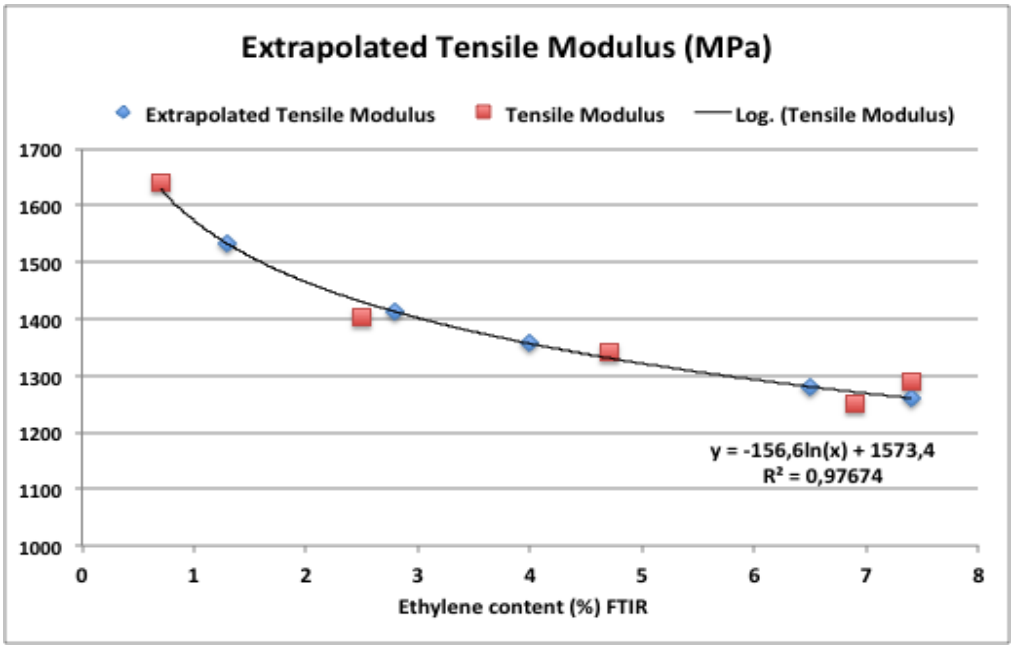

Figure 4.20 *Tensile modulus results for set 1 from second sampling (large samples) and extrapolated values for the original set 1.*

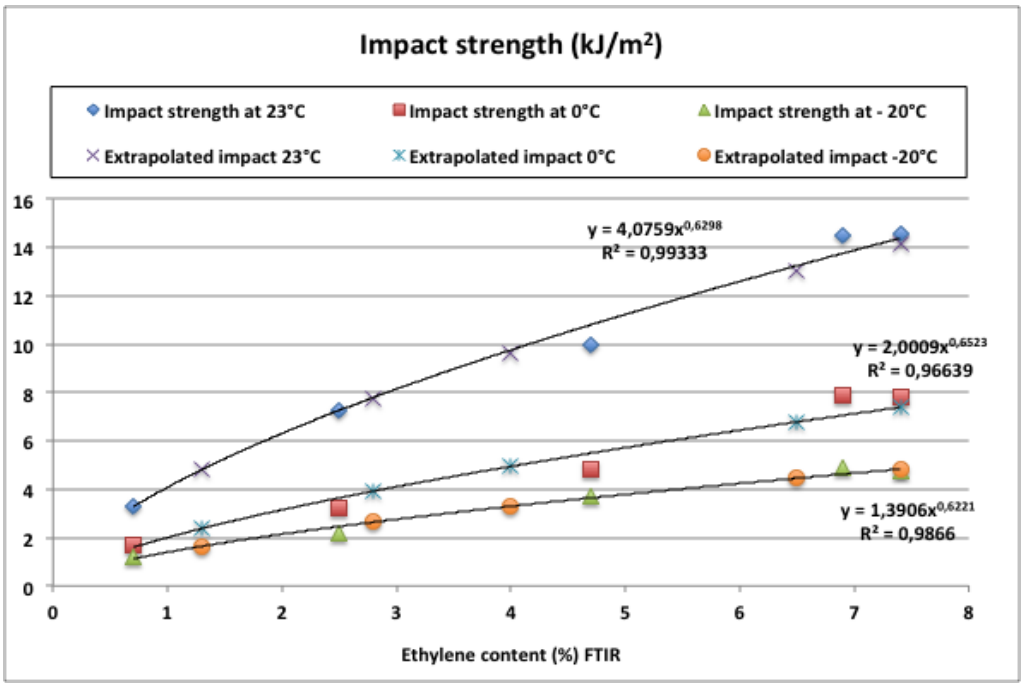

Figure 4.21 *Impact strength results for set 1 from second sampling (large samples) and extrapolated values for the original set 1.*

4.3.3.2 Effect of ethylene incorporation on rubber particle size and distribution for set 1

Broken test bars obtained after physical testing (refer to Table 4.3) were subjected to xylene extraction (as described in Chapter 3), followed by SEM to determine the effect of increasing ethylene incorporation on the size and distribution of the rubber particles. Representative SEM images (one out of the five images used for the statistical analysis for each sample) are shown in Fig. 4.22 to Fig. 4.24 and a breakdown of the average rubber particle size distribution is given for each sample. For calculation of the average particle size distribution, rectangular blocks of approximately 76 μm^2 were selected and all particles within the selected blocks counted and the diameters measured. From these results it can be concluded that the average rubber particle size increases with increasing total ethylene content. Even at ethylene contents as low as 2.5 mol%, rubber particles can be distinguished, however these particles are very small and not well distributed. In this sample all of the particles were larger than 0.18 μm in diameter, supporting the statement by Utracki *et al*. (refer to the DMA results in Section 4.3.3) that phase separation may still exist even though a single T_g is observed [13].

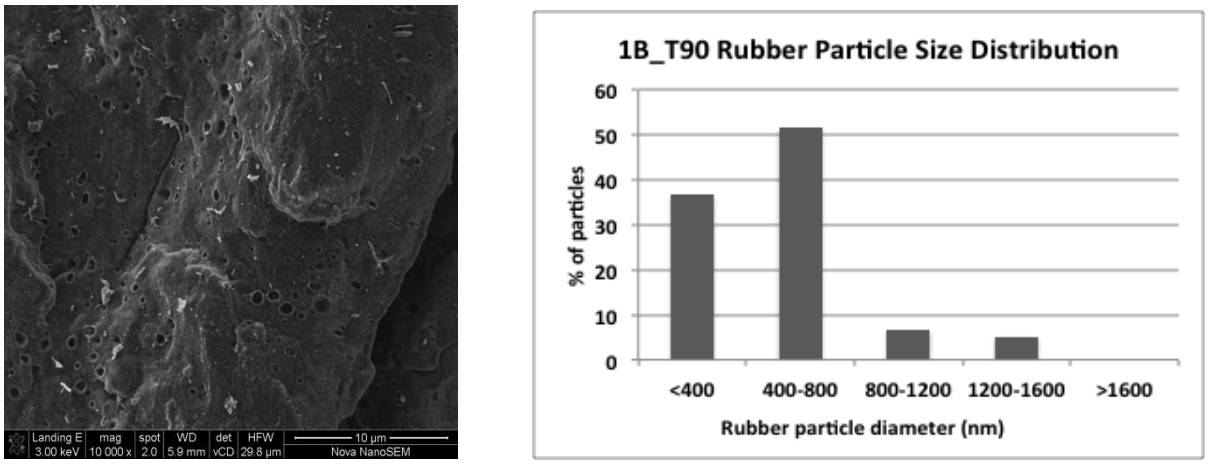

Figure 4.22 *SEM image of sample 1_T90 (2.5 mol% ethylene) after rubber extraction with xylene and particle size distribution of the rubber particles for this sample.*

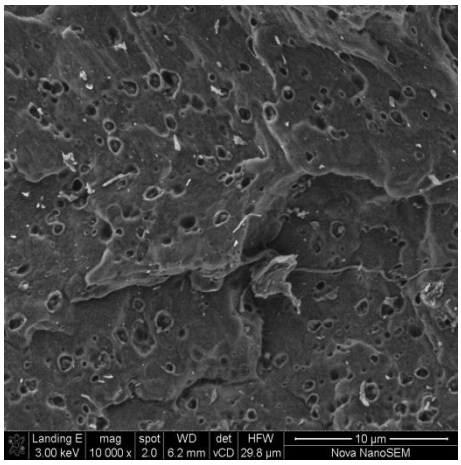

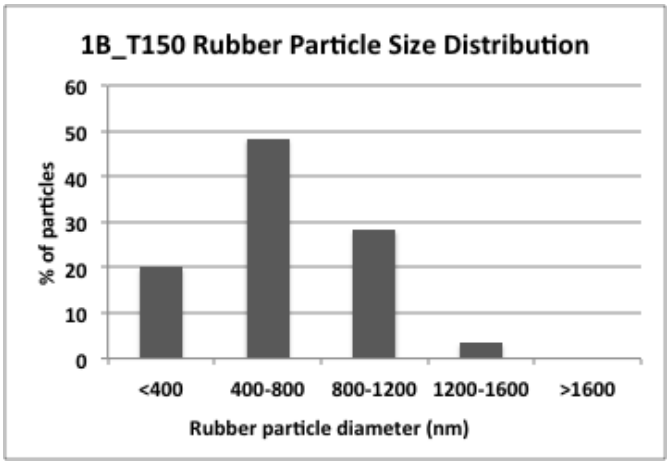

Figure 4.23 *SEM image of sample 1_T150 (4.7 mol% ethylene) after rubber extraction with xylene and particle size distribution of the rubber particles for this sample.*

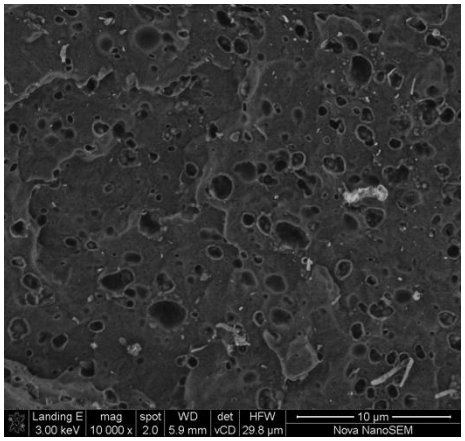

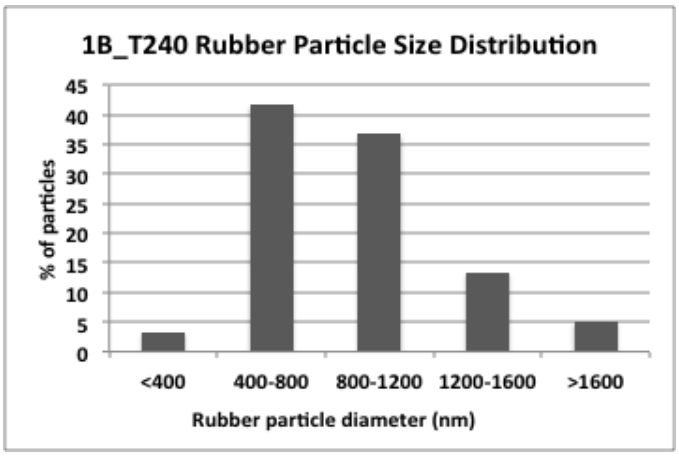

Figure 4.24 *SEM image of sample 1_T240 (7.4 mol% ethylene) after rubber extraction with xylene and particle size distribution of the rubber particles for this sample.*

From the images in Fig. 4.22 to Fig. 4.24 there appears to be a decrease in inter-particle distances and a more even distribution of rubber particles with increasing ethylene content and particle size. The average number of particles counted per area decreased slightly with increasing ethylene content, however the average size of the particles increased significantly. The average distances between particles and particle sizes were investigated in more detail and the result from this statistical analysis is given in Fig. 4.25. Along with an increase in ethylene incorporation, there is a marked growth in the average particle diameter (red trend) as well as a marked reduction in the relative distance between particles (blue trend). Another interesting observation from these trends is that there is a significant step change in particle size and inter-particle distance, for a relatively small change in ethylene content from 6.9 mol% to 7.4 mol%.

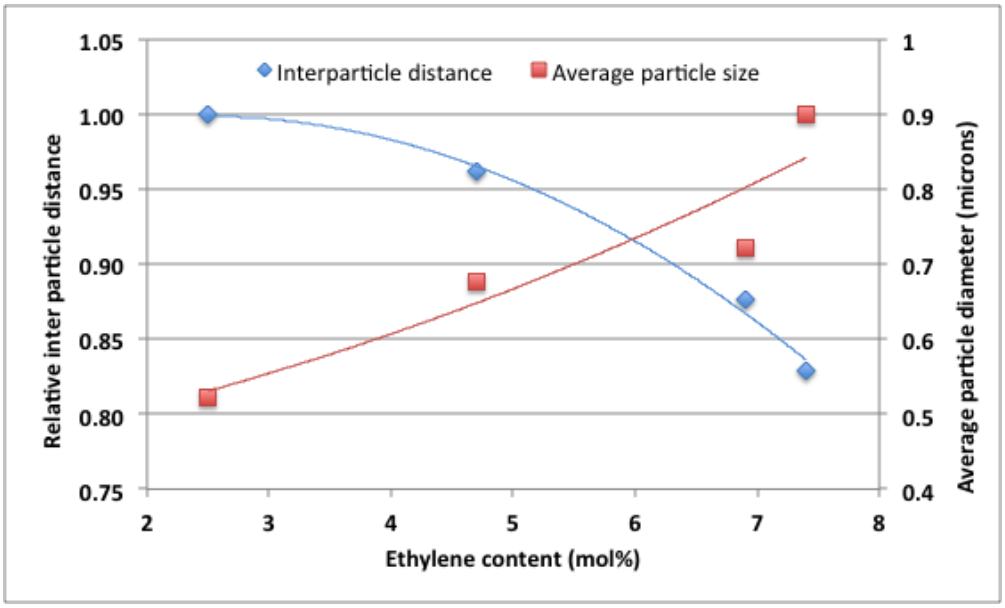

Figure 4.25 *Changes in the relative inter particle distances and average particle diameters with increasing ethylene content.*

Relating the rubber distribution observations to the physical property results, the increase in average particle size and decrease in relative inter particle distance correspond with the observed increase in impact strength as expected. The sharp change in particle size and inter particle distance at higher ethylene content (6-7 mol%) does however not translate into significant stiffness or impact strength properties, indicating that optimal particle size and inter particle distance may have already been achieved at lower ethylene contents. This observation does however not exclude the effect of the step change in rubber particle size and distribution on other particle properties, e.g. hardness and warrants further evaluation to understand the full effect. For the purposes of this study, which is focused on the physical properties typically measured and controlled in industry, it is sufficient to determine the effect on the stiffness-impact balance.

4.3.3.3 Physical properties determined for set 2 samples

For the set 2 samples, large volume sampling (>5 kg) was not possible and therefore a portion of the original 200 g samples was used for injection moulding of smaller test bars. The reduced area was accounted for in the measurements. The storage modulus determined by DMA is shown in Fig. 4.26. It is observed that the storage modulus increases initially, followed by a slight decrease with increasing sample ethylene content.

The difference in storage modulus between -25 °C and 25 °C increases with increasing ethylene content as expected up to a maximum (approximately 12 mol%) and then decreases slightly, indicating that the stiffness is only reduced up to a certain level of ethylene incorporation, beyond which higher ethylene content might contribute towards the observed stiffness. In general for this trend, it doesn't seem as if the storage modulus is significantly affected by the increase in ethylene incorporation in these samples.

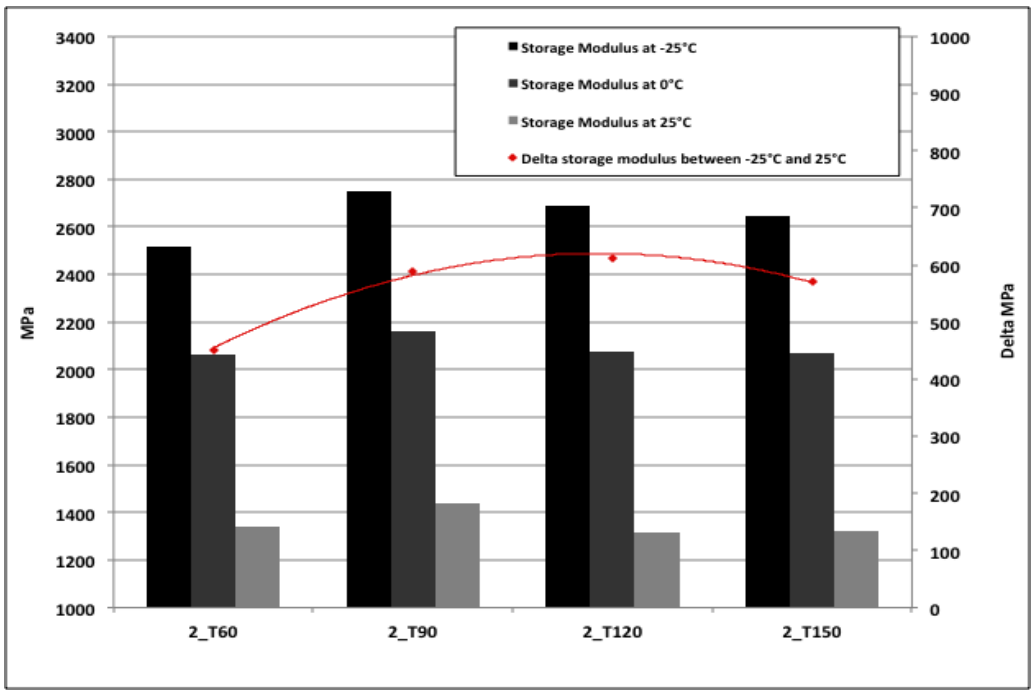

Figure 4.26 *Storage modulus as measured by DMA for moulded samples from set 2 (2_T60 to 2_T150) at different temperatures.*

The damping (tan δ) trends for set 2 are shown in Fig. 4.27. For all samples, except the 2_T60 sample with the lowest ethylene content, two distinct phase transitions are observed. Some of the major transition regions as outlined in Section 4.3.3.1 are also observed in these trends: (1) the α_{am} or amorphous copolymer phase relaxation occurring just above -50 °C and (2) the β_{PP} or relaxation of the polypropylene homopolymer phase between 15-20 °C [12]. There is a noticeable increase in the low temperature peak representative of the α_{am} transition with increasing ethylene content as expected. Furthermore the maximum height of this peak moves towards lower temperatures with increasing ethylene incorporation, increasing the distance between the two peaks, indicative of a greater measure of phase separation. The β_{PP} transition is shifted towards slightly higher temperatures for the 2_T120 sample, compared to the rest of the set.

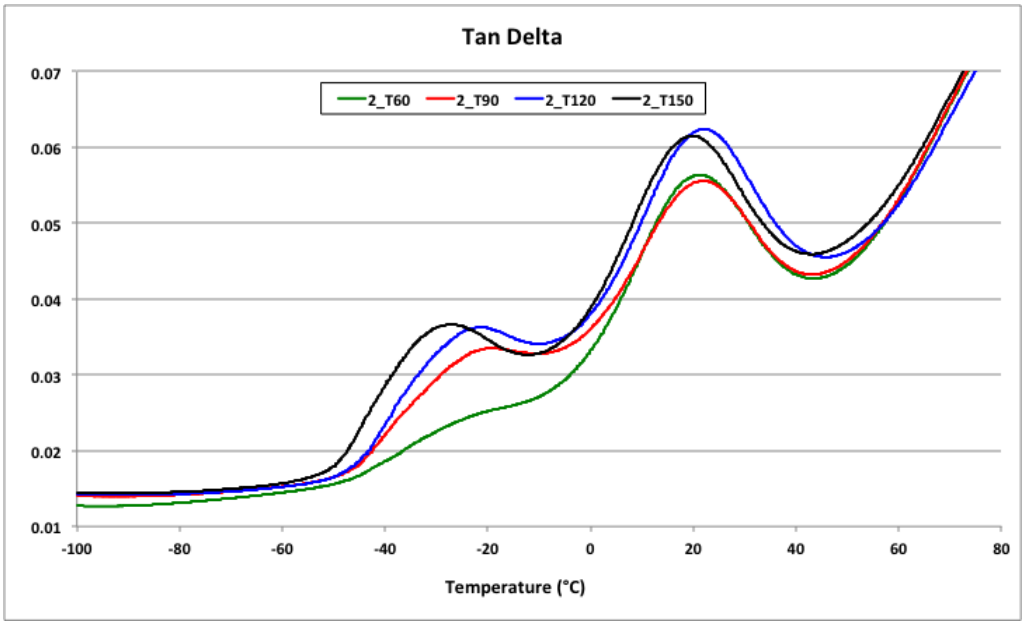

Figure 4.27 *Tan delta curves as measured by DMA for moulded samples from set 2.*

The tensile modulus and impact strength trends obtained for samples with increasing ethylene contents are shown in Fig. 4.28 and Fig. 4.29 respectively.

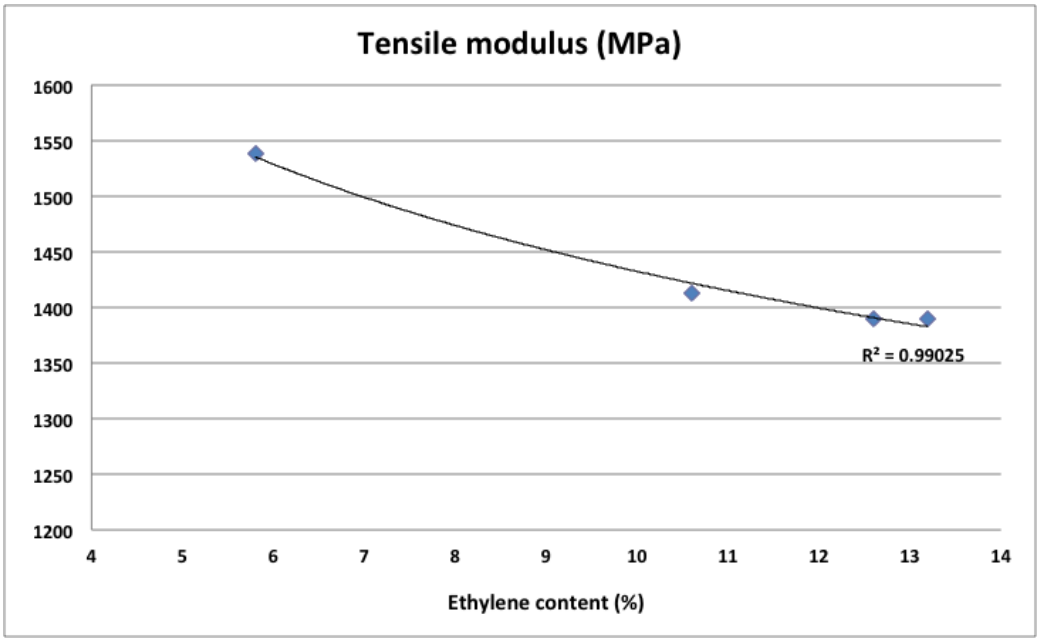

Figure 4.28 *Tensile modulus results for set 2 samples with increasing ethylene contents.*

A clear trend emerged for changes in the tensile modulus with increasing ethylene contents. As expected there is a decrease in the tensile modulus with an increase in ethylene content and this trend flattens at higher ethylene contents (12-13 mol%), indicating that beyond this point, further increases in ethylene content would not significantly reduce product stiffness. This supports the DMA observation that the delta storage modulus is only affected up to a certain level of ethylene incorporation.

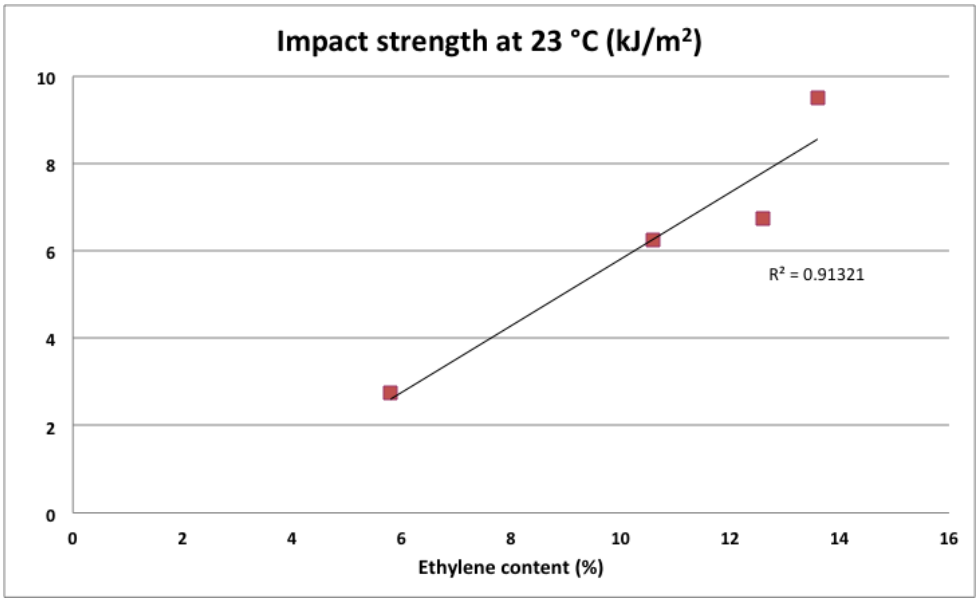

Figure 4.29 *Impact strength results for set 2 samples with increasing ethylene content.*

Simultaneous to a decrease in stiffness, there is an increase in impact strength properties (Fig. 4.29) with increasing ethylene content, as expected. This trend does however not reach a plateau, but continues to increase. It is expected that the impact strength properties could be further increased by increasing the total polymer ethylene content and based on the stiffness results, this could be done without further reducing stiffness beyond the minimum. In this trend the 2_T120 sample appears to be an outlier with slightly lower impact strength than expected. It was also observed in the tan δ trend obtained by DMA that the glass transition of the homopolymer was shifted to slightly higher temperatures, which could contribute to the sample being more brittle.

4.3.3.4 Effect of ethylene incorporation on rubber particle size and distribution for set 2

FE-SEM images of the fractured surfaces of test bars from samples of set 2 with increasing ethylene contents are shown in Fig. 4.30 to Fig. 4.33. As previously seen, the holes in the polymer surface are indicative of rubber particles that were extracted with xylene. For the sample with the lowest ethylene content (2_T60, Fig. 4.30) the rubber particles are very small, with over 60% the particles less than 400 nm in diameter; in fact a substantial amount of the particles are in the range of 0.18 μm, which is on the critical limit above which other groups have observed that phase separation occurs as indicated by Utracki *et a*l. [13]. Despite the small size of the rubber particles in this sample, these particles are well distributed, as observed from the FE-SEM image (Fig. 4.30) and the low calculated inter-particle distances relative to the rest of the set as shown in Fig. 4.34.

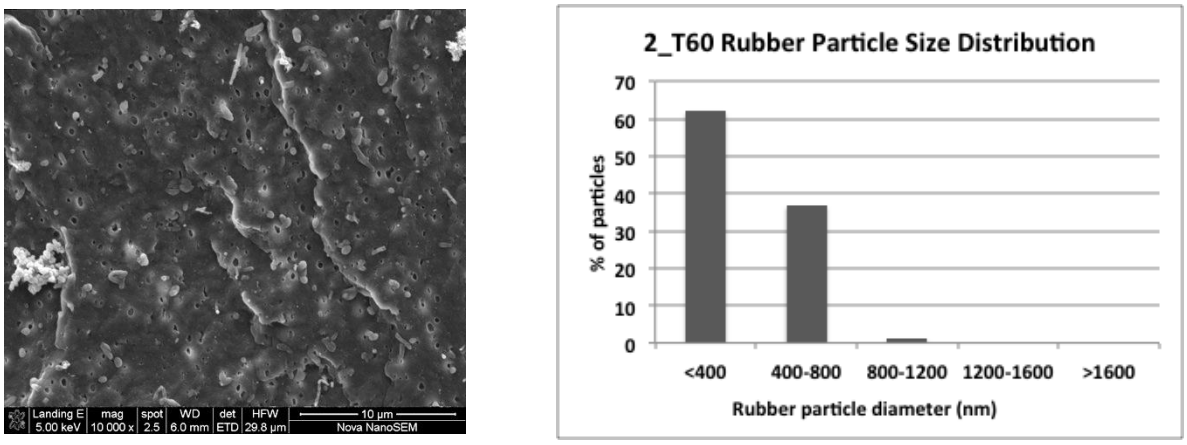

Figure 4.30 *SEM image of sample 2_T60 (5.8 mol% ethylene) after rubber extraction with xylene and particle size distribution of the rubber particles for this sample.*

As the ethylene content of the samples increases, there is a steady increase in the rubber particle size, as observed from the particle size distributions in Fig. 4.31 to Fig. 4.33 as well as the average particle diameter trend in Fig. 4.34. Comparing Fig. 4.31 and Fig. 4.32 representing images from samples with 10.6 mol% and 12.6 mol% ethylene, there is a marked increase in the number of rubber particles, resulting in a significantly reduced inter-particle distance (refer to Fig. 4.34).

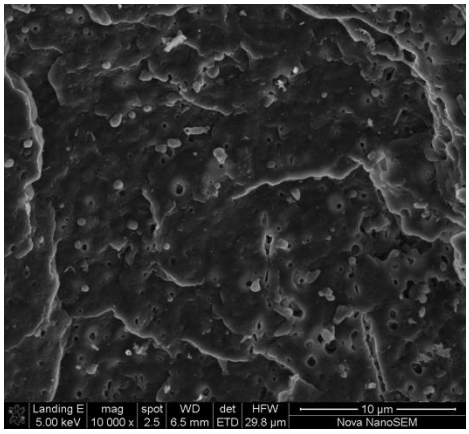

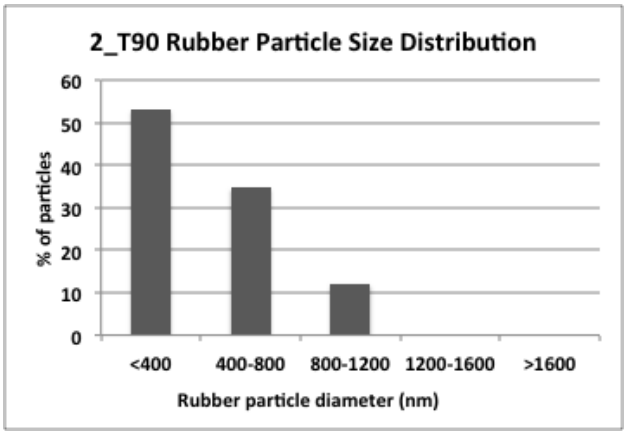

Figure 4.31 *SEM image of sample 2_T90 (10.6 mol% ethylene) after rubber extraction with xylene and particle size distribution of the rubber particles for this sample.*

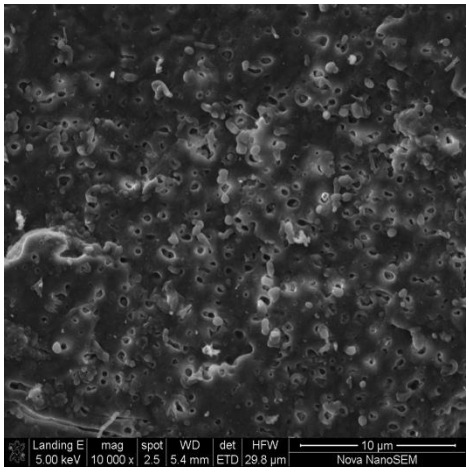

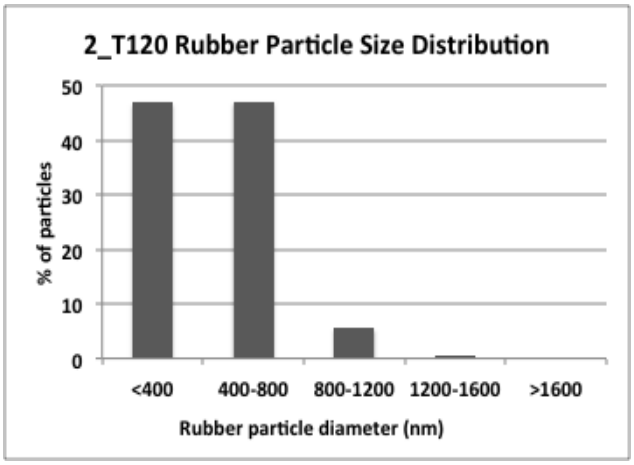

Figure 4.32 *SEM image of sample 2_T120 (12.6 mol% ethylene) after rubber extraction with xylene and particle size distribution of the rubber particles for this sample.*

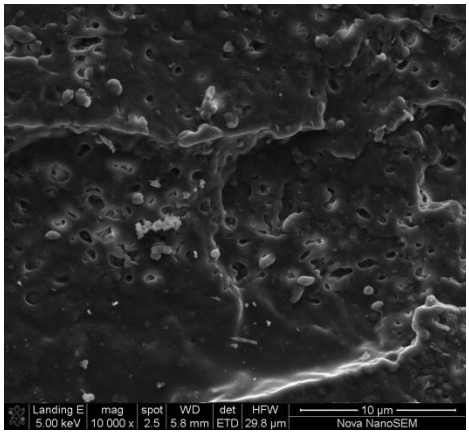

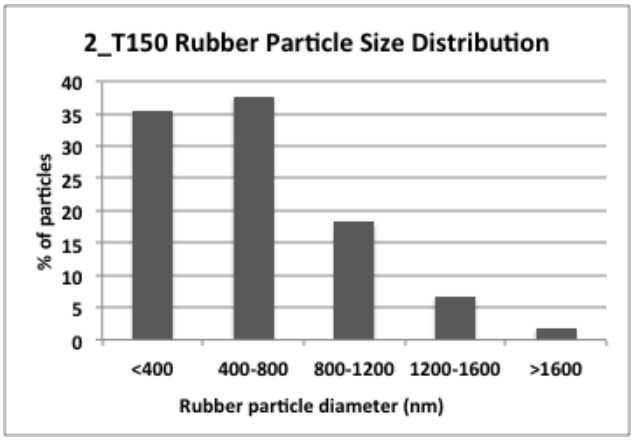

Figure 4.33 *SEM image of sample 2_T150 (13.2 mol% ethylene) after rubber extraction with xylene and particle size distribution of the rubber particles for this sample.*

From the particle size distribution trends above, it is also clear that a significant amount of small sized particles (diameter <400nm) are still present even in samples with high ethylene contents. This makes the calculation of average inter-particle distances and the establishment of an ethylene-dependent trend for changes in the inter particle distances, more complicated. In general one would expect the inter-particle distance to decrease with increasing ethylene content, as the particles become larger and better distributed. The expected trend is however not observed for this set of samples and in fact it seems that the inter-particle distances increase slightly with increasing ethylene content (Fig. 4.34). This is most likely due to the total number of particles that decreases as the ethylene content increases, resulting in larger particles but with greater distances between particles. The exception in this trend is sample 2_T120, which has the shortest inter particle distances in the range. Even though the stiffness of this sample fits the stiffness decrease trend, the impact strength of this sample is lower than expected when considering the impact strength trends. It is evident that an optimal rubber particle size and distribution exists and that even though generally a reduction in inter particle distances leads to improved impact strength properties, there seems to be an optimal inter-particle distance below which a reduction rather than improvement in toughness is observed. The cause of this specific behaviour of the 2_T120 sample is not evident based on the copolymer content or composition, which fits the set 2 trend (refer to Table 4.2) or the nascent particle morphological development (Fig. 4.5E and Fig. 4.16) and is thus considered to be an outlier. Further detailed determination of sample crystallinity, microstructure and chemical composition in the following chapter could shed some more light on this observation.

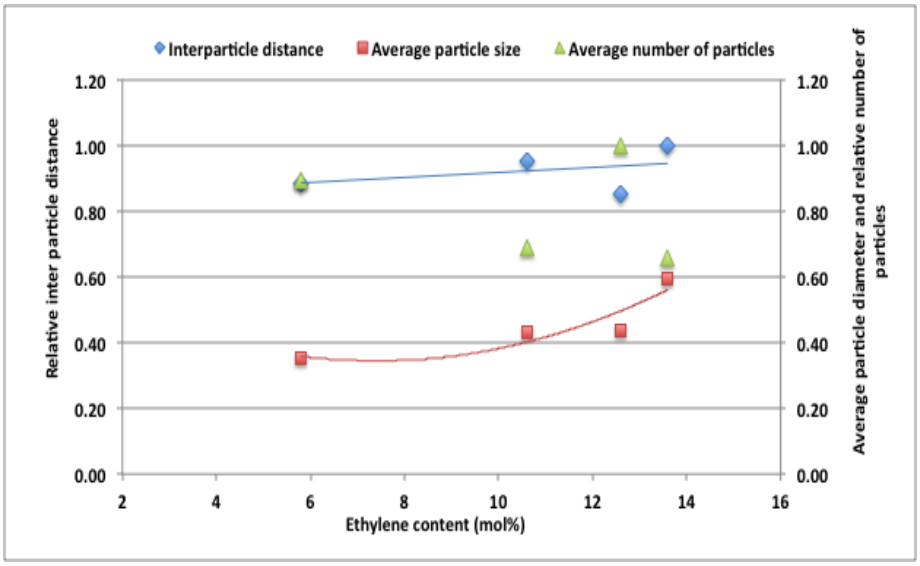

Figure 4.34 *Changes in the relative inter particle distances and average particle diameters with increasing ethylene content.*

In general however, it is observed that with increasing ethylene contents, the average particle size significantly increases along with a decrease in the average number of particles, suggesting that some of the smaller particles may start fusing together, resulting in a more wide-spread distribution. The driver behind this may be a loss in compatibility between the amorphous rubber and crystalline matrix phases, resulting in greater measure of phase separation. This is supported by the DMA damping trends discussed in the preceding section, where in general greater phase separation is observed with increasing ethylene incorporation.

4.3.4 Effect of ethylene incorporation on bulk sample molecular weight and chemical composition

The bulk samples described in Table 4.1 were also analyzed by size exclusion chromatography coupled to FTIR (SEC–FTIR) to study molecular weight and chemical composition distribution. From the Gram-Schmidt plots (Fig. 4.35) it is evident that these samples have a broad molecular weight distribution with the broadening more prominent towards the low molecular weight side (as indicated by longer retention times). The Gram-Schmidt plot is representative of the full FTIR spectrum between 2800 and 3200 cm^{-1}, which is used to indicate the total polymer concentration as it varies with molecular weight distribution. The sample with the highest ethylene content (1_T360) is also noticeably shifted towards higher molecular weights.

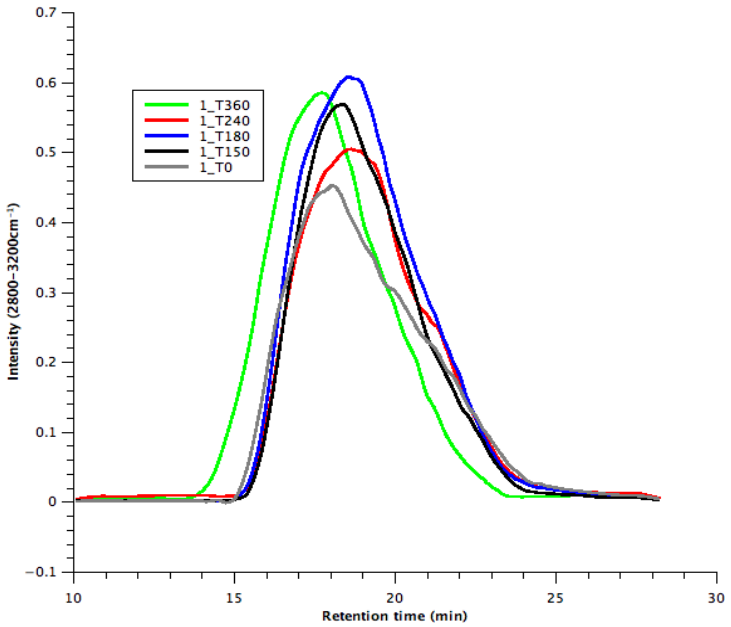

Figure 4.35 *Gram-Schmidt plot of samples analysed by SEC-FTIR.*

Debling and Ray also referred to this trend of increasing molecular weight with increasing ethylene incorporation in their study [4]. This was observed even when the same hydrogen content was used during homo- and copolymerization and it was proposed that the ratio between the increased propagation rate due to the higher reactivity of ethylene, but similar chain transfer rate, due to the same hydrogen content, resulted in longer chains. In industry however, the molecular weight of the copolymer produced in the second reactor is also deliberately controlled by the relative hydrogen feeds to the first and second reactor respectively to be significantly higher than that of the homopolymer.

From size exclusion chromatography (SEC) analysis of samples from set 1 (Table 4.5), it can be seen that there is an increase in average molecular weight and polydispersity with ethylene incorporation; however the 1_T240 sample seems to be an outlier with a higher molecular weight and polydispersity than the rest of the samples. There is a slight change in polydispersity when changing from homopolymer (1_T0) to copolymer, however when making a comparison between samples with different ethylene contents, the polydispersity values are quite similar (with the exception of 1_T240), possibly indicating that the effect of ethylene incorporation on sample heterogeneity, molecular weight and distribution is already present at low ethylene contents and doesn't change much with further ethylene incorporation. It could also be that this method is not sensitive enough to detect subtle changes in polydispersity in the bulk.

Table 4.5 SEC analysis of set 1 samples with increasing ethylene content.

Sample	Mp ($g.mol^{-1}$)	Mn ($g.mol^{-1}$)	Mw ($g.mol^{-1}$)	Mz ($g.mol^{-1}$)	Mv ($g.mol^{-1}$)	PD
1_T0	122 620	33 400	157 510	355 690	136 100	4.72
1_T150	166 340	32 910	249 920	708 350	206 230	7.59
1_T180	152 600	33 580	233 100	620 760	194 850	6.94
1_T240	151 620	14 050	254 470	3 179 010	167 660	18.1
1_T360	119 250	26 250	164 370	442 700	137 740	6.26

Size exclusion chromatography (SEC) analysis of set 2 samples (Table 4.6) also indicates a progression in the weight-average molecular weight (Mw) with increasing ethylene incorporation. There doesn't seem to be a significant change in polydispersity (PD) due to increasing ethylene incorporation. Furthermore it is clear that the set 2 samples have on average significantly higher molecular weights than those of the set 1 samples. This is due to different operating conditions used for the production of the two sets.

Table 4.6 SEC analysis of set 2 samples with increasing ethylene content.

Sample	Mp (g.mol^{-1})	Mn (g.mol^{-1})	Mw (g.mol^{-1})	Mz (g.mol^{-1})	Mv (g.mol^{-1})	PD
2_T0	296 946	61 617	417 924	1 422 804	381 852	7.66
2_T60	301 273	65 428	565 921	2 861 512	437 441	8.65
2_T90	391 249	67 236	554 275	1 587 717	449 335	8.24
2_T120	381 861	75 395	552 502	1 517 616	451 279	7.33
2_T150	487 222	68 027	645 332	1 969 030	517 584	9.49

Ethylene and propylene content as well as crystallinity distribution as a function of molecular weight was also investigated using previously assigned FTIR peak ratios by de Goede *et al*. [14]. The propylene content is indicated by the area ratio of the CH_3 bending band at 1376 cm^{-1} to the CH_2 bending band at 1462 cm^{-1}, as the CH_3 groups are exclusively present in polypropylene. Ethylene content is indicated by the area ratio of the 720 cm^{-1} band, which is indicative of long methylene sequences associated with crystalline polyethylene to the 1150 cm^{-1} polypropylene band. This was used previously to determine copolymer composition in ethylene-propylene block copolymers [14].

From the propylene and ethylene content distribution curves (Fig. 4.36) it can be seen that ethylene content seems to increase with increasing molecular weight and propylene content seems to increase with a decrease in molecular weight. Thus ethylene is predominantly found in the higher molecular weight portion of the polymer. This concurs with the way these polymers are produced in industry, with lower molecular weight homopolymer produced in the first reactor and very high molecular weight copolymer produced in the second reactor for improved impact strength properties.

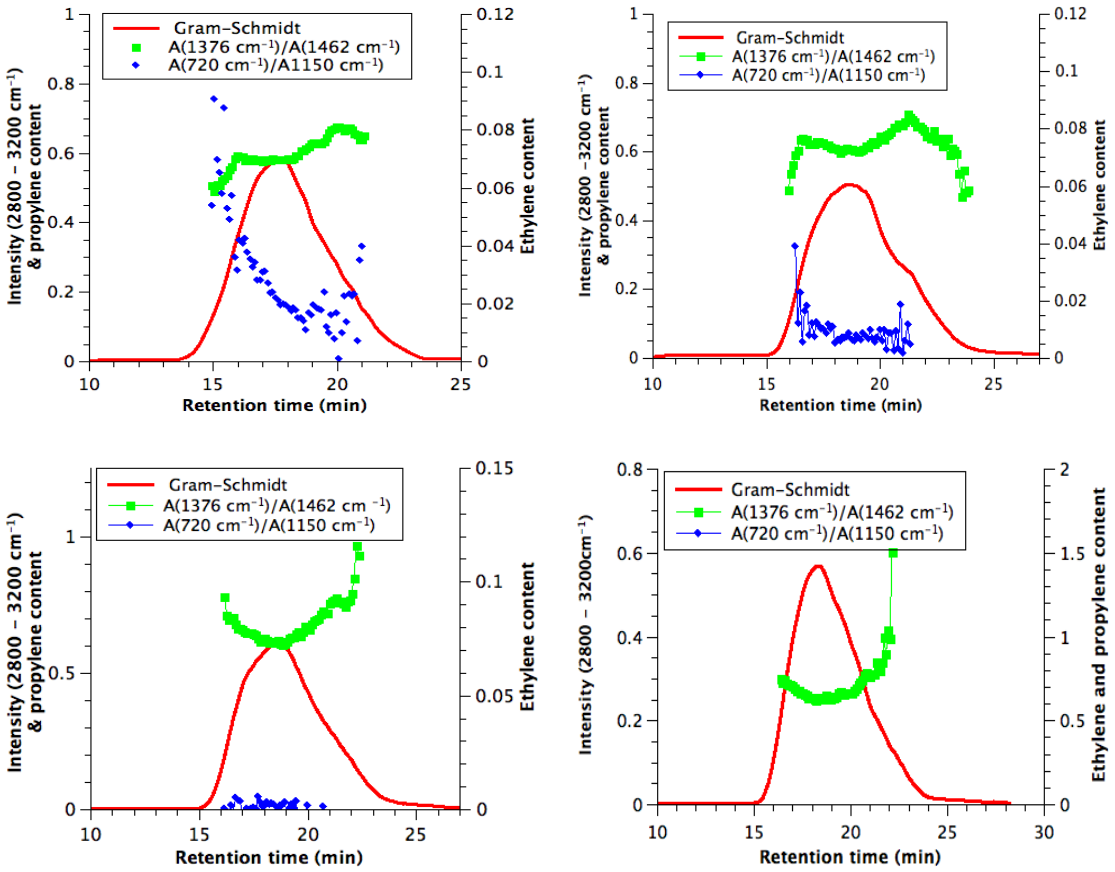

Figure 4.36 *Overlay of propylene and ethylene contents across molecular weight distribution for sample 1_T360 (top left), 1_T240 (top right), 1_T180 (bottom left) and 1_T150 (bottom right.).*

Propylene crystallinity is determined by the band ratio of the 998 cm^{-1} band, representative of long monomer repeat units in the crystalline 3_1 helix of polypropylene to the 973 cm^{-1} band associated with short helix segments. Relative ethylene crystallinity is expressed by the ratio of the 730cm^{-1} band (identified as a true crystallinity band), to the band at 720 cm^{-1}, which is representative of long continuous methylene sequences. It has been observed previously that as the crystallinity of polyethylene increases, the 720 cm^{-1} band splits to form another band at 730 cm^{-1}, of which the intensity increases with an increase in polyethylene crystallinity.

The distribution of propylene and ethylene crystallinity (Fig. 4.37) also shows an increase for propylene crystallinity with decreasing molecular weight. Ethylene crystallinity is very low and resultantly it is difficult to draw any conclusions. It does however seem as if the ethylene crystallinity is fairly constant where ethylene is found, regardless of the molecular weight of the

chains. The 1_T180 and 1_T150 samples did not differ significantly from those discussed above and are therefore not included in the trends. Furthermore, the set 2 samples are also not expected to differ much in terms of ethylene and propylene content and distribution and due to the low level of detail obtained for bulk samples, are not shown here.

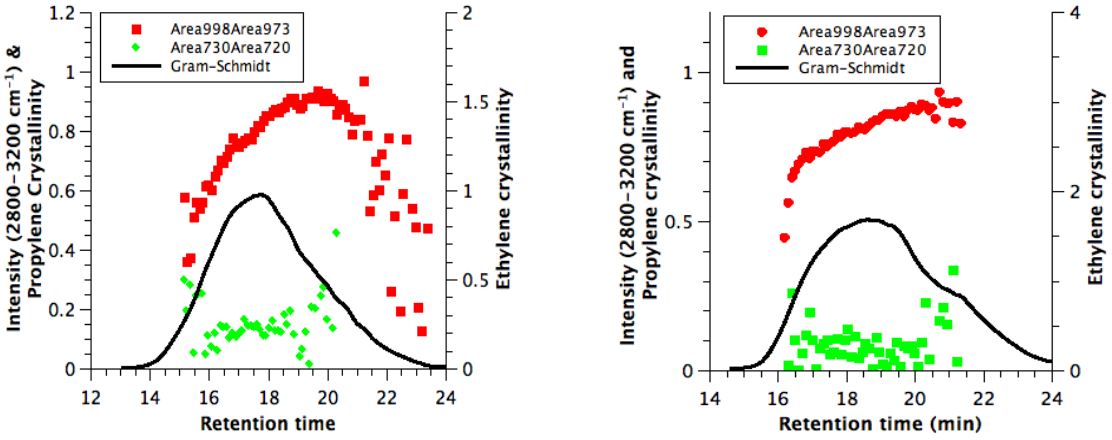

Figure 4.37 *Overlay of propylene and ethylene crystallinities across molecular weight distribution for 1_T360 (left) and 1_T240 (right).*

4.4 Conclusion

Sequentially produced heterophasic impact copolymer (HEPC) samples with different levels of ethylene incorporation were obtained from two different industrial gas-phase processes during a homopolymer to copolymer transition. It was shown that samples with significantly different total ethylene contents could be obtained by this method, which provided some insights into the early development of the copolymer phase and its effect on polymer properties. Due to the nature of the samples used, novel data was generated which was not obtained by previous morphological studies in this field.

Morphological development of the copolymer phase was investigated for samples with increasing ethylene contents for the two different sets, initially by means of SEM and in more detail by FE-SEM. Clear trends for the development of the rubbery copolymer phase with increasing ethylene content were observed, with the copolymer being distributed throughout the whole diameter of each particle.

For the samples from set 1, the external particle surfaces displayed less porosity than the internal surfaces. It was observed even at relatively low ethylene contents that the external surface of the particle was completely covered by a copolymer layer, whereas cracks and pores were clearly visible on the internal surfaces with thin threads of copolymer present. It was also observed that not all of the internal pores were filled with copolymer and that at the higher ethylene content of the range, copolymer was found to pool in certain areas. The mechanism of copolymer phase development for set 1 seemed to be through the growth of the copolymer phase on the surface of existing homopolymer globules. This resulted in a gradual smoothening of the globular surface as well as thickening of homopolymer fibrils, with increasing ethylene content. These morphological observations, supported the observations made by Debling and Ray [4] with regards to the maintenance of internal porosity and Kakugo *et al.* [3] with regards to the location of copolymerization on globule surfaces, but also provided new insights in the sense that the copolymer phase permeated the whole diameter of the particle and did not follow any particular concentration gradient for distribution. This supports the idea that ethylene monomer diffusion limitations don't significantly affect copolymerization radially throughout the particle for these samples.

The successive development of the radial internal distribution of copolymer as well as the external coating of the surface of nascent powder particles with increasing ethylene content also translated into a gradual development of rubber particle size and reduction in inter particle distances in moulded samples as observed by the microscopic analysis of fractured mould surfaces. Good correlation was found for the increase in rubber particle size and reduction in the inter particle distance with the total ethylene content of the sample. Furthermore, the changes in rubber particle size and distribution could also be related to the mechanical properties. From these correlations it was also noted that a certain optimal combination of particle size and inter particle distance was required for high impact strength properties and that altering these parameters beyond their limits did not result in any significant physical property advantages. It was found that stiffness was only affected up to approximately 6 mol% ethylene, but that the impact strength could still be increased beyond these ethylene contents. Good correlation was obtained between the DMA storage modulus and tensile modulus properties, as well as between the DMA damping trends and impact strength properties.

Within the set 2 samples, it was found that even though the homopolymer is very porous before introduction of copolymer, the internal porosity is significantly reduced upon ethylene

incorporation, while some external porosity is maintained. At intermediate ethylene contents, almost no internal pores or homopolymer fibrils were observed, indicating at least for the samples involved that almost complete pore filling occurred internally. This pore-filling observation seemed to support to some extent what was observed by Urdampilleta *et al.* [7] and Chen *et al*. [8], however in this case a clearer distinction between the copolymer and homopolymer phases was observed, instead of the fine distribution of copolymer in the matrix as observed by these authors. Similar to the set 1 observations no concentration gradient was observed for copolymer distribution throughout the particle. As the ethylene content of the samples increased a fine globular surface with a grainy appearance was maintained with the copolymer extending in long strands between globules, possibly flowing into the pores formed by homopolymer globules before copolymerization.

These morphological developments in the nascent powder particles translated into a fine rubber particle distribution in moulded samples as observed by FE-SEM images of rubber extracted mould fracture surfaces. For this set, a significant amount of small rubber particles (less than 400 nm in diameter) were present in all samples regardless of ethylene content. As the ethylene content of the samples increased, the particles gradually grew larger, but there was also a significant decrease in the average number of rubber particles, suggesting that some of the rubber particles may have fused together, resulting in a trend of increasing inter particle distance with increasing ethylene content. Nevertheless, the impact–stiffness balance improved as expected for increasing ethylene content, indicating that the changes in size and distribution of the rubber particles were sufficient to successively improve the toughness of the polymers as the ethylene content of the samples increased. In this set it was observed that sample 2_T120 seemed to be an outlier, based on a large number of rubber particles present in this sample, as well as significantly lower inter particle distances, which resulted in poorer impact strength properties, indicating that an optimal inter particle distance exists for sufficient impact-stiffness balance.

Comparing the proposed morphological developments for the different sample sets as described above, it was clear that the existing homopolymer morphology and porosity as dictated by the catalyst system played a vital role in the development and distribution of the copolymer phase. This has identified an interesting topic for further investigation, as will be done in the next chapter where the effect of copolymer growth on sample crystallinity and microstructure will be investigated. Furthermore, it was also found for both sets that impact strength properties

could be increased without sacrificing stiffness properties beyond a minimum at higher ethylene contents. This process seems to be driven by ethylene and copolymer content, rather than by the catalyst or technology used. Overall, an increase in molecular weight and distribution was seen with increasing ethylene contents, as would be expected from these sequential processes, where the aim is to obtain very long copolymer chains, compared to the homopolymer chains to improve impact strength properties. SEC–FTIR has also shown that the ethylene is found predominantly in the higher molecular weight chains and propylene in the lower molecular weight chains. Resultantly, propylene crystallinity also coincided with the low molecular weight fractions, as would be expected, because in the higher molecular weight chains, propylene crystallinity would be significantly reduced by the presence of incorporated ethylene.

In summary, the observations in Chapter 4 have identified specific mechanisms for copolymer phase development and distribution, with some correlation to what was proposed by previous studies, but also some further elaboration on how the copolymer phase evolves from very low ethylene contents. Ethylene-dependent growth trends as well as the influence of the existing homopolymer and technology set were identified. The morphological developments in the nascent powder particles, as well as in the final molded state were related to the development of physical properties and good correlations were observed between the expected and observed physical property trends.

Based on these initial observations in the bulk, it is still unclear how the copolymer phase develops on a molecular level and what its effect is on sample crystallinity. Understanding how the polymer microstructure develops with increasing ethylene content, as well as how this affects the crystallinity of the sample, will also provide a better understanding of the observed morphological and physical changes in this chapter. Therefore Chapter 5 will focus on changes in the crystallinity and microstructure with increasing ethylene contents.

4.5 References

1. Kissin, Y. *Alkene Polymerization Reactions with Transition Metal Catalysts*. Elsevier. 2008., p.27
2. Kakugo, M., Sadatoshi, H., Yokoyama, M. and Kojima, K. *Transmission electron microscopic observation of nascent polypropylene particles using a new staining method*. Macromolecules. 1989., **22:** p.547-551.
3. Kakugo, M., Sadatoshi, H., Sakai, J. Chapter 27. *Morphology of nascent polypropylene produced by $MgCl_2$ supported Ti catalyst*. Catalytic Olefin Polymerization. Editors: Keii, T., Soga, K. Elsevier. 1990., p.345-354.
4. Debling, J.A. and Ray, W.H. *Morphological development of impact polypropylene produced in gas-phase with a TiCl4/MgCl2 catalyst*. Journal of Applied Polymer Science 2001., **81(13):** p.3085-3106
5. Cecchin, G., Marchetti, E. and Baruzzi, G. *On the Mechanism of Polypropene growth over $MgCl_2/TiCl_4$ Catalyst Systems*. Macromolecular Chemistry and Physics. 2001., **202:** p.1987-1994.
6. McKenna, T.F., Bouzid, D., Matsunami, S., Sugano, T. *Evolution of particle morphology during polymerisation of high impact polypropylene*. Polymer Reaction Engineering. 2003., **11(2):** p.177-197.
7. Urdampilleta, I., González, A., Iruin, J.J., de la Cal, J.C. and Asua, J.M. *Morphology of high impact polypropylene particles*. Macromolecules. 2005., **38(7):** p.2795-2801.
8. Chen, Y., Chen, Y., Chen, W. and Yang, D. *Evolution of phase morphology of high impact polypropylene particles upon thermal treatment*. European Polymer Journal. 2007., **43:** p.2999-3008.
9. Daoust, D., Bebelman, S., Chaupart, N., Legras, R., Devaux, J. and Costa, J. *Characterization of ethylene in EP and in iPP/EP systems by deconvolution of IR spectra*. Journal of Applied Polymer Science. 2000., **75:** p.96-106.
10. Kosek, J., Smolná, K. and Gregor, T. Morphological analysis of high-impact polypropylene using X-Ray microCT and AFM. European Polymer Journal. 2013. *Article in press*.
11. Introduction to Dynamic Mechanical Analysis (DMA). PerkinElmer Inc. USA 2008: p.4-6.
12. Doshev, P., Lohse, G., Henning, S., Krumova, M., Heuvelsland, A., Michler, G. and Radusch, H.J. *Phase interactions and structure evolution of heterophasic ethylene-propylene copolymers as a function of system composition*. Journal of Applied Polymer Science. 2006., **101:** p.2825-2837.
13. Utracki, L., *Polymer alloys and blends.* Carl Hanser: Munich. 1989., p.93
14. de Goede, E., Mallon, P. and Pasch, H. *Fractionation and analysis of an impact poly(propylene) copolymer by TREF and SEC-FTIR*. Macromolecular Materials and Engineering. 2010., **295(4):** p.366-373.

Chapter 5

Results and Discussion: Development of crystallinity and chemical composition

In this chapter the attenuation of sample crystallinity by ethylene incorporation is investigated. Solution- and solid-state NMR is used to determine the development of bulk sample microstructure and chain conformation as well as changes in the semi-crystalline copolymer fractions (representative of the compatibilizing phase between rubber and matrix) for samples with increasing ethylene incorporation. These results are placed within the context of the bulk chemical properties and physical behaviour determined in Chapter 4.

5.1 Introduction

The focus of the detailed studies described in the literature review was to develop models for polymer morphology and phase development in heterophasic ethylene-propylene copolymers (HEPCs). For this reason, mostly microscopic techniques (SEM, TEM and AFM) were used for visualization of the different phases, supplemented by other techniques such as mercury intrusion porosimetry and sorption measurements [1,2]. In the study by Debling and Ray [3], extensive reaction kinetics experiments were done in addition to the microscopy work. Some SEC and DSC work were also done, but due to sample complexity and heterogeneity not much information could be obtained from the bulk HEPCs. Further characterization of the polymers used in the morphological studies, was done only in a few instances, for example Chen *et al*. did a follow-up investigation on their initial morphology study by solvent fractionation of the same samples and further characterization (by means of DSC) of these fractions [4]. Hence in very few previous studies, the observations on morphological development were related to other polymer properties such as chemical composition, crystallinity and chain conformation.

The purpose of this chapter will therefore be to present changes in polymer crystallinity, microstructural and chemical composition development with increasing ethylene incorporation, and to relate these observations to the morphological and physical property observations made in the previous chapter.

Crystallization behaviour of HEPCs has been the main topic of a number of publications in the past few years. A few previous studies that have specifically focused on crystallinity and chemical composition of HEPCs are thus outlined: Zhu *et al*. described a detailed study on crystallization- and melt behaviour of two polypropylene in-reactor alloys containing ethylene-butene and ethylene-propylene copolymers [5]. The compositional heterogeneity of these polymers were broken down by successive-self nucleation and annealing (SSA), which is a DSC technique capable of thermally 'fractionating' polymers into components with increasing lamellar thickness. Microstructural characterization of TREF fractions of these polymers was also done and these were correlated to mechanical properties and phase structures. Li *et al*. produced copolymers by autoclave polymerization, of which different parts (amorphous and crystalline) were blended with polypropylene and subsequently analysed by DSC, polarised optical microscopy, wide angle X-ray diffraction and SEM [6]. It was observed that different components of the copolymer affect the linear spherulitic growth rate to different extents. The same authors further compared the morphology of a conventional HEPC produced by an

industrial two-step process to that of an HEPC produced in autoclave by means of a multi-stage sequential polymerization (MSSP) and interpreted the improved mechanical behaviour of the MSSP product within the context of microstructural differences between these polymers affecting phase separation and crystallization [7].

As with the morphological studies, all of the studies mentioned above are limited in the sense that only the final HEPC product is investigated, therefore no information on how the developing polymer affects crystallinity and microstructure is obtained [5, 8]. In other instances, autoclave products were used, which are not representative of typical HEPCs produced in industry [6]. The samples used in the scope of this thesis however, are in-reactor alloys with increasing ethylene contents and have therefore provided a unique view into the development of the copolymer as it occurs in industry. For this reason, all observations from these sample sets with respect to changes in crystallinity and microstructure would be novel.

Apart from providing information on the development of bulk crystalllinity and average chain ethylene distribution, this chapter will also focus on the use of solid-state NMR as a technique to determine chain conformation and molecular dynamics along with chemical composition. Although solution NMR has been widely used in the characterization of HEPCs [8-11], solid-state NMR has been greatly underutilized for HEPCs and to date, no solid-state investigations exist that have characterised the exact type of polymers used in this thesis. However a few solid-state studies with some relevance to the scope of this thesis are highlighted below:

Comotti *et al*. investigated the crystallization of mixtures of isotactic and syndiotactic polypropylene and developed a deconvolution and peak assignment for changes in the methylene region related to disorder in the chain packing [12]. Alamo *et al*. determined the partitioning of ethylene defects in model random ethylene-propylene copolymers synthesised by metallocene catalysts [13]. Zhu *et al*. used different solid-state techniques (including 2-dimensional wide line separation or WISE experiments) to characterize the chain dynamics and phase structure of a commercial PP/ethylene-α-butylene in-reactor alloy [14]. It was shown that the polymer consisted of a homo-polyethylene matrix, polypropylene dispersed phase and a linear low-density polyethylene (LLDPE) interphase.

In this chapter, solid-state techniques focused on selective observation of crystalline and amorphous regions will be used to obtain a better understanding of the molecular dynamics in

the state the polymers are typically used in. This will also be related to the microstructural development as determined by solution NMR.

Most studies on HEPCs use TREF as a technique to fractionate these highly complex polymers into more homogeneous samples. However, although TREF fractionation yields more homogeneous samples relative to the bulk sample, it is also known that these fractions can still consist of a wide range of molecular weights and chemical compositions. In order to characterize these fractions further a relatively new technique, high temperature high performance chromatography (HT-HPLC) has been developed. The first account of this new method was in a publication by Macko and Pasch where it was shown to have the ability to baseline separate a mixture of polyethylene and different polypropylene molecules with various tacticities [15]. The principle of this technique relies upon the adsorption of polymer chains with different ethylene contents on the stationary phase followed by introducing a solvent gradient with increasing strength for the dissolution of components with increasing ethylene composition. Molecular weight also plays a role in this separation, as statistically the chance of encountering more ethylene insertions is higher with longer copolymer chains. This method has been recently applied to HEPCs and has proven to be particularly useful for further separation of complex HEPC fractions [16-17]. In this chapter the HT-HPLC results of selected TREF fractions will be applied to further investigate the complex composition to determine how the semi-crystalline copolymers develop with increasing ethylene contents.

5.2 Experimental

The experimental techniques are described in detail in Chapter 3 (Prep-TREF, Solution NMR, solid state NMR, HT-HPLC).

5.3 Results and discussion

5.3.1 Ethylene-dependent changes in crystallinity and microstructure for set 1

5.3.1.1 Attenuation of crystallizability with increasing ethylene incorporation

To determine the effect of increasing ethylene incorporation on sample crystallinity and to obtain fractions for further detailed characterization, preparative TREF (prep-TREF) was done. Historical preparative TREF (p-TREF) data from previous studies on HEPCs, was however only available for the “final” impact copolymers, representing the highest ethylene content in the

range, hence some additional information was required to predict the crystallization behaviour of the rest of the transition samples with lower ethylene contents.

Various methods have been established for the fractionation of samples based on crystallization behaviour. Furthermore, some information on the degrees of crystallinity of different components can be obtained. Fractionation methods such as TREF and crystallization fractionation analysis (CRYSTAF) relies upon temperature dependent differences in crystallizability between the various components of the polymer. In TREF, the dissolved polymer is cooled at a very slow rate (this step alone can take up to four days) on an inert support and then in a separate fractionation step, solvent is added at increasing temperatures to the crystallized sample, to dissolve and elute fractions of increasing crystallizability. CRYSTAF is a shorter technique and uses the principle of measuring the concentration of dissolved polymer as it crystallizes out of solution, therefore fractions in order of decreasing crystallizability is obtained. A disadvantage of this technique is that during the process of crystallization, dilution of the measured sample takes place, making this method less sensitive, particularly for the measurement of fractions of lower crystallizability. Also, when considering that the samples used in this study have low contents of less crystallisable components, relative to the crystalline polypropylene matrix (>80%), CRYSTAF might not be sensitive enough to determine these components.

Solution crystallization analysis by laser light scatter (SCALLS) was applied to bulk samples as a faster alternative method to CRYSTAF and a-TREF (analytical TREF) to determine the optimal temperatures for sampling during fractionation with p-TREF. This method did not only enable the retrieval of results in a fraction of the time normally used for TREF or CRYSTAF, but also provided information that has not been previously observed by either of these techniques, as will be demonstrated in the section to follow. The principle of SCALLS is that changes occur in the scatter pattern of a laser beam, which is passed through a polymer in various stages of dissolving in solution (heating experiments) or crystallizing out of solution (cooling experiments) [18-19]. Considering the mechanisms of TREF and CRYSTAF, SCALLS is expected to be analogous to CRYSTAF in cooling mode and to TREF in heating mode. The information obtained by SCALLS or turbidity fractionation analysis (TFA) referred to by Shan *et al*. has been shown to correlate well with TREF and CRYSTAF [18]. The SCALLS technique was previously used to study the solution crystallization behaviour of a series of different polyolefins and was successful in detecting subtle crystallization differences between samples [19].

In Fig. 5.1 the heating trends from 30 °C to 130 °C at a rate of 1.5 °C.min^{-1}, obtained with the blue laser is shown. As the polymer in solution melts with increasing temperature, the turbidity of the solution is measured as a response. It can be observed from the raw data (Fig. 5.1A) that there are two sharp increases in the voltage measurement, the first between 110 °C and 115 °C and the second between 115 °C and 120 °C indicating that most of the crystals melt at these temperatures and also that there are at least two distinct populations from a crystallization perspective. At lower temperatures, around 95-100 °C, it can also be observed that the 1_T240 and 1_T360 samples with higher ethylene contents start melting before the 1_T150 and 1_T180 samples, as observed by the slope of these trends between 90 and 110 °C. This can be explained by the theory that samples with higher ethylene contents should have less perfect crystals, if the ethylene insertions disrupt the regular polypropylene crystal structure, resulting in components that melt at lower temperatures. The significance of this observation is that the semi-crystalline copolymers produced in the second reactor, does seem to have an influence on the crystallinity of the isotactic polypropylene, confirming the presence of interactions between these different reactor products, which is responsible for improved physical properties in contrast to mechanical blends of polypropylene with copolymers, which are known to have poorer physical properties. Furthermore, this level of detail relating to different crystalline components, is not observed when using TREF or CRYSTAF, which are less sensitive to these subtle differences.

From the first derivative curve shown in Fig. 5.1B, there is also a clear bimodality for sample crystallizability, with the highest ethylene content sample 1_T360 even displaying a lower-temperature shoulder at 110 °C. Here the trends for samples with lower ethylene contents also seem to be shifted towards higher temperatures.

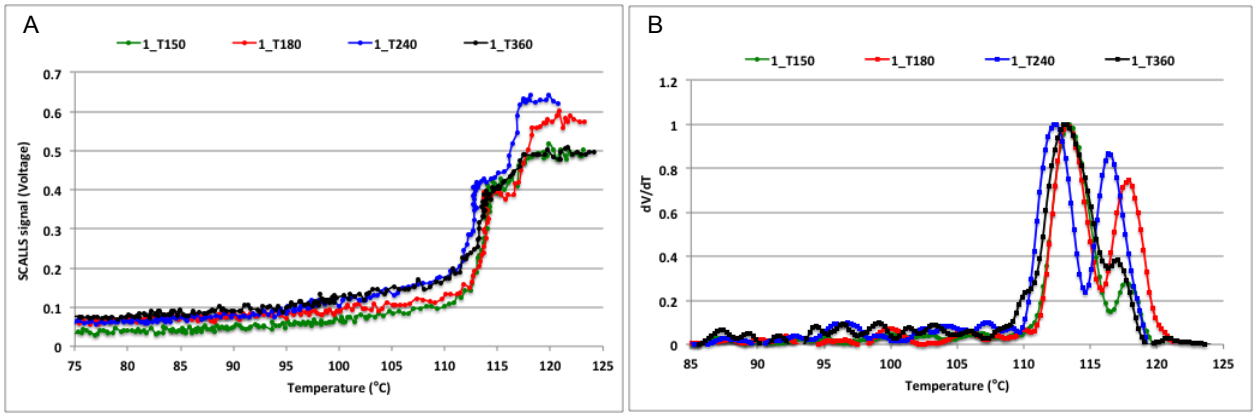

Figure 5.1 *SCALLS heating trends: A (raw voltage signal) and B (first derivative) obtained by blue laser for samples of set 1 with different ethylene contents.*

From the SCALLS data, it was evident that the main components for all the samples were present between 110 and 120 °C, hence it was confirmed that the p-TREF fraction temperatures normally used for heterophasic copolymers (30, 60, 80, 90, 100, 110, 120, 130 °C) would be applicable to samples used in this study.

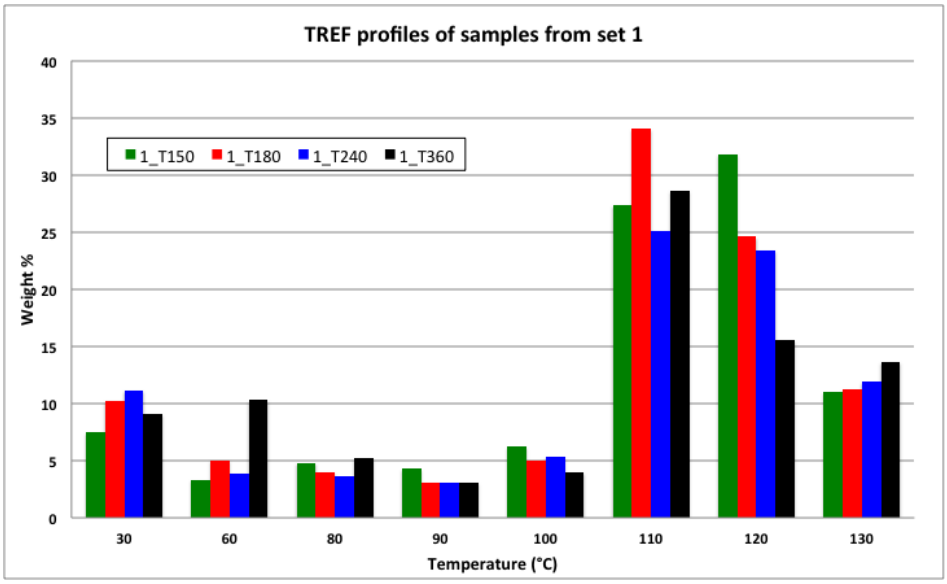

Figure 5.2 *Prep-TREF profiles of samples from set 1 with increasing ethylene content (1_T150 to 1_T360).*

Preparative-TREF was done on bulk samples to obtain more homogeneous fractions for further analysis and also to determine the effect of increasing ethylene incorporation on the composition distribution (Fig. 5.2). From this trend it can be seen that samples with lower ethylene content (1_T150 and 1_T180) have TREF profiles shifted towards higher temperatures and less weight% of the fractions at the lower temperatures, indicative of greater crystallizability, compared to the other samples with higher ethylene contents (1_T240 and 1_T360). It is also observed that the relative weight percentages of the 30-80 °C fractions increases with increasing ethylene content, most possibly due to the development of ethylene-propylene copolymers with reduced crystallizability in samples with increasing ethylene incorporation. The results from further characterization of these fractions will be described in Section 5.3.3.

Furthermore, there is a decrease in the 120 °C fractions with higher crystallizability simultaneous with the increase in the 30 °C fractions. This is due to the replacement of some

propylene by ethylene in the second reactor as increasing amounts of ethylene are incorporated during the transition, thereby reducing the propylene crystallizability. There is also an increase in the 130 °C fraction with increasing ethylene content, which could include a small amount of highly crystalline polyethylene in this fraction.

5.3.1.2 Development of chemical composition distribution

^{13}C solution NMR experiments were carried out on the bulk samples to develop an understanding of how the chemical composition of the polymer develops with increasing amounts of ethylene incorporation. Carbon assignments for solution ^{13}C NMR are shown in Figure 5.3.

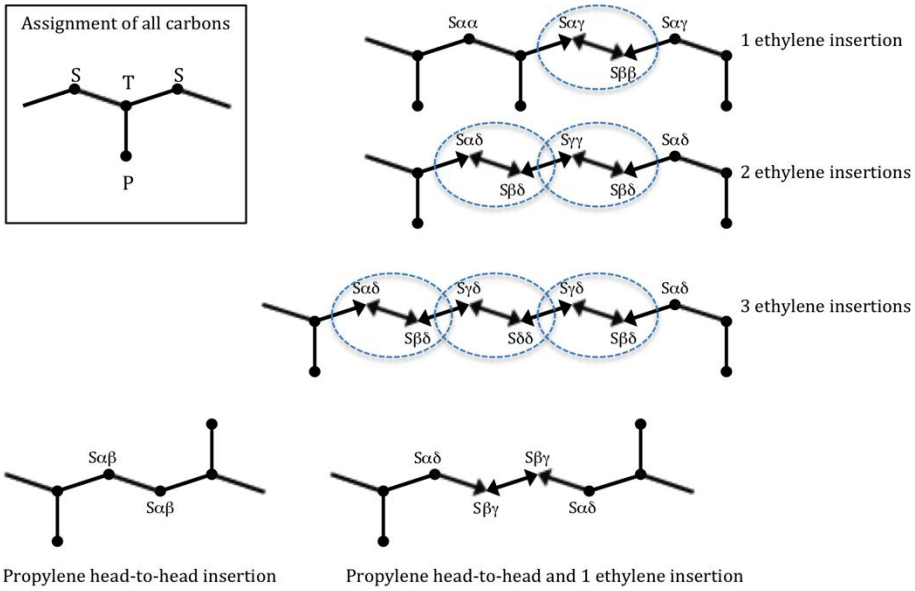

Figure 5.3 *Notation used in the ^{13}C NMR results for assignment of primary, secondary and tertiary carbons (left) adapted from Carman and Wilkes [20] as well as the assignment for various different types of carbons present in propylene-ethylene copolymers (right) adapted from Ray et al. [9].*

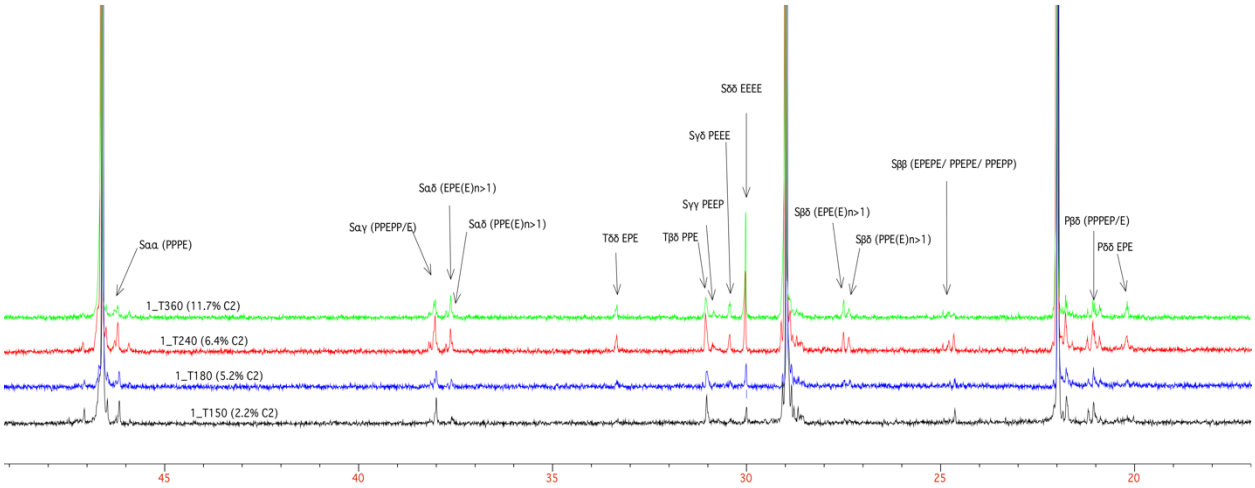

Figure 5.4 *Overlay of solution NMR spectra of samples from set 1.*

In the ^{13}C NMR spectra of the bulk samples (Fig 5.4), three major peaks associated with polypropylene can be distinguished: the methyl peak at approximately 22ppm, the methine peak at 28.5ppm and the methylene peak at 46.5ppm [21]. There are also a few smaller peaks relating to mixed ethylene and propylene sequences.

From the spectrum overlays as well as calculated triad and tetrad distributions (Table 5.1, Fig. 5.5) there is an observed preference in the development of continuous ethylene sequences, above that of isolated ethylene insertions or mixed ethylene/propylene sequences. This is clear when comparing the relative peak intensities of the Sδδ peak at a chemical shift of 30 ppm (≥3 ethylene insertions) to that of the Sββ peaks at 24.6-24.9 ppm (single ethylene insertion). The same is observed for the Sαδ peaks at 37.6–37.7 ppm (≥2 ethylene insertions) which increases rapidly with increasing sample ethylene content compared to the Sαγ peaks at 37.9–38.1 ppm (single ethylene insertion), as well as the growth of the Sδδ peak (EEEE) relative to that of the Syγ peak (PEEP) at 30.8 ppm, which supports the other observations that longer continuous ethylene sequences are found with increasing ethylene incorporation. It is therefore evident that at low ethylene contents some alternating sequences are present, but at higher ethylene contents, ethylene preferentially incorporates in longer continuous sequences. This corresponds with the higher reactivity of ethylene monomer compared to that of propylene, as well as the increased availability of ethylene at the active sites at higher ethylene contents.

When comparing tertiary carbons however, there is a clear increase in the Tδδ peak (EPE sequences), compared to the Tβδ peak (PPE sequences), which stays constant indicating at least some localized random ethylene incorporation. This is also observed for the ratio of the Sαα

carbons at 46.2 ppm and 45.9 ppm representative of EPPE and PPPE sequences respectively. For these sequences the development seems to be purely ethylene dependant, as one would expect for a statistical process. The primary carbons also indicate a growth of ethylene rich sequences such as EPE (Pδδ peak at 20.1 ppm) and EPPEP/E (Pβδ peak at 20.8 ppm) relative to sequences containing more P units such as PPPEP/E (Pβδ peak at 21 ppm), consistent with the trend of increasing ethylene content of these samples.

The calculated ethylene and propylene contents as well as triad and tetrad distributions are given in Table 5.1. These values were calculated using a macro developed by S. Joubert, Sasol Technology, Sasolburg to ensure reproducibility and consistency of spectral analysis. Details on the calculation of specific sequences and monomer contents are given in Chapter 3.

Table 5.1 Microstructural analysis (^{13}C NMR) for set 1 bulk samples – normalised triads and tetrads.

		1_T150	1_T180	1_T240	1_T360
mol %P		97.9%	94.8%	93.7%	88.3%
mol %E		2.1%	5.2%	6.3%	11.7%
Triads	PPP	95.8%	91.3%	89.2%	82.0%
	PPE	1.9%	3.1%	3.3%	4.2%
	PEP	0.9%	1.3%	1.9%	2.1%
	PEE	0.6%	1.1%	2.0%	3.7%
	EEE	0.5%	2.2%	2.5%	6.0%
	EPE	0.3%	1.0%	1.2%	2.0%
Tetrads	PPPP	96.7%	94.3%	92.4%	88.1%
	PPPE	2.1%	2.5%	3.4%	3.4%
	EPPE	0.3%	0.2%	0.8%	0.8%
	PEEP	0.3%	0.6%	0.7%	1.3%
	PEEE	0.3%	1.2%	1.2%	2.6%
	EEEE	0.3%	1.2%	1.5%	3.8%
Ne	Ne	1.7	2.2	2.2	2.9
Np	Np	77.9	42.0	32.3	21.9

The observations made from the NMR spectra are confirmed by the calculated sequence distributions in Table 5.1 as well as the grouping of tetrads with blocky ethylene sequences (PEEE + EEEE) and isolated sequences (EPPE + PEEP) as shown in Fig. 5.5A. From the normalised tetrad data it is confirmed that there is a rapid linear progression of continuous ethylene sequences (PEEE + EEEE), in contrast to shorter or isolated ethylene insertions (EPPE

+PEEP), which seems to reach a plateau in the development trend with increasing ethylene incorporation (Fig 5.5B).

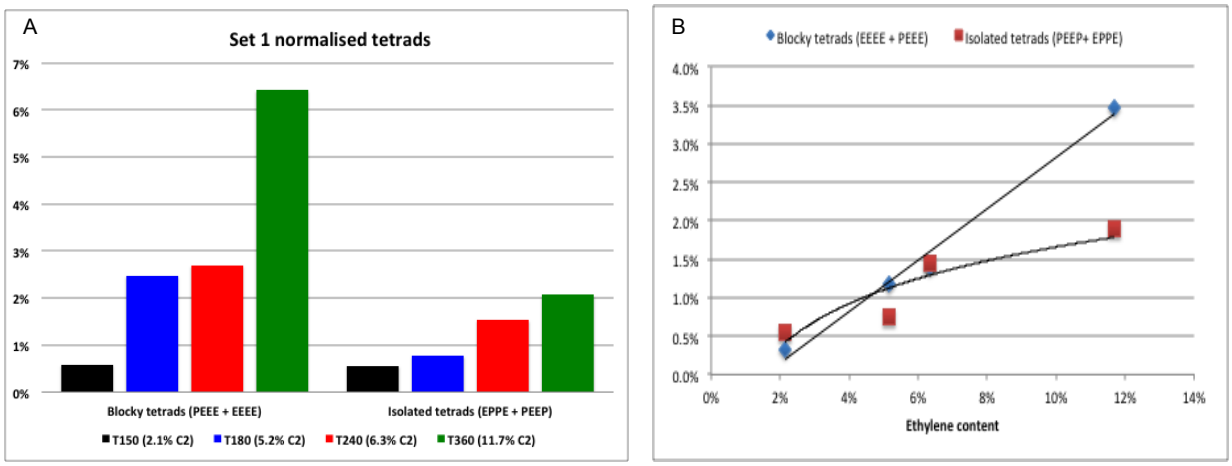

Figure 5.5 *Development of blocky and isolated ethylene sequences for set 1 bulk samples (A) and for increasing ethylene content (B).*

Considering changes in the number average propylene sequence length (Np) with increasing ethylene content (Fig. 5.6A), it is observed that initially the propylene sequence length is significantly reduced at low ethylene contents, with the trend reaching a horizontal asymptote at higher ethylene contents. These results represent statistical chain properties and are consistent with isolated ethylene insertions at low ethylene contents and subsequent continuous ethylene insertions at higher ethylene contents, resulting in the flattening of the trend. In contrast to this, there is almost a linear trend for the development of the number average ethylene sequence length (Ne), as indicated in Fig. 5.6B, but the average ethylene chain length is still quite short as the total ethylene contents of these polymers are low (<13 mol%).

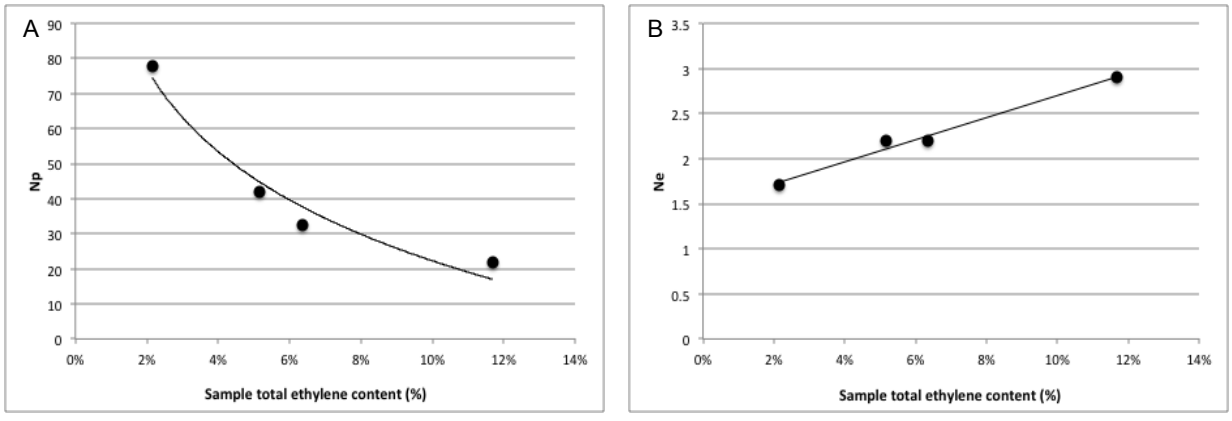

Figure 5.6 *Changes in the number average propylene sequence length (A) number average ethylene sequence length (B) with increasing ethylene contents.*

5.3.1.3 Changes in chain conformation and molecular dynamics for set 1

Complementary to the average chain microstructure information obtained by solution NMR (as described in Section 5.3.1.2), solid-state NMR can be used to obtain information on the actual chain conformations in the solid state. This can be specifically applied to the multiphase solid polymers, such as the ones analysed in this study, because sections of the polymer in different environments have different molecular dynamics and relaxation times, thus enabling the observation of crystalline, amorphous and rigid-amorphous areas separately.

In previous experiments on LLDPE, solid-state experiments with cross polarization and magic angle spinning (CPMAS) indicated a sharp peak at 32.9 ppm representative of trans-trans methylene sequences of polyethylene in the orthorhombic crystalline form as well as a broader peak at 31.0 ppm representative of non-crystalline phases [22].

In contrast with polyethylene and its copolymers with α-olefins, which has been fairly well characterised, only few reports on the solid-state characterization of propylene-ethylene copolymers exist and none could be found to date that characterised the type of polymers used in this study. Alamo *et al*. [13] conducted an extensive study of calculating and experimentally confirming the solid-state assignments of peaks in crystalline and non-crystalline regions for a series of random propylene-ethylene copolymers synthesised with metallocene catalysts. The polymers used in the study of Alamo *et al*. can be considered as model polymers due to the homogeneity obtained with metallocene catalysts; hence these peak assignments are used as reference and are given in Table 5.2 below.

Table 5.2 Solid-state chemical shifts for random propylene-ethylene copolymers synthesised by metallocene catalyst as assigned by Alamo et al. [13]

Carbon source	Carbon type	Chemical shifts (ppm)
Propylene backbone	Methyl (CH_3)	22.1
	Methine (CH)	26.7
	Methylene (CH_2)	44.5
Comonomer (ethylene defect)	Methylene (CH_2)[a]	24.5
	Methine (CH)	31.1
	Methylene (CH_2)	34.7
	Methylene (CH_2)	39.2
Polypropylene stereo- and regio defects	*mrrmm*-stereodefect	16.0, 30.1, 33.1, 47.9 & 50.6
	2,1 erythro-regiodefect	11.5, 31.6, 33.1 & 35.3

[a] When the methyl pendant group is absent due to an ethylene insertion

The CPMAS solid-state NMR experiments conducted on the bulk samples of set 1 (Fig. 5.7) clearly display two polyethylene peaks (amorphous at 31 ppm and crystalline at 33 ppm) for the samples with higher ethylene contents: samples 1_T240 and 1_T360 (6.4-11.7 mol% ethylene), indicating that even for the relatively low total ethylene contents studied here, ethylene is not only present in amorphous regions but also in crystalline environments if a sufficient amount of ethylene is present.

Alamo *et al.* [13] found an ethylene partitioning coefficient of 0.42, which stayed fairly constant irrespective of total ethylene content, which also confirmed that while a significant amount of ethylene is rejected from crystalline structures formed by the copolymer, there are also ethylene carbons present in crystalline areas (note that a partitioning coefficient of 1 indicates full acceptance and 0 full rejection). The 1_T150 and 1_T180 samples of set 1 probably have too low ethylene contents for significant peaks to be detected by this lower resolution method, especially in the bulk. The increase in both the crystalline and amorphous peaks for the 1_T240 and 1_T360 samples is also consistent with the increase in the overall ethylene content of these samples. Furthermore the ethylene appears to be present in almost similar amounts in crystalline and amorphous environments in the 1_T360 sample with the highest ethylene content (11.7%). For the 1_T240 sample (6.4% ethylene), there is less ethylene in crystalline regions than in amorphous areas. Consistent with the solution NMR results, it seems that for set 1, ethylene is incorporated quite randomly at low contents, resulting in a preferential partitioning in amorphous areas as observed by solid-state NMR. As the ethylene content increases and longer ethylene sequences start to form (as shown by solution NMR), there is also a growth of ethylene sequences in crystalline regions (as indicated by solid-state NMR).

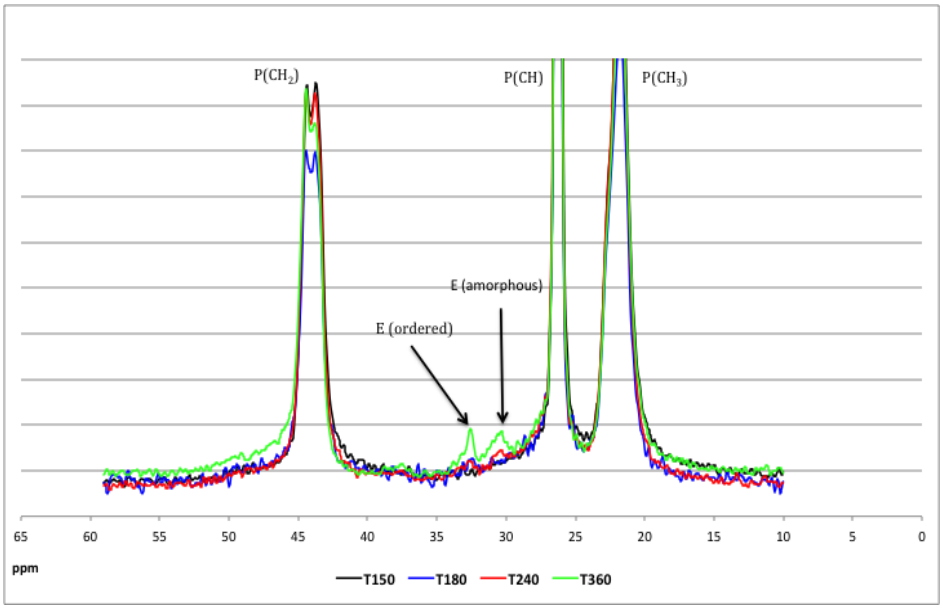

Figure 5.7 *Overlay of solid-state NMR (CPMAS) profiles for samples from set 1 with increasing ethylene content.*

Peak splitting is observed for the methylene (CH_2) peaks of polypropylene between 43 and 45 ppm (Fig. 5.7), indicating that these carbons are experiencing two distinct environments. Furthermore a broadening of the methylene peak, consistent with increased heterogeneity, is observed with increasing ethylene incorporation.

It is well known that pure isotactic polypropylene can exist in various allomorphs (α, β, γ and smectic), which all have a localised 3_1 helix conformation, but differ in terms of the crystal packing of the helices [12, 13, 21-25]. In the α-allomorph, helices of alternating handedness stack together, causing the methylene and methyl carbons to experience two different or non-equivalent environments resulting in a 2:1 methylene peak ratio. In the β-allomorph, helices of the same handedness stack together, hence the methylene carbons are all exposed to equivalent environments and only one peak is observed.

Comotti *et al.* [12] conducted a study on a mixture of isotactic and syndiotactic polypropylene where the methylene peak region of isotactic crystalline polypropylene was deconvoluted into three peaks; one at 44 ppm representative of a disordered α phase (α_d) and two peaks at 44.7 and 43.8 ppm respectively, representing the ordered α phase (α_2), with an expected 2:1 ratio as explained previously for a pure crystalline form. The principle behind the work to follow was that any defect influencing crystal packing interactions should cause a deviation of the 2:1 ratio.

For the set 1 samples, deconvolution of the methylene peak was carried out, the α_2 peak ratios calculated and plotted against total ethylene content (Fig. 5.8). A clear trend of decreasing α_2 peak ratios with increasing ethylene content is observed and it can be concluded that with increasing incorporation of ethylene, the regular crystal packing is disrupted to a greater extent. It should also be noted that even in standard isotactic polypropylene, the peak ratio is slightly less than 2, due to the presence of a small amount of atactic polypropylene sequences, which can also disrupt regular crystal packing, however this contribution is considered to be constant for all the samples in the range.

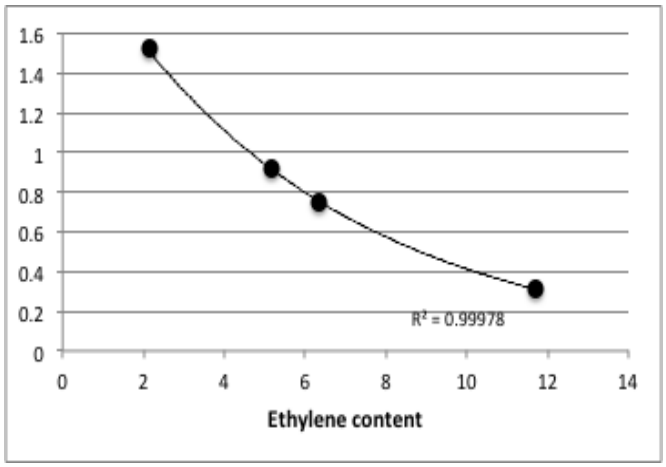

Figure 5.8 *Plot of the α_2 peak ratios for set 1 samples with increasing total ethylene content.*

In order to draw valid conclusions from the deconvolution of the split methylene peak, the α-allomorph should be the sole contributor to this trend. It has been shown previously that a complex polymorphism between the α- and γ-allomorphs can exist in ethylene-propylene copolymers, influencing the 'up' and 'down' orientation of helices in the unit cell of the crystal (Fig. 5.10). This is influenced by thermal treatment of the sample and it was observed that the γ-allomorph started to form upon slow crystallization from the melting point [25]. The nascent powder samples used for the solid-state analysis did however not have any thermal history, thus it was doubtful whether a significant amount of the γ-allomorph would be present in these samples. However to verify this, X-ray diffraction (XRD) was performed on all bulk samples (Fig. 5.9). Films that were quench cooled (to prevent thermal effects from influencing the formation of the γ-allomorph) were prepared from the powder samples for XRD analysis.

Typical X-ray diffraction patterns obtained for the α-, β- and γ-allomorphs as well as their chain conformations are shown in Fig. 5.10. The shaded areas in Fig. 5.10 indicate the diagnostic

peaks used to identify the various allomorphs. For the α-allomorph it is the peak at 2θ=18.6 ° and for the γ-allomorph 2θ= 20 °. From Fig. 5.9, it can be seen that no peaks are present at 20 ° and all the other peaks associated with the different crystal faces present in the α-allomorph are observed. Hence it can be concluded that the disruption of the α_2 peak ratios is due to the effect on chain packing from the α-allomorph alone. In the XRD trends, peak broadening with increasing sample ethylene content is also observed, supporting the solid-state observation of an increase in the heterogeneity of crystalline structures with increasing ethylene incorporation.

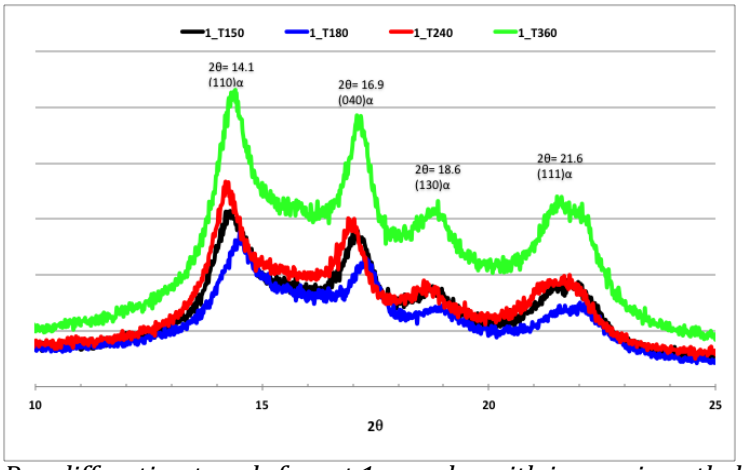

Figure 5.9 *X-Ray diffraction trends for set 1 samples with increasing ethylene contents.*

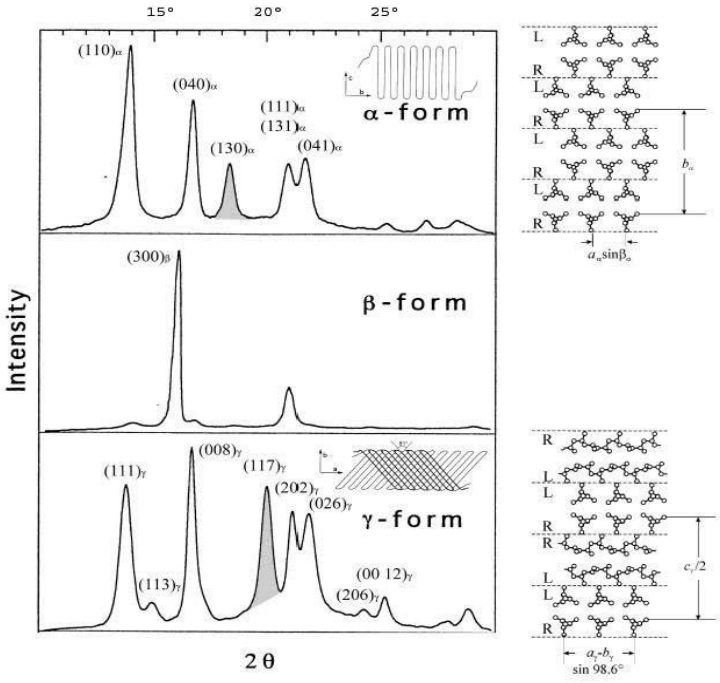

Figure 5.10 *Typical powder X-Ray diffraction patterns for the α, β and γ polymorphs with drawings of corresponding chain conformations [24].*

The solid-state NMR results discussed in the previous section represent samples that have undergone cross polarization between carbon and hydrogen atoms. Due to the nature of this technique, which is dependent on proton density and mobility, peaks representing carbons with low mobility, such as the peak resulting from methine (CH) carbons, appear much sharper as it is central in the carbon backbone of the molecule and movement is hindered by CH_2 and CH_3 groups attached to it. This technique is therefore sensitive to components with low mobility and resolution is lost when some mobility is introduced, as can be observed by the broadening of the CH_2 group with increasing ethylene incorporation. The peak associated with the methyl pendant group (CH_3) is also broader relative to the methine peak due to its higher mobility as it is not located within the backbone, where movement is restricted.

There is however another solid-state technique, termed dipolar dephasing (represented by the IDREF spectra in the section to follow) which allows for the selective visualisation of areas with higher mobility. The principle of this technique relies upon dipolar carbon-proton interactions and for the carbons studied here, with fairly similar proton densities, there is a faster decay of strongly dipolar coupled regions associated with regions of lower mobility. Conversely, since mobility weakens the dipolar interaction, carbons experiencing higher mobility, decay slower and are observed in the dipolar dephasing spectra. This technique was therefore applied to shed some further light on the observed differences in the polypropylene methylene region and ordered-to-amorphous ethylene partitioning.

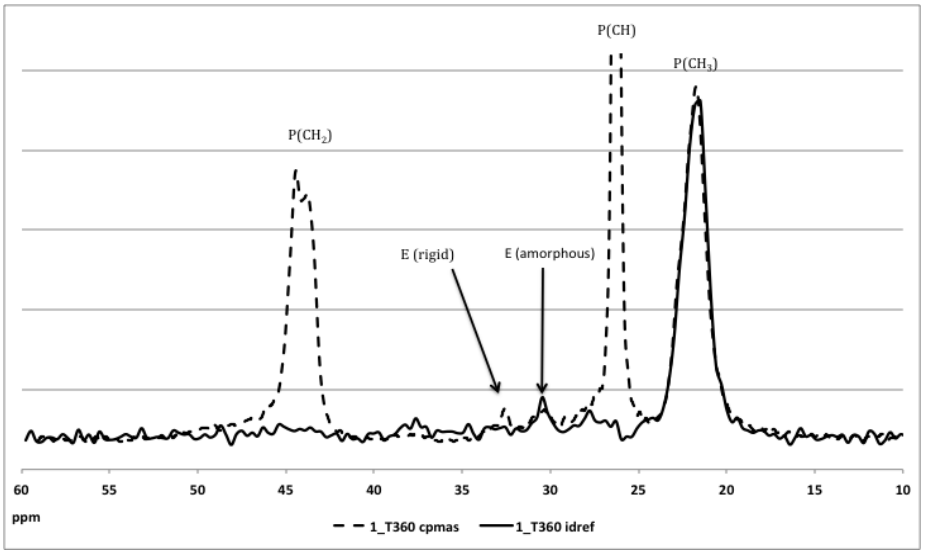

Figure 5.11 *Overlay of solid-state CPMAS (dashed line) and IDREF (solid line) trends of 1_T360, indicating the rigid and mobile contributions respectively.*

In Fig. 5.11 the dipolar dephasing trend is overlaid on the cross polarization trends for the set 1 sample with the highest ethylene content (1_T360). A few observations from the differences between these trends can be made: First, the methylene and methine carbons, almost completely disappear in the IDREF trends. This is to be expected as these carbons form the polypropylene backbone and are not expected to be very mobile. Second, in all samples the methyl pendant group (CH_3) of polypropylene is represented as a pronounced peak as it is quite mobile. Third, the ethylene peak in amorphous environments at approximately 31.1 ppm is also present in the IDREF trend since these amorphous areas are expected to have some mobility. Furthermore, the peak representing ethylene in rigid environments is not present in the IDREF trend, clearly indicating that this type of ethylene carbon has low mobility and must be present within crystalline regions.

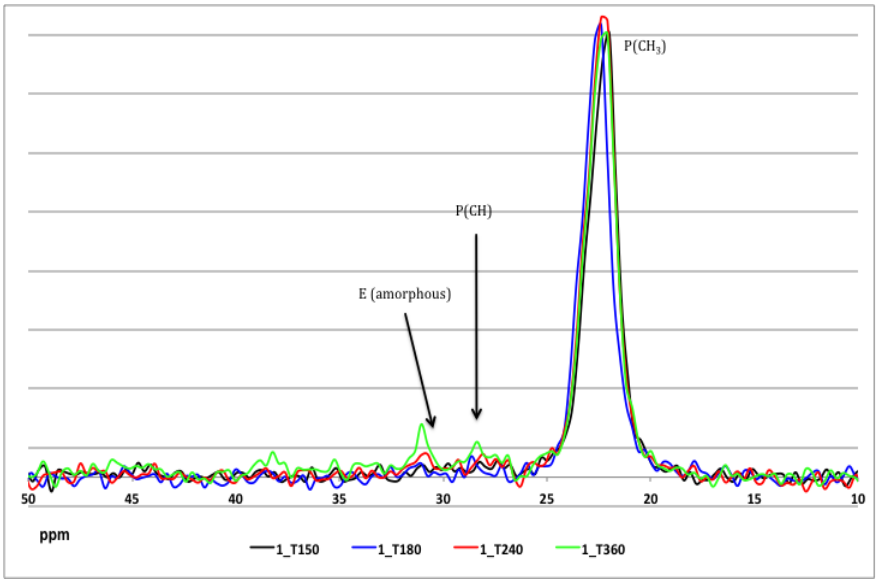

Figure 5.12 *Overlay of solid-state dipolar dephasing (IDREF) trends of samples with increasing ethylene content.*

Overlays of the IDREF curves of all the set 1 samples are shown in Fig. 5.12. It is observed that only those samples with higher ethylene contents (1_T240 and 1_T360 with 6.4 and 11.7 mol% ethylene respectively) display amorphous ethylene peaks, indicating that a certain minimum ethylene content needs to be present to achieve some local chain mobility.

Another interesting observation is that the methine peak, which normally should have low mobility, actually starts to appear in the IDREF curve indicating that some of these carbons start to experience mobility at high ethylene contents. When considering the position of the methine group in the carbon backbone of polypropylene, it is normally shielded by the methyl pendant group however, wherever ethylene is incorporated, the pendant group is absent, resulting in

methylene groups. Alamo *et al*., calculated the effect of one ethylene insertion on the affected methine carbon's chemical shift in their study and confirmed the experimental chemical shift at 24.5 ppm [13, 23]. For the sample with the highest ethylene content (1_T360), there is a shoulder observed at approximately 24.5 ppm on the peak representing the methyl group. The resolution of these bulk spectra is however not sufficient to draw any significant conclusions and therefore further work on this will be discussed in the solid-state analysis of the fractions in Section 5.3.3, focussing specifically on the contribution of the copolymers that are more prominent in the lower temperature fractions.

5.3.1.4 Conclusions on crystallinity and microstructural development for set 1

Changes in the overall polymer crystallinity with increasing ethylene content were investigated by SCALLS and the results corresponded well with the prep-TREF elution profiles. By means of SCALLS analysis, the presence of distinct components with different crystallinities was indicated for each sample, since at least two distinct melting transitions were observed per sample. This level of resolution was not obtained by TREF analysis. Since the samples used in this study represented sequential products obtained from a two-reactor system, subtle changes in sample crystallinity could be detected and a trend for attenuation of crystallinity during the development of the copolymer phase, could be established. The fact that the crystallinity of the first sample could be sufficiently altered by subsequent samples with increasing ethylene incorporation and that ethylene-dependent trends for this could be obtained, confirmed that there are complex interactions present between the products made in the first and second reactor, resulting in the improved physical properties normally observed for in-reactor alloys compared to their mechanical blend counterparts.

Solid-state NMR further confirmed the presence of such interactions in the bulk samples, by the observation that a significant amount of ethylene was found in both crystalline environments, relative to amorphous environments. This type of partitioning of ethylene sequences between both crystalline and amorphous environments was also observed by others directly by means of solid-state experiments performed on random copolymers [13]. Furthermore XRD experiments on ethylene-propylene copolymers showed differences in crystallinity and crystallite thickness that corresponded to changes in comonomer content [25-26] and supported the theory that at least some of the ethylene comonomer was included in the crystals. This emphasises the importance of the chemical composition of the copolymer phase produced in the second reactor.

These copolymers consist of amorphous rubbery components for improving impact resistance, but also semi-crystalline copolymers that control the dispersion of rubber throughout the homopolymer matrix, by being included to some extent within the crystalline structure – hence compatibilizing the rubber with the matrix. Supporting the compatibilization theory, it was observed in the rubber particle analysis in Chapter 4 that an increase in rubber particle size along with a decrease in inter-particle distances and particle distribution occurred with increasing ethylene contents. These semi-crystalline components are therefore of particular interest due to their specific function and highly heterogeneous nature and further characterization of these fractions will be discussed in Section 5.3.3 in this chapter.

Further evidence of the attenuation of crystallinity could also be found due to changes in the splitting of the solid-state methylene peaks with increasing ethylene content. Deconvolution of the methylene peaks indicated an increasing deviation from the ideal 2:1 α_2 peak ratio with increasing ethylene content, confirming a greater extent of disruption of the regular crystal packing. This was also confirmed by the broadening of the XRD peaks representative of the different α-allomorph crystal faces, indicating increased heterogeneity within the crystal structures with increasing ethylene content.

Comparison of different solid–state experiments capable of distinguishing between mobile and rigid components also indicated changes with increasing ethylene incorporation, confirming the presence of some of the ethylene carbons in crystalline environments (from the observed difference between the mobile and rigid trends), but also indicating a slight increase in the mobility of methine groups. This is an interesting observation as methine carbons are normally shielded in the polypropylene 3_1 helix, and are expected to have very low mobility. Therefore the fact that some of the methine carbons are starting to experience some localised mobility is indicative of changes in the crystal structure.

Investigation into the development of ethylene sequences by means of solution NMR indicated that longer ethylene sequences developed more rapidly than isolated ethylene insertions, with increasing ethylene content. This is consistent with the known relative differences in reactivity between ethylene and propylene monomer and is highlighted by solution NMR, which is mostly a statistical method. A linear trend was observed for the development of blocky sequences in contrast to the development of isolated sequences that reached a plateau at higher ethylene contents. These observations are also consistent with the significant reduction in number

average propylene sequence length up to a certain ethylene content, whereas a linear development of the number average ethylene sequence length was observed.

Relating the solution NMR results to those of solid-state NMR, the development of longer continuous ethylene sequences, could explain the observed presence of ethylene in crystalline environments. Furthermore, the interaction of these components with the isotactic polypropylene could be related to the observed changes in the crystallinity and physical performance of the bulk samples as described in Chapter 4.

5.3.2 Ethylene-dependent changes in crystallinity and microstructure for set 2

5.3.2.1 Attenuation of crystallizability with increasing ethylene incorporation

SCALLS heating trends obtained upon second heating with a blue laser are shown in Fig. 5.13 below for the set 2 samples. Compared to the slope of the baseline sample with the lowest ethylene content (2_T60), the other samples appear to start melting at lower temperatures, indicative of reduced crystallinity. This is also consistent with ethylene incorporation, indicating that there is some disruption of the crystalline structures that were present before copolymerization along with increasing ethylene content. For this set, all samples display two distinct temperature transitions, except for the 2_T90 sample, which seems to melt at a higher temperature and display only one peak associated with melting behaviour (Fig. 5.13B). It is also interesting to observe that for the samples with higher ethylene content (2_T120 and 2_T150), small low temperature peaks and shoulders start forming below the main melting peak at approximately 113 °C. This is most pronounced for the 2_T120 sample indicating a distinct portion of the sample with reduced crystallinity. It was also observed for this specific sample in the previous chapter that it had a slightly reduced impact to stiffness balance, compared to the trend followed by the rest of the samples and contained a large number of closely dispersed rubber particles. Therefore it is possible that the low crystalline component in this sample, as identified by SCALLS could be responsible in part for its mechanical behaviour. Most of the samples also display a high temperature peak above 115 °C, indicating the presence of a highly crystalline component in each of these samples as well. From this data, the main melting transition was identified as occurring between 110 and 120 °C, with the melting of smaller crystals at slightly lower temperatures (around 105 °C). Hence the selected prep-TREF temperatures of 30, 60, 80, 90, 100, 110, 120 and 130 °C would also apply to this set, to obtain sufficiently homogeneous fractions for further separation and characterization.

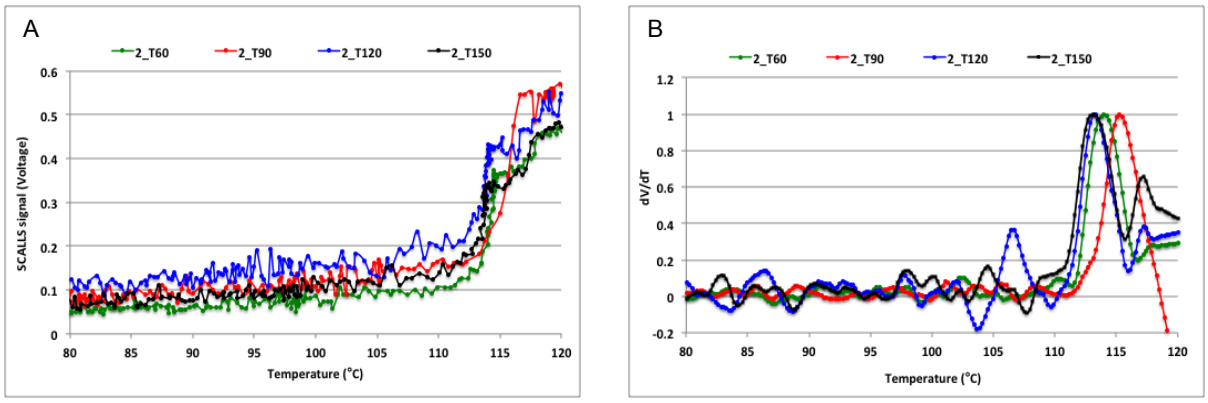

Figure 5.13 *SCALLS heating trends: A (raw voltage signal) and B (first derivative) obtained by blue laser for samples of set 2 with different ethylene contents.*

Similar to what was observed by SCALLS, the prep-TREF profiles (Fig. 5.14) also indicate that the 2_T90 sample appears to be shifted towards higher elution temperatures and that the 2_T120 sample is shifted to slightly lower elution temperatures, relative to the other samples, highlighting the similarities in the results obtained with these two techniques. As mentioned in the previous section, the SCALLS method however provides better resolution that can't be obtained by other methods in the sense that it can distinguish between different components with different levels of crystallinity.

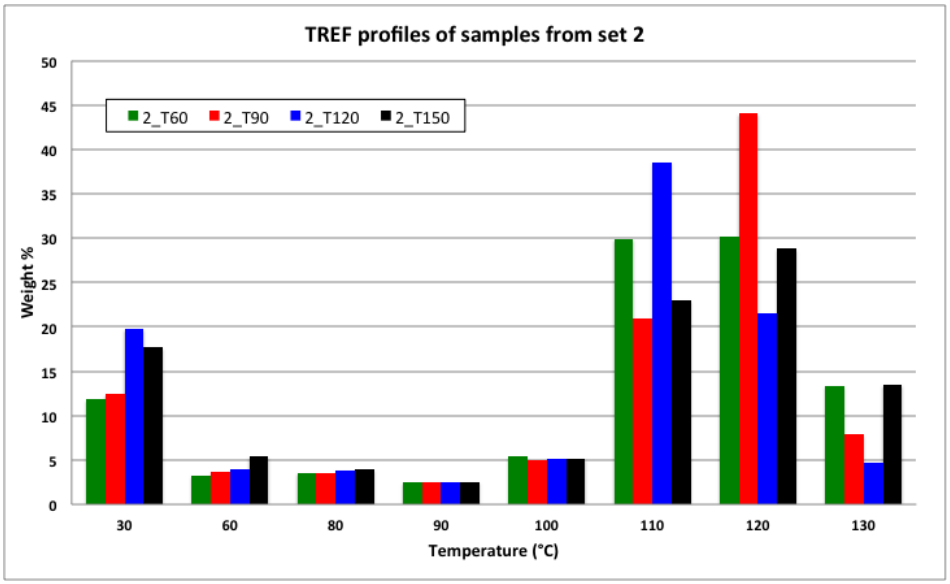

Figure 5.14 *Prep-TREF profiles of samples from set 2 with increasing ethylene content (2_T60 to 2_T150).*

In the prep-TREF profiles, the general trend of loss in weight% of the higher temperature fractions (> 110 °C) along with a gain in the weight% of the low temperature fractions (30 °C and 60 °C) is observed with increasing ethylene incorporation. Judging by the relative weight percentages of sample in each fraction, it also seems that most of each sample is distributed in the 110 to 120 °C fractions, followed by the 30 °C fraction, with a very small percentage of the samples present in the 60 to 100 °C fractions. This narrow distribution was also observed in the SCALLS heating trends (Fig. 5.13B). Furthermore, the 80, 90 and 100 °C fractions stay fairly constant regardless of the total ethylene content of the sample. When considering that these fractions at least have some crystallinity and are expected to act as a compatibilizer between the amorphous rubber (30 °C fraction) and isotactic polypropylene (>100 °C fractions), it will be interesting to observe differences in the microstructure and chemical composition of these fractions for samples with increasing ethylene contents. This will be discussed in more detail in Section 5.3.3.

5.3.2.2 Development of chemical composition distribution

To develop an understanding of the underlying microstructure responsible for the above observations on bulk sample crystallinity, as discussed in the previous section, ^{13}C solution and solid state NMR was done on the bulk samples. The notation for different carbons was described in section 5.3.1.2.

The solution NMR spectra for bulk samples from set 2 is shown in Fig. 5.15. As observed previously, the three main peaks are from the methyl- (22 ppm), methine- (28.5 ppm) and methylene carbons (46.5 ppm) from polypropylene respectively. This is to be expected as at least 80 mol% of these bulk polymers consist of propylene homopolymer. Based on peak intensities, the next most prominent contributor to these spectra are the Sδδ peaks at 30 ppm (≥3 ethylene insertions), representative of polyethylene. The increase in the Sδδ peaks is also consistent with the increase in the total ethylene content of these samples. A few smaller peaks, representative of different propylene and ethylene sequences are also observed.

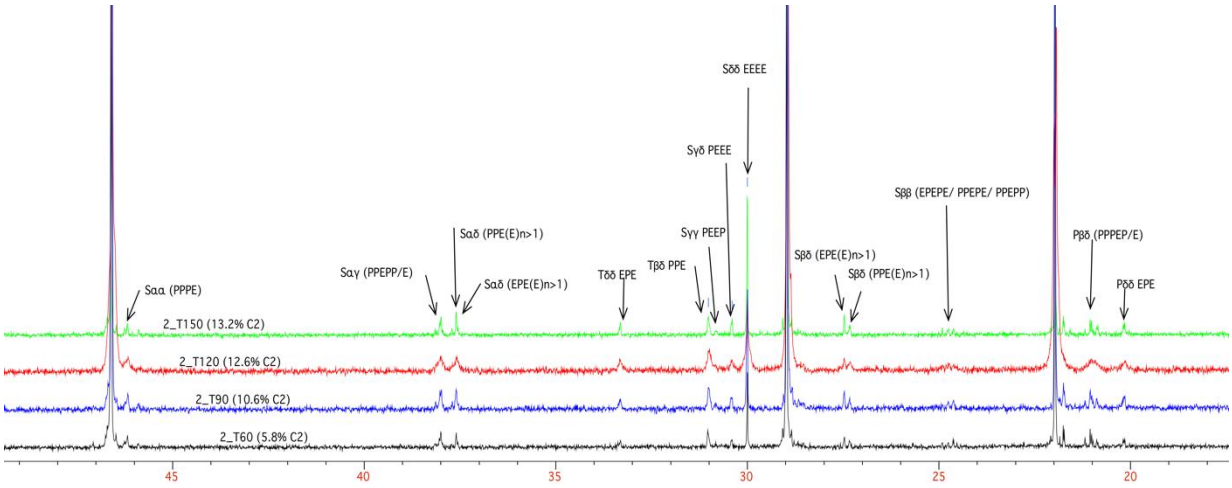

Figure 5.15 *Overlay of solution ^{13}C NMR spectra of samples from set 2.*

Comparing the relative peak intensities of the Sδδ peak at 30ppm to the Sββ peaks at 24.6-24.9ppm (representative of sequences with a single ethylene insertion), it is also clear that in the development of the copolymer phase of these samples, longer ethylene sequences form more rapidly than sequences containing isolated ethylene units. This is also confirmed by the triad and tetrad distributions in Table 5.3 and Fig. 5.16. These results however indicate that although there is a rapid initial development of blocky sequences; this development trend seems to reach a plateau at the higher ethylene contents.

Apart from the pronounced development of the Sδδ peak, there doesn't appear to be much of a progression in the other sequences with increasing ethylene contents. Comparing the Sαδ peaks at 37.6–37.7 (≥2 ethylene insertions) to the Sαγ peaks at 37.9–38.1 ppm (single ethylene insertion) the relative ratios of these peaks stay fairly constant with an increase in ethylene content. It is also clear that there is a significant amount of longer ethylene sequences present. This is evident by comparing the relative intensity of the Sγδ peaks at 30.4ppm (representing PEEE sequences) to those of the Sγγ peaks at 30.7ppm (representing PEEP sequences) for all ethylene contents in the range. The same is true for the two Sβδ peaks between 27-28ppm, and, where the Sβδ peak representative longer ethylene sequences ($EPE(E)_{n>1}$) is consistently higher than the Sβδ peak representing ($PPE(E)_{n>1}$) sequences. There also doesn't appear to be significant changes in the ratio between the two Sαα peaks (PPPE and EPPE) at 46ppm; although the PPPE peak is more pronounced than the EPPE peak, as would be expected considering the total propylene content in these samples, the relative ratio of the two peaks stays the same regardless of ethylene content. These observations can also be related to the

prep-TREF results, which indicated that the sample distribution between the semi-crystalline fractions from 80 to 100 °C stays constant regardless of ethylene content.

Table 5.3 Microstructural analysis (^{13}C NMR) for set 2 bulk samples– normalised triads and tetrads.

		2_T60	2_T90	2_T120	2_T150
mol %P		94.2%	89.4%	87.4%	86.8%
mol %E		5.8%	10.6%	12.6%	13.2%
Triads	PPP	95.8%	91.3%	89.2%	82.0%
	PPE	1.9%	3.1%	3.3%	4.2%
	PEP	0.9%	1.3%	1.9%	2.1%
	PEE	0.6%	1.1%	2.0%	3.7%
	EEE	0.5%	2.2%	2.5%	6.0%
	EPE	0.3%	1.0%	1.2%	2.0%
Tetrads	PPPP	92.8%	89.4%	87.1%	85.5%
	PPPE	3.0%	3.2%	3.4%	4.5%
	EPPE	0.8%	0.8%	1.7%	1.9%
	PEEP	0.5%	0.7%	0.3%	0.8%
	PEEE	1.0%	2.0%	2.7%	2.4%
	EEEE	2.0%	3.9%	4.7%	5.0%
Ne	Ne	2.6	2.9	2.6	3.2
Np	Np	39.9	24.5	16.5	20.1

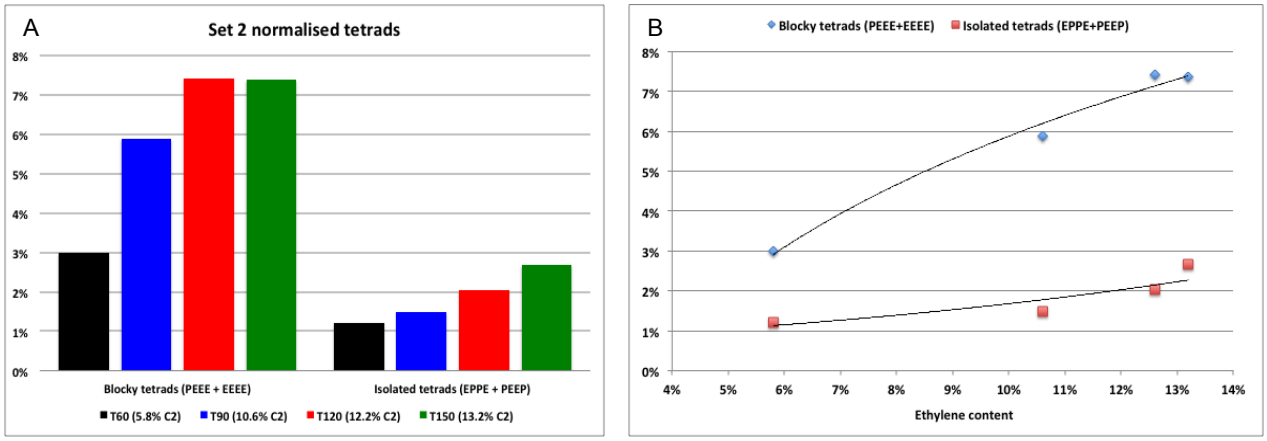

Figure 5.16 *Development of blocky and isolated ethylene sequences for set 2 bulk samples (A) and for increasing ethylene content (B).*

Considering changes in the number average propylene (Np) and ethylene (Ne) sequence length with increasing ethylene incorporation for set 2 (Fig. 5.17), there is a significant decrease in the propylene sequence length, as would be expected for increasing ethylene contents, along with a

slight increase in the number average sequence length. In these trends the 2_T120 sample again doesn't seem to exactly match the existing trend and shows both a reduced number average propylene and ethylene sequence length compared to the other samples. As this is a statistical observation, it could be proposed that on average a typical 2_T120 polymer chain would contain a more random distribution of propylene and ethylene, which would account for the lower crystallinity component observed by SCALLS as well as the lower temperature shift in the TREF trend. Furthermore this is also reflected in the high number of rubber particles and short inter particle distances observed for the 2_T120 moulded samples. This average increase in random distribution is not observed at tetrad level as the measurement is limited to a small number of carbons in sequence.

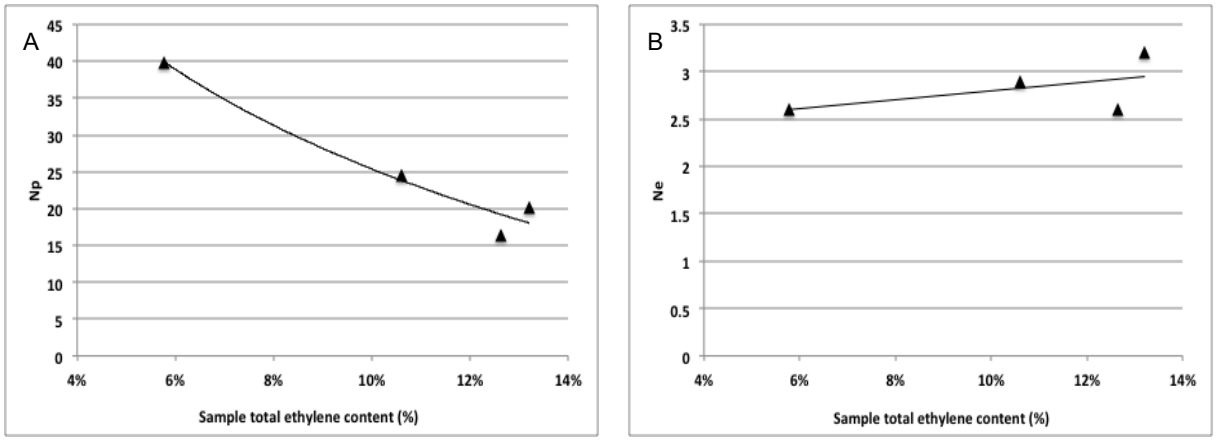

Figure 5.17 *Changes in the number average propylene sequence length (A) and number average ethylene sequence length (B) with increasing ethylene contents for set 2.*

Based on the information from the solution NMR spectra, especially the development of the Sδδ (long ethylene sequence peak), one might expect a more pronounced Ne development. It should however be considered that solution NMR provides mostly statistical results and utilizes a relatively small detection window. Furthermore, solution NMR doesn't provide any information on how local sequences are linked or to which parts of the crystal structure these sequences belong. For this reason, solid-state NMR was also conducted on the bulk samples to provide complementary information on the chemical composition in relation to crystal structure.

5.3.2.3 Changes in chain conformation and molecular dynamics for set 2

Within the context of the solution NMR results, which showed a pronounced development of long ethylene sequences, relative to all other sequences, solid-state NMR was conducted on the bulk samples to determine how these sequences would be distributed within the bulk crystal

structure. The solid-state spectra for the set 2 samples are shown in Fig. 5.18. In these spectra, the polypropylene methyl and methylene carbon peaks indicate a broadening with increasing ethylene incorporation, consistent with increased sample heterogeneity as the ethylene content increases.

Furthermore, the peak representing ethylene in crystalline environments, is consistently higher than that of ethylene in amorphous regions, for all samples except the sample with the lowest ethylene content in the series, 2_T60 (5.8% ethylene). This is also consistent with the solution NMR observation that a significant amount of continuous ethylene sequences are already present in the samples with lower ethylene contents compared to isolated ethylene sequences (as indicated by the relative Sδδ peak to Sγγ peak ratio) and that this doesn't develop further with increasing ethylene content.

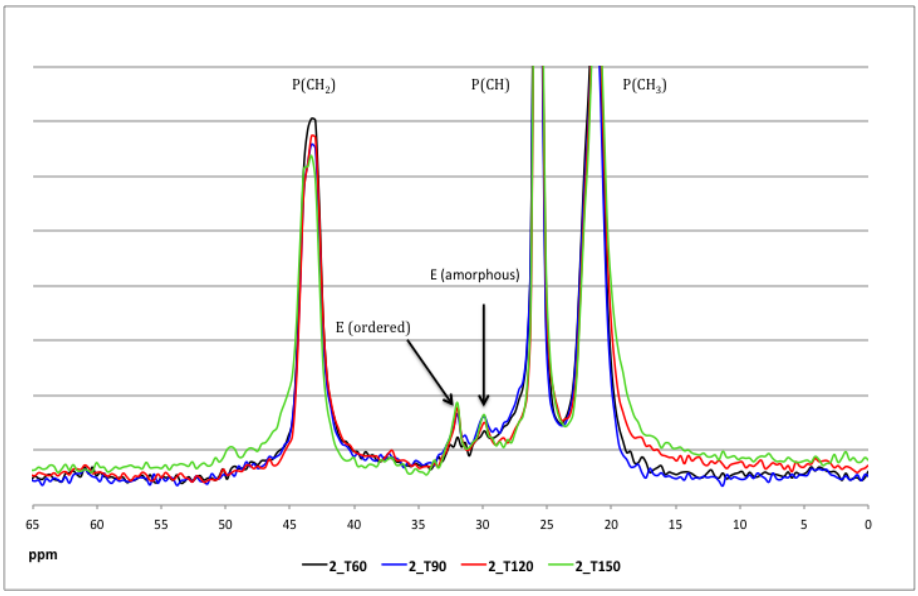

Figure 5.18 *Overlay of solid-state NMR (CPMAS) profiles for samples from set 2 with increasing ethylene content.*

As described previously, splitting of the methylene peaks of polypropylene is normally observed, which can be deconvoluted into three peaks of which two are in a 2:1 ratio when regular crystal packing of the ordered α_2 crystals occurs. Deviations from this perfect 2:1 ratio indicate disruptions of the regular crystal packing. From Fig. 5.18 the splitting of the methylene peak (45 ppm) is not observed for the set 2 samples. In fact, it was impossible to identify three methylene peaks in these samples and resultantly deconvolution of the methylene peaks could not be carried out to determine the deviation from regular crystal packing of the α-allomorph.

This observation may also be due to the presence of other allomorphs, which could influence crystal packing; hence X-ray diffraction was carried out on the bulk samples to identify the different allomorphs in these samples (Fig. 5.19). From the X-ray diffraction patterns in Fig. 5.19, it can be seen that only the α-allomorph is present in these samples as all the identified peaks correspond to the α-allomorph. It may be suggested, based on solid state results that even though the α-allomorph is clearly present, the crystal packing of the α unit cells may be disrupted to such an extent in these samples that the splitting of the methylene peak is lost. This is observed as a single broadened peak resulting from averaging of different signals due to heterogeneous environments brought about by lack of stereoregularity.

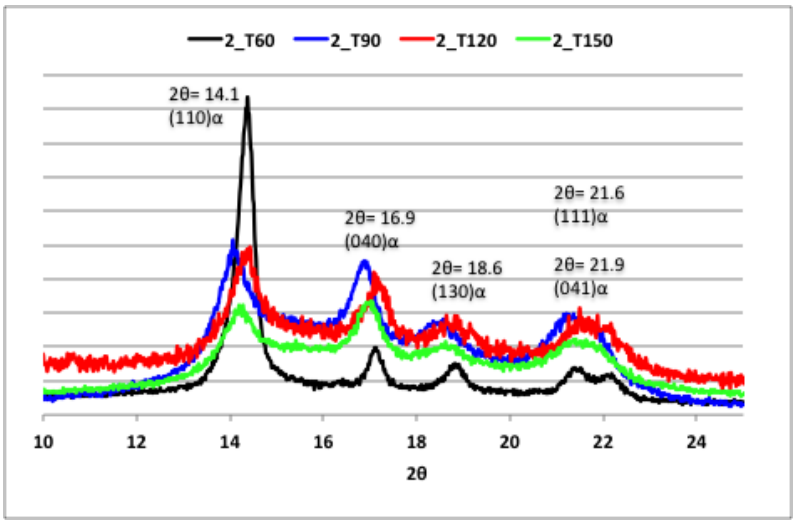

Figure 5.19 *X-ray diffraction patterns of set 2 samples.*

Comparing solid-state spectra generated by rigid (CPMAS) and mobile (IDREF) components as shown in Fig. 5.20 for the set 2 sample with the highest ethylene content (2_T150), it is clear that some of the polypropylene carbons that are considered to be rigid under normal circumstances, become mobile due to ethylene incorporation. As explained previously, the presence of the polypropylene methyl carbons and ethylene carbons in amorphous environments in the IDREF trends can be expected due to some local mobility of these carbons. Furthermore, some methine (CH) carbons start to display a mobile component, possibly due to the loss of shielding by the methyl carbons, as these are lost with increasing ethylene incorporation. It is also observed that a small portion of the methylene peaks (45 ppm) starts to display a peak representing carbons with higher mobility. Since the methylene carbons are part of the backbone it is interesting to see some mobility for these carbons. This observation together with the CPMAS observation concerning the deconvolution of the methylene peak,

suggests that the crystal packing is disrupted to such an extent that at least some of the methylene carbons are starting to experience mobility.

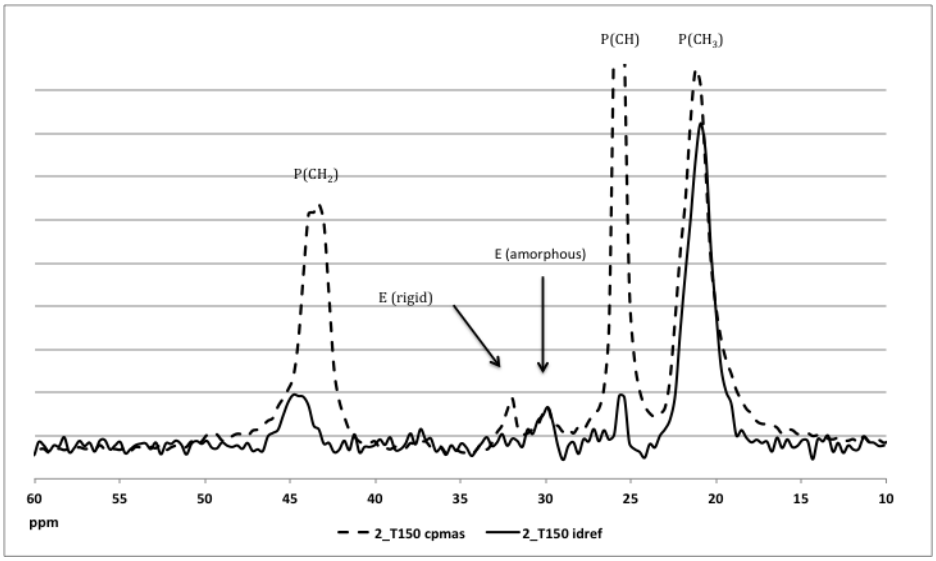

Figure 5.20 *Overlay of solid-state IDREF and CPMAS trends for 2_T150.*

Considering the IDREF trends for all the set 2 samples (Fig. 5.21), there is an increase in the number of small peaks with increasing ethylene content, with the exception of the sample with the lowest ethylene content (2_T60). There however isn't a progression in the development of any specific peak with increasing ethylene content, except for a methylene peak at ~45 ppm, which is only present in the sample with highest ethylene content, but is absent in the rest of the samples. The other two peaks present in these trends, which appear at relatively low ethylene contents and don't seem to develop further with increasing ethylene content, are the peaks at 31.1 ppm representing ethylene in amorphous regions and a methine peak at approximately 25 ppm. The line shape of the methyl peak also appears to be affected, which is also a function of changes in the crystalline environment surrounding these carbons.

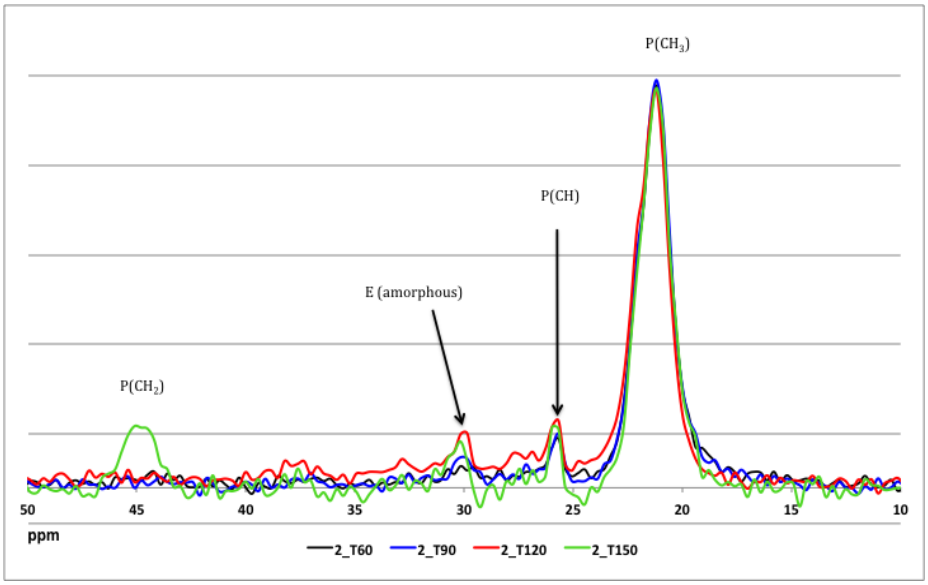

Figure 5.21 *Solid-state IDREF trends for set 2 samples with increasing ethylene content.*

5.3.2.4 Conclusions on crystallinity and microstructural development for set 2

Considering the crystallinity profiles obtained by SCALLS for the set 2 samples, it was clear that each of the samples contained various components with different crystallinities. The 2_T120 sample that showed some irregularity in terms of rubber particle size and distribution as well as impact strength behaviour, was also shown by SCALLS to contain a significant amount of a lower crystallinity component. At least one main crystalline component with a fairly narrow distribution was identified for all samples between 110 and 115 °C, along with smaller high- and low temperature components, for all samples except the 2_T90 sample that only displayed one component, which melted at a slightly higher temperature. This narrow distribution for the 2_T90 sample was also observed in the prep-TREF trends. From the TREF elution profiles it was observed that the weight percentage of the sample in the high temperature fractions (> 100 °C) was reduced with increasing ethylene content, along with an increase in the weight percentage of 30 °C fractions. There didn't appear to be significant ethylene dependent changes in the sample distribution for 80-100 °C fractions. This was also reflected in the solution NMR spectra, where no clear trends for the development of mixed propylene and ethylene sequences could be observed when comparing samples with increasing ethylene content. The only clear ethylene dependent trend observed in this set was the increase in the Sδδ peak at 30 ppm representative

of EEEE sequences. As expected for the higher reactivity of ethylene monomer, there was a marked difference in the development of blocky ethylene sequences relative to sequences containing isolated ethylene units, however it also seemed that towards the higher ethylene contents in the range tested, this trend reached a plateau. It was also observed that for the lowest ethylene content in the range, already significant amounts of continuous ethylene sequences were present.

The above observations in comparison to those observed for set 1, could be a function of the actual ethylene content of the sample range, as the sample with the lowest ethylene content already contained a significant amount of ethylene (5.8 mol%). To determine the influence of total ethylene content as a driver for the development of ethylene sequences, the tetrad distributions for both sample sets were plotted relative to their total ethylene contents (Fig. 5.22). It can be seen from those trends that regardless of the sample set considered, blocky ethylene sequences develop more rapidly than isolated sequences and also that samples from different sets are distributed along the same trend. This observation is a reflection of the statistical nature of solution NMR and the limited number of sequential units than can be observed, emphasising the importance of using complementary methods of investigating chemical composition.

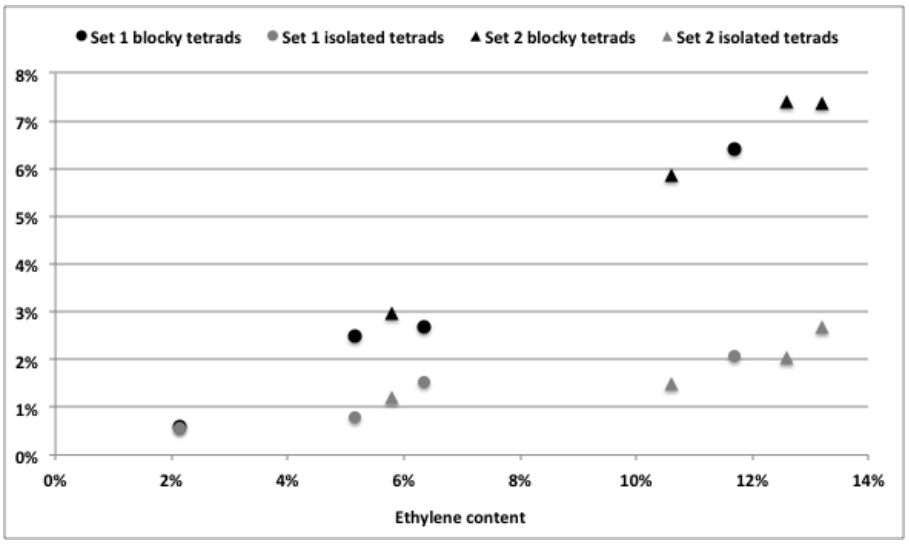

Figure 5.22 *Comparison of ethylene dependent sequence development for different sets.*

To obtain a better idea of the chemical composition in relation to crystal structures, solid-state NMR was also done on these samples. Spectra highlighting the contribution of rigid components (obtained from cross polarization experiments), indicated that there was a significant amount of polyethylene sequences present in crystalline environments, consistent with the development of long ethylene sequences observed by solution NMR and that this did not differ much between samples with different ethylene contents. The only exception for this was the 2_T60 sample, which did not display ethylene peaks for crystalline or amorphous environments, but this was most probably due to the relatively low ethylene content present in this sample.

From the solid-state experiments, it was also noted that even though the solution NMR did not detect subtle developments in any specific sequences, significant differences were present in crystal packing and crystalline environments experienced by the backbone carbons due to ethylene incorporation. The methylene peaks in the CPMAS spectra did not display peak splitting, which suggested a significant disruption of crystal packing in the environment surrounding methylene carbons of polypropylene. This was further supported by the appearance of methylene peaks in the IDREF spectra, which indicated some local mobility experienced by these carbons and which could relate to the severe disruption of crystal packing to such an extent that the splitting of the methylene peak was lost. This phenomenon was only observed in the sample with the highest ethylene content and it could be concluded that a certain minimum amount of ethylene was required to start affecting the mobility of methylene carbons from polypropylene.

5.3.3 Characterization of TREF fractions representing semi-crystalline copolymers

The prep-TREF profiles for the set 1 and set 2 samples were discussed in the previous sections. The 30 °C fraction represents rubbery ethylene-propylene copolymer and some atactic propylene. The 60 to 90 °C fractions represent semi-crystalline ethylene-propylene copolymers of varying ethylene contents and distributions. The 100 °C fractions and higher represent mostly isotactic polypropylene as well as some crystalline polyethylene, which is found in the 130 °C fraction. It is well known in industry that the semi-crystalline copolymers are of importance as this forms an interphase between the amorphous rubber and homopolymer matrix. Variations in the ethylene composition and distribution towards random ethylene incorporation is expected to make these copolymers more compatible with the rubber and

longer or more blocky ethylene sequences in the EPR are expected to be more compatible with the homopolymer matrix. Therefore it is important to understand how these different copolymers, found in fractions of increasing crystallinity develop with increasing ethylene incorporation, as they are responsible for phase interactions and ultimately product properties.

5.3.3.1 Solution NMR characterization of semi-crystalline fractions of set 1

Considering the solution NMR overlays of selected TREF fractions from set 1 samples obtained at 60 °C, 80 °C and 90 °C (Fig. 5.23 to Fig. 5.26), it is clear that the 60 and 80 °C fractions are more alike and in general more ethylene rich, compared to the 90 °C fractions. This is evident by comparing the Sδδ linear ethylene sequence (EEEE) peak at 30ppm relative to the three peaks obtained for polypropylene at 46.5ppm (Sαα), 29ppm (Tββ) and 22ppm (Pββ) respectively. The 90 °C fractions display significantly smaller peaks for propylene-ethylene copolymer sequences relative to the main polypropylene peaks.

Further comparing the spectra overlays in Fig. 5.23 to Fig. 5.26, there is a general decrease in the secondary carbons representing mixed E and P sequences with increasing fractionation temperature; note the decrease in the Sαα (PPPE & EPPE) at ~46 ppm, Sγ (PPEPP/E) at ~38 ppm, Sαδ (EPE$(E)_{n>1}$) at ~ 37.5 ppm, Sβδ (EPE$(E)_{n>1}$ & PPE$(E)_{n>1}$) at ~ 27.5 and 27 ppm and the Sββ peaks (EPEPE/ PPEPE/ PPEPP) at ~ 24.8 ppm as the TREF fraction temperature and thus crystallizability increases. This is to be expected, as isolated ethylene insertions would be present in amorphous copolymers with low crystallinity. Continuous ethylene sequences, depending on the actual length of the sequence (which is difficult to determine by NMR which is limited in the number of units that can be detected at a time) could associate with longer polypropylene stretches and be partially included within crystalline copolymer structures. It is also possible that longer ethylene stretches could crystallize on its own and form a type of LLDPE with some propylene insertions. Furthermore, it is observed that even though there are very few mixed ethylene-propylene sequences in the 90 °C TREF fractions, there is still a substantial amount of relatively long ethylene sequences (EEEE), which could make this fraction more compatible with the polypropylene fractions with higher crystallizability.

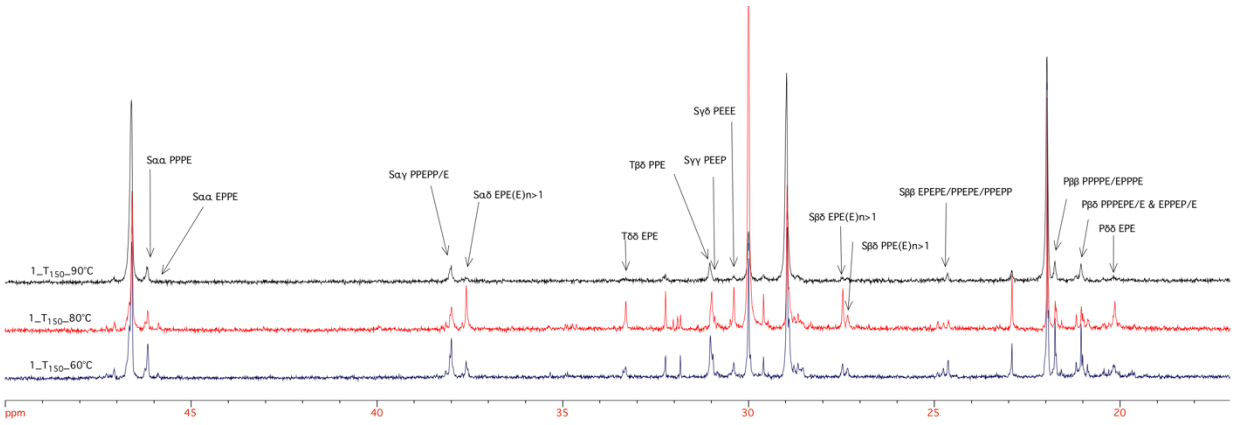

Figure 5.23 *Overlay of the 60 ℃, 80 ℃ and 90 ℃ fractions of 1_T150 (2.1% total ethylene).*

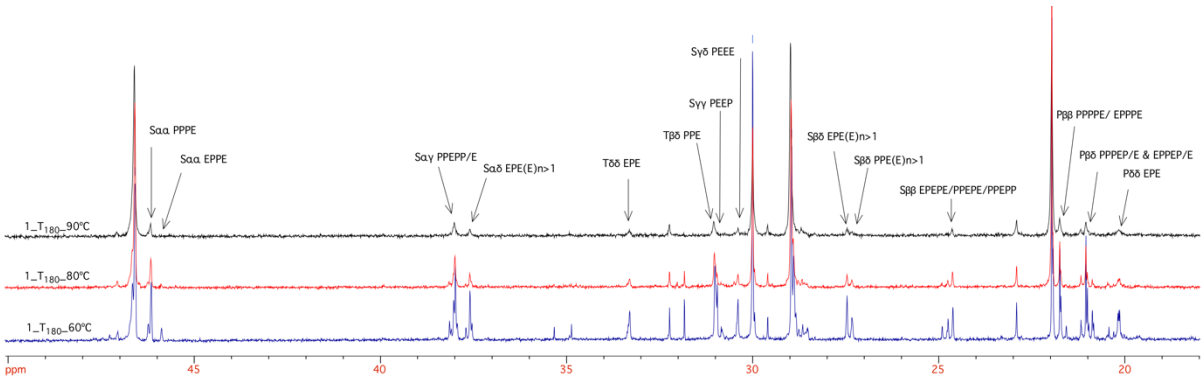

Figure 5.24 *Overlay of the 60 ℃, 80 ℃ and 90 ℃ fractions of 1_T180 (5.2% total ethylene).*

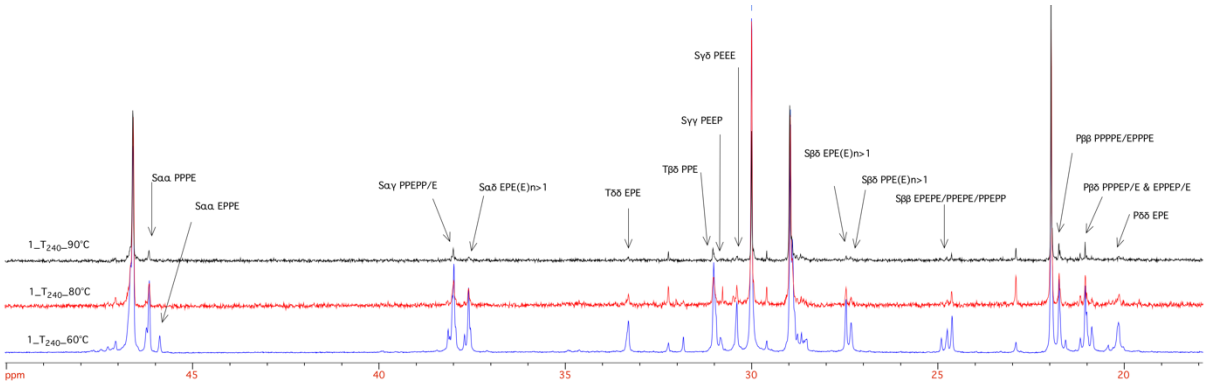

Figure 5.25 *Overlay of the 60 ℃, 80 ℃ and 90 ℃ fractions of 1_T240 (6.3% total ethylene).*

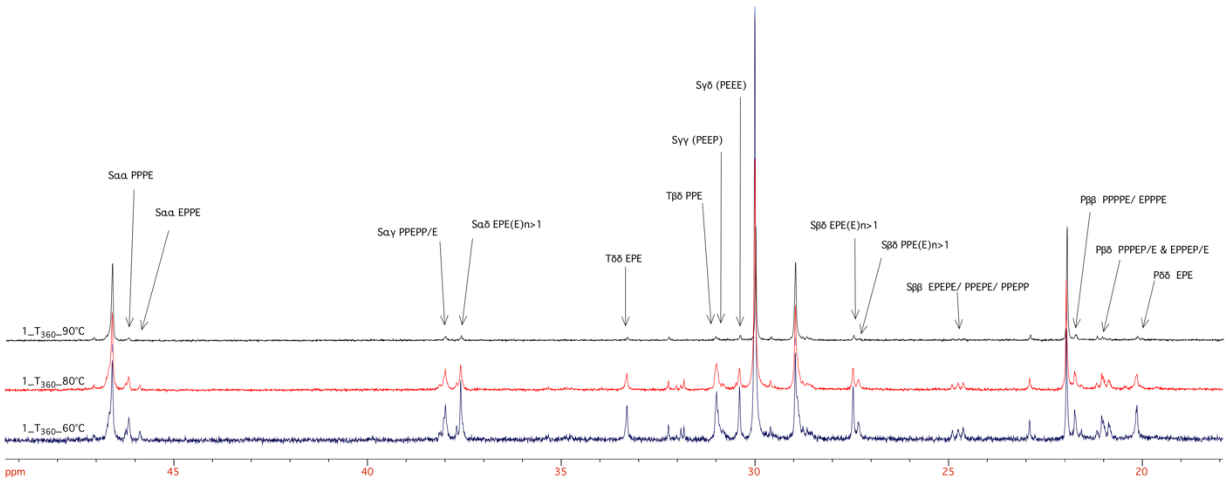

Figure 5.26 *Overlay of the 60 ℃, 80 ℃ and 90 ℃ fractions of 1_T360 (11.7% total ethylene).*

Considering the development of the semi-crystalline fractions for samples with increasing ethylene contents, it is also observed that the relative ratio of propylene to ethylene decreases in similar fractions, comparing samples with increasing ethylene contents, resulting in a significant total amount of ethylene, especially in the 60 °C fractions.

Comparing the total copolymer contents and triad distributions in Table 5.4 and tetrad distributions in Fig. 5.27 to Fig. 5.29, the following observations concerning ethylene sequence distribution development can be made: In Table 5.4 for a specific fraction, there is an increase in total propylene content and decrease in total ethylene content with an increase in the elution temperature of the fraction, as would be expected. Comparing the 60 °C fractions for samples with increasing ethylene contents, the total ethylene content increases, as expected with increasing ethylene content and reaches an almost 50:50 propylene to ethylene distribution in the sample with the highest ethylene content (1_T360).

In general, the triad distributions confirm the bulk observation that consecutive PP or EE sequences are more abundant than alternating E/P sequences (PEP and EPE) for all samples. The trend observed for fractions of increasing crystallizability is that the 60 °C fraction of each sample has the highest percentage of alternating E triads (PEP & EPE) and these triads decrease with increasing crystallizability (TREF elution temperature). The same trend is observed for the isolated tetrad sequences (Fig. 5.27-Fig. 5.29).

Another observation is that even though the number average ethylene sequence length (Ne) is fairly similar for the different fractions in samples 1_T150 to 1_T240, it is significantly higher in the 90 °C fraction of the 1_T360 sample compared to the 60 °C and 80 °C fractions of that sample. This confirms the presence of longer blocky ethylene sequences, in samples with sufficiently high total ethylene contents, which may be able to interact with the polypropylene matrix and co-crystallize at least locally.

Table 5.4 ^{13}C NMR sequence distributions for set 1 semi-crystalline TREF fractions (60 to 90 °C).

Sample	TREF fraction	% P[a]	% E[a]	Normalised triad distributions (%)						Ne	Np
				PPP	PPE	PEP	EPE	PEE	EEE		
1_T150	60 °C	73.2	26.8	56.8	14.9	6.0	3.0	5.1	14.9	2.9	7.9
	80 °C	84.9	15.1	72.9	10.2	3.7	1.4	2.0	9.8	2.7	14.7
	90 °C	86.5	13.5	78.5	6.6	2.1	1.4	2.0	9.5	3.4	21.6
1_T180	60 °C	65.0	35.0	45.2	17.7	7.6	4.4	7.9	17.7	2.9	5.4
	80 °C	75.2	24.8	59.1	13.6	4.3	2.4	4.0	16.6	3.6	10.7
	90 °C	78.1	21.9	70.2	6.4	1.4	1.9	2.4	17.7	5.2	18.4
1_T240	60 °C	64.3	35.7	43.6	15.0	7.6	4.5	9.8	15.0	2.9	5.2
	80 °C	67.8	32.2	53.7	11.8	2.8	2.5	4.1	25.1	5.5	11.4
	90 °C	77.2	22.8	70.8	4.9	1.8	1.6	2.4	18.6	5.3	17.7
1_T360	60 °C	50.4	49.6	27.8	18.4	6.5	7.0	12.2	18.4	3.6	3.7
	80 °C	52.8	47.2	36.4	13.8	4.3	5.0	8.8	31.8	5.0	5.6
	90 °C	66.0	34.0	59.4	3.9	1.3	2.0	3.2	30.2	10.2	20.3

When considering the ethylene sequence development for a specific fraction, it is clear that at low ethylene contents, there are long stretches of polypropylene, with short ethylene insertions. As the ethylene content of the sample increases, the propylene stretches become shorter and the ethylene stretches longer, until there are almost alternating blocks of continuous E and P sequences. This is valid for the 60 and 80 °C fractions, but for the 90 °C fractions the continuous propylene sequences are still much longer than continuous ethylene sequences.

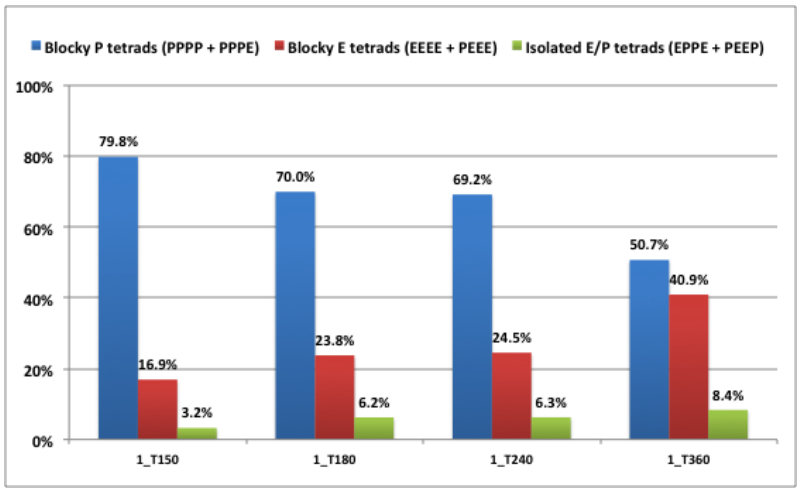

Figure 5.27 *Tetrad distributions for the 60 ℃ fractions of set 1 samples.*

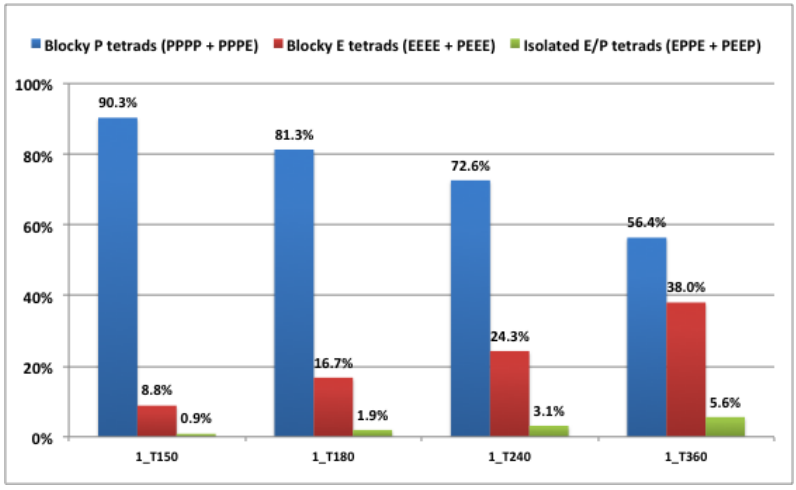

Figure 5.28 *Tetrad distributions for the 80 ℃ fractions of set 1 samples.*

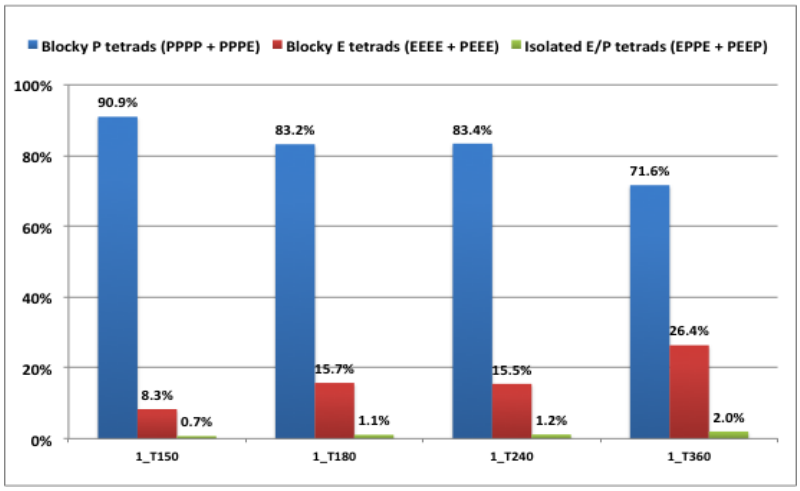

Figure 5.29 *Tetrad distributions for the 90 ℃ fractions of set 1 samples.*

5.3.3.2 Solid-state NMR characterization of semi-crystalline fractions of set 1

Solid-state experiments, similar to those done on the bulk samples, were run on the same TREF fractions described in the previous section, in order to relate the differences in microstructure as described in Section 5.3.1 to changes in chain conformation. Overlays for the semi-crystalline TREF fractions obtained at 60, 80 and 90 °C, for set 1 samples with increasing ethylene contents are shown in Fig. 5.30 to Fig. 5.33. Comparing the spectra obtained for fractionated samples with those of the bulk (Section 5.3.1.3), there are a few additional solid-state peaks present in the fractionated samples, as these contain higher amounts of ethylene-propylene copolymers, highlighting the complexity of these fractions. For each fractionation temperature, the general trend of increasing intensities of the ethylene peaks with total ethylene content of the samples, is observed.

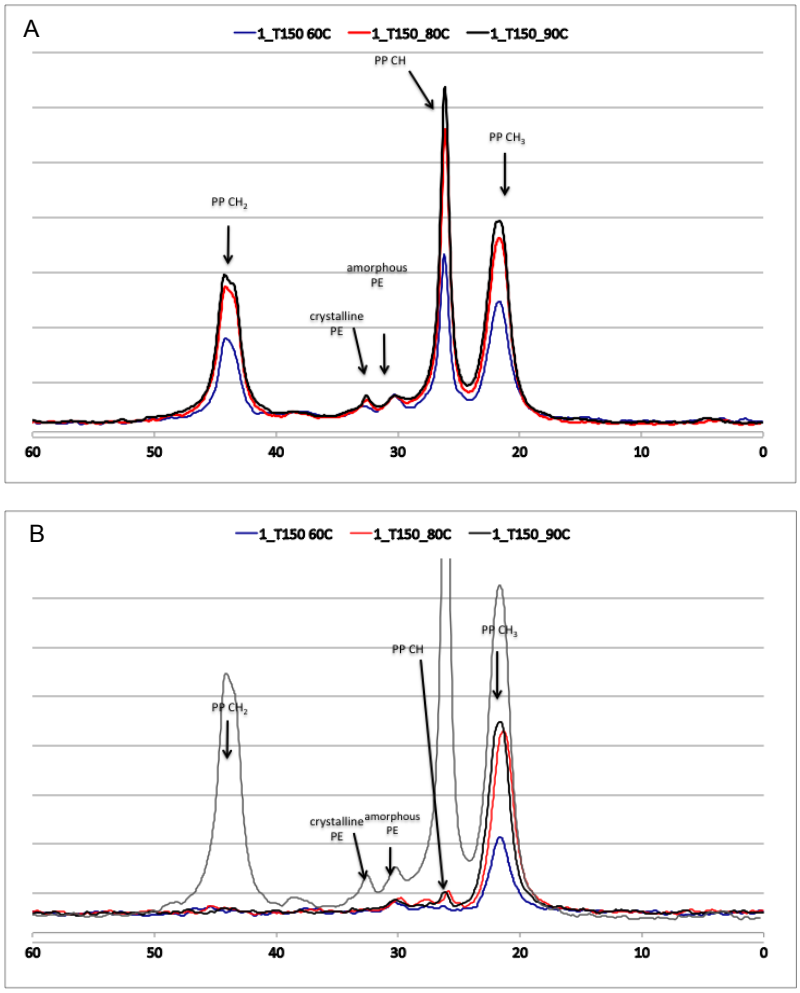

Figure 5.30 *Overlay of solid-state spectra of semi-crystalline TREF fractions from sample 1_T150 (A) CPMAS experiments and (B) IDREF experiments (Grey trend: 1_T150 90 ℃ CPMAS trend as reference).*

In Fig. 5.30A, the CPMAS trends that emphasise carbons with lower mobility, indicate an increase in the peaks representing the polypropylene methyl, methine and methylene carbons with an increase in fractionation temperature, consistent with the increase in crystalline polypropylene with increasing elution temperature. It is also observed that the peak representing crystalline polyethylene is higher in the 80 and 90 °C fractions relative to the 60°C fraction. Furthermore, the splitting of the methylene peaks at 45 ppm only starts to appear in the highest temperature fraction in this range, indicating that in fractions lower than 90 °C, there is a greater deviation from the 2:1 ratio observed for regular crystal packing of the α_2 allomorph. It can therefore be concluded that the ethylene defects present in the 60 and 80 °C fractions disrupt regular crystal packing to a greater extent than in the 90 °C fraction, which is also consistent with the relative crystallinities of these fractions.

The IDREF trends of the 60, 80 and 90 °C fractions are shown in Fig. 5.30B, overlaid on the CPMAS trend of the 90 °C fraction (in grey), to indicate differences between these trends. As expected, peaks representing methyl carbons are present in the IDREF trends of all fractions as these carbons experience some measure of mobility. A small amount of amorphous polyethylene is also found in the mobile contribution. For the 80 and 90 °C fractions, there starts to develop a small peak, in addition to these peaks, which corresponds to the chemical shift of the methine carbon, possibly due to reduced shielding of the methine carbons with increasing ethylene content as explained previously.

Considering the cross-polarized trends for the 1_T180 sample (Fig. 5.31A), there is a noticeable development of the polyethylene peaks, compared to the 1_T150 sample and another peak at 39 ppm starts to appear. This peak was shown by Alamo *et al.* to be the best resonance for quantification of ethylene defects in propylene-ethylene copolymers, as this does not overlap with stereo- and regiodefect resonances [13]. Comparing the partitioning of polyethylene between rigid and amorphous environments, only the 60 °C fraction has a significant amount of ethylene in amorphous- relative to crystalline environments. Considering the IDREF trends in Fig. 5.31B, the amorphous polyethylene peak of the 60 °C fraction is more pronounced than in the corresponding trends for the 1_T150 sample with lower ethylene content, which indicates that the ethylene carbons in amorphous regions experience mobility. There is also a small peak corresponding to methine resonance as seen in Fig. 5.30B as well as the methylene peak at 39 ppm observed in Fig. 5.31A as well, suggesting that these carbons experience some mobility.

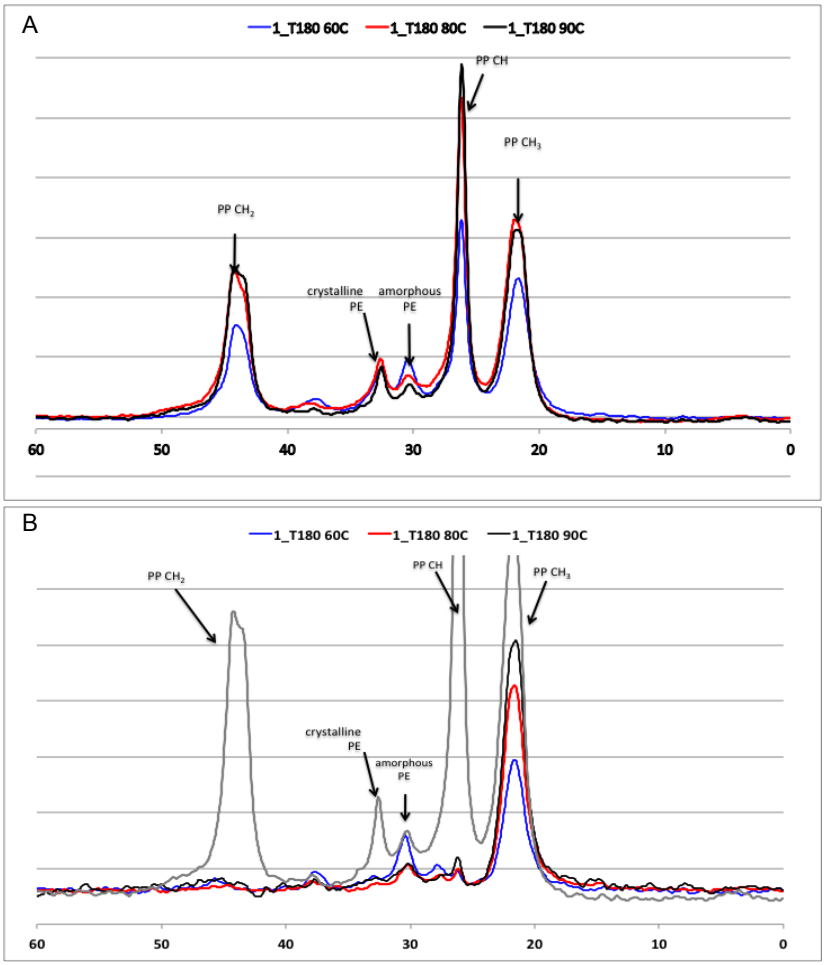

Figure 5.31 *Overlay of solid-state spectra of semi-crystalline TREF fractions from sample 1_T180 (A) CPMAS experiments and (B) IDREF experiments (Grey trend: 1_T180 90 ℃ CPMAS trend as reference).*

The same trends as described above for fractions with increasing elution temperatures are observed in the other samples with increasing ethylene contents (Fig. 5.32 and Fig. 5.33) and comparing trends over samples with increasing ethylene contents, the peak intensities of the ethylene peaks at 30, 31 and 39 ppm increase as expected with ethylene content in the trends obtained by CPMAS experiments. Furthermore, there is a marked development of peaks representing regions with higher mobility with increasing ethylene content, when comparing the trends obtained by IDREF experiments in Fig. 5.30 to Fig. 5.33. This is especially the case for the 60 °C fraction of the highest ethylene content sample (1_T360), where additional peaks and peak splitting is observed compared to the same fractions of the other samples with lower ethylene contents (Fig. 5.33A – blue trend). Also, the splitting observed for the methylene peaks of the bulk samples is only observed in this fraction compared to the same peaks for samples with lower ethylene contents, emphasising the heterogeneity of this fraction. For this sample,

the methine (CH) peak at 26 ppm also splits into two, indicating a dual environment for the methine carbon which is normally shielded to a certain extent in propylene homopolymer, being fixed between the methylene groups of the carbon backbone and the methyl pendant group due to its position in the 3_1 helix. As explained previously, with increasing ethylene incorporation, one would expect less methyl pendant groups to be present and therefore less shielding, thus causing the methine groups to experience different environments, resulting in local mobility, which is observed as a shoulder to the methine peak. In the case of the highest ethylene content sample (1_T360), this shoulder has developed into a peak at approximately 28 ppm. Comotti *et al*. has reported the presence of a methine peak in an amorphous environment at 28.5 ppm [12]. In this study propylene homopolymer with 45% isotactic (*mmmm* = 0.45) and 20% syndiotactic sequences was used, however the same principle of the influence of stereodefects (whether by means of tacticity differences or ethylene incorporation) should apply to the work presented in this thesis.

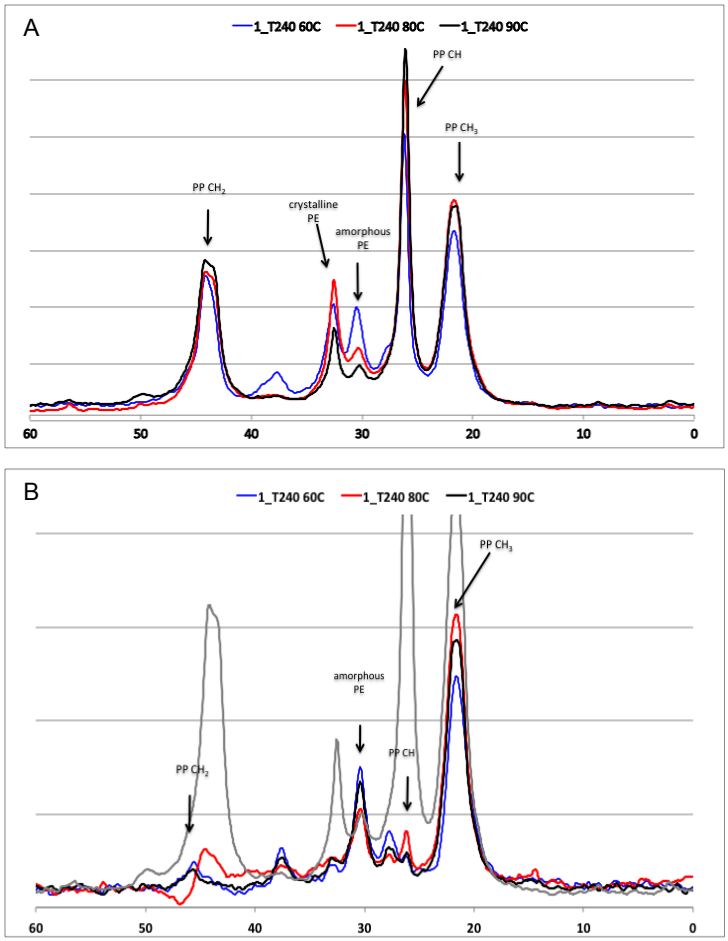

Figure 5.32 *Overlay of solid-state spectra of semi-crystalline TREF fractions from sample 1_T240 (A) CPMAS experiments and (B) IDREF experiments (Grey trend: 1_T180 90 ℃ CPMAS trend as reference).*

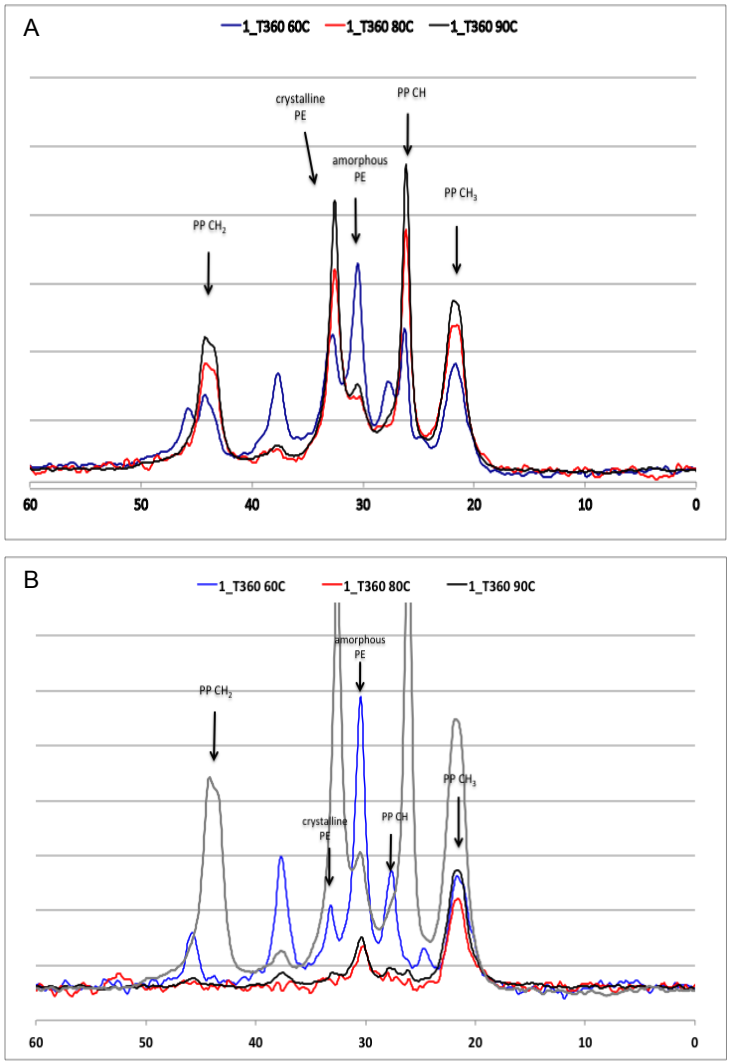

Figure 5.33 *Overlay of solid-state spectra of semi-crystalline TREF fractions from sample 1_T360 (A) CPMAS experiments and (B) IDREF experiments (Grey trend: 1_T180 90 ℃ CPMAS trend as reference).*

Considering the IDREF trends for the 60 °C fraction of 1_T360 there are, apart from a major peak representing amorphous polyethylene, also significant contributions from crystalline polyethylene, as well as the methylene and methine carbons from polypropylene (Fig. 5.33B). These results indicate that the polypropylene crystal structure is significantly affected by the incorporation of ethylene. Caution should however be taken when interpreting solid-state trends for TREF fractions in isolation, as some interactions between fractions (which occur in the bulk) are lost through the physical separation that occurs during fractionation. Having considered that, better resolution and identification of low concentration components are possible by evaluating the solid-state spectra that persists even in fractionated samples and gives an appreciation for the potential of different interactions occurring between different fractions in the bulk and the challenge of developing an understanding of these.

5.3.3.3 HT-SEC and HT-HPLC characterization of set 1 semi-crystalline fractions

As demonstrated in the solution and solid state spectra discussed above, it is clear that each TREF fraction, particularly those eluting between 60 and 90 °C, consists of various ethylene sequences and distributions and should by no means be considered as homogeneous samples. The solution and solid–state NMR experiments described in the previous section have provided much information on chemical composition distribution on average as well as local distribution with respect to crystal structures for samples with varying degrees of crystallinity. Although it could be expected that differences in the molecular weight distribution of these samples, would indirectly influence the observed NMR results, these have not yet been directly accounted for. In this section the molecular weight distributions as determined by high temperature size exclusion chromatography (HT-SEC) will be compared for the different fractions in question and related to the rest of the results. It is well known that apart from a wide molecular weight distribution, these fractions also display a broad chemical composition distribution. To date, the only technique capable of further separating these complex fractions, is high temperature high performance liquid chromatography (HT-HPLC), which will be applied in this study to further separate fractions primarily based on chemical composition distribution, but also affected by the molecular weight distribution of these samples to some extent.

In Fig. 5.34 the HT-SEC elution profiles of selected fractions from set 1 are shown. It is clear from these trends that each fraction consists of chains with a broad range of molecular weights and in some instances a bi- or even trimodal molecular weight distribution. For the lower temperature fractions (30 to 80 °C), the elution profile of the 1_T360 sample with the highest ethylene content is shifted to higher molecular weights. This confirms the bulk observation of an increase in molecular weight as the copolymer content increases. Furthermore the 1_T360 sample does not display a low temperature shoulder as observed for the 30 °C fractions of the samples with lower ethylene contents (Fig. 5.34A). The sample with the lowest ethylene content (1_T150) also shows a very broad molecular weight distribution as well as a distinct low molecular weight portion, which is present in all the low temperature fractions of this sample, but not observed for the other samples. As shown previously in the SEC-FTIR analysis of bulk samples, the low molecular weight portion of the samples corresponds to polypropylene and since the fractions discussed in this section represent fractions with reduced crystallinity (relative to isotactic polypropylene) it is possible that a low amount of random ethylene insertions and atactic polypropylene could be responsible for this observation. It should also be noted that the solution NMR trends indicate the presence of end groups at 32.2 ppm

(representing the third carbon from the end) and 23 ppm (representing the second carbon from the end) in the 60, 80 and 90 °C fractions of all samples, however the intensities of these peaks decrease with increasing ethylene content, supporting the HT-SEC observations.

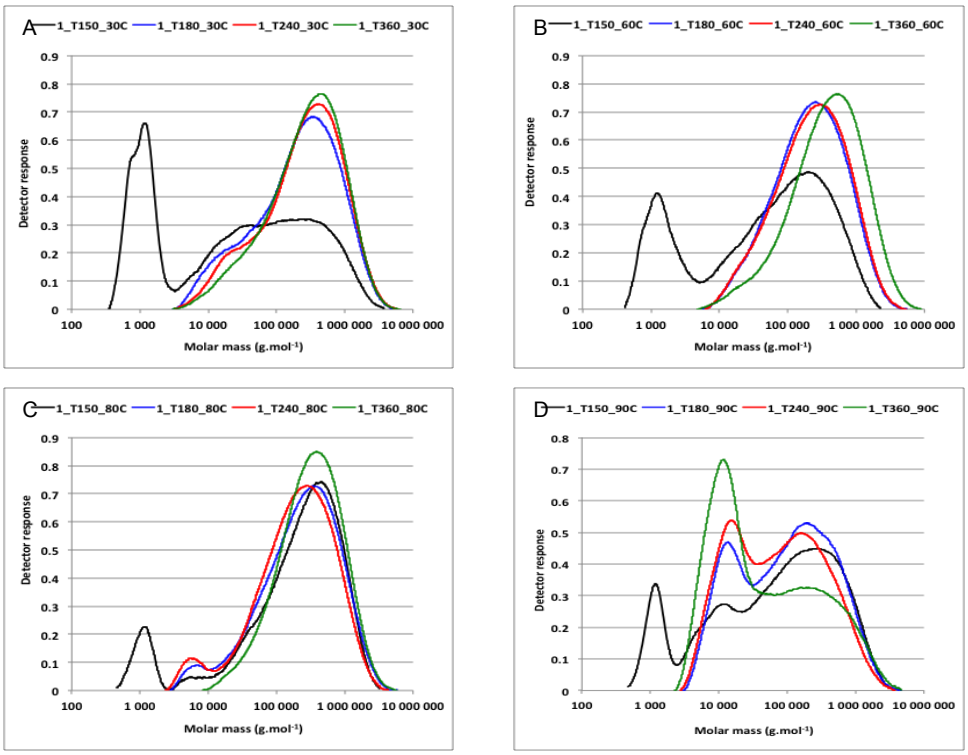

Figure 5.34 *HT-SEC overlays of TREF fractions from set 1 samples with increasing ethylene contents (T180, T240 and T36): 30 ℃ (A), 60 ℃ (B), 80 ℃ (C) and 90 ℃ (D) fractions.*

All samples show at least a bimodal distribution for the 90 °C fraction, however for the 1_T360 sample there is less of the high molecular weight component present in this sample as these components were predominantly found in the lower temperature fractions of this sample (specifically the 60 °C fraction). The higher temperature TREF fractions are not shown here, but the molecular weight distribution of these samples were very similar irrespective of total ethylene content, confirming that these fractions consist mostly of propylene homopolymer.

It is difficult to draw any significant conclusions on the observed trends without considering differences in the chemical composition of these fractions and therefore it is required to evaluate the HT-HPLC trends as well (Fig. 5.35). During HT-HPLC, polypropylene elutes first when using 1-decanol as the mobile phase, as it is a good solvent for polypropylene. A

distribution in retention times around this early elution is therefore only governed by tacticity and molecular weight differences between different polypropylene molecules. The two observed peaks eluting at 1.3 ml and 3.0 ml represent low and high molecular weight isotactic polypropylene respectively. After a cumulative elution volume of 3 ml, a solvent mixture of 1-decanol and trichlorobenzene (TCB) is introduced, following a gradient with an increasing TCB concentration. TCB is a good solvent for polyethylene and therefore the propylene-ethylene copolymers are eluted according to increasing ethylene contents as the composition of this solvent in the mobile phase increases. It should be noted that these copolymers are adsorbed on the HPLC column prior to gradient elution and therefore, the greater the interaction between the polymer and column, the stronger solvent is required to dissolve and elute the polymer from the column. Consequently, at higher ethylene contents or with stronger interactions between the polymer and column (for example with linear as opposed to branched ethylene sequences) higher elution volumes are observed.

In Fig. 5.35 the HT-HPLC elution profiles for the 30 to 90 °C TREF fractions is shown for set 1 samples with increasing ethylene contents. The higher temperature TREF fractions did not indicate any significant ethylene dependent differences as these consist mostly of isotactic polypropylene and are therefore not shown below. It is observed from HT-HPLC chromatograms that the 30 °C TREF fractions (Fig. 5.35a) are by far the most diverse of the different fractions, representing a wide range of ethylene contents and distributions, as judged by the broad elution profiles observed for all samples between 3 and 5 ml. Some polypropylene with low tacticity and/or low molecular weight is observed at a low elution volume (approximately 1 ml). It is also observed that the chromatograms are slightly shifted towards higher elution volumes as the total ethylene content of the sample increases, which is consistent with the expected increase in heterogeneity with higher ethylene content and the principle of separation used in this method. Furthermore, for the sample with the highest ethylene content (1_T360), a small portion of linear polyethylene is observed to elute between 5 and 6 ml for the 60 to 90 °C fractions (Fig. 5.35b – c). This is consistent with what was observed by solution and solid-state NMR and confirms that these semi-crystalline copolymer fractions contain long enough ethylene stretches which could influence the crystallization of the polypropylene helices.

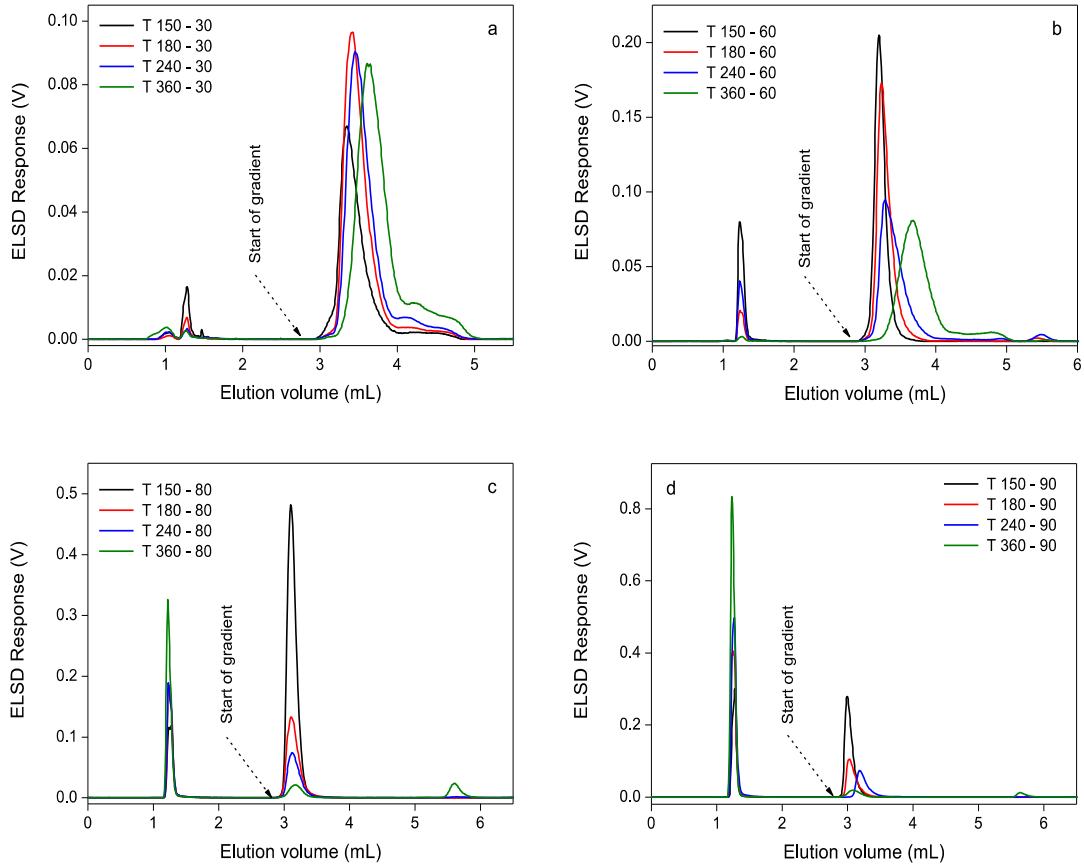

Figure 5.35 *HT-HPLC overlays of TREF fractions from set 1 samples with increasing ethylene contents (1_T150, 1_T180, 1_T240 and 1_T360): 30 ℃ (a), 60 ℃ (b), 80 ℃ (c) and 90 ℃ (d) fractions.*

5.3.3.4 Solution NMR characterization of semi-crystalline fractions of set 2

The solution NMR spectra for the 60, 80 and 90 °C fractions of the set 2 samples are shown in Fig. 5.36 to Fig. 5.39. Considering the sample with the lowest ethylene content in the set (2_T60), there is a significant amount of long ethylene sequences present in all the fractions of this sample, as indicated by the Sδδ peak relative to the three polypropylene peaks (Fig. 5.36). The relative intensity of this peak however decreases with increasing fractionation temperature, so that the trend develops from an ethylene rich copolymer with a significant amount of mixed ethylene-propylene sequences in the 60 °C fraction to a polymer containing either long continuous propylene or -ethylene sequences, but almost no other copolymer sequences in the 90 °C fraction. This is consistent with the different crystallinities of each fraction, where the 90 °C fraction, which is more crystalline contains long ethylene sequences that can co-crystallize with the homopolymer. Alternatively the 60 °C fraction with lower

crystallinity consists of many different ethylene and propylene sequences, which would be expected to be present in more amorphous regions.

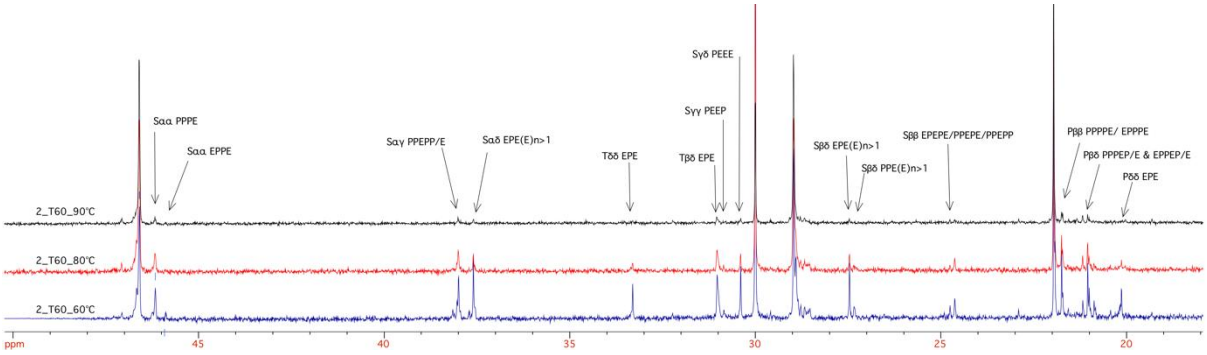

Figure 5.36 *Overlay of the 60 ℃, 80 ℃ and 90 ℃ fractions of 2_T60 (5.8% total ethylene).*

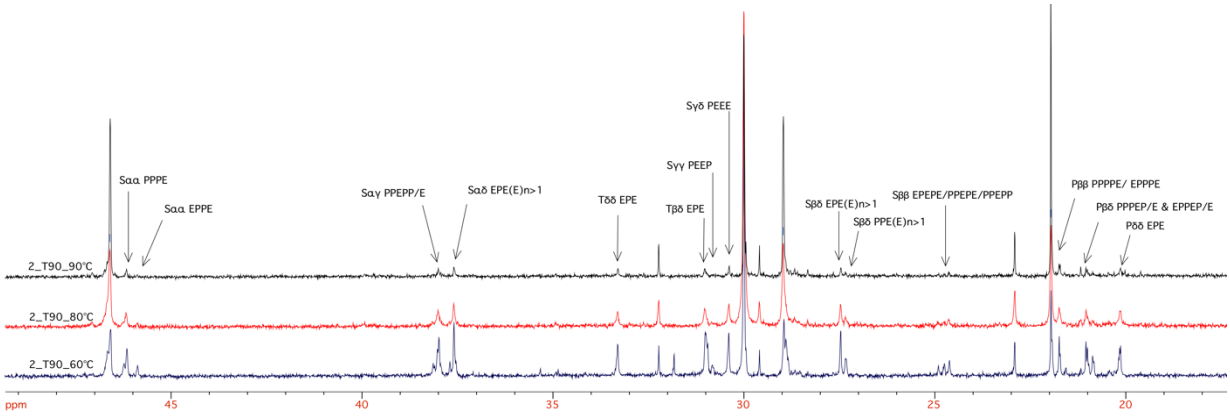

Figure 5.37 *Overlay of the 60 ℃, 80 ℃ and 90 ℃ fractions of 2_T90 (10.6% total ethylene).*

When comparing the progression in the spectra in Fig. 5.36 to Fig. 5.39, it is noticeable that the polypropylene peaks are significantly reduced specifically in the 60 and 80 °C fractions as the sample ethylene content increases. This happens to such an extent that these lower temperature fractions appear to consist mostly of linear low-density polyethylene with propylene being the copolymer, rather than propylene with ethylene copolymer insertions, which is the composition of the bulk samples.

It is also observed for the lower ethylene content (2_T60) sample that the Sαγ to Sαδ peak ratio changes as the fraction temperature and thus crystallinity increases, with the longer ethylene sequences ($EPE(E)_{n>1}$) being more prominent relative to isolated ethylene sequences PPEPP/E in the 60 °C fractions, however this ratio is the opposite in the 80 °C fraction, where isolated ethylene sequences are more prominent than longer sequences. In the higher ethylene content sample (2_T90), the longer ethylene sequences represented by the Sαδ peak is dominant in both

the 60 °C and 80 °C fractions, indicating that even in fractions with low crystallinity, longer ethylene stretches are found. This observation suggests that these longer ethylene stretches could interact with the polypropylene matrix to such an extent, that the crystallinity of the polymers is significantly reduced, resulting in the relatively low elution temperature of these fractions.

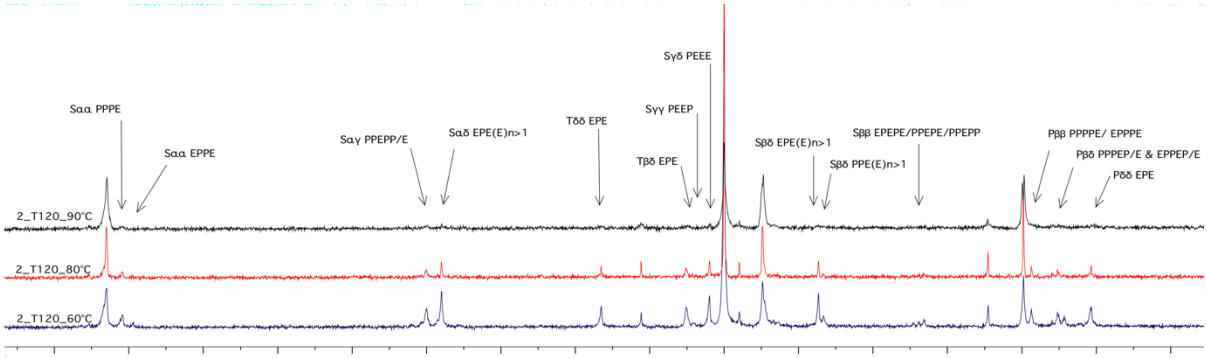

Figure 5.38 *Overlay of the 60 °C, 80 °C and 90 °C fractions of 2_T120 (12.6% total ethylene).*

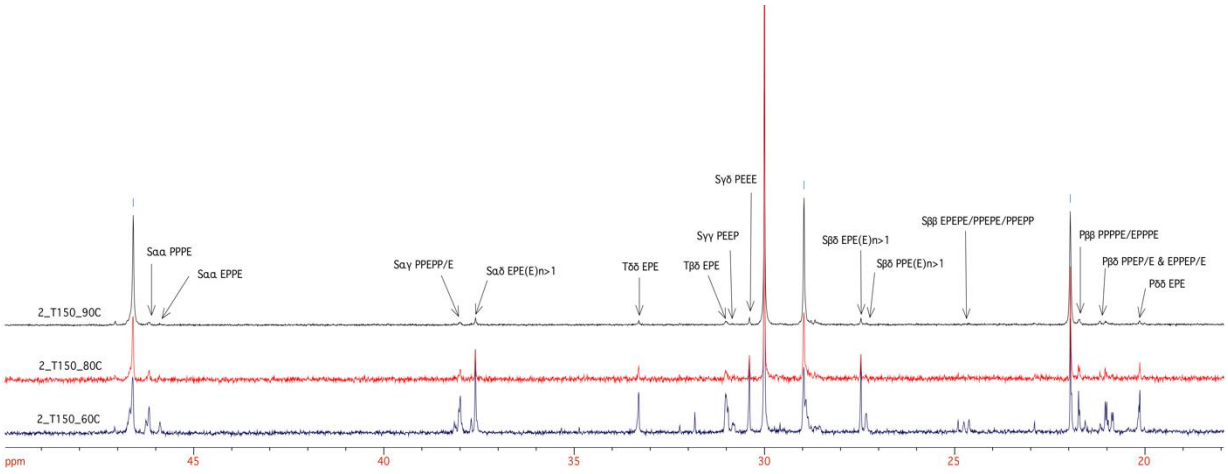

Figure 5.39 *Overlay of the 60 °C, 80 °C and 90 °C fractions of 2_T150 (13.2% total ethylene).*

Comparing the total monomer contents, triad distributions and number average propylene - (Np) and ethylene sequence length (Ne) for the semi-crystalline fractions (Table 5.5), the following observations can be made: As discussed in Section 5.3.3.1., the ethylene content increases as expected with the ethylene content of the bulk sample and also with decreasing fraction temperature within a sample. As observed in the spectra the calculated monomer contents indicate that most of the fractions are quite ethylene-rich, with ethylene contents up to 60 mol%, as observed for the 60 °C fraction of the 2_T120 sample. Except for the 2_T60 sample with the lowest ethylene content, the other samples have more than 50 mol% ethylene present

in the 60 and 80 °C fractions. The monomer content of these fractions doesn't change much for samples with increasing bulk ethylene content, as no clear progression in this distribution is observed for the 2_T90 to 2_T50 samples. The concentration effect of ethylene in these fractions is furthermore evident, when comparing the ethylene composition of the copolymer determined by FTIR analysis of the bulk samples, which also indicated relatively high ethylene contents in the copolymer (43-47 mol%) as seen in Table 4.2 (Chapter 4).

Apart from the significant ethylene content in these fractions, the triad distributions also indicate that the ethylene molecules are predominantly present in blocky runs, when comparing the PEE and EEE sequences to the PEP and EPE sequences in Table 5.5 as well as the tetrad distributions in Fig. 5.40-Fig. 5.42. For the 60 and 80 °C fractions of samples with higher ethylene contents (2_T120 and 2_T150), there are also significantly more EEE sequences, relative to the PPP sequences also highlighting the ethylene-richness of these fractions.

Table 5.5 ^{13}C NMR sequence distributions for set 2 semi-crystalline TREF fractions (60 to 90 °C).

Sample	TREF fraction	% P[a]	% E[a]	Normalised triad distributions (%)						Ne	Np
				PPP	PPE	PEP	EPE	PEE	EEE		
2_T60	60 °C	59.1	40.9	44.5	10.2	5.2	4.3	8.6	27.4	4.5	6.6
	80 °C	69.1	30.9	59.3	6.8	3.2	2.2	3.9	23.2	5.7	12.7
	90 °C	80.7	19.3	75.2	2.8	2.0	0.9	1.3	16.3	9.9	42.7
2_T90	60 °C	48.5	51.5	28.0	15.3	7.3	6.9	13.7	28.9	3.6	3.4
	80 °C	46.0	54.0	34.5	6.8	3.3	4.4	7.1	43.7	7.6	6.5
	90 °C	64.9	35.1	59.1	3.1	1.3	2.9	3.6	29.9	9.0	16.5
2_T120	60 °C	39.7	60.3	26.4	8.1	3.7	6.1	12.1	43.5	5.8	3.8
	80 °C	44.4	55.6	33.3	5.6	2.5	4.4	6.9	47.4	9.0	7.2
	90 °C	62.2	37.8	55.9	3.0	0.7	1.9	3.3	35.2	12.3	20.0
2_T150	60 °C	45.8	54.2	26.3	12.6	5.2	7.0	13.8	35.1	4.4	3.7
	80 °C	43.0	57.0	35.1	4.5	2.4	3.7	7.4	46.8	9.4	7.1
	90 °C	58.0	42.0	52.9	2.7	0.7	1.6	3.1	39.1	17.7	24.5

The tetrad distributions for all the 60 °C fractions (Fig. 5.40), show that with ethylene incorporation the percentage of blocky propylene sequences decreases while the percentage blocky ethylene sequences increase, until a 50:50 distribution of blocky propylene to ethylene sequences is found for the sample with the highest ethylene content. Furthermore, there does not appear to be an ethylene dependent development of isolated sequences, which is consistent with the previous observations made for this sample set. Interestingly, for the 80 °C fractions (Fig. 5.41), the 50:50 blocky ethylene to blocky propylene distribution stays fairly constant for the 2_T90, 2_T120 and 2_T150 samples, which indicates that the crystallinity of the polymer in this fraction is not affected by increasing ethylene incorporation. The 90°C fractions (Fig. 5.42) are propylene rich and also display the expected trends of decreasing blocky propylene sequences and increasing blocky ethylene sequences with increasing ethylene content of the bulk sample. Almost no isolated ethylene sequences are observed for the 90°C fractions, consistent with the crystallinity of these fractions.

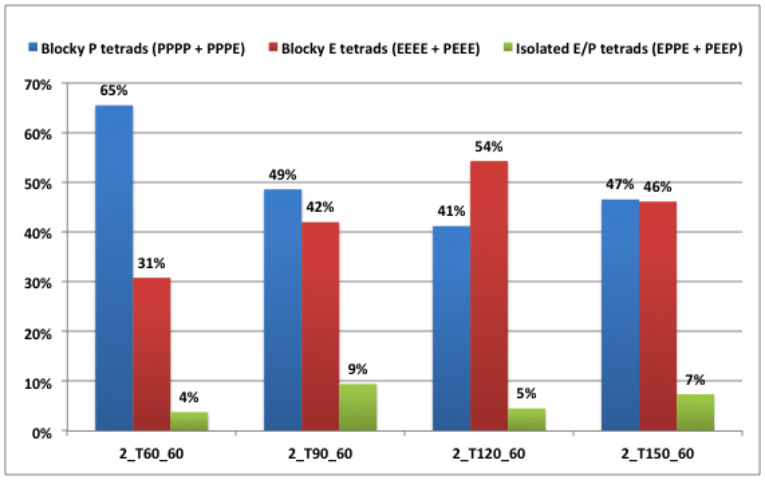

Figure 5.40 *Tetrad distributions for the 60 ℃ fractions of set 2 samples.*

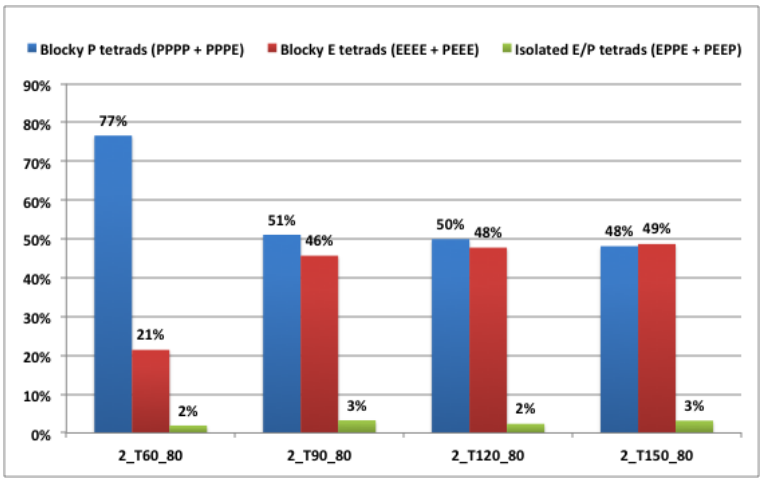

Figure 5.41 *Tetrad distributions for the 80 ℃ fractions of set 2 samples.*

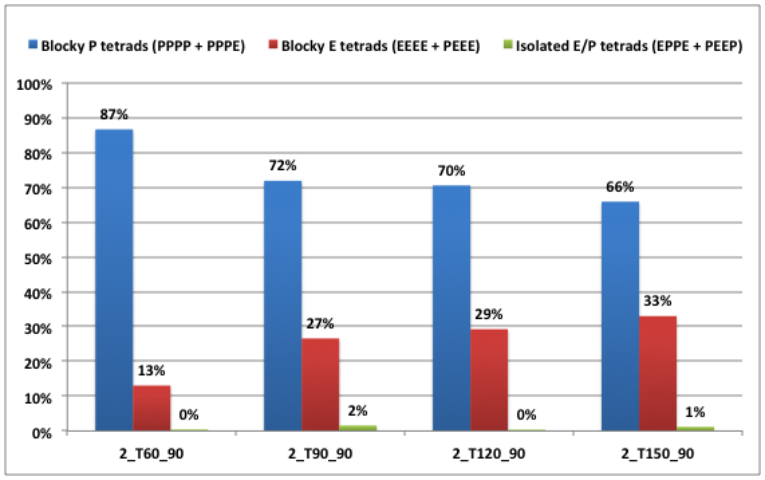

Figure 5.42 *Tetrad distributions for the 90 ℃ fractions of set 2 samples.*

5.3.3.5 Solid-state NMR characterization of semi-crystalline fractions of set 2

Solid-state experiments were conducted to provide more information on changes in the chain dynamics with changes in the chemical composition. It should be noted that the interpretation of these solid-state results are confined to specific fractions and do not provide any information on the interactions between fractions, which was represented in the bulk solid-state analyses. However, in the bulk the resolution of low concentration components is low, so the analyses of fractions could provide samples where the ethylene-propylene copolymers are more concentrated, providing better resolution of these components. In analysing fractions, some observations and interpretations on local chain structure and chain conformation can be made in isolation, along with predictions on the potential interactions and compatibility between different fractions. Accounting for the specific function of these fractions within the bulk should however be kept in mind with the interpretation.

The solid-state overlays of the semi-crystalline fractions of set 2 samples with increasing ethylene contents are shown in Fig. 5.43 to Fig. 5.46. For the sample with the lowest ethylene content in the range (2_T60), it is noteworthy that the CPMAS trends (Fig. 5.43A) already indicate a significant amount of ethylene in crystalline environments, relative to amorphous environments for all fractions. The relative intensity of the crystalline to amorphous polyethylene peaks is at its highest for the 80 °C fraction. Considering the different crystallinities of these fractions, it would make sense that the lower crystallinity 60 °C fractions would contain more amorphous polyethylene which could potentially aid in compatibilization with polymer chains eluting in the 30 °C fraction in the bulk. Regardless of this, however there is still a significant amount of crystalline polyethylene present in this fraction that would not be expected to compatibilize with amorphous sequences. Considering the IDREF trends (Fig. 5.43B) representing carbons with higher mobility, the 60 °C fraction of this sample displays a methylene peak (from polyethylene) at 39 ppm, a peak representing amorphous polyethylene at 31 ppm as well as smaller peaks representing the methine carbons and even crystalline polyethylene at 28.5 ppm and 31.3 ppm respectively. The observation that a small mobile contribution is observed for crystalline polyethylene indicates that this type of carbon experiences some localised mobility, which is consistent with the reduced crystallinity of this fraction.

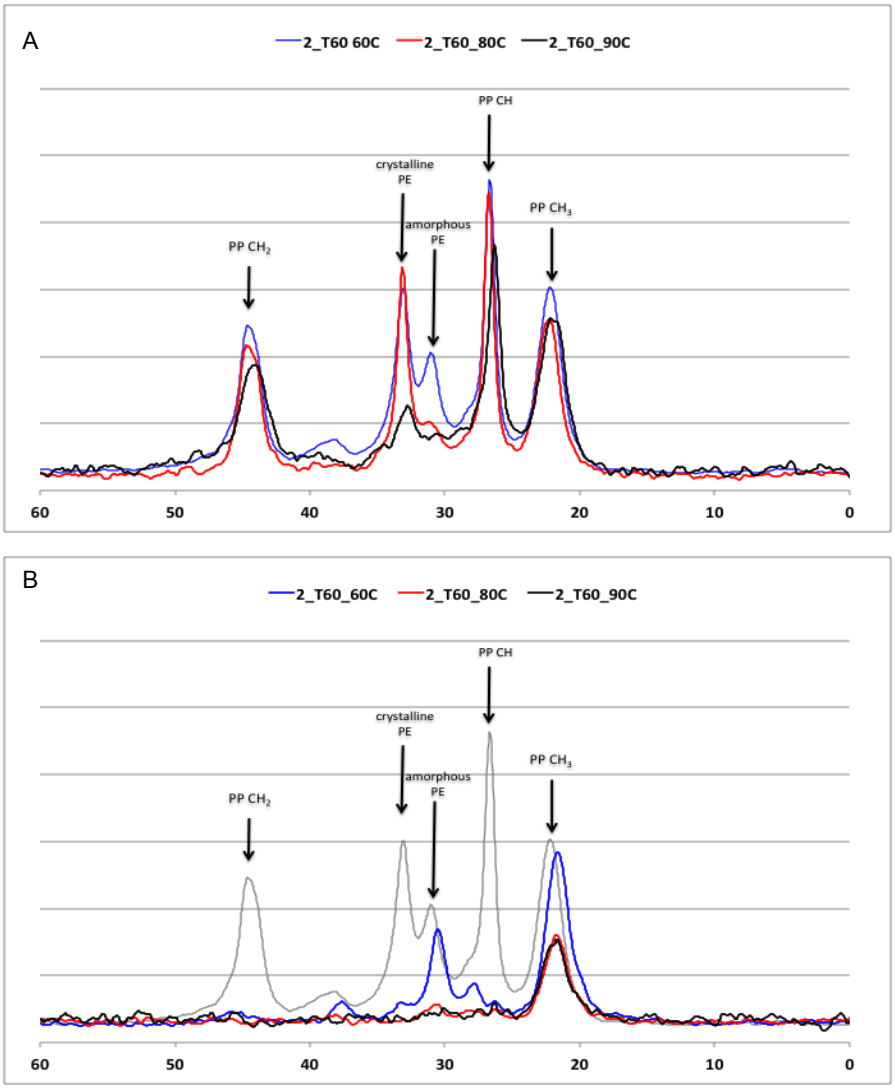

Figure 5.43 *Overlay of solid-state spectra of semi-crystalline TREF fractions from sample 2_T60 (A) CPMAS experiments and (B) IDREF experiments (Grey trend: 2_T60 60 ℃ CPMAS trend as reference).*

The solid-state spectra of the fractions become more complex as the ethylene content of the samples increases. In the CPMAS spectra of the 2_T90 sample (Fig. 5.44A), a shoulder at 28.5 ppm starts to develop next to the methine peak and the methylene peak representative of ethylene carbons at 39 ppm becomes more prominent in the 60 °C fraction of this sample. There is also a broadening of the methyl and methylene peaks in this fraction, indicative of increased heterogeneity. From the IDREF trends of this sample (Fig. 5.44B), the development of a methylene peak at approximately 45 ppm is observed, indicating increased mobility of the methylene carbons in the polypropylene backbone due to ethylene incorporation. In the bulk

samples this phenomenon was only observed for the sample with the highest ethylene content, but by zooming in on the TREF fractions it is evident that this local mobility and disruption of chain packing is already present at lower ethylene contents. Comparing the CPMAS and IDREF trends of this sample, the sudden mobility of methylene carbons coincides with the observed splitting of the methylene peak, which explains why the deviation from the 2:1 ratio of the methylene peak in the bulk could not be determined. Based on the line shape of the methylene peaks present in these samples, the ratio appears to be inverted (1:2 ratio).

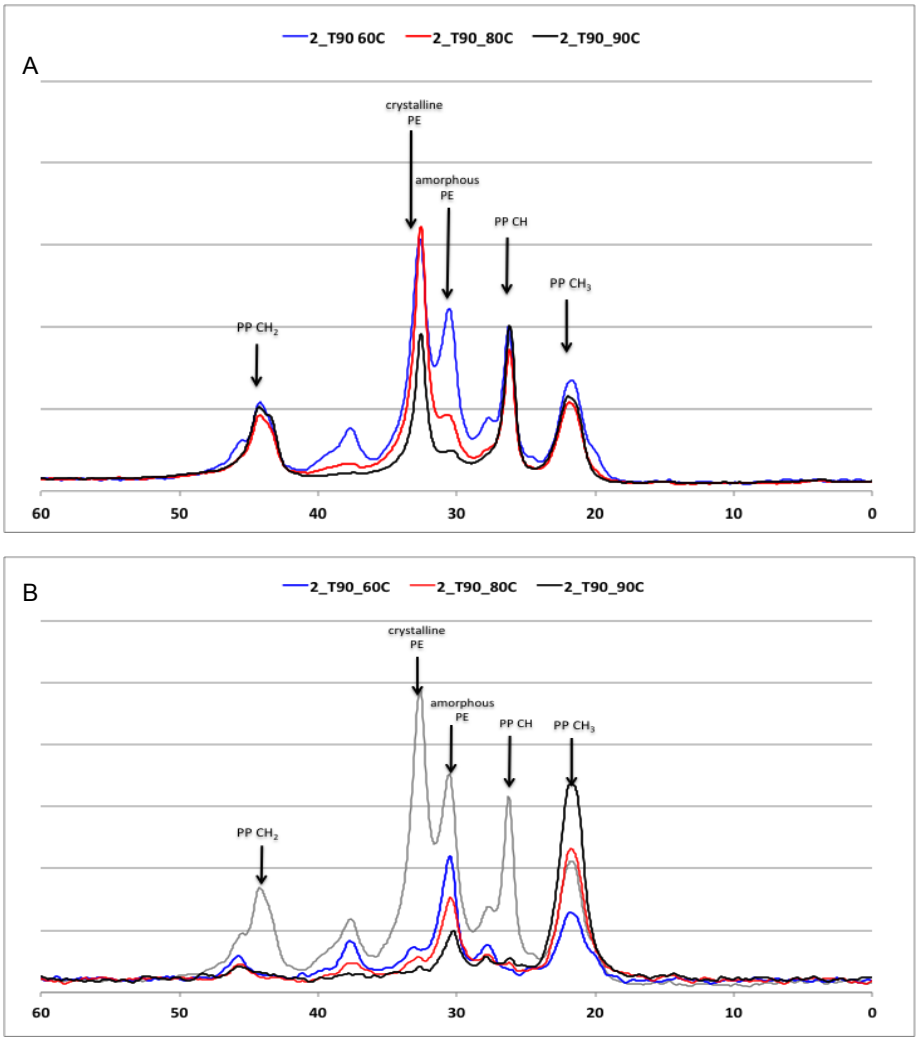

Figure 5.44 *Overlay of solid-state spectra of semi-crystalline TREF fractions from sample 2_T90 (A) CPMAS experiments and (B) IDREF experiments (Grey trend: 2_T90 60 ℃ CPMAS trend as reference).*

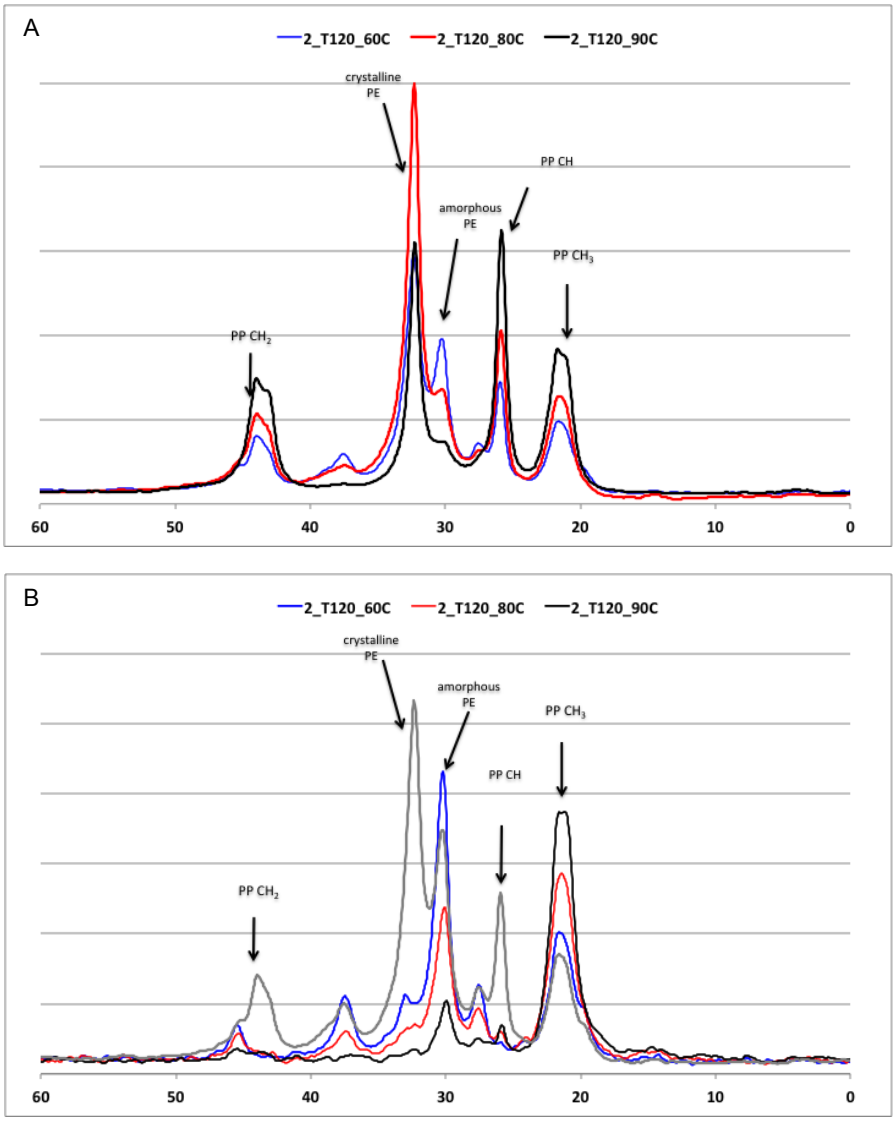

Figure 5.45 *Overlay of solid-state spectra of semi-crystalline TREF fractions from sample 2_T120 (A) CPMAS experiments and (B) IDREF experiments (Grey trend: 2_T90 60 ℃ CPMAS trend as reference).*

The solid-state trends for the sample with the highest ethylene content in the range (2_T150), is quite similar to the preceding samples, with the crystalline polyethylene peak intensity increasing even further, consistent with the total ethylene content of the sample (Fig. 5.46A). Another development in these samples is the further broadening of the methyl peak in the IDREF trend of the 60 °C fraction (Fig. 5.46B), indicating an increase in the heterogeneity of the environment surrounding these carbons as well as an increase in the mobility experienced by these carbons.

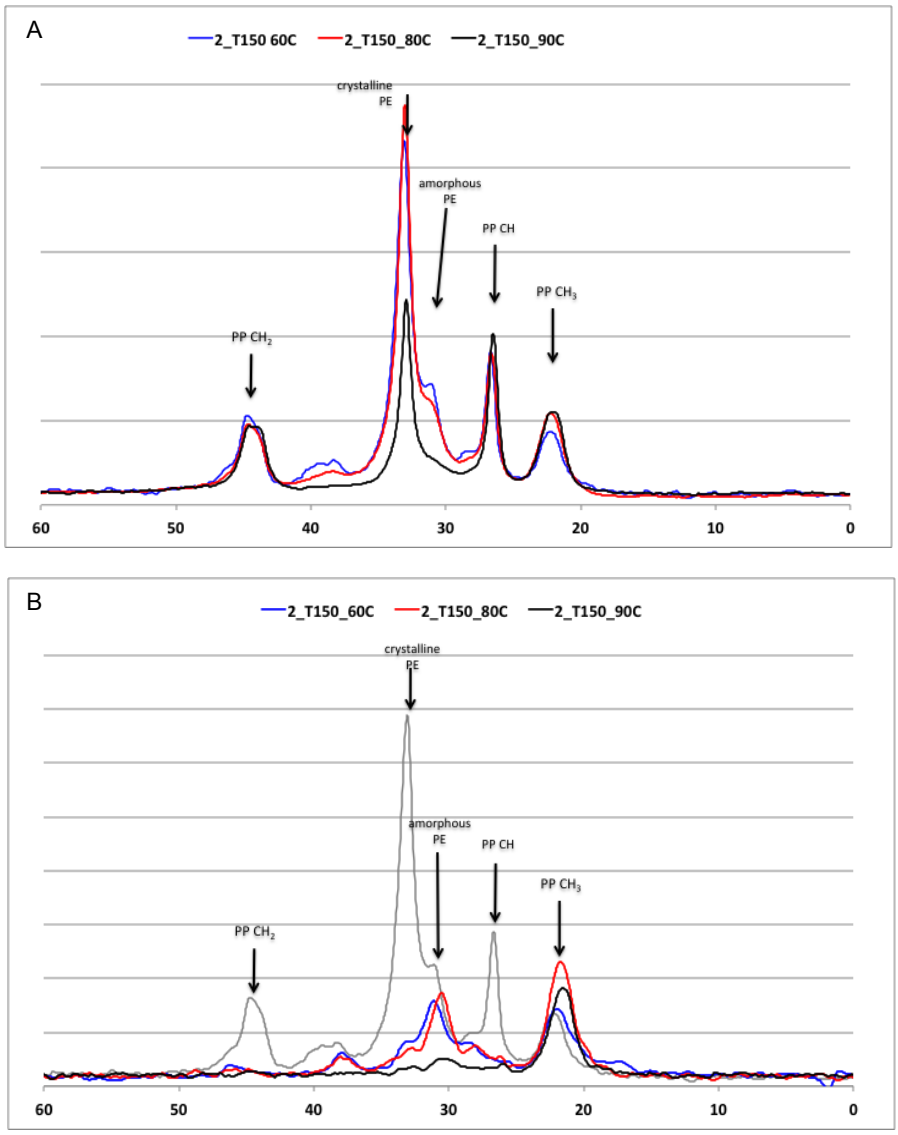

Figure 5.46 *Overlay of solid-state spectra of semi-crystalline TREF fractions from sample 2_T150 (A) CPMAS experiments and (B) IDREF experiments (Grey trend: 2_T150 60 ℃ CPMAS trend as reference).*

5.3.3.6 HT-SEC and HT-HPLC characterization of set 2 semi-crystalline fractions

The molecular weight distribution of the semi-crystalline fractions of set 2 is shown in Fig. 5.47, again emphasising the heterogeneity observed within fractions. The sample with the lowest ethylene content in the range also shows a distinct low molecular weight component in the 30 °C to 80 °C fractions. As observed previously the molecular weight trends are generally shifted towards higher molecular weights with increasing ethylene content, except for the 2_T150

sample that displays a lower molecular weight component. The HT-SEC trends for the 60 °C fractions also show that the 2_T60 and 2_T150 samples are more similar in terms of molecular weight distribution. The higher temperature fractions (80 and 90 °C) indicate a bimodal molecular weight distribution for all samples with a shift towards higher molecular weights consistent with an increase in the total ethylene content of the sample.

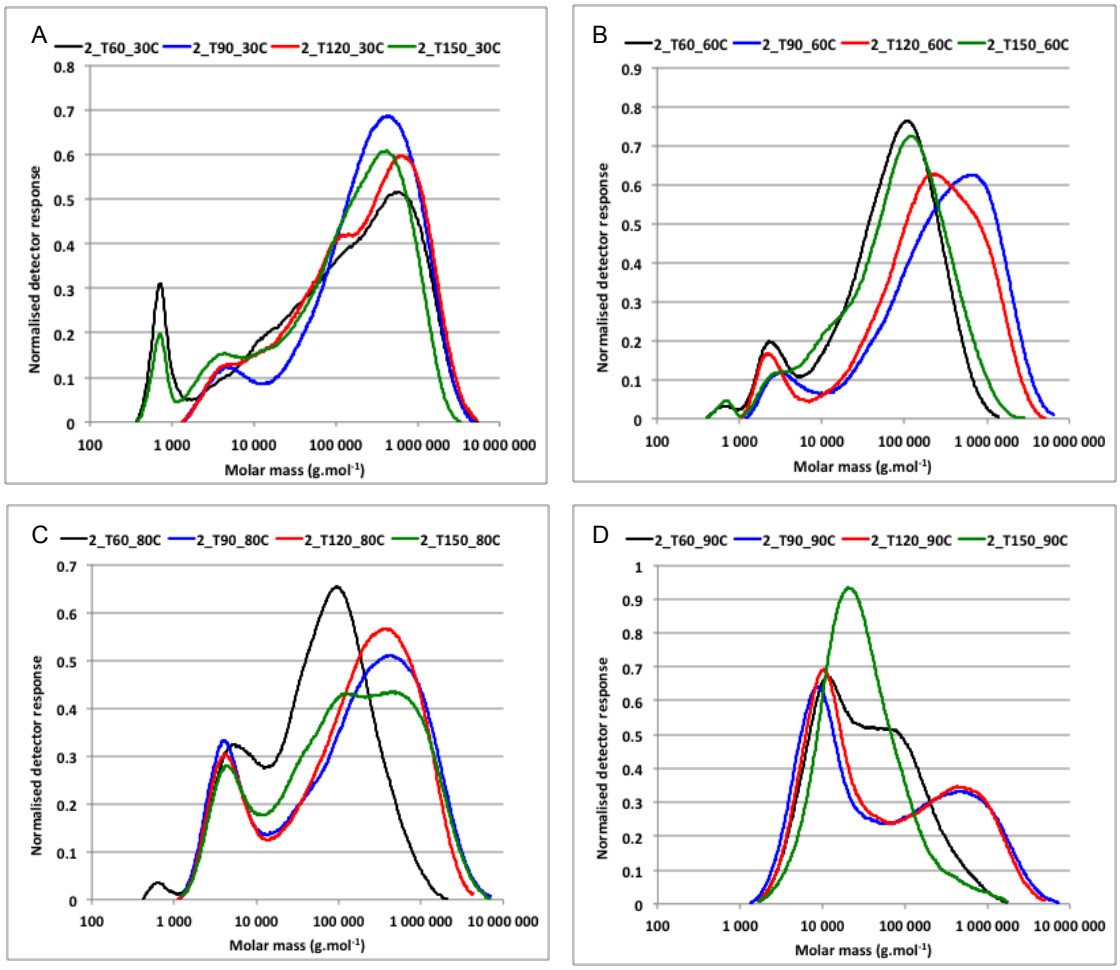

Figure 5.47 *HT-SEC overlays of TREF fractions from set 2 samples with increasing ethylene contents (2_T60, 2_T90, 2_T120, 2_T150): 30 ℃ (A), 60 ℃ (B), 80 ℃ (C) and 90 ℃ (D) fractions.*

From the HT-HPLC trends (Fig. 5.48) of the semi-crystalline fractions from set 2, it is observed that the 30 °C fractions contain a diverse mixture of high and low molecular weight isotactic polypropylene, a distribution of ethylene-propylene copolymer sequences and some linear polyethylene. It is interesting that the sample with the lowest ethylene content contains a portion of linear polyethylene, which is not observed for similar fractions of the other samples. For the 60 and 80 °C fractions it appears that there are two distinct populations with different

ethylene compositions, eluting between 3-4 ml and 5-6 ml respectively. Each of these populations consists of a distribution of different ethylene compositions as indicated by the broadening of the peak at 3-4 ml and some bimodality observed for the peak at 5-6 ml. Furthermore there is a significant amount of the peak representing longer ethylene sequences, compared to the earlier peak representing a lower ethylene composition, which is consistent with the solution NMR and solid-state NMR observations that longer ethylene sequences, as well as ethylene in crystalline environments seem to be prevalent in the set 2 samples.

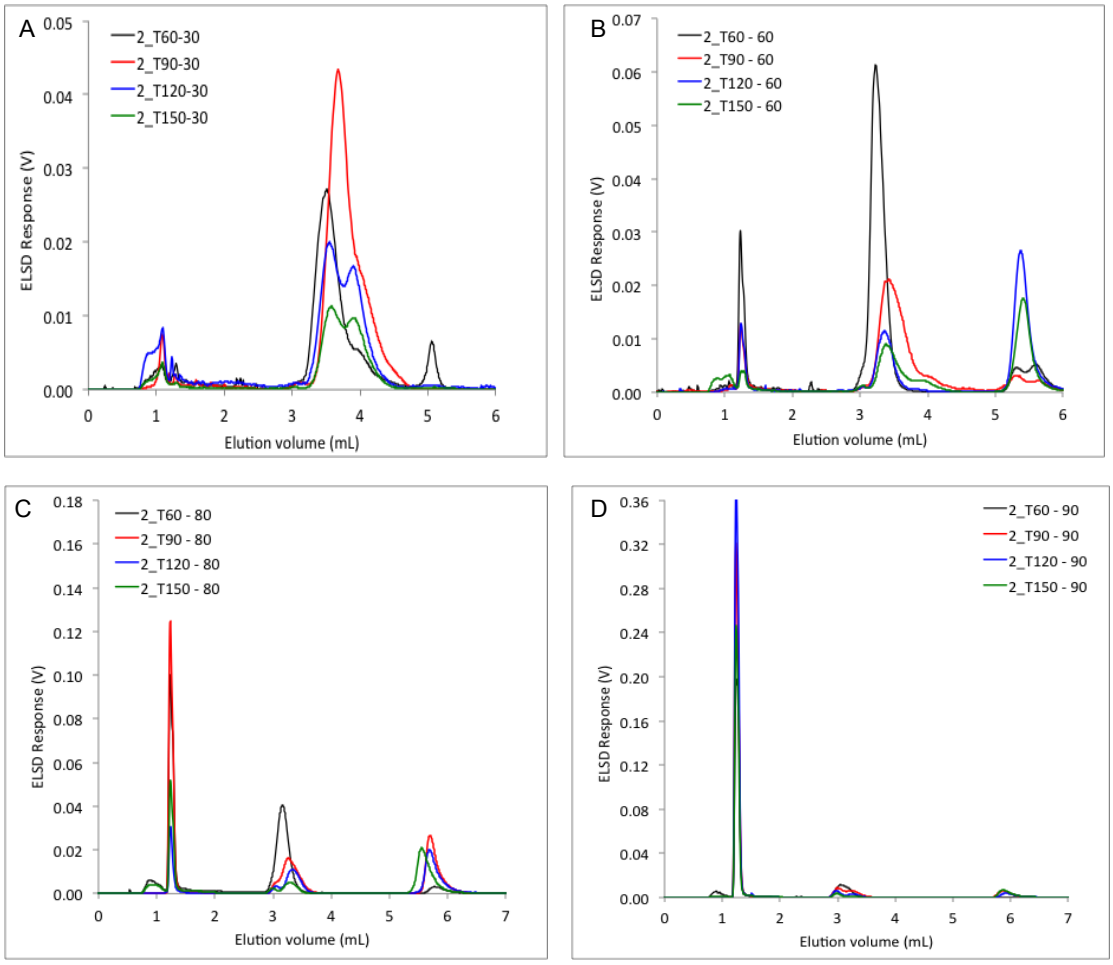

Figure 5.48 *HT-HPLC overlays of TREF fractions from set 2 samples with increasing ethylene contents (2_T60, 2_T90, 2_T120, 2_T150): 30 ℃ (A), 60 ℃ (B), 80 ℃ (C) and 90 ℃ (D) fractions.*

5.4 Conclusions

The effect of ethylene incorporation on bulk sample crystallinity, chemical composition and molecular dynamics was investigated for both sets of samples from different gas-phase processes. Selected samples (obtained by TREF fractionation) of both these sets were further analysed by solution and solid-state NMR as well as HT-SEC and HT-HPLC to determine how the semi-crystalline fractions (where the copolymer is concentrated) develop with increasing ethylene content and how this could contribute to the properties observed for the whole polymer, especially within the context of the compatibilizing function of these fractions between the amorphous rubber and crystalline homopolymer.

For set 1 it was found that the crystallinity of the homopolymer matrix could be successively reduced by increasing ethylene incorporation, as observed by the shift in the crystallinity profiles of the SCALLS and TREF trends towards lower temperatures with increasing ethylene content. It was also observed in the SCALLS trends that these samples displayed discrete groups with different crystallinities. The microstructural analysis of bulk samples showed that blocky ethylene sequences developed more rapidly with ethylene content than isolated ethylene sequences, which corresponds to the higher reactivity of ethylene relative to propylene. It was also shown by solid-state NMR that ethylene was partitioned between amorphous and rigid environments, confirming that some of the copolymer chains are excluded from the crystals while others are able to interact with the existing crystalline structures, thereby altering areas of the original crystal structure of the homopolymer as a result of these interactions. This was observed by changes in the methylene peak region and deconvolution of this multi-modal peak showed deviations from the 2:1 ratio normally observed for the highly crystalline α_2 phase consistent with an increase in the total ethylene content of the samples. Solid-state NMR also provided some information on the development of environments with increased mobility by comparing CPMAS and IDREF trends. The difference of the trends showed an ethylene dependent increase in mobility experienced by the methylene carbons from polyethylene in amorphous areas, as well as the methine carbons of polypropylene due to a loss in shielding around the backbone.

The driver for the inclusion or rejection of copolymer chains from the crystal structure is considered to be the ethylene composition of the copolymer. For this reason the semi-crystalline copolymer fractions were investigated in more detail by solution and solid-state

NMR as well as HT-SEC and HT-HPLC. It was shown in general that the 60 °C fractions contained a greater variety of copolymer sequences which would aid in compatibilization with the rubber phase, whereas the 90 °C fractions consisted mostly of polypropylene and blocky ethylene sequences (EEEE) which would more likely compatibilize with the homopolymer phase. The Sδδ peak intensities (relative to the other peaks) in the 90 °C fractions increased as the total ethylene content of the sample increased. This also corresponded to an increase in the solid-state peak at ~33 ppm, representative of ethylene in crystalline environments with increasing sample ethylene content. This increase was more pronounced for the 80 and 90 °C fractions and is consistent with what would be expected in terms of compatibilization. From the tetrad distributions of the 60 °C fractions, it was observed that with a decrease in blocky propylene tetrads (PPPP and PPPE) there was a corresponding increase in blocky ethylene tetrads (EEEE and PEEE) as the total ethylene content of the sample increased, until a 50:40 split blocky propylene to ethylene distribution was found in the sample with the highest ethylene content (1_T360). In this sample it was also observed that the number average ethylene sequence was equal to the number average propylene sequence length, indicating on average blocks of equal length of each monomer. This was also observed in the 80 °C fraction of the sample with the highest ethylene content. As observed with the bulk, isolated sequences (EPPE and PEEP) did not develop as rapidly as the blocky sequences. For the 80 and 90 °C fractions the blocky propylene to ethylene ratio increased to a 60:40 split and 70:30 split for the final sample in the set as the total ethylene contents in these fractions decreased.

HT-SEC and HT-HPLC provided some insights into the molecular weight and chemical composition distribution of the fractions. The molecular weight distribution trends were shifted towards higher molecular weights as the ethylene content of the sample increased and the sample with the lowest ethylene content in the set showed a distinct lower molecular weight component in all fractions. As the fraction temperature increased the contribution of the high molecular component grew less, consistent with the decrease of the total ethylene content in these fractions (as observed by solution NMR). The HT-SEC observations also support the observations made by SEC-FTIR using bulk samples in the sense that ethylene is predominantly found in chains with high molecular weights. From the HT-HPLC trends a broad chemical composition distribution was observed for the 60 and 80 °C fractions. The trends were also shifted towards higher elution volumes (i.e. higher ethylene contents) consistent with the total ethylene content of the sample. Apart from the broad distribution representing different

ethylene contents, a distinct small peak eluting at a later stage was also observed, representative of long and/or linear ethylene sequences, confirming the preference for the development of longer ethylene sequences with increasing ethylene incorporation.

The set 2 samples in general had fairly narrow SCALLS profiles with a smaller portion of high- and low crystallinity components. The only exception here was the 2_T120 sample that showed a significant amount of a lower crystallinity component. This sample also had reduced impact strength compared to the rest of the samples in the range. Similarly the TREF profiles were also narrow and followed the trend of decreasing crystallinity with increasing ethylene content, however these samples were mainly distributed in fractions above 110 °C or below 30 °C, with very little material in the semi-crystalline fractions. Solution NMR was done on the bulk samples and it was observed that the peaks representing secondary carbons in various ethylene-propylene sequences did not change much with increasing ethylene content. The most pronounced development that was observed for this set was that of longer ethylene sequences (EEEE) relative to isolated ethylene sequences (PEEP). This observation was also reflected in the solid-state spectra, where it was shown that ethylene was predominantly found in crystalline environments for all samples except the first with the lowest ethylene content. It was also observed from the line shape of the peak representing methylene carbons that the disruption of the 2:1 α_2 peak ratio was so great that it could not be quantified. The resulting dipolar dephasing trends indicated that some of the methylene carbons start to experience local mobility upon ethylene incorporation, which would explain the loss in the splitting of the methylene peak. It is therefore evident that the incorporation of ethylene has altered the polypropylene crystalline structure and crystal packing to some extent. Furthermore, it was shown by solution NMR of the semi-crystalline fractions, that significant amounts of blocky ethylene sequences, relative to blocky propylene sequences was found in the 60 and 80 °C fractions. By means of solid-state NMR analysis of the fractions it was shown that all fractions, even the 60 °C fraction, which is expected to compatibilize with the rubber, contained significantly more ethylene in crystalline environments relative to amorphous environments.

Clear ethylene dependent trends in the molecular weight distribution could not be obtained for all fractions of set 2, however it was observed in the 80 °C fraction that the molecular weight increased as the total ethylene content of the sample increased. The sample with the highest ethylene content however had some low molecular weight components present in the other

fractions, which does not correspond with the theory of producing high molecular weight copolymers. The HT-SEC profiles of the set 2 samples showed apart from a broad ethylene composition eluting at low volumes that a significant amount of chains with high ethylene contents, presumably linear polyethylene was present in the 30 to 90°C fractions, which confirms what was observed by solution and solid-state NMR.

5.5 References

1. McKenna, T.F., Bouzid, D., Matsunami, S. and Sugano, T. *Evolution of Particle Morphology During Polymerisation of High Impact Polypropylene.* Polymer Reaction Engineering, 2003. **11**(2): p. 177-197
2. Urdampilleta, I., Gonzalez, A., Iruin, J.J., de la Cal J.C. and Asua, J.M *Morphology of High Impact Polypropylene Particles.* Macromolecules., 2005. **38**: p. 2795-2801
3. Debling, J.A. and Ray, W.H. *Morphological Development of Impact Polypropylene Produced in Gas-phase with a $TiCl_4/MgCl_2$ Catalyst.* Journal of Applied Polymer Science., 2001. **81:** p. 3085-3106
4. Chen, Y., Chen, Y., Chen, W. and Yang, D. *Evolution of phase morphology of high impact polypropylene particles upon thermal treatment*. European Polymer Journal., 2007. **43:** p. 2999-3008
5. Zhu, H., Monrabal, B., Han, C.C. and Wang, D. *Phase structure and crystallization behaviour of polypropylene in-reactor alloys: Insights from both inter- and intramolecular compositional heterogeneity.* Macromolecules., 2008. **41:** p. 826-833
6. Li, Y., Xu, J., Dong, Q., Wang, X., Fu, Z. and Fan, Z. *Effect of microstructure of EPR on crystallization and morphology of PP/EPR blends.* Polymer- Plastics Technology and Engineering., 2008. **47:** p.1242-1249
7. Li, Y., Xu, J., Dong, Q., Fu, Z. and Fan, Z.Q *Morphology of polypropylene/poly(ethylene-co-propylene) in-reactor alloys prepared by multi-stage sequential polymerization and two-stage polymerization.* Polymer., 2009. **50**: 5134-5141
8. Xue, Y., Fan, Y., Bo, S. and Ji, X. *Characterization of the microstructure of impact polypropylene alloys by preparative temperature rising elution fractionation*. European Polymer Journal., 2011. **47:** p.1646-1653
9. Ray, G.J., Johnson., P.E. and Knox, J.R. *Carbon-13 nuclear magnetic resonance determination of monomer composition and sequence distribution in ethylene-propylene copolymers prepared with a stereoregular catalyst system.* Macromolecules., 1977. **10(4):** p.773-778
10. Kakugo, M., Naito Y., Mizunuma, K. and Miyatake, T. *^{13}C NMR determination of monomer sequence distribution in ethylene-propylene copolymers prepared with δ-$TiCl_3$-$Al(C_2H_5)_2Cl$.* Macromolecules., 1982. **15:** p.1150-1152
11. Randall., J.C. *A ^{13}C NMR determination of the comonomer sequence distributions in propylene-butene-1 copolymers.* Macromolecules., 1978. **11(3):** p.33-36

12. Comotti, A., Simonutti, R., Bracco, S., Castellani, L. and Sozzani, P. *Simultaneous crystallization of isotactic and syndiotactic sequences of polypropylene.* Macromolecules., 2001. **34:** p.4879-4885

13. Alamo, R.G., VanderHart, D.L., Nyden, M.R. and Mandelkern, L. *Morphological partitioning of ethylene defects in random propylene-ethylene copolymers.* Macromolecules., 2000. **33:** p.6094-6105

14. Zhu, H., Graf, R., Hou, G., Zhao, Y., Wang, D. and Spiess, H.W. *Solid-state NMR characterization of the multiphase structure of polypropylene in-reactor alloy.* Macromolecular Chemistry and Physics., 2010. **211:** p.1157-1166

15. Macko, T. and Pasch, H. *Separation of linear polyethylene from isotactic, atactic and syndiotactic polypropylene by high-temperature adsorption liquid chromatography.* Macromolecules., 2009. **42:** p.6063-6067

16. Cheruthazhekatt, S., Pijpers, T.J.F., Harding, G.W., Mathot, V.B.F. and Pasch, H. *Compositional analysis of an impact polypropylene copolymer by fast scanning DSC and FTIR of TREF-SEC cross-fractions.* Macromolecules., 2012. **45:** p.5866-5880

17. Cheruthazhekatt, S., Harding, G.W. and Pasch, H. *Comprehensive high temperature two-dimensional liquid chromatography combined with high temperature gradient chromatography-infrared spectroscopy for the analysis of impact polypropylene copolymers.* Journal of Chromatography A., 2013. **1286:** p.69-82

18. Shan, C.L.P., deGroot, W.A., Hazlitt, L.G. and Gillespie, D. *A new turbidimetric approach to measuring polyethylene short chain branching distributions.* Polymer., 2005. **46:** p.11755-11767

19. van Reenen, A.J., Rohwer, E.G., Walters, P., Lutz, M. and Brand, M. *Development and use of a turbidity analyser for studying the solution crystallization of polyolefins.* Journal of Applied Polymer Science., 2008. **109:** p.3238-3243

20. Carman, C.J. and Wikes, C.E. *Monomer sequence distribution in ethylene propylene elastomers. I. Measurement by carbon-13 nuclear magnetic resonance spectroscopy.* Rubber Chemistry and Technology., 1971. **44(3):** p.781-804

21. Bovey, F.A. and Mirau, P.A. *NMR of Polymers.* Academic Press., 1996. p.171

22. Wang, M., Bernard, G.M., Wasylishen, R.E. and Choi, P. *A solid-state ^{13}C NMR investigation of the morphology of single-site and Ziegler-Natta linear low-density polyethylenes with varying branch contents.* Macromolecules., 2007. **40:** p.6594-6599

23. Nyden, M.R., Vanderhart, D.L. and Alamo, R.G. *The conformational structures of defect-containing chains in the crystalline regions of isotactic polypropylene.* Computational and Theoretical Polymer Science., 2001. **11:** 175-18

24. van der Burgt., F.P.T.J. *Crystallization of isotactic polypropylene: The influence of stereo-defects.*, 2002. Technische Universiteit Eindhoven

25. Busico, V., Corradini, P., de Rosa, C. and di Benedetto, E. *Physico-chemical and structural characterization of ethylene-propene copolymers with low ethylene content from isotactic-specific Ziegler-Natta catalysts.* European Polymer Journal. 1985. **21(3):** p.239-244

26. Laihonen, S., Gedde, U.W., Werner, P.E., Westdahl, M., Jääskeläinen, P. and Salazar, J.M. *Crystal structure and morphology of melt-crystallized poly(propylene-stat-ethylene) fractions.* Polymer., 1997. **38(2):** p.371-377

Chapter 6

Conclusion

In this chapter, the main findings from this study are summarized and a model for development of the copolymers in each of the sample sets proposed. The scope for further work is also identified.

6.1 Synopsis, conclusions and recommendations for future work

6.1.1 Introduction

Heterophasic copolymers are valued for their advanced physical properties and mechanical behaviour, while remaining a low cost alternative compared to other materials typically used in similar applications. The compositional heterogeneity of polypropylene ethylene-propylene impact copolymers or HEPCs, however makes it difficult to relate chemical properties to physical performance, suggesting that even better tailoring and optimization of product properties could be possible if structure-function relationships in these complex multi-phase systems could be fully understood. To this end, many previous studies have focussed on developing an understanding of polymer morphological development.

The current study has aimed to provide further, complementary information on the morphological development of these type of polymers, exploring the unique properties of commercial transition samples as opposed to autoclave products used in previous studies. The samples selected for this study were obtained from two different commercial gas-phase processes during a transition from homopolymer to impact copolymer and therefore represents the early sequential development of the copolymer phase with increasing ethylene incorporation.

The main objectives of this study were to determine the effect of increasing ethylene incorporation on the development of polymer morphology and physical properties in the bulk, as well as the effect on sample crystallinity. Furthermore the development of microstructure, chemical composition and crystal packing was observed for increasing ethylene incorporation and related to the observed morphological and physical property development. This was done for bulk samples and selected semi-crystalline fractions obtained by TREF.

6.1.2 Proposed model for copolymer phase development in set 1

Based on the morphological observations made using FE-SEM, as described in Chapter 4, a model is proposed for the sequential development of the copolymer as increasing amounts of ethylene is incorporated in the growing polymer. A schematic representation for the model is shown in Fig. 6.1. It is well known that the growing polymer replicates the morphology of the catalyst in Ziegler-Natta catalysed reactions. Homopolymer chains growing from active centres form submicron sized structures called globules, causing the particle to have a grainy appearance. Homopolymer globules tend to form agglomerates or sub-globules with resultantly a network of cracks and pores between these agglomerates. This initial structure plays an

important role in the development of the copolymer phase, as it was observed for this particular set that due to relatively low homopolymer porosity, the copolymer phase rapidly started to cover the external surfaces of the particle at low ethylene contents. This also resulted in the maintenance of internal porosity even up to the highest ethylene content observed for this set.

The copolymer was observed to form internally at various radial positions in the particle and was not concentrated on either the inner or outer surface of the particle, suggesting that there were not any significant ethylene monomer diffusion limitations present. Furthermore, the growth of copolymer with increasing ethylene content was shown to occur on the surfaces of the existing homopolymer globules as it was observed that the globular surface gradually become smoother with increasing ethylene incorporation. However considering the copolymer distribution over the whole particle, this was not an even covering and the copolymer tended to pool in random areas as observed by smooth patches of copolymer covering the underlying globules. In Fig. 6.1 this is represented as blue blobs on the internal and external surfaces.

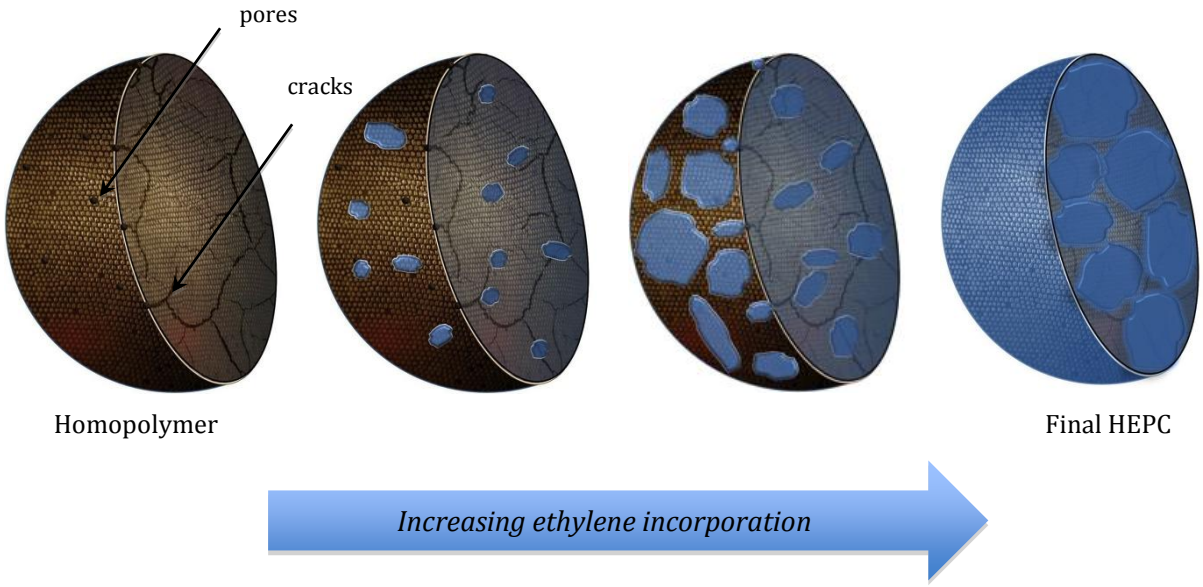

Figure 6.1 *Schematic representation of copolymer development for set 1. Cross sections of polymer particles with external and internal surfaces are shown. Propylene homopolymer is shown in brown and ethylene-propylene copolymers in blue.*

From microscopic investigation of the rubber particle size and distribution in samples moulded from the nascent polymers, it was found that the rubber particle size gradually increased and that the distances between particles gradually decreased with increasing ethylene incorporation while on average the number of rubber particles stayed the same regardless of ethylene content. Resultantly a steady increase in impact resistance was observed with increasing ethylene incorporation as well as a slight decrease in product stiffness as would be

expected. It was also observed that the impact strength could be increased beyond a certain point without sacrificing stiffness any further.

6.1.3 Microstructural changes due to the developing copolymer in set 1

It is well known that the in-reactor alloys produced in industry have superior mechanical properties, compared to blends of propylene homopolymers and copolymers of different compositions. This advantage seems to stem from the fact that in the in-reactor alloys the polypropylene and copolymer chains are physically (covalently) linked which enhances the interaction between these different phases. In this study it was observed that the crystallinity of the existing homopolymer could be attenuated by incorporating increasing amounts of ethylene in the polymer as observed by changes in the SCALLS profiles and shifting of the TREF elution trends to lower temperatures. The effect of copolymer on homopolymer crystallinity was confirmed by solid-state NMR, where it was shown that changes in the crystalline packing of the ordered α_2 allomorph of isotactic polypropylene occurred as observed by changes in the methylene groups which form part of the polypropylene backbone. Furthermore it was also shown that the methine carbons that normally experience environments with low mobility due to its sheltered position in the polypropylene helix and crystal unit, started to experience higher mobility with increasing ethylene incorporation. It was also observed that ethylene units were found in crystalline and amorphous environments in the copolymer. Solid-state NMR has not been used previously on bulk HEPCs and the information obtained from this part of the study has provided some new insights not only on the chemical composition of these highly complex polymers, but also on the molecular dynamics between the various crystal forms and arrangements of the existing homopolymer phase and the developing copolymer.

Solution NMR was used to determine average chain properties and ethylene sequences. It was shown that there was a discontinuous growth of certain ethylene sequences, where blocky or continuous ethylene sequences seemed to develop more rapidly than isolated ethylene sequences. Since solution NMR has a limit to the number of units that can be determined at a time, some information on a larger scale (considering whole polymer chains or phases) is lost. However the power of this technique lies within the statistical averaging that is used in this method, to provide a general idea of what a typical molecule within a distribution could look like. Using the number average sequence lengths that were determined by solution NMR for propylene and ethylene a different microstructural model is proposed here to provide an indication of the distribution of ethylene within the context of the whole polymer (Fig. 6.2A). It can be seen in this scheme that though the bulk is dominated by propylene (blue), there is an increasing frequency of ethylene 'interruptions' (purple) with increasing ethylene content, but

that relative to the propylene sequences the length of the ethylene sequences are still fairly short. Considering the number average sequence length data from the fractions (Fig. 6.2B), it is clear that the 60 °C fractions contain more alternating blocks of ethylene and propylene, which is expected to be more compatible with the amorphous 30 °C fractions, while the number average propylene sequence lengths increases towards the 90 °C fractions, which should create polymers that are more compatible with the isotactic polypropylene. It is also observed that the ethylene blocks in the 90 °C fraction increase in length as the total ethylene content of the sample increases, so that a significant amount of longer ethylene sequences are found in the 90 °C fraction of the final sample of the set (1_T360).

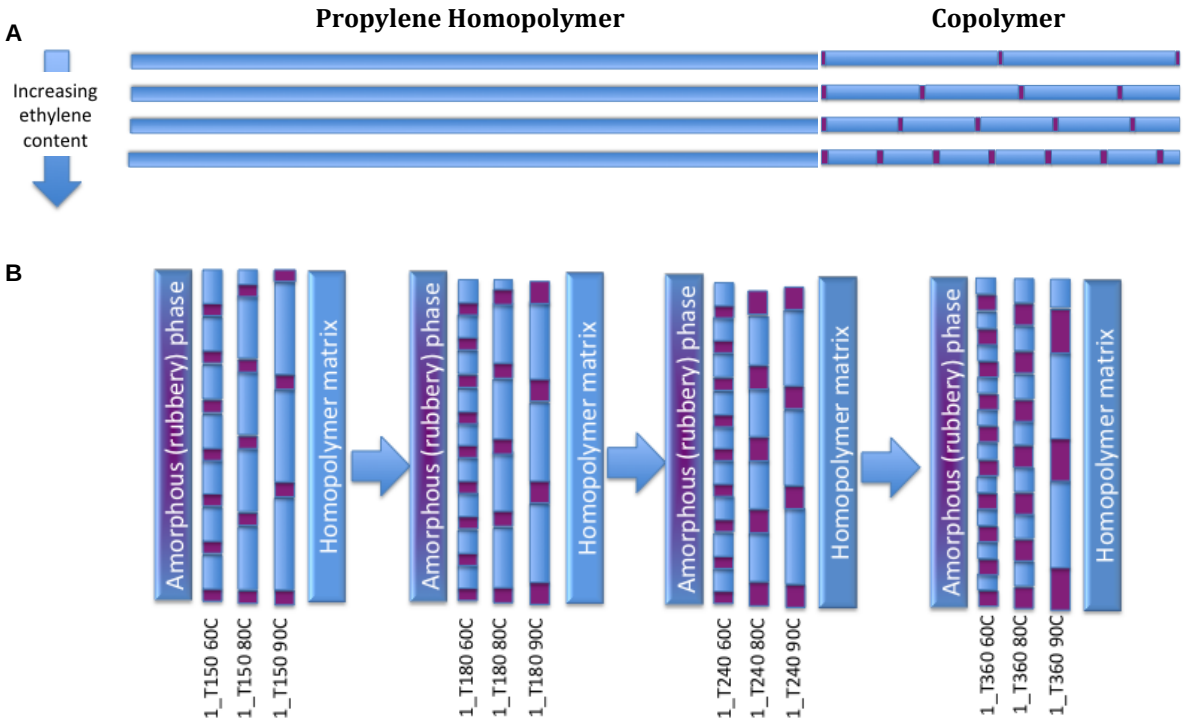

Figure 6.2 *Schematic representation of average ethylene distribution in the bulk samples (A) and fractions (B) for set 1. Propylene units are indicated in blue and ethylene units in purple.*

It was shown by HT-SEC that the copolymer fractions consisted of a wide range of molecular weights and the trends were shifted towards higher molecular weights as the ethylene content of the samples increased. From HT-HPLC of copolymer fractions a wide copolymer composition distribution was observed in the lower temperature fractions (30 and 60 °C) and a small portion of polyethylene (potentially linear PE) was found in the higher temperature fractions (80 and 90 °C), confirming the solution NMR findings as outlined above. Significant amounts of ethylene carbons present in crystalline environments were also observed by solid-state NMR analyses of the fractions.

6.1.4 Proposed model for copolymer phase development in set 2

The growth of the copolymer phase occurred somewhat different for set 2, compared to that of set 1, which was described in the previous section. A schematic representation of this growth is shown in Fig. 6.3. The homopolymer particle is initially very porous, consisting of a multitude of large pores and cracks between clusters of globules. Upon introduction of the ethylene and copolymerization, there is a slower coverage of the external surface areas, as some external pores were observed even for the sample with the highest ethylene content. The number of external pores decreases with increasing ethylene content as these are covered by copolymer. Although external porosity was maintained for this set at higher ethylene contents, internal porosity was rapidly lost as copolymerization continued, as indicated by the absence of pores in images obtained from inner and outer surfaces of microtomed particles. The mode of copolymer growth did not appear to occur solely by surface coverage of globules, as some grainy globular structures were still discernible at higher total ethylene contents and the copolymer phase had the appearance of thin streams stretching between globular structures, possibly filling existing pores and cracks between the globules. These observations are considered to be a function of the initial high porosity of the particles, which resulted in the filling of pores before the smoothening of globular surfaces could occur.

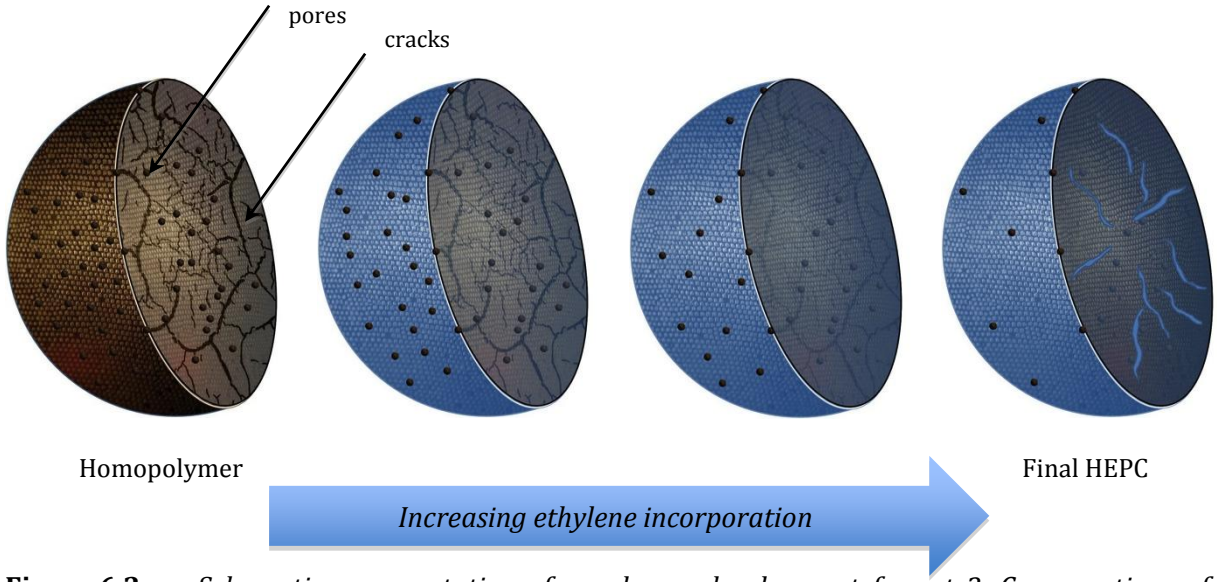

Figure 6.3 *Schematic representation of copolymer development for set 2. Cross sections of polymer particles with external and internal surfaces are shown. Propylene homopolymer is shown in brown and ethylene-propylene copolymers in blue.*

Through microscopic investigation of the fracture surfaces of moulded samples from this set, it was found that although the average rubber particle size increased with increasing ethylene incorporation, the actual number of rubber particles decreased, leading to an increase in inter particle distances with increasing ethylene contents. Despite this, an increase in impact strength

properties as well as a slight decrease in stiffness properties was observed with increasing ethylene incorporation, indicating that the successive distribution of the rubber particles was sufficient to obtain an increase in impact strength. It was also shown that when rubber particles were too closely dispersed, this led to a reduction in impact strength properties. It could be concluded from these observations that in order to obtain an optimal rubber particle distribution for this set, more information on the semi-crystalline copolymers responsible for compatibilization between the rubber and matrix would be required.

6.1.5 Microstructural changes due to the developing copolymer in set 2

On average the HEPC samples from set 2 had a narrower crystallinity distribution, as observed by SCALLS, with small amounts of higher and lower crystallinity components. This was also observed in the TREF profiles where the samples displayed mostly high crystallinity components >100 °C and low crystallinity components < 30 °C, but did not display a significant distribution between the semi-crystalline fractions (60 to 90 °C). This observation was supported by solution NMR of the bulk samples, which showed that the different combined ethylene and propylene sequences did not change much with an increase in sample ethylene content. The most pronounced development in the solution NMR spectra of these samples was the Sδδ peak representing continuous ethylene sequences that increased with an increase in total sample ethylene content. Secondary carbons representative of longer ethylene sequences were also found to be more dominant in these spectra. From the solid-state NMR spectra, the above observations were confirmed as a significant amount of ethylene in crystalline environments was observed, regardless of the total ethylene content of the sample. It was also found that regular polypropylene crystal packing was disrupted in these samples, affecting the methylene region in the spectra and that in the sample with the highest ethylene content, some of the methylene carbons started to experience local mobility, further confirming changes in the crystal packing due to ethylene incorporation. Furthermore the HT-HPLC analyses confirmed a significant amount of linear polyethylene in addition to the distribution of copolymers that eluted from the column.

The number average propylene and ethylene sequence lengths determined by solution NMR are schematically represented in Fig. 6.4. Assuming that alternating sequences of ethylene and propylene exist in a molecule, a predicted average polymer chain from each bulk sample is shown in Fig. 6.4A. Here it is observed that initially at the lowest ethylene content, more frequent ethylene ‘interruptions’ are present, which is considered to be a function of the total ethylene content (as this range starts with a higher ethylene content relative to set 1).

Furthermore, the frequency of the ethylene insertions increases as the total ethylene content of the sample increases, but only up to a certain point, as observed for the last sample in the range, where the frequency of ethylene insertions is slightly lower, but the inserted ethylene units slightly longer.

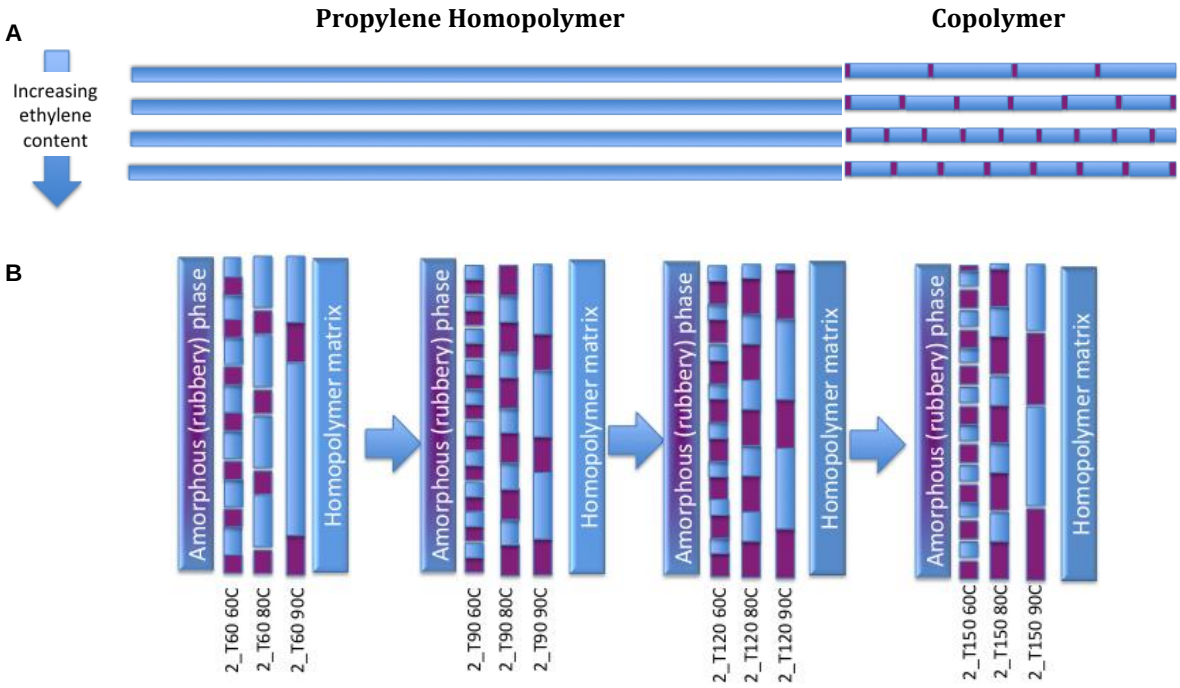

Figure 6.4 *Schematic representation of average ethylene distribution in the bulk samples (A) and fractions (B) for set 2. Propylene units are indicated in blue and ethylene units in purple.*

Considering the representation of an average chain from each semi-crystalline copolymer fraction (Fig. 4.6B), the trend of short propylene and ethylene sequences for fractions with lower crystallinity developing into longer ethylene and propylene sequences in fractions with higher crystallinity is also observed for this set. For the higher ethylene contents in this set (samples 2_T90 to 2_T150), the 60 and 80 °C fractions actually appear to be polyethylene with propylene "insertions" as judged by the length of the ethylene sequence units (purple) relative to that of the propylene (blue). The observation that short continuous propylene and ethylene runs are present in the 60 °C fraction of all the samples, suggests good compatibility of this fraction with the amorphous copolymer (rubber). The only exception is the 2_T120 sample that has slightly longer ethylene runs, which might not be optimal for compatibilization, resulting in less than optimal rubber particle distribution and lower impact strength properties as was observed for this sample. The 90 °C fractions of these samples approach a more blocky distribution with longer ethylene and propylene stretches as the total ethylene content of the sample increases.

6.1.6 Conclusion

This study provided the opportunity to observe the sequential development of copolymers in bulk HEPC samples as these were obtained during a grade transition from homopolymer to HEPC. Samples representing different commercial gas-phase technologies (Set 1 and Set 2) were analysed and a model developed for each set. Even though both technologies used similar Ziegler-Natta catalysts, products with different characteristics were obtained. The catalyst morphology as well as the morphology of the homopolymer prior to the introduction of ethylene were shown to play a significant role in the development and distribution of the copolymer phase. For a homopolymer matrix of low porosity, the complete coverage of external surfaces while some internal porosity was maintained was observed. On the other hand, for a homopolymer matrix with sufficient porosity, internal pore filling occurred preferentially above surface coating, resulting in grainy structures that persisted throughout the particle. For both sets, no radial distribution of copolymer was observed, suggesting that significant ethylene monomer diffusion limitations were not present during polymerization.

During the development of the copolymer phase, continuous ethylene sequences were favoured above isolated ethylene sequences, as determined from the ^{13}C solution NMR spectra and tetrad distributions, which was consistent with the higher reactivity of ethylene compared to propylene. Through solid-state NMR it was shown that partitioning of ethylene between crystalline and amorphous environments occurred and this could be visualised even in the bulk samples, emphasising the potential of this method to discern between longer range chain- and crystal packing interactions. Determination of the relative crystallinities of the samples by means of SCALLS and TREF indicated that the growing copolymer phase attenuated the initial crystallinity of the homopolymer by disrupting crystal packing, emphasising the importance of understanding the various interactions between copolymers with different chemical compositions and the homopolymer phase.

Further analysis of the semi-crystalline fractions by means of solution and solid-state NMR, as well as HT-SEC and HT-HPLC indicated that these fractions contained specific chemical composition and molecular weight distributions that had a combination of characteristics of the fractions eluted before and after the particular fraction, which would aid in the compatibilization of the different fractions in the bulk. This also indicated the potential of manipulating phase compatibility by varying the chemical composition of the copolymer.

6.1.7 Recommendations for future work

The morphological observations were obtained using FE-SEM that provides higher resolution than conventional SEM and allowed the visualization of different structures within the particles up to a sub-micron scale. This technique is however limited in that it is only a surface technique and does not provide any information on the chemical composition of what is observed, or a three-dimensional observation of underlying structures. For the purposes of this study a distinction between the globular homopolymer and smooth copolymer was made to observe the development of the copolymer phase, but it would also be interesting to obtain direct information on the chemical composition of a specific visualised structure. In this study, the chemical composition of fractions was determined and their relative functions within the bulk inferred from what is known in this field of research. However it is evident that a technique such as FTIR-microscopy would provide a direct link between the observed structure and chemical composition that would provide an additional dimension to this study.

Furthermore a relative indication of porosity was obtained for these samples based upon what was visualised in the FE-SEM images. Care was taken to ensure that representative samples were selected for the capturing of microscope images, however it was not possible via this technique to obtain information on the porosity distribution throughout the whole particle. Mercury porosimetry analysis of the bulk samples should provide more information on this.

This study has highlighted the importance of the initial homopolymer morphology and porosity in the subsequent development of the copolymer phase. As the morphology of the homopolymer is a function of the catalyst system used, it follows that different modes of copolymer phase development would be observed for samples obtained from different catalyst systems, which is of industrial relevance as there are always new catalysts being developed and trialled in industry. Furthermore the influence of chain interactions, driven by chemical composition and microstructural development of the copolymer on polymer crystallinity and physical performance, has been established in this study; therefore further work in determining the relationship between these, for a range of different operating conditions would aid the understanding of how to tailor these polymers to obtain the required properties.